STUDY OF N_2O DECOMPOSITION OVER FE-ZSM-5 WITH TRANSIENT METHODS

THÈSE N^{O} 3884 (2007)

PRÉSENTÉE LE 9 NOVEMBRE 2007

À LA FACULTÉ DES SCIENCES DE BASE

Laboratoire de génie de la réaction chimique

SECTION DE CHIMIE ET GÉNIE CHIMIQUE

ÉCOLE POLYTECHNIQUE FÉDÉRALE DE LAUSANNE

POUR L'OBTENTION DU GRADE DE DOCTEUR ÈS SCIENCES

PAR

Petra PRECHTL

M.Sc. Chemieingenieurwesen, Friedrich-Alexander-Universität Erlangen, Allemagne
et de nationalité allemande

acceptée sur proposition du jury:

Prof. P. Vogel, président du jury
Dr L. Kiwi, Prof. A. Renken, directeurs de thèse
Dr G. Foti, rapporteur
Prof. F. Keil, rapporteur
Dr B. Louis, rapporteur

ÉCOLE POLYTECHNIQUE
FÉDÉRALE DE LAUSANNE

Lausanne, EPFL
2007

Acknowledgements

I have worked on this thesis from October 2002 to April 2007 in the Laboratory of Chemical Reaction Engineering (Group of Catalytic Reaction Engineering, since November 2006). First of all I would like to thank Prof. Albert Renken and MER Liouba Kiwi-Minsker for taking me into your group. I thank you for your advices, encouragement, the freedom and the trust you have given to my work.

Many thanks to Prof. Pierre Vogel for having presided the jury and many thanks to Prof. Frerich Keil, Dr. Benoit Louis and Dr. Gyorgy Foti for having taken the time to examinate.

I feel deep gratitude towards Dimitri. Thank you very much for your guidance, inspiration, eternal discussions, availability and the proof reading of my thesis.

Thanks to those who have assisted me in the lab. It would have not been possible to start up the TAP machine without the support of Prof. J.T. Gleaves and Dr. R. Fushimi. Thank you very much for teaching me for one week at your institute in St. Louis, USA. Many thanks also to Dr. G. Yablonsky, Dr. S. Shekhtman, T. Decamp and Dr. Y. Schuurman for your advices on the TAP topic. A big thank you goes to the master students Bryan Bromley and Stéphanie Tissot whose work was very important to complete the experimental part of my thesis.

I am grateful to the technicians Bobo, Jean-Claude, André, the electricians Gaby, Gérard, Supardi, the computer guy PAP and the secretaries Mme Szuman, Mme Anken, Stéphanie, Vida and Sara which always helped in technical and administrative matters and cheered me up when needed.

Special thanks to Chrystèle, Pierre, Pascal, Edi and Sophie for the huge encouragement, for integrating me in Switzerland, teaching me French and the long, long discussions which I appreciated a lot. Edi, thanks a lot for coaching me in alpine sports. Natasha, I owe you a lot for your infinite support and encouragement. Subbu, I always appreciated the inspiring discussions with you and the invitations to your house.

I have had the pleasure to be part of a girls evenings community: Chrystèle, Natasha, Sophie, Béa, Ilaria, Justyna and Elena. Thank you very much for the time we spent together, I cherish it.

To my colleagues: Agnieszka, Anne-Laure, Babis, Benoît, Blanca, Carmen, Eric, Erika, Ester, Gabriele, Hao, Igor, Jonas, Kashid, Kim, Lavax, Marie-Agnès, Marina, Martin, Micaela, Michal, Philip, Sébastien and Yves-Alain thanks for the discussions (professional and non-prof.) as well as the coffees and good moments we have shared.

To the people I owe the most: my parents, thanks for your support and trust as well as to my siblings for always believing in me. Thanks to my friends from Germany who came to visit and cheered me up when needed: Christine & Ralf, Florian, Frank, Gisi & Family, Katja, Simone, Susanne and Ute.

Science is organized knowledge.
Wisdom is organized life.

I. Kant

Abstract

Nitrous oxide is the third most important gas contributing to global warming and its concentration in the atmosphere is still on the rise. Nitric acid production represents the largest source of N_2O in the chemical industry, with a total annual emission of about 400 kt N_2O. An efficient way to reduce the N_2O is the catalytic decomposition into N_2 and O_2. ZSM-5 zeolites containing iron are known to be effective in this reaction involving Fe(II)-extraframework species as active sites. But the nature of these sites and the reaction network is still under debate. Often the N_2O is in the exhaust together with other gases like NO_x, CO_x, oxygen, and water vapor, which may influence the catalyst efficiency towards N_2O decomposition. The effect of these gases on the reaction mechanism is still not understood yet.

The aim of this work is to study the decomposition mechanism of N_2O over isomorphously substituted Fe-ZSM-5 (0.02-0.55% Fe) using transient response methods. Kinetic studies under steady-state conditions give overall information about the reaction, whereas transient experiments lead to information on the individual steps and the possibility to suggest a reaction model. Transient response methods are applied in vacuum using a Temporal Analysis of Products (TAP) setup and at ambient pressure using a Micromeritics AutoChem 2910 analyzer. The influence of different gases such as NO, H_2O and NO_2 on the decomposition of N_2O over Fe-ZSM-5 is investigated to gain insight into their effect on this reaction.

The TAP multifunctional reactor system is used to perform transient pulse experiments for micro-kinetic analysis of complex heterogeneous catalytic reactions. This setup allows to dose precisely reactants and to monitor product formation with sub-millisecond time resolution implying the absence of external mass or heat transfer. A reproducible low hydroxylation level of the catalyst can be attained in vacuum. The results from the transient responses with the Micromeritics analyzer are obtained under conditions more relevant to "*operando*".

The mechanism of N_2O decomposition over Fe containing ZSM-5 was studied by transient response methods at ambient pressure with the Micromeritics analyzer and

under vacuum with the TAP setup. Both approaches showed that the mechanism strongly depends on the reaction temperature, but in all cases involves atomic oxygen loading from N_2O with N_2 evolution as the first reaction step. The surface oxygen, $(O)_{Fe}$, formed from N_2O possesses very high reactivity and oxidizes CO to CO_2 already at 373 K. A complete saturation of the active sites can be reached by the catalyst exposure to N_2O at low temperatures ($T < 600$ K in vacuum, $T < 523$ K at ambient pressure). Under these conditions oxygen is stored and does not desorb. On that basis, the concentration of sites active for the surface atomic oxygen loading from N_2O is determined by pulse experiments using the TAP setup. The concentration of active sites is found to be the same as in a flow experiment with the Micromeritics analyzer.

The mechanism of surface atomic oxygen recombination and desorption as O_2 depends on the temperature. At temperatures higher than 773 K, the mechanism probably involves direct $(O)_{Fe}$ recombination. The investigation of the response profiles upon N_2O pulses at 803 K evidences the O_2 formation is the rate-determining step since the oxygen desorption is found to be slow compared to N_2O and N_2. Furthermore, a fit of the oxygen desorption curve corresponded to a first order dependence on the oxygen surface coverage.

In the range of 523 to 773 K, the O_2 formation is facilitated by NO, which is formed on the catalyst surface from N_2O. The addition of NO to the gas phase confirmed the accelerating effect of NO on the oxygen desorption. NO and $(O)_{Fe}$ are adsorbed on adjacent, but different sites and are not competing for the same ones. Adsorbed NO accommodates oxygen from N_2O forming higher oxidized nitrogen oxide species NO_2/NO_3 which decompose back to NO_{ads} and molecular oxygen. Thus, the recombination of surface oxygen loaded from N_2O is accelerated by a NO/NO_x redox cycle whereas adsorbed NO_x acts as co-catalyst.

Adsorbed NO is oxidized by N_2O easily as shown also by temperature-programmed desorption (TPD) experiments. Therefore, the interaction of gaseous NO_2 with Fe-ZSM-5 at 523 K in vacuum and at ambient pressure is investigated and demonstrates the formation of two different NO_x surface species accompanied by the evolution of gaseous NO. These surface species block the sites for oxygen loading from N_2O whereas the amount of reversible adsorbed N_2O stays constant compared to the standard pre-treated catalyst. The formation of reactive surface oxygen from NO_2 could neither be evidenced in TPD nor with CO oxidation experiments.

Adsorbed water strongly influences the N_2O decomposition inhibiting it completely, at least at temperatures ≤ 673 K. Water pulses at 523 and 593 K result in partial desorption of the loaded atomic surface oxygen as O_2, indicating the competition of water for the same adsorption sites. The residual adsorbed oxygen desorbs during TPD experiments at 849 K instead of 715 K for the dry catalyst and it can not oxidize CO to CO_2. It means that the active sites are transformed into an inactive form in the

presence of water. The oxygen which stays on the catalyst seems to participate in the Fe(II) oxidation to the hydroxylated Fe(III) species. These Fe(III) species are inactive in N_2O decomposition and could be activated again by high temperature treatment in He or in vacuum.

During TAP experiments only small amounts of water are dosed and the water desorption is facilitated due to vacuum. Therefore, the effect of water could be shown to be reversible at temperatures > 700 K. At 803 K oxygen desorbs significantly faster with increasing water amount suggesting a water assisted O_2 desorption. Simultaneously, the catalyst activity decreases to about a half of the initial activity of the dry zeolite.

To conclude, from the TAP reactor data obtained under vacuum conditions and the results from the transient flow experiments at ambient pressure it follows that the mechanism of the N_2O decomposition over Fe-containing ZSM-5 depends strongly on the reaction temperature and on the presence of NO, H_2O and NO_2. In general, below 523 K only surface atomic oxygen loading from N_2O takes place with simultaneous evolution of N_2 in the gas phase. The O_2 formation proceeds via direct $(O)_{Fe}$ recombination at temperatures above 773 K. In the range of 523 to 773 K, the recombination of the atomic oxygen involves NO_x adsorbed on the catalyst surface.

Keywords: N_2O Decomposition, Fe-containing HZSM-5, TAP, Transient Method, Mechanism

Version abrégée

Le protoxyde d'azote est le troisième gaz le plus important contribuant à l'effet de serre et sa concentration dans l'atmosphère ne cesse d'augmenter. La production d'acide nitrique est la plus grande source industrielle de N_2O répandue dans l'environnement, avec un total d'émission annuel proche de 400 kt. Une alternative efficace pour réduire cette valeur est la décomposition de ce gaz en N_2 et O_2. La zéolithe ZSM-5 contenant du fer est connue pour être un bon catalyseur de cette réaction impliquant du Fe(II) hors maille cristalline comme sites actifs. Cependant la nature de ces sites ainsi que le mécanisme réactionnel est encore débattu. Souvent, le N_2O libéré dans les gaz industriels est mélangé avec d'autres gaz comme les NO_x, les CO_x, l'oxygène et la vapeur d'eau qui peuvent avoir une influence non négligeable sur l'efficacité du catalyseur. Les effets de ces gaz sur le mécanisme de décomposition du N_2O ne sont encore pas bien compris.

L'objectif de ce travail est d'étudier le mécanisme de la décomposition du N_2O sur de la zéolithe Fe-ZSM-5, substituée de manière isomorphe (0.02-0.55% Fe), par des méthodes de réponses transitoires. Les études cinétiques à l'état stationnaire donnent des informations générales sur la réaction alors que les expériences transitoires amènent des informations sur les étapes individuelles si bien qu'il devient possible de suggérer un schème réactionnel. Les méthodes de réponses transitoires sont effectuées sous vide à l'aide d'un système TAP (Temporal Analysis of Product) et à pression ambiante avec un analyseur Micromeritics Autochem 2910. L'influence des différents gaz comme le NO, le H_2O et le NO_2 dans la décomposition du N_2O sur la Fe-ZSM-5 est examinée afin de connaître leur effet sur cette réaction.

Le système réactionnel multifonctionnel TAP est utilisé pour effectuer des expériences d'injection transitoire pour une analyse de la micro-cinétique des réactions catalytiques hétérogènes complexes. Cette installation permet de doser précisément les réactants et de mesurer la formation des produits dans une résolution de l'ordre de la milliseconde sans limitation de transfert de masse externe et de transfert de chaleur externe. Un niveau faible d'hydroxylation du catalyseur peut être atteint de manière

reproductible sous vide. Les résultats obtenus par méthode transitoire avec l'analyseur Micromeritics concernent des conditions plus *"operando"*.

Le mécanisme de décomposition du N_2O sur de la ZSM-5 contenant du fer est étudié par la méthode des réponses transitoires à pression ambiante avec l'analyseur Micromeritics et sous vide avec l'installation TAP. Les deux approches ont montré que le mécanisme dépendait beaucoup de la température, mais dans tous les cas, la première étape est la déposition de l'oxygène atomique à partir du N_2O produisant alors du N_2. L'oxygène à la surface, $(O)_{Fe}$, formé à partir du N_2O possède une très haute activité et oxyde le CO en CO_2 déjà à 373 K. Une saturation complète des sites actifs peut être atteinte lors de l'exposition du catalyseur au N_2O à basses températures ($T < 600$ K sous vide, $T < 523$ K à pression atmosphérique). Sous ces conditions, l'oxygène s'accumule car il ne parvient pas à désorber. Sur cette base, il est possible de déterminer la concentration des sites actifs à la décomposition du N_2O en effectuant une série d'injections grâce à l'installation TAP. Cette concentration de sites actifs mesurée est identique à celle estimée lors des expériences avec l'analyseur Micromeritics.

Le mécanisme de recombinaison de l'oxygène atomique à la surface du catalyseur ainsi que la désorption de l'O_2 dépend de la température. Aux températures plus hautes que 773 K, le mécanisme implique probablement une association directe des $(O)_{Fe}$. L'observation des profils due à l'injection de N_2O à 803 K met en évidence que la formation de l'O_2 est l'étape limitante comme la désorption de l'oxygène est lente comparée à la disparition du N_2O et la libération du N_2. En outre, la tendance de la courbe de désorption de l'oxygène correspond à une dépendance du premier ordre en fonction de la quantité d'oxygène à la surface.

Entre 523 et 773 K, la formation d'O_2 est facilitée par le NO, qui est formé à la surface du catalyseur à partir de la décomposition du N_2O. L'addition du NO dans la phase gazeuse confirme l'effet accélérateur de ce gaz sur la désorption de l'oxygène. Le NO et l'$(O)_{Fe}$ sont adsorbés sur des sites différents mais adjacents et ne rentrent pas en compétition. Le NO adsorbé permet à l'oxygène du N_2O de former différentes espèces d'oxyde d'azote NO_2/NO_3 qui se décomposent ensuite en NO_{ads} et en oxygène moléculaire. Ainsi, l'association de l'oxygène adsorbé à la surface déposé par le N_2O est accélérée par un cycle redox NO/NO_x où le NO_x adsorbé agit comme co-catalyseur.

Le NO adsorbé est oxydé facilement par le N_2O comme le démontre les expériences TPD (Temperature-Programmed Desorption). Par conséquent, les interactions du NO_2 gazeux avec la Fe-ZSM-5 à 523 K, sous vide et à pression atmosphérique, ont été étudiées et démontrent la formation de deux espèces NO_x différentes à la surface qui accompagnent la formation du NO gazeux. Ces espèces à la surface bloquent les sites pour la déposition de l'oxygène du N_2O tandis que la quantité de N_2O adsorbé de façon réversible reste constante en comparaison avec le catalyseur prétraité de façon standard. La formation de l'oxygène actif à la surface à partir du NO_2

ne peut être mise en évidence ni par les mesures TPD ni par les expériences d'oxydation du CO.

L'adsorption de l'eau influence fortement la décomposition du N_2O jusqu'à l'inhiber complètement à des températures plus faibles que 673 K. Les résultats de l'injection d'eau à 523 et 593 K entrainent une désorption partielle de l'oxygène atomique à la surface en O_2, ce qui démontre une compétition pour les mêmes sites. L'oxygène résiduel désorbe lors des mesures TPD à une température de 849 K au lieu de 715 K dans le cas d'un catalyseur sec et ne peut pas oxyder le CO en CO_2. Cela signifie que les sites actifs sont désactivés en présence d'eau. L'oxygène restant sur le catalyseur semble participer à l'oxydation du Fe(II) à la forme hydroxylée Fe(III). Ces espèce Fe(III) sont inactives à la décomposition du N_2O mais peuvent être réactivées par un traitement à haute température sous hélium ou sous vide.

Durant les expériences avec l'installation TAP, seule une faible quantité d'eau est mesurée et sa désorption est facilitée par la faible pression interne du système. Par conséquent, les effets de l'eau peuvent être démontrés comme étant réversibles aux températures inférieures à 700 K. À 803 K l'oxygène désorbe sensiblement plus rapidement en présence d'eau ce qui peut indiquer un mécanisme de formation de l'oxygène gazeux assistée par l'eau. Simultanément, l'activité du catalyseur diminue de moitié par rapport à l'activité initiale de la zéolite sèche.

Pour conclure, les résultats obtenus sous vide par le réacteur TAP ainsi que par les flux transitoires sous pression ambiante, il s'ensuit que le mécanisme de la décomposition du N_2O sur la ZSM-5 contenant du fer dépend fortement de la température ainsi que de la présence de certains constituants dans la phase gazeuse comme le NO, le H_2O et le NO_2. En règle générale, à une température inférieure à 523 K, seule la déposition de l'oxygène prend place en même temps que la formation du N_2 lors de la décomposition du N_2O. La formation de l'O_2 s'effectue via une recombinaison directe de l'$(O)_{Fe}$ aux températures supérieures à 773 K. Entre ces deux températures (523 à 773 K), la recombinaison de l'oxygène atomique implique du NO_x adsorbé sur la surface du catalyseur.

Mots-clés: Décomposition de N_2O, HZSM-5 contenant du fer, TAP, méthode transitoire, mécanisme

Table of Contents

Symbol List & Abbreviations

A	s^{-1}	Preexponential factor
c_{N2O}	mol/m^3	Concentration of N_2O at the reactor outlet
$c_{N2O,0}$	mol/m^3	Concentration of N_2O at the reactor inlet
$C_{Fe}^{N_2O}$	sites/g	Amount of deposited oxygen from N_2O on the catalyst
C_{Fe}^{TPD}	sites/g	Amount of molecular oxygen evolved during temperature-programmed desorption
C_{Fe}^{CO}	sites/g	Amount of deposited oxygen active in low-temperature CO oxidation
d_i	m	Average interparticle distance
d_p	nm	Circular cross section
D_{eAr}	m^2/s	Effective Knudsen diffusivity
E_a	kJ/mol	Activation energy
F_{Ar}	mol/s	Flow of Ar at the reactor outlet
$\overline{F_{Ar}}$	-	Dimensionless flow of Ar at the reactor outlet
H_p	s^{-1}	Peak height of the area-normalized exit flow
I_{O2}	mol/s	Flow of O_2 at the reactor outlet
k	s^{-1}	Rate constant
k_1	s^{-1}	Rate constant
k'	s^{-1}	Parameter
L	m	Length of the reactor
m	-	Index of infinite series

m/e	-	Mass to charge ratio
M_{Ar}	kg/mol	Molecular weight of Ar
n	-	Reaction order
N_{Ar}	mol	Number of moles of Ar in the inlet pulse
R	J/mol/K	Ideal gas constant
t	s	Time
T	K	Temperature
X	-	Conversion

Greek Letters

ε_b	-	Fractional voidage of the packed bed in the reactor
θ_O	mol	Coverage of active sites with oxygen
τ	-	Dimensionless time
τ_b	-	Tortuosity
τ_p	-	Dimensionless time at which the exit flow is at maximum
τ_{res}	s	Mean residence time

Subscripts

ads	Adsorption
p	Peak

Abbreviations

AMU	Atomic Mass Unit
CFCs	Chlorofluorocarbons
CVD	Chemical Vapor Deposition
DFT	Density Functional Theory
DRIFTS	Diffuse Reflectance Infrared Fourier Transform Spectroscopy

EXAFS	Extended X-ray Absorption Fine Structure
FBC	Fluidized-Bed Combustor
FTIR	Fourier Transform Infrared Spectroscopy
GWP	Global Warming Potential
IPCC	Intergovernmental Panel on Climate Change
IR	Infrared
MCT	Mercury Cadmium Telluride
MFI	Crystalline structure of ZSM-5 zeolite (Mobil Five)
MMO	Methane Monooxygenase
MS	Mass Spectrometer
NSCR	Non Selective Catalytic Reduction
SBU	Secondary Building Unit
SCR	Selective Catalytic Reduction
SDC	Standard Diffusion Curve
STP	Standard Temperature Pressure
TAP	Temporal Analysis of Products
TPD	Temperature-Programmed Desorption
TPR	Temperature-Programmed Reaction
TZTR	Thin-Zone TAP Reactor
UNFCCC	United Nations Framework Convention on Climate Change
UV	Ultraviolet
WIE	Wet Ion Exchange

Chapter 1

INTRODUCTION

N_2O is a very potent greenhouse gas due to its longevity in the earth's atmosphere and its special adsorption properties for infrared radiation [1-4]. Any concentration perturbation that occurs will last for centuries. One metric ton of nitrous oxide has the same effect in the atmosphere as 310 metric tons of CO_2. Nitrous oxide is thus part of efforts to reduce greenhouse gas emissions, such as the Kyoto Protocol [5]. Nitrous oxide is the third most important gas that contributes to global warming behind carbon dioxide and methane. Nitrous oxide also destroys ozone in the stratosphere, aggravating the excess amount of UV light striking the earth's surface in recent decades [6-8].

The recently published Fourth Assessment Report of the Intergovernmental Panel of Climate Change stated that the warming of the climate system is unequivocal [9]. The global atmospheric N_2O concentration increased from a pre-industrial value of about 270 ppb to 319 ppb in 2005 and its concentration is still on the rise. More than a third of all nitrous oxide emissions are anthropogenic and are primarily due to agriculture, but control of these emissions is difficult due to the very diffuse nature of N_2O emissions. However, N_2O emissions that can be reduced in the short term are associated with chemical production and energy industry [10-12]. 35% of the N_2O emission in the European Union is concentrated in a limited number of large N_2O sources, which holds promise for an economic and efficient reduction strategy to fulfill

the Kyoto commitment. Nitric acid production represents the largest source of N_2O in the chemical industry, with a global annual emission of 400 kt N_2O [13].

An efficient way to reduce the N_2O emission is its catalytic decomposition into N_2 and O_2. ZSM-5 zeolites containing iron are known as promising catalysts. The reaction involves iron complexes stabilized in the ZSM-5 matrix and proceeds via surface atomic oxygen and gaseous nitrogen formation from N_2O. This reaction takes place at temperatures lower than 600 K. Oxygen recombines only at higher temperatures indicating the in general accepted rate-limiting step in N_2O decomposition the desorption of oxygen from the catalyst surface [14-16]. The catalyst activity is known to be sensitive to the presence of other gases like H_2O, NO, hydrocarbons, CO, etc. The addition of gaseous NO enhances the activity of Fe containing zeolites [14, 16-18] while their activity is diminished in the presence of water vapors [14]. Slow NO formation on the catalyst surface from N_2O interaction is observed over Fe- and Cu-zeolites [19-23]. NO/NO_2 [16, 18, 24] as well as nitrite/nitrate [25] redox cycles are proposed for active sites regeneration in N_2O decomposition apart from direct recombination from atomic surface oxygen related to a Fe(II)/Fe(III) redox cycle.

The Fe-ZSM-5 catalyst shows no inhibition by oxygen, since it does not react with the active iron sites [26]. Only N_2O can oxidize the Fe(II) sites to Fe(III) upon formation of so-called "α-oxygen" [27, 28]. The atomic surface oxygen deposited from N_2O on Fe-ZSM-5 exhibits a very high, unusual reactivity. The active oxygen rapidly exchanges with $^{18}O_2$ at 523 K, whereas Fe-ZSM-5 that is not treated with N_2O is completely inactive for the isotope exchange at that temperature [26, 29]. It oxidises CO and H_2 even at low temperature (~373 K) [26, 30]. Furthermore, it is shown to insert into C-H bonds analog to the enzyme methane monooxygenase (MMO) [27, 29, 31, 32], converting methane to methoxy species at room temperature [29, 33-36] and oxidising benzene to phenol [37, 38]. α-oxygen possesses a high potential as selective oxidant.

The aim of this work is to study the mechanism of the decomposition of N_2O over isomorphously substituted Fe-ZSM-5 (0.02-0.55% Fe) using transient response methods. Transient experiments have the potential to provide considerably more information than steady-state experiments. Whereas steady-state experiments give an integrated picture of a reaction system, transient experiments give information on individual steps. The elucidation of the detailed mechanism of heterogeneous catalysis serves to establish the underlying elementary steps for reaction models which are very valuable in the catalyst development process.

The Temporal Analysis of Products (TAP) multifunctional reactor system is an apparatus that is used to perform transient pulse experiments for micro-kinetic analysis of complex heterogeneous catalytic reactions. The TAP reactor system was developed in 1988 by John T. Gleaves and co-workers for the advancement of industrial heterogeneous catalysts [39, 40]. It has been extensively applied in experimental studies

on catalytic reaction mechanisms and other surface processes [41-46]. The setup is very suitable to dose precisely reactants, to study product sequences with sub-millisecond time resolution and to dehydroxylate the catalyst in vacuum implying the absence of external mass or heat transfer. Hydroxylation is well known to influence the ZSM-5 activity for N_2O decomposition in a negative way [47-49], falsifying mechanistic observations which can be minimized in TAP studies with vacuum conditions and small amounts of reactants. The influence of different test molecules such as NO, H_2O and NO_2 on the decomposition of N_2O over Fe-ZSM-5 is investigated to gain supplementary mechanistic aspects.

The transient response method is also applied at atmospheric pressure using a Micromeritics AutoChem 2910 analyzer in order to obtain quantitative results and information on the reaction mechanism under more relevant industrial conditions. Mainly temperature and concentration perturbations are imposed on the catalytic system and useful information on the mechanism is gained from the resultant response.

References

1. *Intergovernmental Panel on Climate Change (IPCC)* 1995.
2. Badr, O.; Probert, S. D., Environmental Impacts of Atmospheric Nitrous-Oxide. *Applied Energy* **1993,** 44, (3), 197-231.
3. Donner, L.; Ramanathan, V., Methane and Nitrous-Oxide - Their Effects on the Terrestrial Climate. *Journal of the Atmospheric Sciences* **1980,** 37, (1), 119-124.
4. Ramanathan, V.; Cicerone, R. J.; Singh, H. B.; Kiehl, J. T., Trace Gas Trends and Their Potential Role in Climate Change. *Journal of Geophysical Research-Atmospheres* **1985,** 90, (ND3), 5547-5566.
5. Kyoto Protocol to the United Nations Framework Convention on Climate Change.
6. *Intergovernmental Panel on Climate Change (IPCC)* 1992.
7. Crutzen, P. J., Ozone Production Rates in an Oxygen-Hydrogen-Nitrogen Oxide Atmosphere. *Journal of Geophysical Research* **1971,** 76, (30), 7311.
8. Wennberg, P. O.; Cohen, R. C.; Stimpfle, R. M.; Koplow, J. P.; Anderson, J. G.; Salawitch, R. J.; Fahey, D. W.; Woodbridge, E. L.; Keim, E. R.; Gao, R. S.; Webster, C. R.; May, R. D.; Toohey, D. W.; Avallone, L. M.; Proffitt, M. H.; Loewenstein, M.; Podolske, J. R.; Chan, K. R.; Wofsy, S. C., Removal of Stratospheric O_3 by Radicals - in-Situ Measurements of OH, HO_2, NO, NO_2, ClO, and BrO. *Science* **1994,** 266, (5184), 398-404.
9. *Intergovernmental Panel on Climate Change (IPCC)* 2007.
10. Centi, G.; Perathoner, S.; Vazzana, F., Catalytic control of non-CO_2 greenhouse gases - Methane, flourocarbons, and especially nitrous oxide can be decomposed and even reused by implementing new catalytic techniques. *Chemtech* **1999,** 29, (12), 48-55.
11. Centi, G.; Perathoner, S.; Vazzana, F.; Marella, M.; Tomaselli, M.; Mantegazza, M., Novel catalysts and catalytic technologies for N_2O removal from industrial

emissions containing O_2, H_2O and SO_2. *Advances in Environmental Research* **2000,** 4, (4), 325-338.
12. Kapteijn, F.; RodriguezMirasol, J.; Moulijn, J. A., Heterogeneous catalytic decomposition of nitrous oxide. *Applied Catalysis B-Environmental* **1996,** 9, (1-4), 25-64.
13. Perez-Ramirez, J.; Kapteijn, F.; Schoffel, K.; Moulijn, J. A., Formation and control of N_2O in nitric acid production - Where do we stand today? *Applied Catalysis B-Environmental* **2003,** 44, (2), 117-151.
14. Bulushev, D. A.; Kiwi-Minsker, L.; Renken, A., Dynamics of N_2O decomposition over HZSM-5 with low Fe content. *Journal of Catalysis* **2004,** 222, (2), 389-396.
15. Kiwi-Minsker, L.; Bulushev, D. A.; Renken, A., Low temperature decomposition of nitrous oxide over Fe/ZSM-5: Modelling of the dynamic behaviour. *Catalysis Today* **2005,** 110, (3-4), 191-198.
16. Perez-Ramirez, J.; Kapteijn, F.; Mul, G.; Moulijn, J. A., NO-assisted N_2O decomposition over Fe-based catalysts: Effects of gas-phase composition and catalyst constitution. *Journal of Catalysis* **2002,** 208, (1), 211-223.
17. Mul, G.; Perez-Ramirez, J.; Kapteijn, F.; Moulijn, J. A., NO-assisted N_2O decomposition over ex-framework FeZSM-5: mechanistic aspects. *Catalysis Letters* **2001,** 77, (1-3), 7-13.
18. Sang, C. M.; Kim, B. H.; Lund, C. R. F., Effect of NO upon N_2O decomposition over Fe/ZSM-5 with low iron loading. *Journal of Physical Chemistry B* **2005,** 109, (6), 2295-2301.
19. Bulushev, D. A.; Renken, A.; Kiwi-Minsker, L., Formation of the surface NO during N_2O interaction at low temperature with iron-containing ZSM-5. *Journal of Physical Chemistry B* **2006,** 110, (1), 305-312.
20. El-Malki, E. M.; van Santen, R. A.; Sachtler, W. M. H., Active sites in Fe/MFI catalysts for NO_x reduction and oscillating N_2O decomposition. *Journal of Catalysis* **2000,** 196, (2), 212-223.
21. Grubert, G.; Hudson, M. J.; Joyner, R. W.; Stockenhuber, M., The room temperature, stoichiometric conversion of N_2O to adsorbed NO by Fe-MCM-41 and Fe-ZSM-5. *Journal of Catalysis* **2000,** 196, (1), 126-133.
22. Shimokawabe, M.; Tadokoro, K.; Sasaki, S.; Takezawa, N., Temperature programmed desorption and infrared spectroscopic studies of nitrogen monoxide adsorbed on ion-exchanged copper mordenite catalysts. *Applied Catalysis A-General* **1998,** 166, (1), 215-223.
23. Turek, T., Kinetics of nitrous oxide decomposition over Cu-ZSM-5. *Applied Catalysis B-Environmental* **1996,** 9, (1-4), 201-210.
24. Bulushev, D. A.; Renken, A.; Kiwi-Minsker, L., Role of adsorbed NO in N_2O decomposition over iron-containing ZSM-5 catalysts at low temperatures. *Journal of Physical Chemistry B* **2006,** 110, (22), 10691-10700.
25. Sang, C. M.; Lund, C. R. F., Possible role of nitrite/nitrate redox cycles in N_2O decomposition and light-off over Fe-ZSM-5. *Catalysis Letters* **2001,** 73, (1), 73-77.
26. Panov, G. I.; Sobolev, V. I.; Kharitonov, A. S., The Role of Iron in N_2O Decomposition on ZSM-5 Zeolite and Reactivity of the Surface Oxygen Formed. *Journal of Molecular Catalysis* **1990,** 61, (1), 85-97.
27. Dubkov, K. A.; Ovanesyan, N. S.; Shteinman, A. A.; Starokon, E. V.; Panov, G. I., Evolution of iron states and formation of alpha-sites upon activation of FeZSM-5 zeolites. *Journal of Catalysis* **2002,** 207, (2), 341-352.
28. Pirngruber, G. D.; Grunwaldt, J. D.; Roy, P. K.; Van Bokhoven, J. A.; Safonova, O. V.; Glatzel, P., The nature of the active site in the Fe-ZSM-5/N_2O system

studied by (resonant) inelastic X-ray scattering. *Catalysis Today* **2006,** 126, (1-2), 127-134.
29. Dubkov, K. A.; Sobolev, V. I.; Panov, G. I., Low-temperature oxidation of methane to methanol on FeZSM-5 zeolite. *Kinetics and Catalysis* **1998,** 39, (1), 72-79.
30. Dubkov, K. A.; Paukshtis, E. A.; Panov, G. I., Stoichiometry of oxidation reactions involving alpha-oxygen on FeZSM-5 zeolite. *Kinetics and Catalysis* **2001,** 42, (2), 205-211.
31. Dubkov, K. A.; Sobolev, V. I.; Talsi, E. P.; Rodkin, M. A.; Watkins, N. H.; Shteinman, A. A.; Panov, G. I., Kinetic isotope effects and mechanism of biomimetic oxidation of methane and benzene on FeZSM-5 zeolite. *Journal of Molecular Catalysis A-Chemical* **1997,** 123, (2-3), 155-161.
32. Panov, G. I.; Sobolev, V. I.; Dubkov, K. A.; Parmon, V. N.; Ovanesyan, N. S.; Shilov, A. E.; Shteinman, A. A., Iron complexes in zeolites as a new model of methane monooxygenase. *Reaction Kinetics and Catalysis Letters* **1997,** 61, (2), 251-258.
33. Knops-Gerrits, P. P.; Goddard, W. A., Methane partial oxidation in iron zeolites: theory versus experiment. *Journal of Molecular Catalysis A-Chemical* **2001,** 166, (1), 135-145.
34. Panov, G. I.; Uriarte, A. K.; Rodkin, M. A.; Sobolev, V. I., Generation of active oxygen species on solid surfaces. Opportunity for novel oxidation technologies over zeolites. *Catalysis Today* **1998,** 41, (4), 365-385.
35. Wood, B. R.; Reimer, J. A.; Bell, A. T.; Janicke, M. T.; Ott, K. C., Methanol formation on Fe/Al-MFI via the oxidation of methane by nitrous oxide. *Journal of Catalysis* **2004,** 225, (2), 300-306.
36. Yoshizawa, K.; Shiota, Y.; Yumura, T.; Yamabe, T., Direct methane-methanol and benzene-phenol conversions on Fe-ZSM-5 zeolite: Theoretical predictions on the reaction pathways and energetics. *Journal of Physical Chemistry B* **2000,** 104, (4), 734-740.
37. Panov, G. I., Advances in Oxidation Catalysis. Oxidation of Benzene to Phenol by Nitrous Oxide. *CATTECH* **2000,** 4, (1), 18-32.
38. Panov, G. I.; Dubkov, K. A.; Starokon, E. V., Active oxygen in selective oxidation catalysis. *Catalysis Today* **2006,** 117, (1-3), 148-155.
39. Gleaves, J. T.; Ebner, J. R.; Kuechler, T. C., Temporal Analysis Of Products (Tap) - A Unique Catalyst Evaluation System With Submillisecond Time Resolution. *Catalysis Reviews-Science and Engineering* **1988,** 30, (1), 49-116.
40. Gleaves, J. T.; Yablonskii, G. S.; Phanawadee, P.; Schuurman, Y., TAP-2: An interrogative kinetics approach. *Applied Catalysis A-General* **1997,** 160, (1), 55-88.
41. Fushimi, R.; Shekhtman, S. O.; Gaffney, A.; Han, S.; Yablonsky, G. S.; Gleaves, J. T., TAP vacuum pulse-response and normal-pressure studies of propane oxidation over MoVTeNb oxide catalysts. *Industrial & Engineering Chemistry Research* **2005,** 44, (16), 6310-6319.
42. Kondratenko, E. V.; Perez-Ramirez, J., Mechanism and kinetics of direct N_2O decomposition over Fe-MFI zeolites with different iron speciation from temporal analysis of products. *Journal of Physical Chemistry B* **2006,** 110, (45), 22586-22595.
43. Olafsen, A.; Slagern, A.; Dahl, I. M.; Olsbye, U.; Schuurman, Y.; Mirodatos, C., Mechanistic features for propane reforming by carbon dioxide over a Ni/Mg(Al)O hydrotalcite-derived catalyst. *Journal of Catalysis* **2005,** 229, (1), 163-175.
44. Baerns, M.; Imbihl, R.; Kondratenko, V. A.; Kraehnert, R.; Offermans, W. K.; van Santen, R. A.; Scheibe, A., Bridging the pressure and material gap in the

catalytic ammonia oxidation: structural and catalytic properties of different platinum catalysts. *Journal of Catalysis* **2005,** 232, (1), 226-238.

45. Goguet, A.; Shekhtman, S. O.; Burch, R.; Hardacre, C.; Meunier, F. C.; Yablonsky, G. S., Pulse-response TAP studies of the reverse water-gas shift reaction over a Pt/CeO_2 catalyst. *Journal of Catalysis* **2006,** 237, (1), 102.
46. van Veen, A. C.; Hinrichsen, O.; Muhler, M., Mechanistic studies on the oxidative dehydrogenation of methanol over polycrystalline silver using the temporal-analysis-of-products approach. *Journal of Catalysis* **2002,** 210, (1), 53-66.
47. El-Malki, E. M.; van Santen, R. A.; Sachtler, W. M. H., Isothermal oscillations during N_2O decomposition over Fe/ZSM-5: effect of H_2O vapor. *Microporous and Mesoporous Materials* **2000,** 35-6, 235-244.
48. Roy, P. K.; Pirngruber, G. D., The surface chemistry of N_2O decomposition on iron-containing zeolites(II) - The effect of high-temperature pretreatments. *Journal of Catalysis* **2004,** 227, (1), 164-174.
49. Yuranov, I.; Renken, A.; Kiwi-Minsker, L., Zeolite/sintered metal fibers composites as effective structured catalysts. *Applied Catalysis A-General* **2005,** 281, (1-2), 55-60.

Chapter 2

STATE OF THE ART

2.1. Characteristics of N_2O

Nitrous oxide (dinitrogen oxide, N_2O) is a colorless, non-flammable gas with a pleasant, slightly sweet odor under ambient conditions. It was discovered in 1772 by Joseph Priestly, who called it "diminished nitrous air", from the reduction of NO with iron or iron/sulphur mixtures [1]. Sir Humphrey Davy inhaled N_2O during his medical training in 1799, as part of a study on the physiological effects of several newly discovered gases, and he discovered the ability of N_2O to promote lightheadedness. It is used in surgery and dentistry for its anesthetic effects, where it is commonly known as laughing gas due to the euphoric effects of inhaling it.

N_2O is a linear molecule that is isoelectronic to CO_2. The electronic structure and geometrical structure can be understood in the context of the valence bond resonance forms shown in Figure 2.1. Bond distances determined from rotational spectroscopy measurements are given as well [2].

N_2O is a very potent greenhouse gas due to its longevity in the earth's atmosphere and its special adsorption properties for infrared radiation [3-6]. The half-life of atmospheric N_2O is estimated between 110 and 168 years [7, 8]. Thus, any concentration perturbation that occurs will last for centuries. One metric ton of nitrous oxide has the same effect in the atmosphere as 310 metric tons of CO_2. Nitrous oxide is

thus part of efforts to curb greenhouse gas emissions, such as the Kyoto Protocol. Nitrous oxide is the third most important gas that contributes to global warming behind carbon dioxide and methane, which has 23 times the greenhouse warming potential of carbon dioxide (over 100 years). Nitrous oxide also destroys ozone in the stratosphere, aggravating the excess amount of UV light striking the earth's surface in recent decades [9-11].

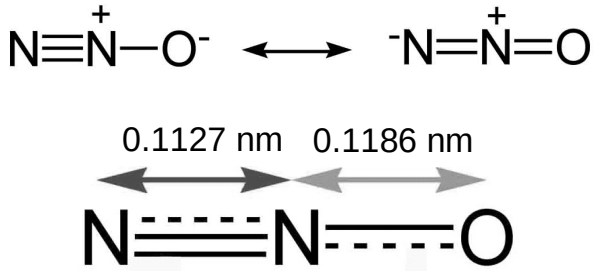

Figure 2.1: Resonance forms of nitrous oxide and bond distances.

Nitrous oxide is naturally emitted by bacteria in soils and oceans. Agriculture is the main source of human-produced nitrous oxide: cultivating soil, the use of nitrogen fertilizers, and animal waste handling can all stimulate naturally occurring bacteria to produce more nitrous oxide. The livestock sector (primarily cows, chickens, and pigs) produces 65% of human-related nitrous oxide [12]. Industrial sources make up only about 20% of all anthropogenic sources, and include the production of nylon and nitric acid and the burning of fossil fuel in internal combustion engines.

N_2O was until recently allowed to be emitted into the atmosphere without restrictions. However, after N_2O was recognized as a relevant greenhouse gas and designated as such in the Kyoto Protocol [13] limitations for N_2O emissions have been set from the legislation of signatory nations. Agriculture is a major anthropogenic source, but control of these emissions is difficult due to the very diffuse nature of N_2O emissions. N_2O emissions can be reduced in the short term with chemical production and the energy industry. The major industrial source of N_2O is the production of nitric acid (400 kt N_2O per year), which is a key bulk chemical in the fertilizer industry [14]. The greenhouse gas effect as well as possibilities to limit the N_2O emission of chemical production plants and combustion processes is discussed in the following sections.

Nitrous oxide is applied in medical and dental use, as food additive e. g. in whipped cream and for filling packages of potato chips as well as oxidiser in rocket engines. There are a number of selective oxidation reactions with N_2O over iron containing MFI type zeolites. An overview is given on studies which target to involve N_2O into organic synthesis as an oxidant in section 2.1.3.

2.1.1. The Greenhouse Effect

The natural greenhouse effect raises the temperature of the planet by 33 K, thus making it habitable. On average, 343 W/m^2 of sunlight fall on the earth, roughly 1/3 of which is reflected back into space. The other 2/3 reaches the ground, which re-radiates it as longer wavelength, infrared radiation. Some of this is blocked by greenhouse gases, thereby warming the atmosphere. Naturally occurring greenhouse gases include water vapor, carbon dioxide (CO_2), methane (CH_4) and nitrous oxide (N_2O) [15].

Human activity is emitting extra amounts of greenhouse gases, especially CO_2, N_2O, CH_4 and Chlorofluorocarbons (CFCs) which alter the amounts of radiation trapped by the atmosphere and so have an effect on climate. In order to be able to compare the effect of different gases in enhancing the greenhouse effect, a method has been developed of estimating their global warming potentials (GWP). The GWP index is the cumulative enhancement occurring between now and a chosen later time caused by a unit mass of the gas emitted now. It is a relative scale which compares the gas in question to that of the same mass of CO_2, whose GWP is by definition 1. Some examples of Global Warming Potentials referenced to CO_2 are presented in Table 2.1. The GWP is based on a number of factors, including the radiative efficiency (heat-absorbing ability) of each gas relative to that of carbon dioxide, as well as the decay rate of each gas (the amount removed from the atmosphere over a given number of years) relative to that of carbon dioxide. GWPs have inherent uncertainties, because of the range of assumptions done for their calculation [5].

Table 2.1: Global Warming Potentials, referenced to CO_2 [5].

Gas	*GWP for various time horizons*		
	20 years	100 years	500 years
CO_2	1	1	1
CH_4	56	21	6.5
N_2O	280	310	170
HFC-23	9100	11700	9800
HFC-32	2100	650	200
SF_6	16300	23900	34900

The recently published contribution of Working Group I of the fourth assessment report of the Intergovernmental Panel on Climate Change (IPCC) clearly stated that warming of the climate system is unequivocal, as is now evident from observations of increases in global average air and ocean temperatures, widespread melting of snow and ice, and rising global average sea level illustrated in Figure 2.2 [16]. Eleven of the last twelve years (1995-2006) rank among the 12 warmest years in the instrumental record of global surface temperature (since 1850). Global average sea level

rose at an average rate of 1.8 mm per year over 1961 to 2003. The rate was faster over 1993 to 2003, about 3.1 mm per year. Mountain glaciers and snow cover have declined on average in both hemispheres.

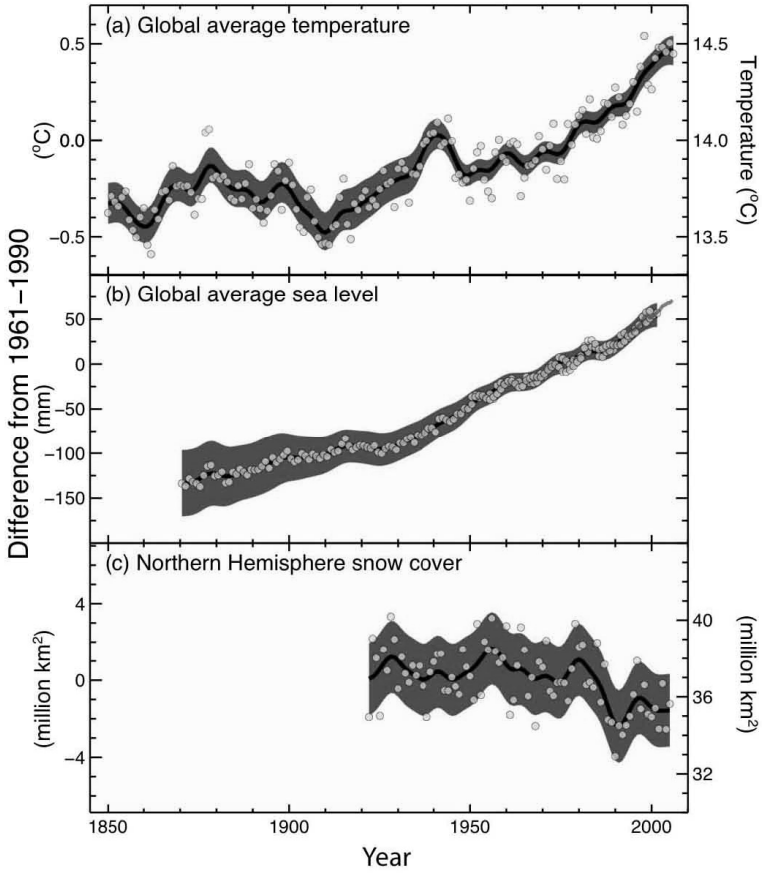

Figure 2.2: Observed changes in global average surface temperature (a), global average sea level rise (b) and Northern Hemisphere snow cover for March-April (c). All changes are relative to corresponding averages for the period 1961-1990. Smoothed curves represent decadal averaged values while circles show yearly values. The shaded areas are the uncertainty intervals estimated from a comprehensive analysis of known uncertainties (a and b) and from the time series (c) [16].

Most of the observed increase in globally averaged temperatures since the mid-20th century is very likely due to the observed increase in anthropogenic greenhouse gas concentrations. Global atmospheric concentrations of CO_2, CH_4 and N_2O have increased markedly as a result of human activities since 1750 and now far exceed pre-industrial

values determined from ice cores spanning many thousands of years. The global increases in CO_2 concentration are due primarily to fossil fuel use and land-use change, while those of CH_4 and N_2O are primarily due to agriculture. CO_2 is the most important anthropogenic greenhouse gas. The global atmospheric concentration of carbon dioxide has increased from a pre-industrial value of about 280 ppm to 379 ppm in 2005. CH_4 concentration increased from 715 ppb to 1774 ppb and N_2O from 270 ppb to 319 ppb. The atmospheric concentration incline of N_2O over the last 10000 years is illustrated in Figure 2.3. The growth rate of N_2O has been approximately constant since 1980. More than a third of all nitrous oxide emissions are anthropogenic and are primarily due to agriculture [16].

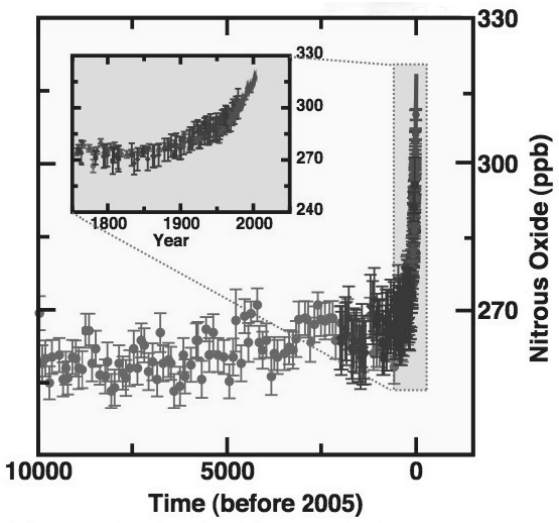

Figure 2.3: Atmospheric concentration of N_2O over the last 10000 years and since 1750 (inset). Measurements are shown from ice cores and atmospheric samples [16].

For the next two decades a warming of about 0.2 K per decade is projected for a range of emission scenarios. Even if the concentrations of all greenhouse gases and aerosols had been kept constant at year 2000 levels, a further warming of about 0.1 K per decade would be expected. Continued greenhouse gas emissions at or above current rates would cause further warming and induce many changes in the global climate system during the 21st century that would very likely be larger than those observed during the 20th century. Anthropogenic warming and sea level rise would continue for centuries due to the timescales associated with climate processes and feedbacks, even if greenhouse gas concentrations were to be stabilized [16].

However, if the rate of climate change can be limited to a low level, then natural and human systems will find it easier to adapt. Therefore, an important way to slow the rate of change is to reduce emissions of greenhouse gases. The second assessment report of the Intergovernmental Panel on Climate Change (IPCC 1996) formed the basis of negotiations over Kyoto Protocol. The Kyoto Protocol to the United Nations Framework Convention on Climate Change is an amendment to the international treaty on climate change, assigning mandatory targets for the reduction of greenhouse gas emissions to signatory nations. The Kyoto Protocol is an agreement made under the United Nations Framework Convention on Climate Change (UNFCCC) [13]. Countries that ratify this protocol commit to reduce their emissions of carbon dioxide and five other greenhouse gases (CH_4, N_2O, HFCs, PFCs and SF_6), or engage in emissions trading if they maintain or increase emissions of these gases. The objective is the stabilization of greenhouse gas concentrations in the atmosphere at a level that would prevent dangerous anthropogenic interference with the climate system [17]. The Kyoto Protocol is an agreement under which industrialized countries will reduce their collective emissions of greenhouse gases by 5.2% compared to the year 1990 - calculated as an average over the five-year period of 2008-12. It should be mentioned that, compared to the emissions levels that would be expected by 2010 without the Protocol, this target represents a 29% cut. National limitations range from 8% reductions for the European Union and some others to 7% for the US, 6% for Japan, 0% for Russia, and permitted increases of 8% for Australia and 10% for Iceland. Possibilities for reduction of N_2O emission of chemical production and the energy industry are presented in the following section.

2.1.2. Reduction of N_2O Emission from Industrial Sources

The major industrial source of N_2O is the production of nitric acid and contributes with a global annual emission of 400 kt to the global warming [14]. Therefore, the elimination of nitrous oxide from nitric acid plants can make an important contribution to the protection of the Earth's climate. N_2O is also produced during the manufacture of adipic acid, caprolactam, acrylonitrile, glyoxal, and in general organic syntheses using HNO_3 as the oxidant or reactions involving ammonia oxidation.

The reduction of N_2O emissions from nitric acid plants would effectively contribute or even fulfil the Kyoto commitments of several European countries, which presents an extra motivation for the development of technology. Therefore, promising options to control N_2O emissions in nitric acid plants are pointed out in this section. The production of weak nitric acid is based on the Oswald process and consists of the following basic chemical operations [18]:

- Catalytic oxidation of ammonia with air to nitric oxide:

$$4NH_3 + 5O_2 \rightarrow 4NO + 6H_2O \tag{2.1}$$

In a catalytic converter NH_3 is mainly converted to NO (selectivity about 97%) and water using a platinum-rhodium gauze with a composition of 90% Pt and 10%Rh. N_2O (typically 1.5-2%) and N_2 are formed as unwanted side-products:

$$\begin{aligned} 4NH_3 + 4O_2 &\rightarrow 2N_2O + 6H_2O \\ 4NH_3 + 3O_2 &\rightarrow 2N_2 + 6H_2O \end{aligned} \tag{2.2}$$

- Oxidation of nitric oxide to nitrogen dioxide:

$$2NO + O_2 \rightleftarrows 2NO_2 \rightleftarrows N_2O_4 \tag{2.3}$$

The nitrous gases are cooled to promote further oxidation to NO_2. NO reacts non-catalytically with residual O_2 to form NO_2 and its liquid dimer, N_2O_4. Operating at low temperatures and high pressures promotes maximum production of NO_2 within a minimum reaction time.

- Absorption of nitrogen dioxide in water to produce nitric acid:

$$3NO_2 + H_2O \rightarrow 2HNO_3 + NO \tag{2.4}$$

The cooled NO_2/N_2O_4 mixture is introduced into an absorption process to produce weak nitric acid. The tail-gas leaving the absorber column at a temperature of 293-303 K contains N_2O and traces of NO_x. Typical values of the tail-gas composition at the outlet of the NO_2 absorber are shown in Table 2.2.

Table 2.2: Composition of tail gas at the outlet of the NO_2 absorber (N_2 balance gas) for a nitric acid plant of 1500 ton HNO_3 per day and tail gas flow of $2 \cdot 10^5$ Nm^3/h [19].

Gas	*Concentration*	
NO_x	100-3500 ppm	(200 ppm)
N_2O	300-3500 ppm	(1500 ppm)
O_2	1-4 vol%	(2.5 vol%)
H_2O	0.3-2 vol%	(0.5 vol%)

The tail gas is heated and used in a tail gas expander for energy recovery. For additional NO_x abatement a selective catalytic reduction (SCR) facility is in many cases incorporated up- or down stream the tail gas expander. The current technology for NO_x

removal is selective catalytic reduction (SCR) using ammonia as a reductant and in many cases vanadium-pentoxide-type catalysts. Unfortunately, the conventional NH_3-DeNO_x catalysts do not reduce N_2O emissions [20]. The flowsheet of weak nitric acid production according to the dual-pressure configuration is presented in Figure 2.4. Techniques for N_2O abatement can be applied in the following locations in the nitric acid production process [21]:

- Preventing N_2O being formed in the ammonia burner (1)
- Removing N_2O from the NO_x gases between the ammonia converter and the absorption column (2)
- Process integrated upstream the tail gas expander (3)
- End-of-pipe downstream the tail gas expander (4)

The above listed locations of the different abatement technologies are marked in Figure 2.4 and will be discussed as follows.

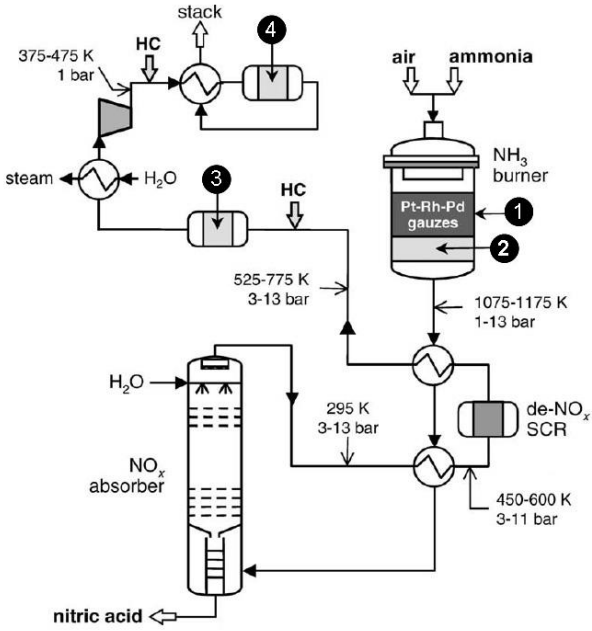

Figure 2.4: Flowsheet of a dual-pressure nitric acid plant with the possible locations for N_2O abatement technologies [22].

The emission of N_2O depends exclusively on the ammonia combustions process. Once formed, N_2O passes unreacted through the plant and is not affected by the NO_2 absorber or the after-treatment for NO_x removal of the tail gas. Production of N_2O can be minimized by optimizing the catalytic oxidation of NH_3 to NO. However, the catalytic

conversion process is already one of the most efficient processes known. An optimized NO yield is expected to be limited by changing any parameter.

The second abatement measure aims on the thermal or catalytic decomposition of N_2O in the high-temperature zone immediately downstream of the ammonia burner. N_2O is not stable at elevated temperature and pressure and will decompose if given time. Norsk Hydro, therefore, investigated the possibility to extend the reaction chamber of the oxidation reactor, thus, improving autonomous decomposition of N_2O [23]. Instead of increasing the reactor chamber, the decomposition of nitrous oxide can be promoted using a catalyst for selective decomposition. Possible drawbacks are that catalyst life may be short due to harsh conditions (temperature of 1075-1175 K and total pressure up to 13 bar) and that the selectivity to NO decreases, since NO decomposition may be also catalyzed. BASF reported 80 and 70% reduction of N_2O using Cu-based mixed oxide spinel during tests in dual-pressure and atmospheric pressure plants, respectively [24, 25]. Other companies are also investigating this option [26-28].

The third abatement possibility is the implementation of process integrated N_2O reduction measures upstream the tail gas expander, but behind the nitrogen oxides absorption section, which offers the advantage of not influencing the nitric acid production process. The pressure (3-13 bar) and especially the temperature (500-773 K) of the tail gas are essential parameters to determine the optimal process option. Thermal decomposition of N_2O in the tail gas is economically unfeasible since its temperature needs to be raised up to 1023-1273 K by external heat supply for the decomposition of only 1500 ppm N_2O.

At nitric acid plants with high-temperature tail-gases (700-773 K) direct catalytic decomposition of N_2O over a catalyst without addition of reducing agents is an attractive and economical option to reduce N_2O emissions. The use of Fe-ZSM-5 seems viable [14]. This catalyst shows no inhibition by oxygen and an improved activity in the presence of NO_x. However, water severely inhibits the reaction.

Uhde developed a process for the combined reduction of N_2O and NO_x emissions from nitric acid plants, called EnviNOx®. As seen in Figure 2.5 the central component is a so-called combi-reactor located between the tail gas heater and the tail gas turbine. It contains two catalyst beds operated at the same pressure and temperature, and a device for the intermediate addition of NH_3. In the first stage- the so-called DeN_2O® stage- N_2O decomposition takes place over an iron zeolite under full NO_x load. In the second stage, NO_x reduction is effected using NH_3 as a reduction agent, while N_2O abatement continues simultaneously. The concept requires a tail gas temperature of more than 673 K and was for the first time successfully implemented in a dual-pressure HNO_3 plant in Linz, Austria [29].

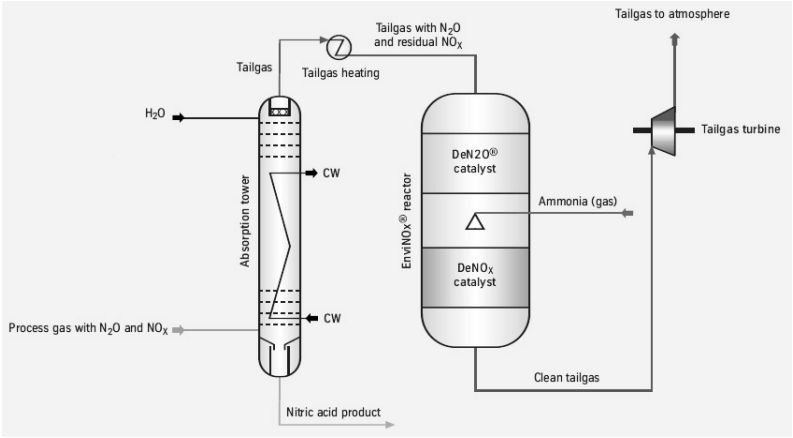

Figure 2.5: Integration of the EnviNOx® reactor into the HNO_3 process [29].

Furthermore, non selective catalytic reduction (NSCR) has been developed for NO_x removal and has shown to be capable of reducing N_2O as well. A reducing agent like hydrogen, natural gas or naphtha is added and oxidised, aided by a Pd catalyst. First, all free oxygen in the tail gas is consumed and thereafter oxygen holding components like NO_x and N_2O to levels below 50 ppm, having an efficiency > 98%. The NSCR technology is already applied in the nitric acid industry, commercialized by GIAP especially in Russia and the USA. Disadvantageous is the high fuel consumption levels and high secondary emissions, slip of fuel occurs and when using CH_4 as a reductant, large amounts of CO are produced [21].

The selective catalytic reduction (SCR) of N_2O with hydrocarbons as reducing agent has been investigated over Fe zeolites [20, 21, 29-32]. The use of hydrocarbons (e.g. propane, propene, natural gas) leads to an increase of the operation costs, due to the high cost associated with the reductant. Reduction of N_2O with ammonia is also possible, but it generally requires higher temperatures than N_2O reduction with hydrocarbons [33, 34]. Suppliers of N_2O removal by SCR technology are ECN and Grande Paroisse [35, 36].

For low-temperature tail gases (500-523 K) a catalyst is required with high activity at low temperatures and stability in the presence of other gases in the feed such as NO_x, H_2O, O_2, SO_2. None of the catalysts proposed in literature show a good activity and stability in N_2O conversion under realistic conditions of feed composition and space velocities [37, 38]. Additional extra-heat by a heat-exchanger or the addition of hydrocarbons as reducing agents is necessary.

As a fourth option the N_2O abatement process can be located end-of-pipe downstream of the tail gas expander. The temperature level is moderate (373-473 K), well below the ignition temperature of all catalysts found. Therefore, in all cases pre-heating is required which makes it a costly and less favourable option. Also the pressure

is about atmospheric, so the volume of the equipment will be larger. However, limitations for retrofit are not so strict for end-of-pipe applications [21].

Combustion processes of fossil fuels, biomass and waste in fluidized-bed combustors (FBCs) also contribute significantly to N_2O emissions [39-42]. The low combustion temperature at which FBCs operate results in low emission levels of NO_x, which matches with the optimal conditions for sulphur-capture. Unfortunately, these benefits are connected to a strongly increased emission of N_2O [43]. Options to control N_2O emissions in fluidized-bed combustors are discussed [22]. The major requirement for a working catalyst is the tolerance of the catalyst against deactivation by SO_2. Fe-ZSM-5 can be used for direct N_2O decomposition, due to the promotion effect of SO_2 on the reaction rate.

Catalytic and thermal abatement technologies have been successfully developed for adipic acid plants, due to the high N_2O concentrations in the tail gas (25-40 vol%) and the exothermicity of the N_2O decomposition reaction, a large increase in the temperature occurs within the catalyst bed [38, 40, 44]. The adiabatic temperature rise of the gas is considerable and renders a temperature range possible in which a large number of catalysts are effective.

2.1.3. N_2O as an Oxidant

The selective oxidation of hydrocarbons is one of the most challenging fields of catalytic chemistry. The main difficulty is the creation of selective catalysts, which activate dioxygen generating some catalyst-bound oxygen species of a proper reactivity and activate the organic compound to direct the reaction to the desired products [45, 46]. The optimization of both these parameters simultaneously is a very difficult task, since one cannot tune them independently. For many catalytic oxidation reactions a reasonable selectivity has not been achieved so far and therefore complex multi-step processes are used instead.

N_2O which was considered not very toxic but practically useless compound appeared to possess remarkable oxidation chemistry. A brief overview for N_2O as oxidant will be given. N_2O as an oxidant is very interesting in relation to phenol production, which is one of the most bulky chemicals with the annual world production exceeding 6 million tons. Theoretically, the selective oxidation could be done in a single step by adding oxygen to benzene. However, many attempts to accomplish this reaction were unsuccessful. Therefore, at present the cumene technology includes three steps as illustrated in Figure 2.6 [47]:

- Alkylation of benzene with propylene to produce cumene
- Oxidation of cumene to cumene hydroperoxide
- Decomposition of cumene hydroperoxide to phenol and co-product acetone

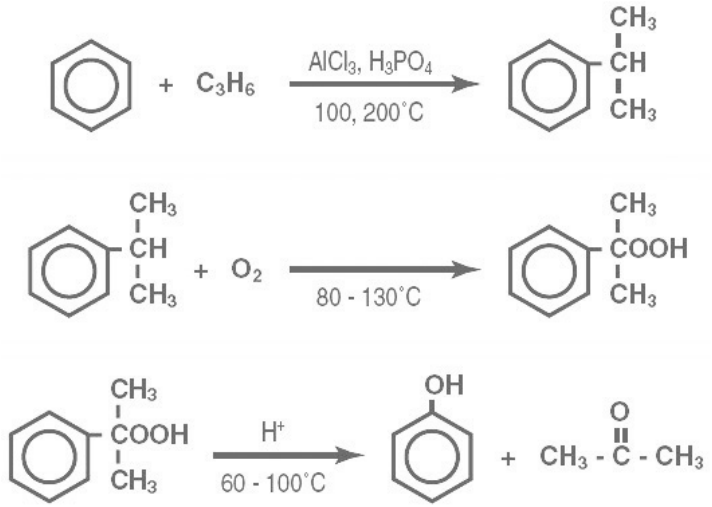

Figure 2.6: Main reactions for phenol and acetone production via cumene.

Despite its great success the cumene process has some disadvantages: a multi-step process, the formation of an explosive intermediate (cumene hydroperoxide), and co-production of acetone in 1:1 stoichiometry.

In 1983 the first use of N_2O for the oxidation of benzene over a vanadia catalyst was reported by Iwamoto et al. [48]:

Figure 2.7: Phenol production via benzene oxidation with N_2O.

At 823 K, the reaction selectivity exceeded 70%. This work has stimulated further efforts and in 1988 three groups of researchers [49-51] independently found ZSM-5 zeolites to be the best catalyst for the oxidation of benzene to phenol. The catalysts allowed the reaction to proceed at much lower temperature and with the

selectivity approaching 100%. The oxidation of benzene to phenol using N_2O as an oxidant has basically two benefits: one-step process and the formation of environmentally friendly molecular nitrogen as a by-product. Based on the direct oxidation of benzene by N_2O, Solutia Inc. and the Boreskov Institute of Catalysis (BIC) developed jointly a new phenol process, which uses a Fe-ZSM-5 catalyst and was called the AlphOx™ [52, 53].

Two different explanations are suggested for the nature of the catalytic activity of ZSM-5. One approach is based on the acidity of the zeolites with strong Brönsted and Lewis sites [54, 55]. The other one relates to the common oxidation catalysis, which might be provided by the presence of a transition metal. Iron was identified to be present in zeolites at least at the level of a few hundred ppm [56, 57]. Presently it is generally accepted that in the micropore space of the high silica zeolite matrix, iron can form some active sites, which catalyze the reaction and were called by Panov "α–sites" [52].

Furthermore, active oxygen deposited from N_2O on Fe-ZSM-5 was shown to be capable of converting methane to methoxy species at room temperature [58-62]. Upon heating, the methoxy species decompose without the formation of methanol. Methanol can be formed, however, by hydrolyzing the methoxy groups on the zeolite surface by washing the catalyst with water. The direct conversion of methane to useful chemical products has so far failed due to its severe thermodynamic stability. At present, to produce methanol, methane is first converted to a mixture of H_2 and CO and after that the latter mixture is converted to methanol. However, the partial oxidation of methane to methanol area holds considerable potential for use of the large, worldwide reserves of natural gas.

The surface oxygen deposited from N_2O on Fe-ZSM-5 exhibits an extremely high reactivity. It oxidises CO and H_2 even at low temperature (~373 K) [63, 64]. Panov et al. [52] gives an overview of data demonstrating the selectivities toward hydroxylation products obtained in the oxidation of various substrates with N_2O over zeolite catalyst. Quite good selectivities were achieved in the oxidative dehydrogenation of alkanes [65, 66] and in the epoxidation of propylene to propylene oxide [67, 68]. Liquid phase oxidation of alkanes with N_2O into carbonyl compounds can be applied to a variety of substrates including aliphatic, cyclic, heterocyclic alkenes and their derivatives. These reactions proceed non-catalytically in the temperature range of 423-523 K yielding ketones and aldehydes as the main products and are summarized by Panov et al. [52].

2.2. Mechanistic Aspects of N_2O Decomposition

Mixed oxides, noble metals and transition metal exchanged zeolites [69, 70] are efficient catalysts for the direct decomposition of N_2O into N_2 and O_2. An overview of different catalysts is given in section 2.3 whereas more detailed information concerning preparation and activation are summarized for the Fe-ZSM-5 which was the only catalyst investigated in this study.

The decomposition of N_2O over Fe-ZSM-5 involves iron containing sites, $(\ )_{Fe}$, and proceeds via surface atomic oxygen and gaseous nitrogen formation from N_2O [56, 62-64, 71, 72]:

$$N_2O + (\ )_{Fe} \rightarrow N_2 + (O)_{Fe} \quad (2.5)$$

This reaction takes place at temperatures lower than 573 K. At temperatures higher than 573 K $(O)_{Fe}$ can recombine forming O_2:

$$N_2O + (\ )_{Fe} \rightarrow N_2 + O_2 + (\ )_{Fe} \quad (2.6)$$

It is important that the oxygen formed at low temperatures (T < 573 K), called "α-oxygen" by Panov and co-workers [72, 73], possesses very high, unusual reactivity. The active oxygen rapidly exchanges with $^{18}O_2$ even at room temperature, whereas Fe-ZSM-5 that was not treated with N_2O is completely inactive for the isotope exchange at that temperature [58, 64]. Oxygen loaded from N_2O on the catalyst surface converts CO to CO_2 [56, 63, 64, 74]. The most interesting property of α-oxygen is that it can insert into a C-H bond. It selectively oxidizes benzene to phenol [47, 75], and it even converts methane to methanol [58-62]. The potential of α-oxygen as selective oxidant is discussed in section 2.1.3.

The structure of the active sites has been much debated. They are Fe(II) sites, but they do not react with O_2 [64]. Only N_2O can oxidize them to Fe(III) upon formation of α-oxygen [72, 76]. The active sites were described as binuclear iron clusters [62, 77]. The proposal was partly based on the observation that the ratio of O/Fe was close to 0.5. A second argument made for the notion of a binuclear iron was due to its capability to insert into C-H bonds analog to the enzyme methane monooxygenase (MMO) [58, 72, 77, 78]. The active site of MMO consists of a binuclear iron core. It is interesting to note that the half of the active sites of a Fe-ZSM-5 are blocked by water and another half is still reactive toward N_2O decomposition militating as well in favor of binuclear iron sites [56]. However, other studies suggested isolated iron sites [79-82] as well as FeO_x nanoclusters and Fe_3O_4 particles [82, 83, 79, 84]. In general, it can be stated that iron speciation strongly depends on the method of iron introduction and the subsequent

treatments [79, 83, 85-90]. Furthermore, an exact structural characterization of the active sites is extremely difficult since Fe-ZSM-5 with high Fe loading (1-6 wt%) is a very complex and heterogeneous material while iron zeolite samples with the larger part of active iron (~90%) are generated from a low integral iron loading (~0.01-0.1 wt%).

In literature two possible rate-determining steps for the N_2O decomposition are discussed. Mechanistic studies have substantiated that O_2 formation is the rate-determining step in N_2O decomposition over iron containing zeolites [56, 71, 91-96]. On the other side as rate-determining step in N_2O decomposition over Fe-ZSM-5, the dissociation of N_2O [97, 98] was suggested and the catalyst reduction by N_2O [99-101]. The absence of an inverse dependence on O_2 partial pressure for the rate of N_2O decomposition has led a number of authors to the conclusion that O_2 desorption is rapid and irreversible and consequently not rate-determining [64, 90, 97, 100, 102, 103]. Additionally, if O_2 desorption were rate-determining, the catalyst surface would be saturated with oxygen atoms and the N_2O decomposition would be zero order in N_2O partial pressure, in contrast to most experimental findings, which show that the rate of N_2O decomposition is first order in N_2O. However, Kiwi-Minsker et al. showed that the reaction kinetics was first order towards N_2O during the transient period, and of zero order under steady-state conditions at 583 K [104]. This is in accordance with mechanistic studies using transient techniques, which have potential for providing deeper mechanistic insights into complex catalytic reactions and substantiated that O_2 formation is the rate-determining step in N_2O decomposition over iron containing zeolites [71, 92-95].

There is no consensus on the reaction pathways leading to gas-phase O_2. A few authors concluded that O_2 formation occurs via the removal of adsorbed oxygen species by N_2O [99-101]:

$$N_2O + (O)_{Fe} \rightarrow N_2 + O_2 + (\ )_{Fe} \tag{2.7}$$

Atomic oxygen species deposited over iron sites can recombine [66, 71, 105] to give gas-phase O_2 according to the following equation.

$$2(O)_{Fe} \rightarrow O_2 + 2(\ )_{Fe} \tag{2.8}$$

Detailed mechanistic DFT investigations by Heyden et al. [97, 103] concluded that O_2 is formed via the decomposition of triatomic oxygen species yielding an iron site with monoatomic oxygen species (Equation (2.9)), which further participates in N_2O decomposition.

$$\begin{aligned} N_2O \;+\; (O_2)_{Fe} \;&\rightarrow\; (O_3)_{Fe} \;+\; N_2 \\ (O_3)_{Fe} \;&\rightarrow\; (O)_{Fe} \;+\; O_2 \end{aligned} \tag{2.9}$$

Considering this reaction scheme, Kondratenko and Perez-Ramirez [94, 106] proposed upon micro kinetic analysis from transient experiments in the TAP reactor that adsorbed biatomic oxygen species undergo a transformation to another biatomic oxygen species, which ultimately desorbs as gas-phase O_2 as in the following equations:

$$\begin{aligned} (O-O)_{Fe} \;&\rightarrow\; (O_2)_{Fe} \\ (O_2)_{Fe} \;&\rightarrow\; (\;)_{Fe} \;+\; O_2 \end{aligned} \tag{2.10}$$

Evidence was presented that adsorbed NO and NO_x species are also formed during N_2O interaction with iron containing zeolites [71, 91, 107-110]:

$$N_2O \;+\; (\;)_{Fe} \;\rightarrow\; N_2 \;+\; (O)_{Fe}, NO_x \tag{2.11}$$

Adsorbed NO species are slowly accumulated on the surface of Fe-ZSM-5 catalyst with low iron content and strongly affect the dynamics of N_2O decomposition, leading to an increase of the reaction rate with time [71, 104, 110]. This autocatalytic behavior was related to the facilitation of atomic oxygen recombination/desorption [74]. A considerable increase of the N_2O decomposition rate upon NO introduction to the reaction mixture was reported by different studies [92, 95, 100, 111, 112]. NO is proposed to act as an intermediate oxygen storage. Adsorbed NO on the catalyst reacts with the oxygen atom that N_2O deposits on the catalyst surface and forms adsorbed NO_2 (Equation (2.12)). O_2 desorption occurs by recombination of the second deposited oxygen atom with an oxygen atom from NO_2 (Equation (2.13)).

$$(O)_{Fe}, NO_{ads} \;\rightarrow\; (\;)_{Fe}, NO_{2,ads} \tag{2.12}$$

$$(\;)_{Fe}, NO_{2,ads} \;+\; (O)_{Fe} \;\rightarrow\; O_2 \;+\; (\;)_{Fe}, NO_{ads} \tag{2.13}$$

The role of NO in the cycle is purely catalytic. Adsorbed NO may even facilitate the migration of atomic oxygen to enhance their recombination [92, 113]. NO/NO_2 [74, 92, 111] as well as nitrite/nitrate [114] redox cycles are proposed for active sites regeneration in N_2O decomposition. Surface NO can be further oxidized to adsorbed NO_2 species [91, 92, 95, 110, 115, 116]. They are proposed to participate in the catalytic cycle and function as intermediate oxygen storage.

2.3. Catalysts for N_2O decomposition

The catalytic decomposition of N_2O into its elements can be carried out with varying degrees of efficiency by mixed oxides, noble metals and transition metal exchanged zeolites [69, 70]. Zeolites are unique matrices allowing the stabilization of small metal complexes, which can barely form over more open surfaces. Fe-zeolites of various framework types (MFI, BEA, FER, MOR, FAU) [85, 109, 117-120], compositions (silicates, titanosilicates, aluminosilicates, gallosilicates, borosilicates, germanosilicates) [121] and containing transition metals especially Fe, Co and Cu [69, 70, 100, 113, 122] and noble metals such as Pt, Rh, Ru [69, 70, 123] are studied.

A significant effect of the framework type of zeolites on the catalytic activity was observed. Pentasyl-type frameworks (BEA, FER, MFI) loaded with iron are more efficient catalysts for direct N_2O decomposition than other zeolites such as MOR, FAU, MAZ, and OFF [33, 124, 125].

Platinum [126-128], rhodium [126, 129, 130] and Pt-Rh alloys [129, 131] are studied in N_2O decomposition. Noble metal catalysts have very high intrinsic activities for N_2O decomposition [70]. But in the exhaust gas stream for adipic and nitric acid plants, N_2O is present together with NO and other components, such as O_2, H_2O and SO_2. Most noble metal catalysts are strongly deactivated by the presence of these other components, particularly NO [69, 132]. Iron zeolites show the opposite behavior a remarkable activity and stability for nitrous oxide decomposition in the presence of these poisons for other catalysts. This includes the insensitivity to O_2, the positive effect of NO and SO_2 on the rate of N_2O conversion and an acceptable resistance towards deactivation by H_2O [22, 132-134].

A synergism for N_2O decomposition between Fe and Ru or Rh, loaded in high-silica zeolites was reported [135, 136.]. Such bimetallic mordenite and ferrierite catalysts have also shown considerable N_2O decomposition activity in the presence of NO [136]. However, the most studied catalyst for N_2O decomposition into N_2 and O_2 is Fe-ZSM-5. The zeolite possesses excellent activity and selectivity in direct N_2O decomposition and generates with N_2O a very efficient oxidant at low temperatures [66].

2.3.1. ZSM-5 Zeolite

Zeolites, in a narrow definition, are porous crystalline aluminosilicates having a uniform pore structure and exhibiting ion-exchange behaviour. The framework of zeolites consists of SiO_4 and AlO_4 tetrahedron sharing oxygen ions located at their apices [137]. Since aluminium is trivalent, every AlO_4 unit carries a negative charge, which is compensated by a positive charge associated with a cation, usually protons or metal

cations from the I and II main group. The topology of the framework defines a structure type symbolized by group of three letters, e.g., MFI for the structure type of zeolite ZSM-5. A list of the ~130 currently accepted structure types, with their type materials, can be found in the Atlas of Zeolite Framework Types [138]. The description and classification of the topology of zeolites is based on the concept of larger units known as secondary building units (SBU) [138].

Pentasil zeolites with five-membered rings as secondary building unit are a class of industrially important molecular sieves. Synthetic materials with the MFI (Mobile Five) structure are the most prominent examples and have also been employed in the present work. The hollow tube model of the pore structure of the MFI structure is presented in Figure 2.8. The MFI-type topology shows a three-dimensional channel system. Due to its sorption and catalytic properties, ZSM-5 arouse great interest. It is a high-silica zeolite with Si/Al larger than ca. 7 first reported in 1972 by Argauer and Landolt in the Mobile Oil Corporation laboratories [139]. The all-silica end member is called silicalite-1 and was synthesized by Flanigen et al. in 1977 [140].

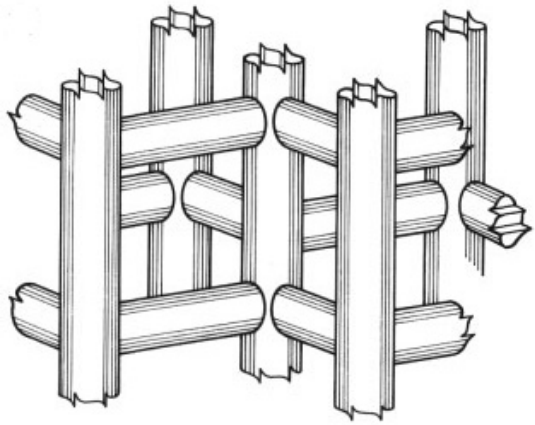

Figure 2.8: Channel system of MFI framework structure [141].

The pore system of ZSM-5 is of intermediate size and consists of channels formed by puckered 10-membered rings. Straight parallel channels with nearly circular cross section ($d_p \approx 0.55$ nm) are linked together by zig-zag shaped continuous pores with elliptical shape (0.52×0.58 nm) and ten-ring apertures perpendicular to the channels, resulting in a three-dimensional cavity system. The framework density is 1.8 g/cm^3 and the specific micropore volume is 0.19 ml/g [142].

2.3.2. Preparation of Iron Containing ZSM-5

The preparation procedure of iron zeolites strongly influences the nature and distribution of iron species in the final material and the associated catalytic performance. Iron zeolites can be prepared by introducing the iron into the zeolite framework during the synthesis, so called hydrothermal synthesis, and into the zeolite matrix by post-synthesis modification. Depending on the preparation method iron species of different nature are produced and illustrated in Figure 2.9. These include isolated ions either (a) in framework positions (isomorphously substituted) or (b) in cationic positions in the zeolite channels, (c) binuclear and, in general, oligonuclear iron complexes in extra-framework positions, (d) iron oxide FeO_x nanoparticles of size $\leq$ 2 nm, and (e) larger iron oxide particles (Fe_2O_3) in a wide distribution (up to 25 nm in size) located at the surface of the zeolite crystal [83, 82, 84].

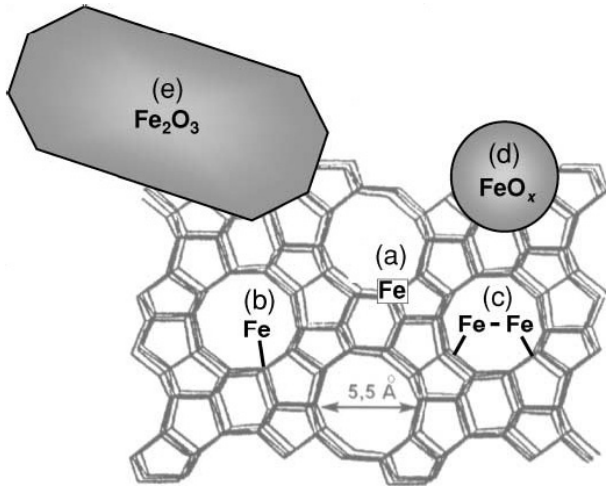

Figure 2.9: Schematic representation of the different Fe species identified in Fe-ZSM-5 [84].

Isomorphously substituted ZSM-5 is prepared by hydrothermal synthesis. Iron is incorporated in the crystalline lattice located in tetrahedral position. An iron source such as $Fe(NO_3)_3$, $FeCl_3$ is either explicitly added to the synthesis solution [143, 144, 72] or a "natural" impurity level of Fe is incorporated into the zeolite framework. ZSM-5 contains about 200 ppm Fe from the synthesis with deionized water and 70 ppm Fe using bidistilled water, respectively [56]. The method guarantees a high dispersion of iron which results in selective and stable catalysts for N_2O decomposition.

By post-synthesis modification, iron is introduced into the zeolite matrix by gas-phase [145-147], aqueous [82] and solid-state [142, 82, 148, 144] ion exchange using different types of Fe-salts. Framework AlO_4 units carry a negative charge which is compensated by a positive charge associated with a cation. This cation is replaced by iron with the ion-exchange method. The ion-exchange capacity of a zeolite depends on the chemical composition, i.e., a higher ion-exchange capacity is observed in zeolites of low SiO_2/Al_2O_3 ratio. The specific ion-exchange capacity varies with the structure of the zeolite and the exchange cation. During preparation of Fe-ZSM-5 by wet ion exchange (WIE), only about the half of the full exchange capacity was achieved without the formation of small iron oxide particles [79, 91].

Very high iron loading can be attained by sublimation also called chemical vapour deposition (CVD) of $FeCl_3$ onto the parent H-ZSM-5 zeolite [145, 146,147]. Fe loadings as high as Fe/Al=1 are reached, but it is generally observed that after washing and calcination iron is clustered to inactive FeO_x [149]. However, a small fraction of Fe yields excellent performance for N_2O decomposition (typically 0.5 wt%) [150-152].

Impregnation of zeolites is employed when the quantity of metal ion to be introduced is greater than would be obtainable by ion exchange, e.g. high-silica zeolites, but the distribution is more uniform in the ion-exchange sample [153]. The anion as well as the cation is introduced. The parent zeolite is soaked with a $FeCl_3$ solution and thereafter calcined [72, 144, 154]. In industrial applications, wet ion exchange (WIE) and impregnation are the simplest methodologies, because they involve few steps and the process parameters are easily accessible.

2.3.3. Activation of Fe-ZSM-5 for N_2O Decomposition

The pre-treatment conditions such as temperature and medium have a strong influence on the N_2O decomposition activity of the Fe-ZSM-5 catalyst. Nitrous oxide decomposition rates over Fe-ZSM-5 catalysts strongly increase after high-temperature calcination and high-temperature steaming [83, 89, 148, 152, 155, 156]. The catalytic activity is related to extra-framework iron species which are formed at this stage. Mechanistic details are still unclear, including such important aspects as the structure and nuclearity of the active iron sites.

High-temperature treatments can have various effects on the iron zeolite. However, in general, calcination in inert at high temperature leads to de-hydroxylation and auto-reduction of iron centers. Water vapour accelerates the hydrolysis of zeolite matrix bonds leading to Fe and Al extra-framework formation.

Iron ions of isomorphously synthesized zeolites migrate during calcination from the crystalline lattice into zeolite micropores or extra-framework iron ions are rearranged

to create active sites. EXAFS measurements performed on a isomorphously substituted Fe-ZSM-5 indicate that before activation at 1123 K in He, iron is located in tetrahedral positions in the MFI framework, but that after activation, the iron migrates to the charge-exchange positions associated with framework Al and is presented as isolated Fe(III) cation [80]. Active iron sites once formed upon calcination in He at 1323 K do not disappear due to re-hydroxylation [155]. An in situ Mössbauer spectroscopy study showed that the activation process (calcination in air, in vacuum, or in the presence of water vapour) causes an intensive reduction of iron, yielding binuclear Fe(II) complexes [72].

Steaming resulted in dealumination of the framework and growth and ordering of the iron oxide aggregates [83, 84]. Moreover, some of the occluded neutral iron oxide nanoparticles were transformed into charge-compensating iron complexes upon a protolysis reaction with the Brönsted protons [83]. The beneficial effect of severe activation treatments to sublimed Fe-ZSM-5, where iron is introduced at extra-framework positions, is taken as an indication that removal of lattice aluminium is important for the generation of active sites [152]. High-temperature treatment induces profound changes in the distribution of iron species, most notably a substantial fraction of oligonuclear and cationic Fe species are converted to Fe species stabilized by extra-framework Al (Fe-O-Al species) in zeolite pores [148]. Protons are known to accelerate the process of steam-induced aluminium migration [157] and steam-dealumination is likely to precede the clustering of iron in Fe-ZSM-5 [120].

2.4. Analysis Methods

Transient experiments were performed in this study to gain useful mechanistic information of the decomposition of N_2O over Fe-ZSM-5. Transient response techniques are a powerful tool for gaining insight into the mechanisms of complex catalytic reactions and to derive rate constants for the individual steps involved [158]. Under steady-state conditions, all elementary steps in series are progressing at the same rate and hence the measured rates hardly tell the precise kinetic structure, or mechanism, of catalytic reactions which usually consist of several elementary steps including adsorption of reactants, surface reaction, and desorption of products. When some perturbations are imposed on a reaction system under steady state, the transient response of the system as it approaches a new steady state exhibits a characteristic behaviour reflecting the nature of the sequence of steps which underlie observed kinetics but cannot be unveiled by the steady-state experiment. The transient response technique was applied with a Micromeritics AutoChem 2910 analyzer at atmospheric pressure and with the TAP setup in vacuum.

2.4.1. Transient Response Techniques at Atmospheric Pressure

The aim of the transient response method is to perturbate the reaction system to acquire useful information on the mechanism of the reactions from the resultant response. Any kind of variables that defines the chemical reaction system may be used for this purpose, i.e., concentration, temperature, pressure or flow rate. In imposing perturbation of any one of these variables, a well-defined forcing function must be used for the sake of simplicity of the analysis of the response. The possible functions will be rectangular step functions, rectangular pulses and ramp functions [158].

In the study of heterogeneous catalysis, it has been recognized that presence of impurities and the formation of intermediates on the catalyst surface plays an important role in surface catalysis. The pre-adsorption of a test molecule prior to a rectangular step function of the reactant provides information about the role of the test molecule on the chemical reaction. By measuring the transient response of the conversion or of side products, the probe molecule can be identified for example as inhibitor, promoter, co-catalyst, intermediate.

A powerful tool used to investigate the desorption, decomposition and reaction of species on the catalyst surface is the temperature-programmed desorption (TPD). A temperature programmer heats the catalyst at a constant rate. Decomposition and desorption of the surface species is followed with a mass spectrometer. The temperature at which a molecule desorbs also reflects how strongly it is bound to the surface [159]. Reaction intermediates, products and side products can be identified and the initial amount of the adsorbate before desorption quantified.

The transient response technique has been proved to be useful for the kinetic and mechanistic study of heterogeneous catalysis by furnishing information complementary to that obtained by steady-state experiments.

2.4.2. Temporal Analysis of Products

The TAP reactor system was originally created by John T. Gleaves in 1988 [160] to assist the catalyst development process. Improvements have been made from then on by optimizing the detection sensitivity as realized with the TAP-2 reactor setup [161], and by adding extra mass spectrometer analysis, as is the case with the Multitrack reactor setup [162, 163]. The TAP reactor system is an apparatus that is used to perform transient pulse experiments for micro kinetic analysis of complex heterogeneous catalytic reactions. It has been extensively applied in experimental studies on catalytic reaction mechanisms and other surface processes.

The critical difference between TAP and TAP-2 reactor systems is the positioning of the microreactor and the detector that measures the reactor effluent. In the TAP-2 system, the two devices are physically much closer, and as a result the detection efficiency of the TAP-2 system is much higher [164].

In heterogeneous catalysis, there are two known kinetic strategies, traditional experiments over industrial multicomponent catalyst under normal conditions (Continuous Stirred Tank Reactor and Plug Flow Reactor, working mostly in a steady-state regime) and surface science experiments under high vacuum conditions mostly over single crystals with well-defined surfaces which are very different from the industrial multicomponent catalyst. Consequently, traditional applied kinetics and surface science kinetics are separated by a "pressure" and "material" gap. The TAP approach can be defined as a "third kinetic strategy", which is bridging these "gaps". The TAP pulse response pressure domain (10^{-2}-10^{-1} Pa) is located at the boundary between the traditional applied kinetics and surface science kinetics, and this domain can be extended [164]. Unlike surface science experiments, TAP pulse response experiments can be performed on practical catalytic materials at pressures higher than those used in surface science experiments.

The Temporal Analysis of Products (TAP) reactor system allows fast transient experiments in the millisecond time regime with submillisecond signal sampling [160]. In contrast, a nonsteady-state reactor setup operating at atmospheric pressure provides a time resolution of only about one second. Several advantages can be attributed to the operation in high vacuum. Since gas transport through the catalyst is governed by Knudsen diffusion, external mass and heat transfer limitations are completely absent and the diffusivities of the individual component of a gas mixture are independent of pressure, concentration, or the composition of the gas mixtures. This simplifies the equations needed to model the system significantly. Moreover, the collisions between gas-phase molecules are limited so that the transient response of product molecules in the TAP system is a measure of gas-solid interactions. The overall surface coverage is lower in vacuum minimizing hydroxylation and side reactions. The catalyst zone is isothermal even in the case of strongly exo- or endothermic reactions due to the small quantity of reactants introduced in the reactor.

TAP-2 Reactor Setup

The TAP-2 reactor system can be used to perform transient as well as steady-state experiments at pressures ranging from 10^{-7} to 250 kPa, and temperatures ranging from 300 to 1200 K. A simplified scheme of the key parts of a TAP-2 reactor system is presented in Figure 2.10. In a TAP experiment catalyst particles are sandwiched between inert particle beds in a small fixed bed microreactor. One end of the microreactor is attached to a manifold containing one or more high-speed pulse valves, and the other

end is attached to an ultra-high vacuum system that has a very high pumping speed. The gas exiting the reactor is monitored as a function of time with a quadrupole mass spectrometer detector. The intensity of the transient response is proportional to the exit flow rate of the corresponding gas. Introducing one or more very short pulses of reactant gas into the evacuated microreactor performs a standard TAP experiment. At sufficiently low pulse intensities the total gas pressure becomes negligible and the gas molecules move through the reactor via Knudsen diffusion.

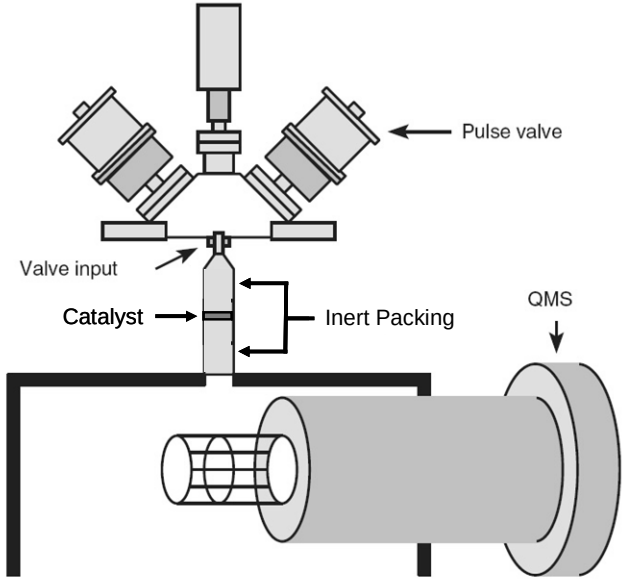

Figure 2.10: The key parts of a TAP-2 reactor system with thin-zone packing [165].

The time-dependent gas flow [molecule/s] that escapes the microreactor is measured by a mass spectrometer, which makes it possible to measure very small signals with precise time resolution. A single pulse is typically very small (~10^{13} to 10^{17} molecules/pulse), and gas transport through the particle bed occurs by Knudsen diffusion. An important feature of this flow regime is that the diffusivities of the individual components of a gas mixture are independent of pressure, concentration, or the compositions of the gas mixture. The number of molecules per pulse is usually much smaller than the total number of active sites in the catalyst, and reaction of a single pulse typically changes the catalyst composition by less than 0.1% [166].

The simplest TAP reactor configuration is the one-zone reactor which is uniformly packed with particles. In practice, it is difficult to obtain temperature

uniformity at high temperatures in a one-zone reactor and was therefore advanced by sandwiching the catalyst zone between two inert zones, called the three-zone reactor [167].

The main advantage of the three-zone TAP reactor compared to the one-zone configuration is that the catalyst zone can be more easily maintained under isothermal conditions. However, it is difficult to maintain a uniform profile of the surface catalyst composition because of the gas concentration gradient, which is the driving force of diffusional transport.

In 1999, Shekhtman et al. [168] proposed the thin-zone TAP reactor (TZTR) in which the thickness of the catalyst zone is made very small compared to the whole length of the reactor. Then, the change of gaseous concentration across the thin catalyst zone can be neglected, and the catalyst composition can be considered as uniform. Uniformity of catalyst composition and model simplicity make the thin-zone TAP reactor configuration very useful [164].

Types of Experiments

Depending on the kind of information required different experimental modes are used. The reactant gas can be introduced into the microreactor in a variety of transient formats at both vacuum and atmospheric pressures as well as in form of pulses and as continuous gas feed.

Single Pulse TAP Experiments

TAP pulse experiments in vacuum include the pulse input train from a single pulse valve and the reactor output that is measured by the mass spectrometer. Key features are illustrated in Figure 2.11. The output transient response spectrum indicated that different products are characterized by different transient responses and that the individual product responses can change with pulse number. Information on the catalytic performance is obtained by pulsing a mixture of a reactant and an inert reference gas. The integral size of the pulse responses allows calculation of conversions and yield, whereas the size and shape of the reference gas represents the dosed amount of reactant. Due to the high time resolution, information on the sequence of product formation can often be obtained by a comparison of the normalized pulse responses for different products [169-171]. The product formation on the surface requires a certain period of time for each step in the reaction sequence. Therefore, the pulse responses of secondary products are delayed in comparison to those of primary products while components formed during the same reaction step appear simultaneously. However, the former statement is only valid if the time for the diffusive mass transport is significantly smaller than the time required for reaction and if the desorption of products into the gas phase is a fast process and if the surface reactions are virtually irreversible [172].

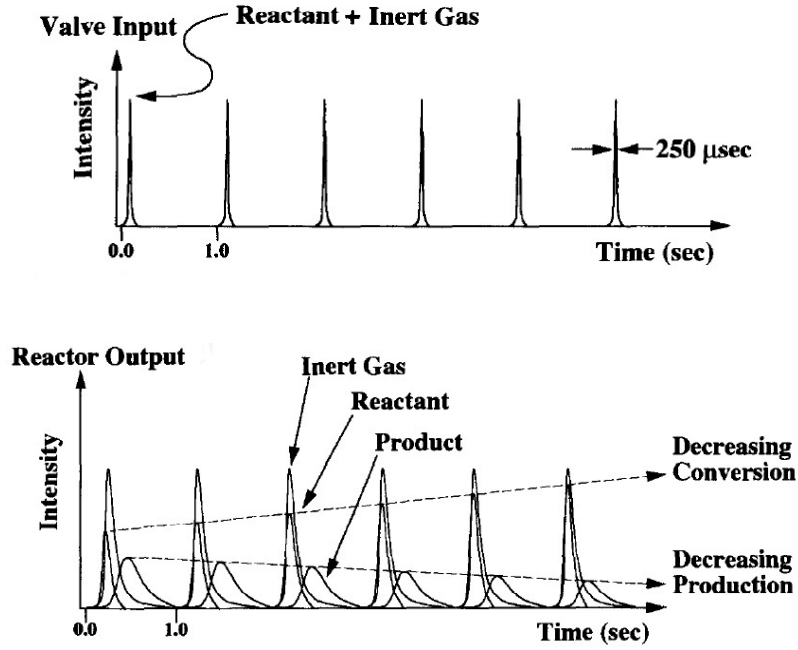

Figure 2.11: Key features of a single pulse TAP experiment showing a train of input pulses and the output transient responses [161].

Furthermore, the surface state of the catalyst can be changed in a distinct way by introducing a large number of pulses in a so-called multi-pulse experiment. This allows for example the surface reduction of an oxide catalyst when pulsing a reactive hydrocarbon or the titration of active sites with an irreversibly adsorbing reactant [173-176]. These experiments may also probe the performance of the catalyst under different working conditions [177-179].

Pump-probe TAP Experiments

In pump-probe experiments, different reactant-inert mixtures are introduced sequentially from separate pulse valves. Figure 2.12 illustrates the input pulses and transient response of such a sequential pulse experiment. The output transient response now contains products pulses coinciding with both valve inputs. For example, one valve may contain a reducing agent and the other valve an oxidizing agent. By varying the delay between the two single pulses and the frequency of repeating the cycle, information on the life-time and reactivity of the adsorbed species are obtained [173, 180-182]. Theses species are created during the first single pulse and probed during the second single pulse.

The pump-probe format is also useful for investigating catalyst activation. In this case, one pulse-valve is used to introduce the activating agent, and the other pulse-valve is used to introduce a reactive probe to monitor the state of the catalyst surface. By monitoring a number of reaction products, changes in activity and selectivity can be observed, and correlated with the incorporation of the activating species [161, 183].

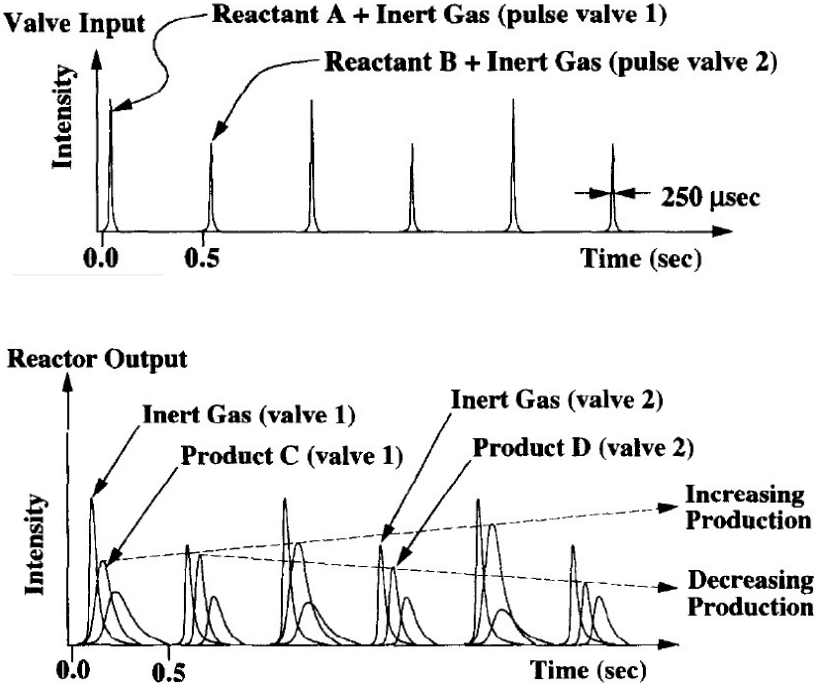

Figure 2.12: Key features of a pump-probe TAP experiment using two pulse valves. The input pulse train which consists of alternating pulses of reactant A and B as well as the output transient responses are shown [161].

Elevated Pressure Experiments

In the elevated pressure configuration the microreactor can be operated as a conventional steady-flow or pulsed microreactor. Continuous gas feed allows the use of larger amounts of reactants which is often required for the pre-treatment of a catalyst. More pronounced changes in the state of the catalyst are applied at elevated pressures while the reactor effluent is continuously recorded and subsequently performing pulse experiments under evacuated conditions [184, 185].

Temperature-Programmed Experiments

The reactor may be operated isothermally or may be temperature programmed. Applications such as temperature-programmed desorption (TPD), surface reaction (TPSR), oxidation (TPO) or reduction (TPR) can be performed. TPD experiments allow the characterization of adsorbates on the catalyst [186-188].

Modeling of TAP Experiments

The composition of the flow provides information on the types of chemical transformations that have occurred in the microreactor, and the time dependence of the flow contains information on gas transport and kinetics. The determination of reaction rate constants for the elementary reaction steps requires setting up a model which describes the transient response of the system. The theoretical basis of TAP experiments is fully developed and well established [164, 165, 167, 168, 189-194]. TAP pulse response experiments are described by a set of partial differential equations that can be solved for certain cases analytically and for more complex systems numerically. Different calculation methods including regression analysis and moment analysis have been used for parameter estimation. The regression analysis involves comparing the experimental response to the model response based on the least square fit. The moment method can be performed when moment or moment-related expressions for the exit flow rate are known.

Quantitative information of the phenomena in the reactor can be extracted from the size and the shape of the responses by the use of mathematical models that describe the diffusion-reaction processes in the reactor. The required mathematical solution therefore describes the gas exit flow rate. The experimental gas exit flow rate can be determined only when the absolute calibration factor has been obtained. Matching of the experimental and the model exit flow rates provide the estimated parameters. When using the experimental response curve without converting into the exit flow rate curve, only the shape of the response is concerned.

Knudsen diffusion is the dominant mass transport mechanism in pulse TAP experiments apart from some viscous influence at the time of the introduction of the reactant pulse, in case the microreactor filling is non-porous. Knudsen diffusion occurs at sufficient low pressure (small gas density) or in small pores when the mean free path of the molecule is much greater than the distance to the surrounding walls. This implies that the collisions between molecules and the solid particles dominate and that intermolecular collisions are negligible. The simple hydrodynamics (mostly Knudsen flow) allows one to focus on the intrinsic kinetic equations.

In case of microporous solids (zeolites, active carbons) the situation is more complicated. The mass transport may be conducted by configurational diffusion where

the molecular diameter is comparable to the channel diameter. Studies have shown that the direct access of molecules to the micropores is highly improbable [195, 196]. Thus, a sequential mechanism can be postulated consisting of the collision and sorption of the molecules with the outer particle surface, random mobility at the outer surface similar to a two-dimensional gas, the entering into the micropores, and diffusion to sorption sites inside the pores [197]. A number of studies deal with the determination of diffusivities in microporous zeolites [163, 198-200] and other porous materials [201, 202] by using the TAP reactor. The modeling was extended to biporous materials (meso- and micropores) including first order reaction within the micropores [203, 204]. The existence of internal diffusion limitations on porous particles needs to be verified carefully as concentration profiles inside the pores for transient experiments might arise even in the absence of chemical reaction [201, 205-208]. In the case of microporous solids internal mass transport has to be accounted for explicitly [205].

2.5. References

1. Mellor, J. W., *A Comprehensive Treatise on Inorganic and Theoretical Chemistry*. New York, 1922; Vol. III.
2. Griggs, J. L.; Rao, K. N.; Jones, L. H.; Potter, R. M., Vibration Rotation Bands of $^{15}N_2{}^{18}O$ - Determination of Precise Values of Internuclear Distances. *Journal of Molecular Spectroscopy* **1968,** 25, (1), 34-&.
3. Donner, L.; Ramanathan, V., Methane and Nitrous-Oxide - Their Effects on the Terrestrial Climate. *Journal of the Atmospheric Sciences* **1980,** 37, (1), 119-124.
4. Ramanathan, V.; Cicerone, R. J.; Singh, H. B.; Kiehl, J. T., Trace Gas Trends and Their Potential Role in Climate Change. *Journal of Geophysical Research-Atmospheres* **1985,** 90, (ND3), 5547-5566.
5. *Intergovernmental Panel on Climate Change (IPCC)* 1995.
6. Badr, O.; Probert, S. D., Environmental Impacts of Atmospheric Nitrous-Oxide. *Applied Energy* **1993,** 44, (3), 197-231.
7. Cicerone, R. J., Analysis of Sources and Sinks of Atmospheric Nitrous-Oxide (N_2O). *Journal of Geophysical Research-Atmospheres* **1989,** 94, (D15), 18265-18271.
8. Prinn, R.; Cunnold, D.; Rasmussen, R.; Simmonds, P.; Alyea, F.; Crawford, A.; Fraser, P.; Rosen, R., Atmospheric Emissions and Trends of Nitrous-Oxide Deduced from 10 Years of Ale-Gauge Data. *Journal of Geophysical Research-Atmospheres* **1990,** 95, (D11), 18369-18385.
9. *Intergovernmental Panel on Climate Change (IPCC)* 1992.
10. Crutzen, P. J., Ozone Production Rates in an Oxygen-Hydrogen-Nitrogen Oxide Atmosphere. *Journal of Geophysical Research* **1971,** 76, (30), 7311-&.
11. Wennberg, P. O.; Cohen, R. C.; Stimpfle, R. M.; Koplow, J. P.; Anderson, J. G.; Salawitch, R. J.; Fahey, D. W.; Woodbridge, E. L.; Keim, E. R.; Gao, R. S.; Webster, C. R.; May, R. D.; Toohey, D. W.; Avallone, L. M.; Proffitt, M. H.; Loewenstein, M.; Podolske, J. R.; Chan, K. R.; Wofsy, S. C., Removal of Stratospheric O_3 by Radicals - in-Situ Measurements of OH, HO_2, NO, NO_2, ClO, and BrO. *Science* **1994,** 266, (5184), 398-404.
12. http://www.virtualcentre.org/en/library/key_pub/longshad/A0701E00.htm.

13. Kyoto Protocol to the United Nations Framework Convention on Climate Change.
14. Perez-Ramirez, J.; Kapteijn, F.; Schoffel, K.; Moulijn, J. A., Formation and control of N_2O in nitric acid production - Where do we stand today? *Applied Catalysis B-Environmental* **2003,** 44, (2), 117-151.
15. http://www.ieagreen.org.uk/climate.html.
16. *Intergovernmental Panel on Climate Change (IPCC)* 2007.
17. http://unfccc.int/essential_background/convention/background/items/1353.php.
18. Onken, U.; Behr, A., *Chemische Prozesskunde*. Thieme: 1996.
19. *Best available techniques for Pollution Prevention and Control in European Fertilizers Industry, Booklet no. 2 of 8: Production of Nitric Acid, 2000*; available at http://www.efma.org/Publications.
20. Van den Brink, R. W.; Booneveld, S.; Pels, J. R.; de Bruijn, F. A.; Gent, M. M. C.; Smit, A. W. *Combined Catalytic Removal of NO_x and N_2O in a Single Reactor from the Tail Gas of a Nitric Acid Plant*; ECN: 2002.
21. Smit, A. W.; Gent, M. M. C.; Van den Brink, R. W., Market Potential for Reduction of N_2O Emissions at Nitric Acid Facilities. *Jacobs Engineering Nederland* 2001.
22. Perez-Ramirez, J.; Kapteijn, F.; Mul, G.; Xu, X. D.; Moulijn, J. A., Ex-framework FeZSM-5 for control of N_2O in tail-gases. *Catalysis Today* **2002,** 76, (1), 55-74.
23. Fareid, E.; Kongshaug, G.; Hjornevik, L.; Nirisen, O.; NorskHydro EP 0359286A2, 1993.
24. Kuhn, G.; Schumacher, V.; Wagner, E. In Proceedings of the International Fertilizer Society, 1999; 1999; p 1.
25. Schumacher, V.; Bürger, G.; Fetzer, T.; Baier, M.; Hesse, M.; BASF DE 19819882A1, 1999.
26. Koch, T.; DuPont US 5478549, 1995.
27. Vernooy, P.; DuPont WO 00/51715 A1, 2000.
28. Kubisa, R.; Klein, M.; L&CSteinmüller WO 99/07638, 1999.
29. Schwefer, M.; Siefert, R.; Groves, M. *Uhde EnviNO$_x$ process for the combined reduction of N_2O and NO_x emissions from nitric acid plants*; ThyssenKrupp techforum 2005, noJUILL pp 66-71.
30. van den Brink, R. W.; Booneveld, S.; Pels, J. R.; Bakker, D. F.; Verhaak, M., Catalytic removal of N_2O in model flue gases of a nitric acid plant using a promoted Fe zeolite. *Applied Catalysis B-Environmental* **2001,** 32, (1-2), 73-81.
31. Centi, G.; Vazzana, F., Selective catalytic reduction of N_2O in industrial emissions containing O_2, H_2O and SO_2: behavior of Fe/ZSM-5 catalysts. *Catalysis Today* **1999,** 53, (4), 683-693.
32. Kameoka, S.; Kita, K.; Takeda, T.; Tanaka, S.; Ito, S.; Yuzaki, K.; Miyadera, T.; Kunimori, K., Simultaneous removal of N_2O and CH_4 as the strong greenhouse-effect gases over Fe-BEA zeolite in the presence of excess O_2. *Catalysis Letters* **2000,** 69, (3-4), 169-173.
33. Mauvezin, M.; Delahay, G.; Kiesslich, F.; Coq, B.; Kieger, S., Catalytic reduction of N_2O by NH_3 in presence of oxygen using Fe-exchanged zeolites. *Catalysis Letters* **1999,** 62, (1), 41-44.
34. Coq, B.; Mauvezin, M.; Delahay, G.; Butet, J. B.; Kieger, S., The simultaneous catalytic reduction of NO and N_2O by NH_3 using an Fe-zeolite-beta catalyst. *Applied Catalysis B-Environmental* **2000,** 27, (3), 193-198.
35. GrandeParoisse; AtoFina In *The Selective Catalytic Reduction of N_2O by NH_3 on a Fe-BEA Catalyst*, 12th International Congress on Catalysis, Granada, 2000; Granada, 2000.

36. ECN Method for the Conversion of Dinitrogen Oxide. PCT WO 99/49954, 1999.
37. Kapteijn, F.; RodriguezMirasol, J.; Moulijn, J. A., Heterogeneous catalytic decomposition of nitrous oxide. *Applied Catalysis B-Environmental* **1996,** 9, (1-4), 25-64.
38. Reimer, R. A.; Slaten, C. S.; Seapan, M.; Lower, M. W.; Tomlinson, P. E., Abatement of N_2O Emissions Produced in the Adipic Acid Industry. *Environmental Progress* **1994,** 13, (2), 134-137.
39. Bahillo, A.; Armesto, L.; Cabanillas, A.; Otero, J., NO_x and N_2O emissions during fluidized bed combustion of leather wastes. *Journal of Energy Resources Technology-Transactions of the Asme* **2006,** 128, (2), 99-103.
40. Centi, G.; Perathoner, S.; Vazzana, F., Catalytic control of non-CO_2 greenhouse gases - Methane, flourocarbons, and especially nitrous oxide can be decomposed and even reused by implementing new catalytic techniques. *Chemtech* **1999,** 29, (12), 48-55.
41. Liu, H.; Feng, B.; Lu, J. D.; Zheng, C. G., Coal property effects on N_2O and NO_x formation from circulating fluidized bed combustion of coal. *Chemical Engineering Communications* **2005,** 192, (10-12), 1482-1489.
42. Xie, J. J.; Yang, X. M.; Zhang, L.; Ding, T. L.; Song, W. L.; Lin, W. G., Emissions of SO_2, NO and N_2O in a circulating fluidized bed combustor during co-firing coal and biomass. *Journal of Environmental Sciences-China* **2007,** 19, (1), 109-116.
43. Wojtowicz, M. A.; Pels, J. R.; Moulijn, J. A., Combustion of Coal as a Source of N_2O Emission. *Fuel Processing Technology* **1993,** 34, (1), 1-71.
44. Zeng, H. C.; Pang, X. Y., Catalytic decomposition of nitrous oxide on alumina-supported ruthenium catalysts Ru/Al_2O_3. *Applied Catalysis B-Environmental* **1997,** 13, (2), 113-122.
45. Belansky, A.; Haber, J., *Oxygen in Catalysis*. Marcel Dekker: New York, 1966.
46. Boreskov, G. K., Catalytic activation of dioxygen. In *Catalytic Science and Technology*, Andersen, J.; Boudart, M., Eds. Springer-Verlag: Berlin, 1982; Vol. 3.
47. Panov, G. I., Advances in Oxidation Catalysis. Oxidation of Benzene to Phenol by Nitrous Oxide. *CATTECH* **2000,** 4, (1), 18-32.
48. Iwamoto, M.; Hirata, J.; Matsukami, K.; Kagawa, S., Catalytic-Oxidation by Oxide Radical Ions .1. One-Step Hydroxylation of Benzene to Phenol over Group-5 and Group-6 Oxides Supported on Silica-Gel. *Journal of Physical Chemistry* **1983,** 87, (6), 903-905.
49. Gubelmann, M. H.; Tirel, P. J. 1988. Fr. Pat. 2630735.
50. Kharitonov, A. S.; Aleksandrova, T. N.; Vostrikova, L. A.; Sobolev, V. I.; Ione, K. G.; Panov, G. I. USSR Pat. 1805127, 1988.
51. Suzuki, E.; Nakashiro, K.; Ono, Y., Hydroxylation of Benzene with Dinitrogen Monoxide over H-ZSM-5 Zeolite. *Chemistry Letters* **1988**, (6), 953-956.
52. Parmon, V. N.; Panov, G. I.; Uriarte, A.; Noskov, A. S., Nitrous oxide in oxidation chemistry and catalysis: application and production. *Catalysis Today* **2005,** 100, (1-2), 115-131.
53. Uriarte, A. K.; Rodkin, M. A.; Gross, M. J.; Kharitonov, A. S.; Panov, G. I., Direct hydroxylation of benzene to phenol by nitrous oxide. In *3rd World Congress on Oxidation Catalysis*, 1997; Vol. 110, pp 857-864.
54. Esteves, P. M.; Louis, B., Experimental and DFT study of the partial oxidation of benzene by N_2O over H-ZSM-5: Acid catalyzed mechanism. *Journal of Physical Chemistry B* **2006,** 110, (33), 16793-16800.
55. Kustov, L. M.; Tarasov, A. L.; Bogdan, V. I.; Tyrlov, A. A.; Fulmer, J. W., Selective oxidation of aromatic compounds on zeolites using N_2O as a mild

oxidant - A new approach to design active sites. *Catalysis Today* **2000,** 61, (1-4), 123-128.
56. Kiwi-Minsker, L.; Bulushev, D. A.; Renken, A., Active sites in HZSM-5 with low Fe content for the formation of surface oxygen by decomposing N_2O: is every deposited oxygen active? *Journal of Catalysis* **2003,** 219, (2), 273-285.
57. Pirutko, L. V.; Chernyavsky, V. S.; Uriarte, A. K.; Panov, G. I., Oxidation of benzene to phenol by nitrous oxide - Activity of iron in zeolite matrices of various composition. *Applied Catalysis A-General* **2002,** 227, (1-2), 143-157.
58. Dubkov, K. A.; Sobolev, V. I.; Panov, G. I., Low-temperature oxidation of methane to methanol on FeZSM-5 zeolite. *Kinetics and Catalysis* **1998,** 39, (1), 72-79.
59. Knops-Gerrits, P. P.; Goddard, W. A., Methane partial oxidation in iron zeolites: theory versus experiment. *Journal of Molecular Catalysis a-Chemical* **2001,** 166, (1), 135-145.
60. Wood, B. R.; Reimer, J. A.; Bell, A. T.; Janicke, M. T.; Ott, K. C., Methanol formation on Fe/Al-MFI via the oxidation of methane by nitrous oxide. *Journal of Catalysis* **2004,** 225, (2), 300-306.
61. Yoshizawa, K.; Shiota, Y.; Yumura, T.; Yamabe, T., Direct methane-methanol and benzene-phenol conversions on Fe-ZSM-5 zeolite: Theoretical predictions on the reaction pathways and energetics. *Journal of Physical Chemistry B* **2000,** 104, (4), 734-740.
62. Panov, G. I.; Uriarte, A. K.; Rodkin, M. A.; Sobolev, V. I., Generation of active oxygen species on solid surfaces. Opportunity for novel oxidation technologies over zeolites. *Catalysis Today* **1998,** 41, (4), 365-385.
63. Dubkov, K. A.; Paukshtis, E. A.; Panov, G. I., Stoichiometry of oxidation reactions involving alpha-oxygen on FeZSM-5 zeolite. *Kinetics and Catalysis* **2001,** 42, (2), 205-211.
64. Panov, G. I.; Sobolev, V. I.; Kharitonov, A. S., The Role of Iron in N_2O Decomposition on ZSM-5 Zeolite and Reactivity of the Surface Oxygen Formed. *Journal of Molecular Catalysis* **1990,** 61, (1), 85-97.
65. Bulanek, R.; Wichterlova, B.; Novoveska, K.; Kreibich, V., Oxidation of propane with oxygen and/or nitrous oxide over Fe-ZSM-5 with low iron concentrations. *Applied Catalysis A-General* **2004,** 264, (1), 13-22.
66. Kondratenko, E. V.; Perez-Ramirez, J., Oxidative functionalization of propane over FeMFI zeolites effect of reaction variables and catalyst constitution on the mechanism and performance. *Applied Catalysis A-General* **2004,** 267, (1-2), 181-189.
67. Duma, V.; Honicke, D., Gas phase epoxidation of propene by nitrous oxide over silica-supported iron oxide catalysts. *Journal of Catalysis* **2000,** 191, (1), 93-104.
68. Zhang, Q. H.; Guo, Q.; Wang, X. X.; Shishido, T.; Wang, Y., Iron-catalyzed propylene epoxidation by nitrous oxide: Toward understanding, the nature of active iron sites with modified Fe-MFI and Fe-MCM-41 catalysts. *Journal of Catalysis* **2006,** 239, (1), 105-116.
69. Centi, G.; Galli, A.; Montanari, B.; Perathoner, S.; Vaccari, A., Catalytic decomposition of N_2O over noble and transition metal containing oxides and zeolites. Role of some variables on reactivity. *Catalysis Today* **1997,** 35, (1-2), 113-120.
70. Li, Y. J.; Armor, J. N., Catalytic Decomposition of Nitrous-Oxide on Metal Exchanged Zeolites. *Applied Catalysis B-Environmental* **1992,** 1, (3), L21-L29.
71. Bulushev, D. A.; Kiwi-Minsker, L.; Renken, A., Dynamics of N_2O decomposition over HZSM-5 with low Fe content. *Journal of Catalysis* **2004,** 222, (2), 389-396.

72. Dubkov, K. A.; Ovanesyan, N. S.; Shteinman, A. A.; Starokon, E. V.; Panov, G. I., Evolution of iron states and formation of alpha-sites upon activation of FeZSM-5 zeolites. *Journal of Catalysis* **2002,** 207, (2), 341-352.
73. Sobolev, V. I.; Kharitonov, A. S.; Paukshtis, Y. A.; Panov, G. I., Stoichiometric Reaction of Benzene with Alpha-Form of Oxygen on FeZSM-5 Zeolites - Mechanism of Aromatics Hydroxylation by N_2O. *Journal of Molecular Catalysis* **1993,** 84, (1), 117-124.
74. Bulushev, D. A.; Renken, A.; Kiwi-Minsker, L., Role of adsorbed NO in N_2O decomposition over iron-containing ZSM-5 catalysts at low temperatures. *Journal of Physical Chemistry B* **2006,** 110, (22), 10691-10700.
75. Panov, G. I.; Dubkov, K. A.; Starokon, E. V., Active oxygen in selective oxidation catalysis. *Catalysis Today* **2006,** 117, (1-3), 148-155.
76. Pirngruber, G. D.; Grunwaldt, J. D.; Roy, P. K.; Van Bokhoven, J. A.; Safonova, O. V.; Glatzel, P., The nature of the active site in the Fe-ZSM-5/N_2O system studied by (resonant) inelastic X-ray scattering. *Catalysis Today* **2006,** in press.
77. Panov, G. I.; Sobolev, V. I.; Dubkov, K. A.; Parmon, V. N.; Ovanesyan, N. S.; Shilov, A. E.; Shteinman, A. A., Iron complexes in zeolites as a new model of methane monooxygenase. *Reaction Kinetics and Catalysis Letters* **1997,** 61, (2), 251-258.
78. Dubkov, K. A.; Sobolev, V. I.; Talsi, E. P.; Rodkin, M. A.; Watkins, N. H.; Shteinman, A. A.; Panov, G. I., Kinetic isotope effects and mechanism of biomimetic oxidation of methane and benzene on FeZSM-5 zeolite. *Journal of Molecular Catalysis A-Chemical* **1997,** 123, (2-3), 155-161.
79. Lobree, L. J.; Hwang, I. C.; Reimer, J. A.; Bell, A. T., Investigations of the state of Fe in H-ZSM-5. *Journal of Catalysis* **1999,** 186, (2), 242-253.
80. Choi, S. H.; Wood, B. R.; Bell, A. T.; Janicke, M. T.; Ott, K. C., X-ray absorption fine structure analysis of the local environment of Fe in Fe/Al-MFI. *Journal of Physical Chemistry B* **2004,** 108, (26), 8970-8975.
81. Choi, S. H.; Wood, B. R.; Ryder, J. A.; Bell, A. T., X-ray absorption fine structure characterization of the local structure of Fe in Fe-ZSM-5. *Journal of Physical Chemistry B* **2003,** 107, (43), 11843-11851.
82. Joyner, R.; Stockenhuber, M., Preparation, characterization, and performance of Fe-ZSM-5 catalysts. *Journal of Physical Chemistry B* **1999,** 103, (29), 5963-5976.
83. Hensen, E. J. M.; Zhu, Q.; Hendrix, M.; Overweg, A. R.; Kooyman, P. J.; Sychev, M. V.; van Santen, R. A., Effect of high-temperature treatment on Fe/ZSM-5 prepared by chemical vapor deposition of $FeCl_3I$. Physicochemical characterization. *Journal of Catalysis* **2004,** 221, (2), 560-574.
84. Perez-Ramirez, J.; Mul, G.; Kapteijn, F.; Moulijn, J. A.; Overweg, A. R.; Domenech, A.; Ribera, A.; Arends, I., Physicochemical characterization of isomorphously substituted FeZSM-5 during activation. *Journal of Catalysis* **2002,** 207, (1), 113-126.
85. Berlier, G.; Spoto, G.; Bordiga, S.; Ricchiardi, G.; Fisicaro, P.; Zecchina, A.; Rossetti, I.; Selli, E.; Forni, L.; Giamello, E.; Lamberti, C., Evolution of extraframework iron species in Fe silicalite 1. Effect of Fe content, activation temperature, and interaction with redox agents. *Journal of Catalysis* **2002,** 208, (1), 64-82.
86. Fejes, P.; Lazar, K.; Marsi, I.; Rockenbauer, A.; Korecz, L.; Nagy, J. B.; Perathoner, S.; Centi, G., Isomorphously substituted Fe-ZSM-5 zeolites as catalysts causes of catalyst ageing as revealed by X-band EPR, Mossbauer and Si-29 MAS NMR spectra. *Applied Catalysis A-General* **2003,** 252, (1), 75-90.

87. Kumar, M. S.; Schwidder, M.; Grunert, W.; Bruckner, A., On the nature of different iron sites and their catalytic role in Fe-ZSM-5 DeNO(x) catalysts: new insights by a combined EPR and UV/VIS spectroscopic approach. *Journal of Catalysis* **2004,** 227, (2), 384-397.
88. Marturano, P.; Drozdova, L.; Kogelbauer, A.; Prins, R., Fe/ZSM-5 prepared by sublimation of $FeCl_3$: The structure of the Fe species as determined by IR, Al-27 MAS NMR, and EXAFS spectroscopy. *Journal of Catalysis* **2000,** 192, (1), 236-247.
89. Perez-Ramirez, J.; Kapteijn, F.; Groen, J. C.; Domenech, A.; Mul, G.; Moulijn, J. A., Steam-activated FeMFI zeolites. Evolution of iron species and activity in direct N_2O decomposition. *Journal of Catalysis* **2003,** 214, (1), 33-45.
90. Zhu, Q.; Mojet, B. L.; Janssen, R. A. J.; Hensen, E. J. M.; van Grondelle, J.; Magusin, P.; van Santen, R. A., N_2O decomposition over Fe/ZSM-5: effect of high-temperature calcination and steaming. *Catalysis Letters* **2002,** 81, (3-4), 205-212.
91. El-Malki, E. M.; van Santen, R. A.; Sachtler, W. M. H., Active sites in Fe/MFI catalysts for NO_x reduction and oscillating N_2O decomposition. *Journal of Catalysis* **2000,** 196, (2), 212-223.
92. Perez-Ramirez, J.; Kapteijn, F.; Mul, G.; Moulijn, J. A., NO-assisted N_2O decomposition over Fe-based catalysts: Effects of gas-phase composition and catalyst constitution. *Journal of Catalysis* **2002,** 208, (1), 211-223.
93. Pirngruber, G. D., The surface chemistry of N_2O decomposition on iron containing zeolites (I). *Journal of Catalysis* **2003,** 219, (2), 456-463.
94. Kondratenko, E. V.; Perez-Ramirez, J., Mechanism and kinetics of direct N_2O decomposition over Fe-MFI zeolites with different iron speciation from temporal analysis of products. *Journal of Physical Chemistry B* **2006,** 110, (45), 22586-22595.
95. Mul, G.; Perez-Ramirez, J.; Kapteijn, F.; Moulijn, J. A., NO-assisted N_2O decomposition over ex-framework FeZSM-5: mechanistic aspects. *Catalysis Letters* **2001,** 77, (1-3), 7-13.
96. Wood, B. R.; Reimer, J. A.; Bell, A. T.; Janicke, M. T.; Ott, K. C., Nitrous oxide decomposition and surface oxygen formation on Fe-ZSM-5. *Journal of Catalysis* **2004,** 224, (1), 148-155.
97. Heyden, A.; Bell, A. T.; Keil, F. J., Kinetic modeling of nitrous oxide decomposition on Fe-ZSM-5 based on parameters obtained from first-principles calculations. *Journal of Catalysis* **2005,** 233, (1), 26-35.
98. Heyden, A.; Hansen, N.; Bell, A. T.; Keil, F. J., Nitrous oxide decomposition over Fe-ZSM-5 in the presence of nitric oxide: A comprehensive DFT study. *Journal of Physical Chemistry B* **2006,** 110, (34), 17096-17114.
99. Fu, C. M.; Korchak, V. N.; Hall, W. K., Decomposition of Nitrous-Oxide on Fey Zeolite. *Journal of Catalysis* **1981,** 68, (1), 166-171.
100. Kapteijn, F.; Marban, G.; RodriguezMirasol, J.; Moulijn, J. A., Kinetic analysis of the decomposition of nitrous oxide over ZSM-5 catalysts. *Journal of Catalysis* **1997,** 167, (1), 256-265.
101. Leglise, J.; Petunchi, J. O.; Hall, W. K., N_2O Decomposition over Iron-Exchanged Mordenite. *Journal of Catalysis* **1984,** 86, (2), 392-399.
102. Chang, Y. F.; McCarty, J. G.; Zhang, Y. L., N_2O Decomposition over [Fe]-ZSM-5 and Fe-HZSM-5 Zeolites. *Catalysis Letters* **1995,** 34, (1-2), 163-177.
103. Heyden, A.; Peters, B.; Bell, A. T.; Keil, F. J., Comprehensive DFT study of nitrous oxide decomposition over Fe-ZSM-5. *Journal of Physical Chemistry B* **2005,** 109, (5), 1857-1873.

104. Kiwi-Minsker, L.; Bulushev, D. A.; Renken, A., Low temperature decomposition of nitrous oxide over Fe/ZSM-5: Modelling of the dynamic behaviour. *Catalysis Today* **2005,** 110, (3-4), 191-198.
105. Pirngruber, G. D.; Luechinger, M.; Roy, P. K.; Cecchetto, A.; Smirniotis, P., N_2O decomposition over iron-containing zeolites prepared by different methods: a comparison of the reaction mechanism. *Journal of Catalysis* **2004,** 224, (2), 429-440.
106. Kondratenko, E.; Perez-Ramirez, J., Micro-kinetic analysis of direct N_2O decomposition over steam-activated Fe-silicalite from transient experiments in the TAP reactor. *Catalysis Today* **2006,** in press.
107. El-Malki, E. M.; van Santen, R. A.; Sachtler, W. M. H., Isothermal oscillations during N_2O decomposition over Fe/ZSM-5: effect of H_2O vapor. *Microporous and Mesoporous Materials* **2000,** 35-6, 235-244.
108. Grubert, G.; Hudson, M. J.; Joyner, R. W.; Stockenhuber, M., The room temperature, stoichiometric conversion of N_2O to adsorbed NO by Fe-MCM-41 and Fe-ZSM-5. *Journal of Catalysis* **2000,** 196, (1), 126-133.
109. Novakova, J.; Sobalik, Z., N_2O decomposition and formation of NO_x species on fe-ferrierite. Effect of NO and CO addition on the decomposition and the role of surface species. *Catalysis Letters* **2005,** 105, (3-4), 169-177.
110. Bulushev, D. A.; Renken, A.; Kiwi-Minsker, L., Formation of the surface NO during N_2O interaction at low temperature with iron-containing ZSM-5. *Journal of Physical Chemistry B* **2006,** 110, (1), 305-312.
111. Sang, C. M.; Kim, B. H.; Lund, C. R. F., Effect of NO upon N_2O decomposition over Fe/ZSM-5 with low iron loading. *Journal of Physical Chemistry B* **2005,** 109, (6), 2295-2301.
112. Kogel, M.; Abu-Zied, B. M.; Schwefer, M.; Turek, T., The effect of NO_x on the catalytic decomposition of nitrous oxide over Fe-MFI zeolites. *Catalysis Communications* **2001,** 2, (9), 273-276.
113. Smeets, P. J.; Groothaert, M. H.; Van Teeffelen, R. M.; Leeman, H.; Hensen, E. H. M.; Schoonheydt, R. A., Direct NO and N_2O decomposition and NO-assisted N_2O decomposition over Cu-zeolites: Elucidating the influence of the Cu-Cu distance on oxygen migration. *Journal of Catalysis* **2007,** 245, 356-366.
114. Sang, C. M.; Lund, C. R. F., Possible role of nitrite/nitrate redox cycles in N_2O decomposition and light-off over Fe-ZSM-5. *Catalysis Letters* **2001,** 73, (1), 73-77.
115. Pirngruber, G. D.; Pieterse, J. A. Z., The positive effect of NO on the N_2O decomposition activity of Fe-ZSM-5: A combined kinetic and in situ IR spectroscopic study. *Journal of Catalysis* **2006,** 237, (2), 237-247.
116. Lobree, L. J.; Hwang, I. C.; Reimer, J. A.; Bell, A. T., An in situ infrared study of NO reduction by C_3H_8 over Fe-ZSM-5. *Catalysis Letters* **1999,** 63, (3-4), 233-240.
117. Kaucky, D.; Sobalik, Z.; Schwarze, M.; Vondrova, A.; Wichterlova, B., Effect of FeH-zeolite structure and Al-Lewis sites on N_2O decomposition and NO/NO_2-assisted reaction. *Journal of Catalysis* **2006,** 238, (2), 293-300.
118. Novakova, J.; Sobalik, Z., Comparison of O-18 isotopic exchange after and during the interaction of N_2O, NO, and NO_2 with Fe ions in ferrierites. *Catalysis Letters* **2003,** 89, (3-4), 243-247.
119. Kumar, A. S.; Perez-Ramirez, J.; Debbagh, M. N.; Smarsly, B.; Bentrup, U.; Bruckner, A., Evidence of the vital role of the pore network on various catalytic conversions of N_2O over Fe-silicalite and Fe-SBA-15 with the same iron constitution. *Applied Catalysis B-Environmental* **2006,** 62, (3-4), 244-254.
120. Pieterse, J. A. Z.; Pirngruber, G. D.; Vansanten, R. A.; Booneveld, S., Hydrothermal stability of Fe-ZSM-5 and Fe-BEA prepared by wet ion-exchange for N_2O decomposition. *Applied Catalysis B: Environmental* **2006,** 71, 16-22.

121. Perez-Ramirez, J.; Gallardo-Llamas, A., Framework composition effects on the performance of steam-activated FeMFI zeolites in the N_2O-mediated propane oxidative dehydrogenation to propylene. *Journal of Physical Chemistry B* **2005,** 109, (43), 20529-20538.
122. Turek, T., Kinetic oscillations during the catalytic decomposition of nitrous oxide. *Catalysis Today* **2005,** 105, (2), 275-282.
123. Tanaka, S.; Yuzaki, K.; Ito, S.; Kameoka, S.; Kunimori, K., Mechanism of O-2 desorption during N_2O decomposition on an oxidized Rh/USY catalyst. *Journal of Catalysis* **2001,** 200, (2), 203-208.
124. Guzman-Vargas, A.; Delahay, G.; Coq, B., Catalytic decomposition of N_2O and catalytic reduction of N_2O and N_2O+NO by NH_3 in the presence of O_2 over Fe-zeolite. *Applied Catalysis B-Environmental* **2003,** 42, (4), 369-379.
125. Oygarden, A. H.; Perez-Ramirez, J., Activity of commercial zeolites with iron impurities in direct N_2O decomposition. *Applied Catalysis B-Environmental* **2006,** 65, (1-2), 163-167.
126. Hahn, T.; Lintz, H. G.; Omay, I. Y. E.; Zambranamontan, E., Kinetics of a Nitrous-Oxide Carbon-Monoxide Interaction on Polycrystalline Platinum, Palladium and Rhodium Foils at Low-Pressures. *Zeitschrift Fur Physikalische Chemie-International Journal of Research in Physical Chemistry & Chemical Physics* **1994,** 186, 195-213.
127. Hinshelwood, C. N.; Prichard, C. R., A comparison between the homogeneous thermal decomposition of nitrous oxide and its heterogeneous catalytic decomposition on the surface of platinum. *Journal of the Chemical Society* **1925,** 127, 327-336.
128. Takoudis, C. G.; Schmidt, L. D., Kinetics of N_2O Decomposition on Polycrystalline Platinum. *Journal of Catalysis* **1983,** 80, (2), 274-279.
129. Granger, P.; Malfoy, P.; Leclercq, G., Kinetics of the CO+N_2O reaction over noble metals - II. Rh/Al_2O_3 and Pt-Rh/Al_2O_3. *Journal of Catalysis* **2004,** 223, (1), 142-151.
130. Tanaka, S.; Yuzaki, K.; Ito, S.; Uetsuka, H.; Kameoka, S.; Kunimori, K., Mechanism of N_2O decomposition over a Rh black catalyst studied by a tracer method - The reaction of N_2O with O-18(a). *Catalysis Today* **2000,** 63, (2-4), 413-418.
131. Kondratenko, E. V.; Perez-Ramirez, J., Transient studies of direct N_2O decomposition over Pt-Rh gauze catalyst. Mechanistic and kinetic aspects of oxygen formation. *Catalysis Letters* **2003,** 91, (3-4), 211-216.
132. Centi, G.; Perathoner, S.; Vazzana, F.; Marella, M.; Tomaselli, M.; Mantegazza, M., Novel catalysts and catalytic technologies for N_2O removal from industrial emissions containing O_2, H_2O and SO_2. *Advances in Environmental Research* **2000,** 4, (4), 325-338.
133. Perez-Ramirez, J.; Kapteijn, F.; Mul, G.; Moulijn, J. A., Superior performance of ex-framework FeZSM-5 in direct N_2O decomposition in tail-gases from nitric acid plants. *Chemical Communications* **2001**, (8), 693-694.
134. Perez-Ramirez, J.; Kapteijn, F.; Mul, G.; Moulijn, J. A., Highly active SO_2-resistant ex-framework FeMFI catalysts for direct N_2O decomposition. *Applied Catalysis B-Environmental* **2002,** 35, (3), 227-234.
135. Pirngruber, G. D.; Frunz, L.; Pieterse, J. A. Z., The synergy between Fe and Ru in N_2O decomposition over FeRu-FER catalysts: A mechanistic explanation. *Journal of Catalysis* **2006,** 243, (2), 340-349.

136. Pieterse, J. A. Z.; Mul, G.; Melian-Cabrera, I.; van den Brink, R. W., Synergy between metals in bimetallic zeolite supported catalyst for NO-promoted N_2O decomposition. *Catalysis Letters* **2005,** 99, (1-2), 41-44.
137. Weitkamp, J.; Puppe, L., *Catalysis and Zeolites*. Springer-Verlag: Berlin Heidelberg, 1999.
138. Baerlocher, C.; Meier, W. M.; Olson, D. H., *Atlas of Zeolite Framework Types*. 5th revised ed.; Elsevier Science B.V.: Amsterdam, 2001.
139. Argauer, R. J.; Landolt, G. R. US Pat 3702886, 1972.
140. Flanigen, E. M.; Bennett, J. M.; Grose, R. W.; Cohen, J. P.; Patton, R. L.; Kirchner, R. M.; Smith, J. V., Silicalite, a New Hydrophobic Crystalline Silica Molecular-Sieve. *Nature* **1978,** 271, (5645), 512-516.
141. Roland, E.; Kleinschmit, P., *Ullmann's Encyclopedia*. VCH Wiley: 2000.
142. Kärger, J.; Ruthven, D. M., *Diffusion in zeolites*. John Wiley & Sons: New York, 1992.
143. Yuranov, I.; Bulushev, D. A.; Renken, A.; Kiwi-Minsker, L., Benzene hydroxylation over FeZSM-5 catalysts: which Fe sites are active? *Journal of Catalysis* **2004,** 227, (1), 138-147.
144. Mohamed, M. M.; Ali, I. O.; Eissa, N. A., Effect of thermal treatment on surface and bulk properties of Fe/ZSM-5 zeolites prepared by different methods. *Microporous and Mesoporous Materials* **2005,** 87, (2), 93-102.
145. Chen, H. Y.; Sachtler, W. M. H., Activity and durability of Fe/ZSM-5 catalysts for lean burn NO_x reduction in the presence of water vapor. *Catalysis Today* **1998,** 42, (1-2), 73-83.
146. Chen, H. Y.; Sachtler, W. M. H., Promoted Fe/ZSM-5 catalysts prepared by sublimation: de-NO_x activity and durability in H_2O-rich streams. *Catalysis Letters* **1998,** 50, (3-4), 125-130.
147. Pirngruber, G. D.; Roy, P. K.; Weiher, N., An in situ x-ray absorption spectroscopy study of N_2O decomposition over Fe-ZSM-5 prepared by chemical vapor deposition of $FeCl_3$. *Journal of Physical Chemistry B* **2004,** 108, (36), 13746-13754.
148. Sun, K. Q.; Xia, H.; Hensen, E.; van Santen, R.; Li, C., Chemistry of N_2O decomposition on active sites with different nature: Effect of high-temperature treatment of Fe/ZSM-5. *Journal of Catalysis* **2006,** 238, (1), 186-195.
149. Bitter, J. H.; Battiston, A. A.; van Donk, S.; de Jong, K. P.; Koningsberger, D. C., Accessibility of the Fe-species in Fe/ZSM-5 prepared via $FeCl_3$ sublimation. *Microporous and Mesoporous Materials* **2003,** 64, (1-3), 175-184.
150. Melian-Cabrera, I.; Espinosa, S.; Groen, J. C.; van de Linden, B.; Kapteijn, F.; Moulijn, J. A., Utilizing full-exchange capacity of zeolites by alkaline leaching: Preparation of Fe-ZSM5 and application in N_2O decomposition. *Journal of Catalysis* **2006,** 238, (2), 250-259.
151. Roy, P. K.; Pirngruber, G. D., The surface chemistry of N_2O decomposition on iron-containing zeolites(II) - The effect of high-temperature pretreatments. *Journal of Catalysis* **2004,** 227, (1), 164-174.
152. Zhu, Q.; van Teeffelen, R. M.; van Santen, R. A.; Hensen, E. J. M., Effect of high-temperature treatment on Fe/ZSM-5 prepared by chemical vapor deposition of $FeCl_3$II. Nitrous oxide decomposition, selective oxidation of benzene to phenol, and selective reduction of nitric oxide by isobutane. *Journal of Catalysis* **2004,** 221, (2), 575-583.
153. Koranyi, T. I.; Vandeven, L. J. M.; Welters, W. J. J.; Dehaan, J. W.; Debeer, V. H. J.; Vansanten, R. A., Comparison of (Non)-Sulfided Ninay-Zeolite Catalysts

Prepared by Ion-Exchange and Impregnation by Xenon Adsorption and Xe-129 Nmr. *Catalysis Letters* **1993,** 17, (1-2), 105-116.
154. Dubkov, K. A.; Starokon, E. V.; Paukshtis, E. A.; Volodin, A. M.; Panov, G. I., Mechanism of the low-temperature interaction of hydrogen with alpha-oxygen on FeZSM-5 zeolite. *Kinetics and Catalysis* **2004,** 45, (2), 202-208.
155. Kiwi-Minsker, L.; Bulushev, D. A.; Renken, A., Transient response method for characterization of active sites in HZSM-5 with low content of iron during N_2O decomposition. *Catalysis Today* **2004,** 91-92, 165-170.
156. Jia, J. F.; Wen, B.; Sachtler, W. M. H., Identification by isotopic exchange of oxygen deposited on Fe/MFI by decomposing N_2O. *Journal of Catalysis* **2002,** 210, (2), 453-459.
157. Jia, C.; Massiani, P.; Barthomeuf, D., Characterization by Infrared and Nuclear-Magnetic-Resonance Spectroscopies of Calcined Beta-Zeolite. *Journal of the Chemical Society-Faraday Transactions* **1993,** 89, (19), 3659-3665.
158. Kobayashi, H.; Kobayashi, M., Transient-Response Method in Heterogeneous Catalysis. *Catalysis Reviews-Science and Engineering* **1974,** 10, (2), 139-176.
159. Chorkendorff, I.; Niemantsverdriet, J. W., *Concepts of Modern Catalysis And Kinetics*. Wiley-VCH Verlag: Weinheim, 2003.
160. Gleaves, J. T.; Ebner, J. R.; Kuechler, T. C., Temporal Analysis Of Products (Tap) - A Unique Catalyst Evaluation System With Submillisecond Time Resolution. *Catalysis Reviews-Science And Engineering* **1988,** 30, (1), 49-116.
161. Gleaves, J. T.; Yablonskii, G. S.; Phanawadee, P.; Schuurman, Y., TAP-2: An interrogative kinetics approach. *Applied Catalysis A-General* **1997,** 160, (1), 55-88.
162. Nijhuis, T. A.; Makkee, M.; van Langeveld, A. D.; Moulijn, J. A., New insight in the platinum-catalyzed CO oxidation kinetic mechanism by using an advanced TAP. *Applied Catalysis A-General* **1997,** 164, (1-2), 237-249.
163. Nijhuis, T. A.; van den Broeke, L. J. P.; Linders, M. J. G.; van de Graaf, J. M.; Kapteijn, F.; Makkee, M.; Moulijn, J. A., Measurement and modeling of the transient adsorption, desorption and diffusion processes in microporous materials. *Chemical Engineering Science* **1999,** 54, (20), 4423-4436.
164. Yablonsky, G. S.; Olea, M.; Marin, G. B., Temporal analysis of products: basic principles, applications, and theory. *Journal of Catalysis* **2003,** 216, (1-2), 120-134.
165. Constales, D.; Shekhtman, S. O.; Yablonsky, G. S.; Marin, G. B.; Gleaves, J. T., Multi-zone TAP-reactors theory and application - IV. Ideal and non-ideal boundary conditions. *Chemical Engineering Science* **2006,** 61, (6), 1878-1891.
166. Fushimi, R.; Gleaves, J. T.; Yablonsky, G. S.; Gaffney, A.; Clark, M.; Han, S., Combining TAP-2 experiments with atomic beam deposition of Pd on quartz particles. *Catalysis Today* **2006,** in press.
167. Yablonsky, G. S.; Shekhtman, S. O.; Phanawadee, P.; Gleaves, J. T., General expression for primary characterization of catalyst activity using TAP pulse response experiment. *Catalysis Today* **2001,** 64, (3-4), 227-231.
168. Shekhtman, S. O.; Yablonsky, G. S.; Chen, S.; Gleaves, J. T., Thin-zone TAP-reactor - theory and application. *Chemical Engineering Science* **1999,** 54, (20), 4371-4378.
169. Olafsen, A.; Slagern, A.; Dahl, I. M.; Olsbye, U.; Schuurman, Y.; Mirodatos, C., Mechanistic features for propane reforming by carbon dioxide over a Ni/Mg(Al)O hydrotalcite-derived catalyst. *Journal of Catalysis* **2005,** 229, (1), 163-175.
170. Pantazidis, A.; Bucholz, S. A.; Zanthoff, H. W.; Schuurman, Y.; Mirodatos, C., A TAP reactor investigation of the oxidative dehydrogenation of propane over a V-Mg-O catalyst. *Catalysis Today* **1998,** 40, (2-3), 207-214.

171. Dewaele, O.; Geers, V. L.; Froment, G. F.; Marin, G. B., The conversion of methanol to olefins: a transient kinetic study. *Chemical Engineering Science* **1999,** 54, (20), 4385-4395.
172. Hinrichsen, O.; Van Veen, A. C.; Zanthoff, H. W.; Muhler, M., TAP Reactor Studies. In *In-Situ Spectroscopy in Heterogeneous Catalysis*, Haw, J. F., Ed. Wiley VCH Verlag: Weinheim, 2002; pp 237-269.
173. Perez-Ramirez, J.; Kondratenko, E. V.; Debbagh, M. N., Transient studies on the mechanism of N_2O activation and reaction with CO and C_3H_8 over Fe-silicalite. *Journal of Catalysis* **2005,** 233, (2), 442-452.
174. Vaccaro, A. R.; Mul, G.; Perez-Ramirez, J.; Moulijn, J. A., On the activation of Pt/Al_2O_3 catalysts in HC-SCR by sintering: determination of redox-active sites using Multitrack. *Applied Catalysis B-Environmental* **2003,** 46, (4), 687-702.
175. Olea, M.; Kunitake, M.; Shido, T.; Asakura, K.; Iwasawa, Y., Temporal analysis of products (TAP) study of the adsorption of CO, O_2, and CO_2 on a Au/Ti(OH)(4)* catalyst. *Bulletin of the Chemical Society of Japan* **2001,** 74, (2), 255-265.
176. Kabin, K. S.; Khanna, P.; Muncrief, R. L.; Medhekar, V.; Harold, M. P., Monolith and TAP reactor studies of NO_X storage on $Pt/BaO/Al_2O_3$: Elucidating the mechanistic pathways and roles of Pt. *Catalysis Today* **2006,** 114, (1), 72-85.
177. Shekhtman, S. O.; Yablonsky, G. S.; Gleaves, J. T.; Fushimi, R., "State defining" experiment in chemical kinetics - primary characterization of catalyst activity in a TAP experiment. *Chemical Engineering Science* **2003,** 58, (21), 4843-4859.
178. Mergler, Y. J.; Hoebink, J.; Nieuwenhuys, B. E., CO oxidation over a $Pt/CoO_x/SiO_2$ catalyst: A study using temporal analysis of products. *Journal of Catalysis* **1997,** 167, (2), 305-313.
179. Schuurman, Y.; Marquez-Alvarez, C.; Kroll, V. C. H.; Mirodatos, C., Unraveling mechanistic features for the methane reforming by carbon dioxide over different metals and supports by TAP experiments. *Catalysis Today* **1998,** 46, (2-3), 185-192.
180. Fathi, M.; Monnet, F.; Schuurman, Y.; Holmen, A.; Mirodatos, C., Reactive oxygen species on platinum gauzes during partial oxidation of methane into synthesis gas. *Journal of Catalysis* **2000,** 190, (2), 439-445.
181. Goguet, A.; Shekhtman, S. O.; Burch, R.; Hardacre, C.; Meunier, F. C.; Yablonsky, G. S., Pulse-response TAP studies of the reverse water-gas shift reaction over a Pt/CeO_2 catalyst. *Journal of Catalysis* **2006,** 237, (1), 102.
182. Gleaves, J. T.; Sault, A. G.; Madix, R. J.; Ebner, J. R., Ethylene Oxidation on Silver Powder - a Tap Reactor Study. *Journal of Catalysis* **1990,** 121, (1), 202-218.
183. Olofsson, G.; Hinz, A.; Andersson, A., A transient response study of the selective catalytic oxidation of ammonia to nitrogen on $Pt/CuO/Al_2O_3$. *Chemical Engineering Science* **2004,** 59, (19), 4113-4123.
184. Rigas, N. C.; Svoboda, G. D.; Gleaves, J. T., Activation of Silver Powder for Ethylene Epoxidation at Vacuum and Atmospheric Pressures. *Acs Symposium Series* **1993,** 523, 183-203.
185. Fushimi, R.; Shekhtman, S. O.; Gaffney, A.; Han, S.; Yablonsky, G. S.; Gleaves, J. T., TAP vacuum pulse-response and normal-pressure studies of propane oxidation over MoVTeNb oxide catalysts. *Industrial & Engineering Chemistry Research* **2005,** 44, (16), 6310-6319.
186. Dewaele, O.; Froment, G. F., TAP study of the sorption of CO and CO_2 on gamma Al_2O_3. *Applied Catalysis A-General* **1999,** 185, (2), 203-210.
187. van Veen, A. C.; Hinrichsen, O.; Muhler, M., Mechanistic studies on the oxidative dehydrogenation of methanol over polycrystalline silver using the temporal-analysis-of-products approach. *Journal of Catalysis* **2002,** 210, (1), 53-66.

188. Hinz, A.; Andersson, A., Propane ammoxidation on an Al-Sb-V-W-oxide catalyst. A mechanistic study using the TAP-2 reactor system. *Chemical Engineering Science* **1999,** 54, (20), 4407-4421.
189. Constales, D.; Yablonsky, G. S.; Marin, G. B.; Gleaves, J. T., Multi-zone TAP-reactors theory and application: II. The three-dimensional theory. *Chemical Engineering Science* **2001,** 56, (5), 1913-1923.
190. Constales, D.; Yablonsky, G. S.; Marin, G. B.; Gleaves, J. T., Multi-zone TAP-reactors theory and application: I. The global transfer matrix equation. *Chemical Engineering Science* **2001,** 56, (1), 133-149.
191. Constales, D.; Yablonsky, G. S.; Marin, G. B.; Gleaves, J. T., Multi-zone TAP-reactors theory and application. III Multi-response theory and criteria of instantaneousness. *Chemical Engineering Science* **2004,** 59, (17), 3725-3736.
192. Shekhtman, S. O. Interrogative Kinetics a New Methodology for Catalyst Characterization. Washington University, Saint Louis, 2003.
193. Shekhtman, S. O.; Yablonsky, G. S., Thin-zone TAP reactor versus differential PFR: Analysis of concentration nonuniformity for gas-solid systems. *Industrial & Engineering Chemistry Research* **2005,** 44, (16), 6518-6522.
194. Yablonskii, G. S.; Shekhtman, S. O.; Chen, S. R.; Gleaves, J. T., Moment-based analysis of transient response catalytic studies (TAP experiment). *Industrial & Engineering Chemistry Research* **1998,** 37, (6), 2193-2202.
195. Jentys, A.; Mukti, R. R.; Tanaka, H.; Lercher, J. A., Energetic and entropic contributions controlling the sorption of benzene in zeolites. *Microporous and Mesoporous Materials* **2006,** 90, (1-3), 284-292.
196. Skoulidas, A. I.; Sholl, D. S., Kinetics of hard sphere and chain adsorption into circular and elliptical pores. *Journal of Chemical Physics* **2000,** 113, (10), 4379-4387.
197. Jentys, A.; Mukti, R. R.; Lercher, J. A., On the sticking probability of aromatic molecules on zeolites. Comment on "Sticking Probability on Zeolites". *Journal of Physical Chemistry B* **2006,** 110, (35), 17691-17693.
198. Delgado, J. A.; Nijhuis, T. A.; Kapteijn, F.; Moulijn, J. A., Determination of adsorption and diffusion parameters in zeolites through a structured approach. *Chemical Engineering Science* **2004,** 59, (12), 2477-2487.
199. Keipert, O. P.; Baerns, M., Determination of the intracrystalline diffusion coefficients of alkanes in H-ZSM-5 zeolite by a transient technique using the temporal-analysis-of-products (TAP) reactor. *Chemical Engineering Science* **1998,** 53, (20), 3623-3634.
200. van Veen, A. C.; Farrusseng, D.; Rebeilleau, M.; Decamp, T.; Holzwarth, A.; Schuurman, Y.; Mirodatos, C., Acceleration in catalyst development by fast transient kinetic investigation. *Journal of Catalysis* **2003,** 216, (1-2), 135-143.
201. Colaris, A. H. J.; Hoebink, J.; de Croon, M.; Schouten, J. C., Intrapellet diffusivities from TAP pulse responses via moment-based analysis. *Aiche Journal* **2002,** 48, (11), 2587-2596.
202. Li, W.; Xie, L.; Gao, L.; Zhao, X.; Hu, R.; Cheng, Y.; Wang, D., The measurement of gas diffusivity in porous materials by temporal analysis of products (TAP). *Catalysis Today* **2006,** 121, (3-4), 246-254.
203. Schuurman, Y.; Delattre, C.; Pitault, I.; Reymond, J. P.; Forissier, M., Effect of coke deposition on transport and sorption in FCC catalysts studied by temporal analysis of products. *Chemical Engineering Science* **2005,** 60, (4), 1007-1017.
204. Schuurman, Y.; Pantazidis, A.; Mirodatos, C., The TAP-2 reactor as an alternative tool for investigating FCC catalysts. *Chemical Engineering Science* **1999,** 54, (15-16), 3619-3625.

205. Schuurman, Y., Assessment of kinetic modeling procedures of TAP experiments. *Catalysis Today* **2006,** 121, (3-4), 187-196.
206. Huinink, J. P.; Hoebink, J.; Marin, G. B., Pulse experiments over catalyst beds: A window of measurable reaction rate coefficients. *Canadian Journal Of Chemical Engineering* **1996,** 74, (5), 580-585.
207. Wang, D. Z.; Li, F. X.; Zhao, X. L., Diffusion limitation in fast transient experiments. *Chemical Engineering Science* **2004,** 59, (22-23), 5615-5622.
208. Phanawadee, P.; Phongaksorn, M.; Chaimongkol, N.; Jaree, A.; Limtrakul, J., Mathematical analysis of TAP models for porous catalysts. *Chemical Engineering Journal* **2005,** 115, (1-2), 51-62.

Chapter 3

EXPERIMENTAL PART

3.1. Studied Catalysts

Three different ZSM-5 zeolites were used in the present study. Extrudates, Fe-ZSM-5_{5500}, were kindly provided by Zeochem AG (Uetikon, Switzerland). They were found to contain 5500 ppm of iron as an impurity originating from a binder used for pelletizing. The zeolite was calcined in a flow of He (60 ml (STP)/min) for 1 h at 1323 K for activation.

The isomorphously substituted ZSM-5 containing 350 ppm Fe (Fe-ZSM-5_{350}) was synthesized via hydrothermal route [1]. The hydrothermal synthesis for the Fe-ZSM-5_{200} containing 200 ppm Fe and its characterization is described elsewhere [2,3]. It is important to note that an iron source was not added intentionally to the synthesis solution in order to obtain zeolite samples containing a "natural" impurity level of Fe. Therefore, the Fe-ZSM-5_{200} was prepared with deionized water. The catalysts were activated by heating at 1323 K in He (50 ml (STP)/min) for 1 h and 8 h, respectively. The main characteristics of the parent zeolites are summarized in Table 3.1.

Table 3.1: Main characteristics of the studied Fe-ZSM-5 catalysts.

Catalyst	*Fe loading, wt%*	*Si/Al ratio*	*Method of catalyst activation*	Fe(II) sites, 10^{18} sites/g		
				$C_{Fe}^{N_2O}$	C_{Fe}^{TPD}	C_{Fe}^{CO}
Fe-ZSM-5_{200}	0.020	42	1323 K, 8h in He	2.0	1.2	1.4
Fe-ZSM-5_{350}	0.035	42	1323 K, 1h in He	2.8	1.9	2.06
Fe-ZSM-5_{5500}	0.550	25	1323 K, 1h in He	3.4	2.6	2.6

The active Fe(II) sites concentrations listed in Table 3.1 were determined by D. Bulushev in transient response experiments with the Micromeritics AutoChem 2910 analyzer. The fraction of iron sites involved in the formation of surface oxygen, $(O)_{Fe}$, from N_2O was measured via transient response methods during N_2O decomposition over the catalyst at 523 K. The determination of the active sites concentration, abbreviated as $C_{Fe}^{N_2O}$, is discussed in detail in section 5.2. The deposited oxygen, which is able to recombine forming O_2, and the concentration of the corresponding Fe(II) sites, C_{Fe}^{TPD}, were estimated from the amount of molecular oxygen evolved during temperature-programmed desorption (523-873 K). The deposited oxygen, which is active in low-temperature CO oxidation, C_{Fe}^{CO}, was measured via the transient response of CO_2 during CO oxidation at 523 K. These methods were described in detail elsewhere [4]. Studies of the N_2O decomposition [4-9] and the hydroxylation of benzene to phenol with N_2O [1, 3] were already published with the catalysts summarized in Table 3.1.

3.2. Temporal Analysis of Products

3.2.1. Setup

The interaction of N_2O, CO, NO, NO_2, H_2O and O_2 with iron containing ZSM-5 and its surface species were investigated by multi-pulse, pump-probe and temperature-programmed desorption experiments in a TAP-2 setup [10] pictured in Figure 3.1. It consists of the four main parts: a gas mixing station, a microreactor with four high-speed pulse valves, a vacuum system, and a mass spectrometer. A scheme of the main parts of the TAP setup is presented in Figure 3.2.

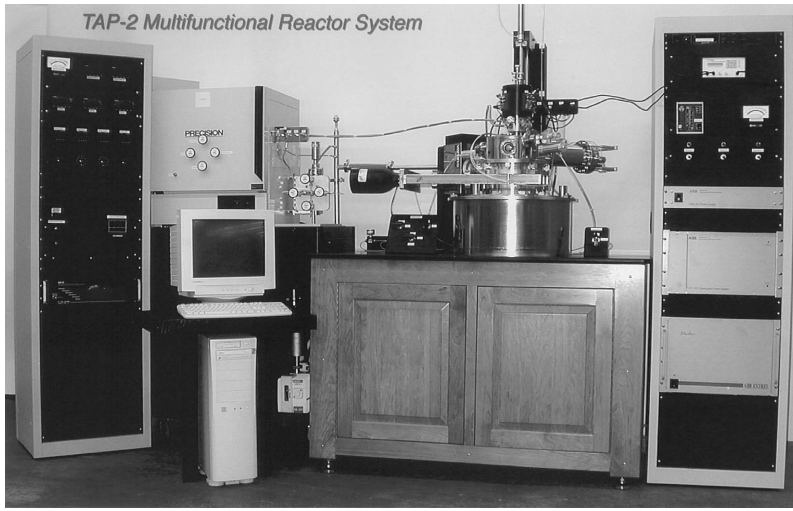

Figure 3.1: Photo of TAP-2 system. Courtesy of Prof. J.T. Gleaves.

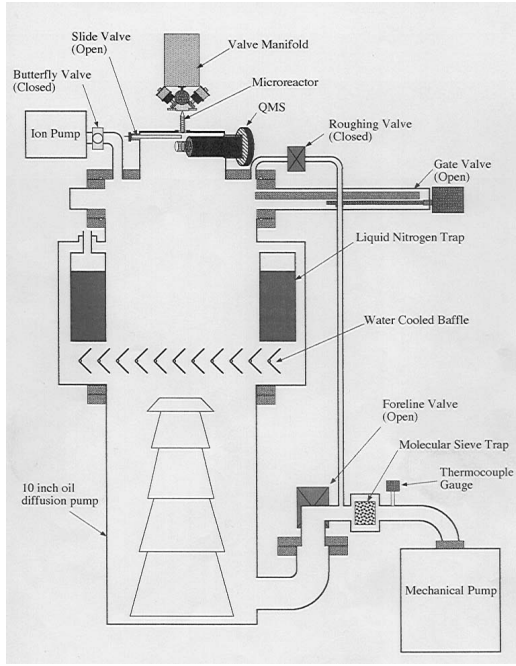

Figure 3.2: Scheme of TAP-2 system [10].

An enlarged image of the pulse valves, microreactor and the analyzer is presented in Figure 3.3.

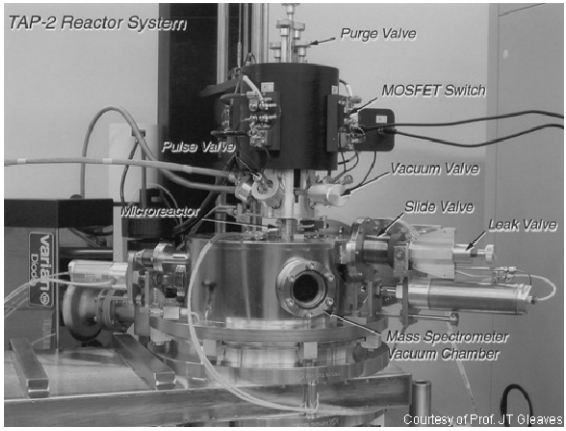

Figure 3.3: Photo of the TAP pulse valves, reactor and analyzer. Courtesy of Prof. J.T. Gleaves.

The tubular microreactor is constructed of stainless steel with an inner diameter of 6.4 mm and 31.8 mm in length. The entrance of this reactor seals via a small volume against the valve-manifold assembly through an O-ring. The reactor outlet is continuously evacuated by an oil diffusion pump that is pumped by a mechanical pump. The pulse valves allow a rapid injection of very small amounts of reactant with a typical pulse width between 80 and 200 μs into the microreactor. The responses of a reactant and products are recorded as a function of time with the quadrupole mass spectrometer (ABB Extrel) located directly underneath the reactor exit. Three gas blending stations serve to prepare certain gas mixtures and to determine the size of the gas pulse by means of a pressure transducer. Typical pulse intensities in vacuum experiments range from 10^{13} to 10^{17} molecules/pulse [10]. The purchased TAP system contained two gas blending stations and a third one was home-made with the same functionality as the original stations in order to be able to pulse three different reaction mixtures over the catalyst in a short period of time.

3.2.2. Description of the Experiments

A Fe-ZSM-5 layer of 50 mg was placed between two beds of quartz particles (200-250 μm particle size) and exposed to vacuum (< 10^{-5} Pa). The temperature of the reactor was measured by a thermocouple positioned in the centre of the catalyst bed. TAP experiments were carried out at 523 K, 593 K, 661 K, 703 K, 803 K and 946 K with different gas mixtures, which were introduced by pulses in the microreactor. Prior

to the measurements, the catalyst was evacuated in the TAP reactor at 946 K for 30 min, and then cooled to the studied temperature. This pre-treatment will be referred to from now on as "standard" in TAP experiments.

The utilized gases were provided by Carbagas (Lausanne, Switzerland) and are summarized in Table 3.2 with their purities and the typical inlet pulse size. Ar served as an inert tracer. The gas blends were produced on the basis of pure gases in the gas blend stations besides the CO and NO mixtures which were purchased already diluted with Ar. The inlet pulse size was calculated from the number of pulses necessary to reduce the pressure of a closed volume. The typical inlet pulse size of the utilized blends was small enough to allow the transport in the reactor to occur through Knudsen diffusion.

Water was dozed gaseous without Ar as tracer. About 50 ml of deionized water were filled into the gas blend reservoir, then the blend station and the feed line were evacuated and the whole gas blend station as well as all parts which lead to the reactor heated to 323 K. Water evaporates and saturates the void. The vapour pressure of 12,3 kPa is adjusted for water at 323 K [11].

Table 3.2: Gas blends for TAP studies, their purities and typical pulse size.

Gas mixture	*Purity of reactant gas*	*Pulse size, 10^{14} molecules/pulse*
Ar	> 99.998%	-
10 vol% CO in Ar	> 99.997%	5
80 vol% N_2 in Ar	> 99.995%	5
80 vol% N_2O in Ar	> 99.0%	5
10 vol% NO in Ar	> 99.9%	6.5
60 vol% NO_2 in Ar	> 99.0%	5.5
25 vol% O_2 in Ar	> 99.95%	1.5

System control and data acquisition are performed with a computer. A pulse is injected within 200 μs, depending on gas and reactor temperature, it takes from 100 ms to a few seconds to pass the reactor. The time period, called cycle time, between the pulse injection until the next pulse is kept constant and usually larger than the time the reactant needs to pass the reactor. To accurately capture these transients it is necessary to sample the reactor output at a submillisecond data acquisition rate. Since the ABB Extrel mass spectrometer requires at least one second for a typical spectral scan, it is not possible to collect high-speed transients. Consequently, vacuum pulse response data are obtained by fixing the mass to charge number at a specific value during a pulse and monitoring the change of the detector response as a function of time. During the following cycle another mass to charge ratio is registered. Reactant, reaction products and inert tracer are analyzed sequential in real-time using the MS. Thus, each collected transient response originates from another pulse. Since the amount of reactants in a

single pulse is much smaller than the amount of active sites a single pulse causes only a very small perturbation of the catalytic system. Several pulses are representative for one defined catalyst state. However, during a train of pulses the catalyst state can be gradually changed and the individual reactant or products response can change with pulse number.

Depending on the type of experiment the following mass to charge ratios (*m*/*e*) were registered simultaneously by the mass spectrometer: 18 (H_2O), 28 (N_2, N_2O, CO), 30 (NO, N_2O, NO_2), 32 (O_2), 40 (Ar), 44 (N_2O, CO_2), 46 (NO_2). The mass spectrometer was only calibrated for the titration of active sites discussed in section 5.2. Since there is no possibility to by-pass the reactor in the TAP system, the reactor content needs to be changed from the catalyst to an inert material for calibration. This takes too much time regarding the instability of mass spectrometer. Calibration factors with ± 30% error could be reached which is not satisfactory for quantification regarding the time and effort which was invested to obtain the calibration factors. Furthermore, the pulse size can only be determined by an indirect measurement via pressure drop in a closed volume correlated to a high number of pulses. This brings in an additional source of error. Therefore, the main part of this study was done without quantification of the transient responses.

In principle, three transient methods were applied:

1) A series of pulses from a single valve served for treating the catalyst with different reactants (N_2O, CO, NO, NO_2, H_2O). The reactant was introduced by repetitive pulsing. The cycle time was fixed in the range of 3 s to 15 s depending on the time the involved compounds needed to desorb. Fe-ZSM-5_{5500} was studied with large numbers of pulses so-called multi-pulses. The pulse responses of N_2O/Ar were investigated at a temperature range from 523 K to 946 K. N_2O and NO interactions at 523 K and 593 K with the catalyst were carried out in general with 600 pulses. NO_2 treatments at 523 K were performed with 300 pulses. H_2O was pulsed at 593 K and 703 K until the saturation of the catalyst was detected with the mass spectrometer. CO served as reducing agent for surface oxygen at 523 K and 593 K and was fed into the reactor as long as CO_2 was formed. O_2/Ar was only pulsed at 803 K.

2) In pump-probe experiments different reactant mixtures were introduced sequentially from separate pulse valves. One valve contained for example N_2O/Ar and the other valve either CO/Ar, H_2O/Ar or NO/Ar. The first reactant (usually N_2O, pump) formed intermediates on the catalyst during the first pulse. When the second reactant (e. g. CO, probe) was fed into the reactor, chemical reactions occurred and product formation is observed. The time delay between the first and second pulse was variable from 0.01 s to 9.5 s. The sequence was repeated and the total cycle time was fixed to 10 s or 20 s. The Fe-ZSM-5_{5500} was investigated by dual-pulse experiments at 523 K with N_2O/CO and at 803 K with N_2O/H_2O. The Fe-ZSM-5_{5500} and Fe-ZSM-5_{200}

were studied in N_2O/NO and NO/N_2O pump-probe experiments at 661 K, 803 K and 946 K.

3) Complementary, TPD (temperature-programmed desorption) experiments were carried out to gain information about surface species. Hence, after a defined sequence of pulses the catalyst temperature was increased linearly by 45 K/min from the studied temperature to 916 K in vacuum. Almost all multi-pulse experiments with the Fe-ZSM-5_{5500} at 523 K and 593 K were completed by a TPD run.

3.2.3. Preliminary Tests

Experimental pulse responses of the inert gas Ar were compared with criterions of the Knudsen regime in order to verify that the TAP-2 system was well adjusted. The beginning of the Knudsen regime was determined by lowering the pulse intensity and observing when the pulse shape becomes independent of the pulse intensity. Additionally, the Knudsen regime was evidenced by comparing the experimental response transformed to dimensionless form to the standard diffusion curve. If the curves match then the gas flow is in the Knudsen regime and the supposed boundary conditions are fulfilled.

For any TAP pulse response experiment that involves only gas transport (no reaction or adsorption) the plot of the dimensionless exit flow versus dimensionless time will give one curve regardless of the gas, bed length, particle size, or reactor temperature. The curve is called the standard diffusion curve (SDC) [10]. The dimensionless exit flow $\overline{F_{Ar}}$ as a function of dimensionless time τ is expressed in the following equation:

$$\overline{F_{Ar}} = \pi \sum_{m=0}^{\infty} (-1)^m (2m+1) \exp\left(-(m+0.5)^2 \pi^2 \tau\right) \tag{3.1}$$

The standard diffusion curve was generated with MATLAB® based on Equation (3.1) and is compared in Figure 3.4 to the dimensionless form of an experimental Ar response. Pure Ar was pulsed within 125 μs into the reactor filled with quartz particles (200-250 μm particle size) at 373 K. The peak height H_p of the area-normalized Ar flow was determined to 7.3 s^{-1}. The parameter k' was derived from the following equation:

$$H_p = 1.85 \frac{D_{eAr}}{\varepsilon_b L^2} \quad \Rightarrow \quad k' = \frac{D_{eAr}}{\varepsilon_b L^2} = \frac{H_p}{1.85} \tag{3.2}$$

The dimensionless form of the experimental Ar response was generated from the area-normalized Ar flow $\frac{F_{Ar}(t)}{N_{Ar}}$ by using the constant k and the following correlations:

$$\overline{F_{Ar}}(\tau) = \frac{\varepsilon_b L^2}{D_{eAr}} \cdot \frac{F_{Ar}(t)}{N_{Ar}} \quad and \quad \tau = t \cdot \frac{D_{eAr}}{\varepsilon_b L^2} \tag{3.3}$$

The dimensionless flow was derived by the product of the area-normalized flow and 1/k'. The dimensionless time was calculated by multiplying the time with k'. The theoretical standard diffusion curve and the dimensionless curve generated from an experimental Ar response in Figure 3.4 overlap perfectly. Therefore, it can be concluded that the gas flow was in the Knudsen regime.

Another way of distinguishing the Knudsen diffusion regime without having to determine the effective diffusivity of the gas, the length of the reactor, or the fractional voidage of the bed is the characteristics of the curve maximum. Provided the gas transport is in Knudsen diffusion regime, the product of peak height $\overline{F}_{Ar,p}$ and peak time τ_p is equal to 0.31 which is correct for the dimensionless curve generated from the experimental Ar response:

$$\overline{F}_{Ar,p} \cdot \tau_p = 0.31 \tag{3.4}$$

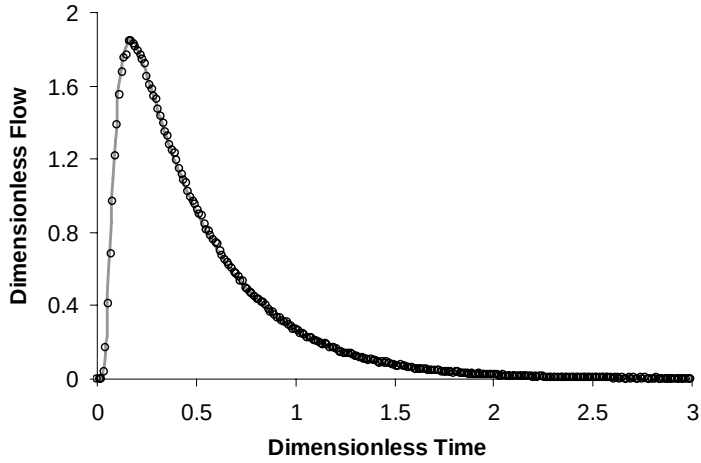

Figure 3.4: Standard diffusion curve (solid line) compared to dimensionless form of experimental Ar response (open symbols).

Further, experiments with different pulse valves and at different temperatures showed also the accordance between TAP theory and experimental response data. Figure 3.5 presents the results from an experiment in which Ar was pulsed over inert quartz pellets while the temperature was varied. The peak height H_p is plotted as a function of the square root of the temperature. In a diffusion controlled process the peak height H_p is directly proportional to the effective diffusion coefficient D_{eAr} which is a function of the square root of the temperature as shown in Equation (3.5). Thus, the data in Figure 3.5 should be a straight line. The results confirmed the Knudsen diffusion regime.

$$H_p = 1.85\frac{D_{eAr}}{\varepsilon_b L^2} \quad and \quad D_{eAr} = \frac{\varepsilon_b d_i}{\tau_b 3}\sqrt{\frac{8RT}{\pi M_{Ar}}} \quad \Rightarrow \quad H_p \sim \sqrt{T} \tag{3.5}$$

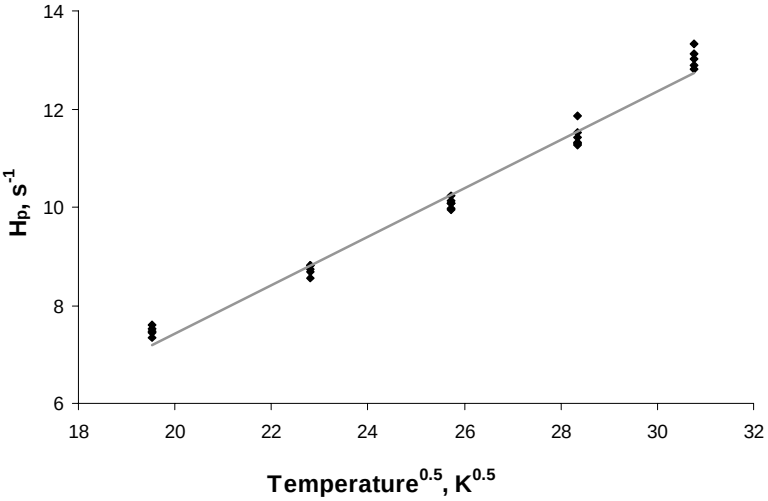

Figure 3.5: Peak height of area-normalized Ar response as function of the square rout of the reactor temperature.

The results in this section demonstrate the validity of the Knudsen flow assumptions for the experiments with an inert gas performed with the TAP-2 system. In particular, the functionality of the setup was proven therewith. However, the gas movement through the catalyst governed by Knudsen diffusion was not of first priority in this study since extensive micro kinetic modeling was not performed.

3.3. Micromeritics AutoChem 2910 Analyzer

All transient response experiments at atmospheric pressure were performed in a AutoChem 2910 analyzer (Micromeritics) illustrated in Figure 3.6.

Figure 3.6: Image of the Micromeritics AutoChem 2910 analyzer.

A simplified scheme of the analyzer is shown in Figure 3.7. It is provided with a ThermoStar 200 (Pfeiffer Vacuum) quadrupole mass spectrometer to analyze the composition of the gas phase. The setup as well as a fused silica capillary connected to the mass spectrometer were heated up to 383 K.

The following mass to charge ratios were monitored simultaneously by the mass spectrometer: 4 (He), 18 (H_2O), 28 (N_2, N_2O, CO), 30 (NO, N_2O, NO_2), 32 (O_2), 40 (Ar), 44 (N_2O, CO_2), 46 (NO_2). It was calibrated using gaseous mixtures of known compositions. Therefore, crawled data, gas concentrations, without the contribution of fragments of other gases are presented throughout the work from measurements with the Micromeritics analyzer. The utilised gas mixtures were provided by Carbagas (Lausanne, Switzerland), used without further purification and summarized in Table 3.3 with their purities. Ar served as an inert tracer and He as inert carrier gas. Other mixtures were created by mixing different gas blends or by diluting with He in the Micromeritics analyzer. The total flow rate of the different gas mixtures was kept always constant at 20 ml (STP)/min. Deionized water was pulsed on the catalyst using a 5 µl syringe via an injector into a 20 ml (STP)/min He flow. Adsorption of water was controlled by the mass spectrometer.

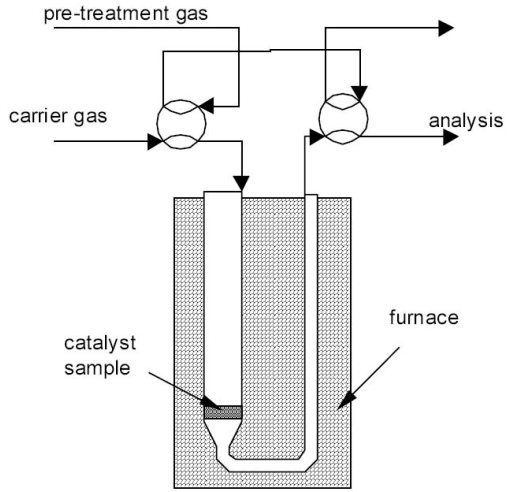

Figure 3.7: Scheme of the Micromeritics AutoChem 2910 analyzer.

0.40 g of Fe-ZSM-5 was placed in a quartz plug-flow reactor. Before every run the catalyst was pre-treated in He (50 ml (STP)/min) at 1323 K for 1 h, then cooled to the studied temperature. To this pre-treatment is hereafter referred as "standard" pre-treatment at atmospheric pressure. The reactor was purged by He (50 ml (STP)/min) for 10 min after each treatment in order to clean the feed lines and to desorb weakly adsorbed species from the catalyst.

Table 3.3: Utilized gas mixtures and their purities.

Gas mixture	*Purity of reactant gas*
Ar	> 99.998%
He	> 99.999%
3 vol% CO, 2 vol% Ar in He	> 99.997%
2 vol% CO_2 in He	> 99.998%
2 vol% N_2 in He	> 99.999%
2 vol% N_2O, 2 vol% Ar in He	> 99.998%
0.5 vol% NO, 0.5 vol% Ar in He	> 99.9%
0.5 vol% NO_2, 0.5 vol% Ar in He	> 99.0%
2 vol% O_2 in He	> 99.998%

Temperature-programmed desorption (TPD) measurements were performed in a He flow of 20 ml (STP)/min in the range of 523-1323 K with a 30 K/min ramp. During temperature-programmed reaction (TPR) studies the catalyst was heated in a He flow of 20 ml (STP)/min with 10 K/min.

The amounts of evolved gases in the transient flow, TPR and TPD runs were determined by integration of the measured curves. Transient response experiments at atmospheric pressure with the Micromeritics setup were performed mainly with NO_2 (chapter 7) and H_2O (chapter 8) as reactants investigating the Fe-ZSM-5_{5500} and Fe-ZSM-5_{350} at temperatures in the range of 523 K to 673 K. The amount of sites active in N_2O decomposition at 523 K of the Fe-ZSM-5_{5500} and of the Fe-ZSM-5_{350} are determined in section 5.2 and section 7.2, respectively. NO and O_2 flow experiments at 523 K with the Fe-ZSM-5_{350} are discussed in section 6.3.

3.4. Diffuse Reflectance Infrared Fourier Transform Spectroscopy

A Perkin-Elmer FTIR spectrometer with a MCT detector was used for the DRIFTS experiments. The Fe-ZSM-5_{350} (~0.015 g) ground in an agate mortar was placed into a cup of a SpectraTech 003-102 DRIFTS cell with CaF_2 windows. The cell was attached to a setup described earlier [12]. Pure Ar and a mixture of 0.5 vol% NO_2, 0.5 vol% Ar in He (purities in Table 3.3) were used with a flow rate of 20 ml (STP)/min to investigate the surface species formed on the catalyst from NO_2 at room temperature and 523 K. Before every run the activated catalyst was pre-treated in the cell in Ar at 823 K for 1 h. DRIFT spectra taken every 0.5 min were obtained by averaging 32 scans with a resolution of 4 cm^{-1}. A single beam spectrum of the catalyst before introduction of the NO_2 containing mixture into the cell at the studied temperature was taken as a background.

3.5. References

1. Yuranov, I.; Bulushev, D. A.; Renken, A.; Kiwi-Minsker, L., Benzene hydroxylation over FeZSM-5 catalysts: which Fe sites are active? *Journal of Catalysis* **2004,** 227, (1), 138-147.
2. Louis, B.; Tezel, C.; Kiwi-Minsker, L.; Renken, A., Synthesis of structured filamentous zeolite materials via ZSM-5 coatings of glass fibrous supports. *Catalysis Today* **2001,** 69, (1-4), 365-370.
3. Louis, B. PhD Thesis. EPFL, 2002.

4. Kiwi-Minsker, L.; Bulushev, D. A.; Renken, A., Active sites in HZSM-5 with low Fe content for the formation of surface oxygen by decomposing N_2O: is every deposited oxygen active? *Journal of Catalysis* **2003,** 219, (2), 273-285.
5. Bulushev, D. A.; Kiwi-Minsker, L.; Renken, A., Dynamics of N_2O decomposition over HZSM-5 with low Fe content. *Journal of Catalysis* **2004,** 222, (2), 389-396.
6. Bulushev, D. A.; Renken, A.; Kiwi-Minsker, L., Role of adsorbed NO in N_2O decomposition over iron-containing ZSM-5 catalysts at low temperatures. *Journal of Physical Chemistry B* **2006,** 110, (22), 10691-10700.
7. Bulushev, D. A.; Renken, A.; Kiwi-Minsker, L., Formation of the surface NO during N_2O interaction at low temperature with iron-containing ZSM-5. *Journal of Physical Chemistry B* **2006,** 110, (1), 305-312.
8. Kiwi-Minsker, L.; Bulushev, D. A.; Renken, A., Transient response method for characterization of active sites in HZSM-5 with low content of iron during N_2O decomposition. *Catalysis Today* **2004,** 91-92, 165-170.
9. Kiwi-Minsker, L.; Bulushev, D. A.; Renken, A., Low temperature decomposition of nitrous oxide over Fe/ZSM-5: Modelling of the dynamic behaviour. *Catalysis Today* **2005,** 110, (3-4), 191-198.
10. Gleaves, J. T.; Yablonskii, G. S.; Phanawadee, P.; Schuurman, Y., TAP-2: An interrogative kinetics approach. *Applied Catalysis A-General* **1997,** 160, (1), 55-88.
11. Haar, L.; Gallagher, J. S.; Kell, G. S., *NBS/NRC Steam Tables*. Hemisphere Publishing Corp.: New York, 1984.
12. Bulushev, D. A.; Kiwi-Minsker, L.; Renken, A., Vanadia/titania catalysts for gas phase partial toluene oxidation - Spectroscopic characterisation and transient kinetics study. *Catalysis Today* **2000,** 57, (3-4), 231-239.

Chapter 4

CO OXIDATION AS MEASURE FOR REACTIVITY OF SURFACE OXYGEN

N_2O decomposition over iron containing ZSM-5 has been suggested to proceed via Fe(II) transition to Fe (III) generating active oxygen species called by Panov and co-workers atomic "α-oxygen" [1, 2]. This oxygen is capable of selectively oxidizing benzene to phenol, CH_4 to methoxy species and H_2 to H_2O at low temperatures [3-5]. α-Oxygen possesses also high reactivity in converting CO to CO_2 at low temperatures (< 523 K) [6-9]. The ability of surface oxygen to oxidize CO is used in this manuscript as measure for its reactivity. If the deposited oxygen is able to oxidize CO it is considered as α-oxygen and will be symbolized by "$(O)_{Fe}$" with the suffix "Fe" standing for active iron site. Oxygen in brackets with another suffix signifies surface oxygen inactive in CO oxidation.

4.1. Reactivity of Oxygen Deposited by N_2O on Fe-ZSM-5

The reactivity of surface oxygen was characterized by its capacity to oxidize CO to CO_2. Surface atomic oxygen was loaded on the Fe-ZSM-5_{5500} at 523 K by introducing 600 pulses of N_2O using the TAP-2 setup. Upon this pre-treatment the interaction of CO with the catalyst was studied at the same temperature. The unreacted part of the CO pulses is shown in Figure 4.1a while the formed CO_2 is pictured in Figure 4.1b. The generation of CO_2 during the first 180 pulses was clearly observed accompanied by the partial consumption of CO. CO_2 was formed as long as surface oxygen was available to oxidize CO. After the consumption of the reactive surface oxygen pool, CO didn't undergo further reactions since the area below the last 120 pulses stayed equal. CO_2 is known to adsorb reversibly on the catalyst [6] which is observed by its broad pulse response. Thus, the oxygen loaded by N_2O on the Fe-ZSM-5 was reactive, oxidizing CO to CO_2 and therefore considered as reactive α-oxygen symbolized with $(O)_{Fe}$ in this manuscript.

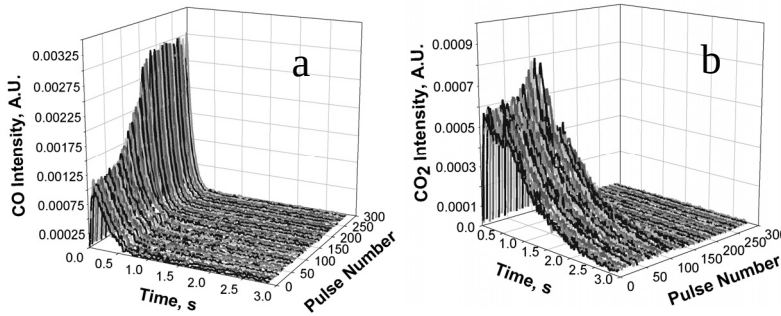

Figure 4.1: Transient CO (a) and CO_2 (b) pulse responses obtained during the interaction of CO with the Fe-ZSM-5_{5500} loaded with atomic surface oxygen from 600 N_2O pulses at 523 K.

The surface oxygen before and after CO interaction was studied also by TPD experiments. The typical oxygen TPD profile after oxygen loading from N_2O on the Fe-ZSM-5_{5500} at 523 K is shown in Figure 4.2, curve 1. The TPD profile of oxygen after N_2O pre-treatment followed by CO interaction presented in Figure 4.2, curve 2 indicates that no surface oxygen remained after the CO treatment which would desorb between 523 and 916 K. For the TAP measurements it can be concluded that the oxygen loaded from N_2O on the Fe-ZSM-5_{5500} at 523 and as well at 593 K (not shown), which was desorbed during TPD experiments, was found to be completely reactive regarding CO oxidation:

$$\begin{aligned} N_2O &\rightarrow (O)_{Fe} + N_2 \\ (O)_{Fe} + CO &\rightarrow CO_2 + (\ )_{Fe} \end{aligned} \qquad (4.1)$$

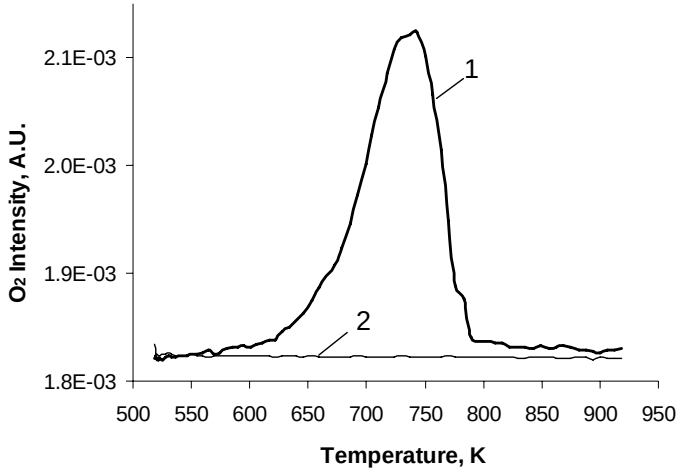

Figure 4.2: TPD profiles of oxygen after its loading from N_2O (1) and after N_2O interaction followed by CO treatment (2) at 523 K of the Fe-ZSM-5_{5500}.

These results are in line with the observations reported by Kiwi-Minsker et al. with a very similar catalyst using the Micromeritics AutoChem 2910 setup at atmospheric pressure [9]. N_2O generated surface oxygen which oxidized CO to CO_2 and the subsequent TPD showed no oxygen desorption between of 550 and 1250 K. Furthermore, the authors reported also that the total amount of consumed surface oxygen only corresponded to about 65% of the total amount of oxygen chemisorbed from N_2O. Sachtler and co-workers found during the study of the isotopic exchange of oxygen on Fe/MFI as well that the number of exchangeable oxygen atoms was smaller than the number of O atoms adsorbed from N_2O, and assigned this difference to the partial consumption of oxygen from the re-oxidation of pre-reduced iron species [10]. Therefore, it can not be concluded straightforward that every loaded oxygen is active in CO oxidation. Even though, CO oxidation with α-oxygen in a static vacuum setup showed that the amount of formed CO_2 was equal to [6] or only 10% below [7] the amount of pre-loaded oxygen from N_2O.

4.2. Summary of CO Interaction with the Fe-ZSM-5 after different Pre-treatments

CO interaction with the Fe-ZSM-5_{5500} was performed using the TAP setup after several pre-treatments in order to probe for reactive surface species. Table 4.1 summarizes these experiments whereas the evolution of CO_2 indicates reactive $(O)_{Fe}$. The listed experiments and the obtained results are discussed in detail in the following chapters.

Table 4.1: Summary of CO interaction with the Fe-ZSM-5_{5500} after different pre-treatments at 523 and 593 K performed with the TAP setup.

Temperature, K	*Pre-treatment*	*CO_2 evolution during CO interaction*	*Discussed in section*
523	N_2O	+	4.1
593	N_2O	+	4.1
523	NO	-	6.4
	$N_2O \rightarrow NO$	very small	6.4
	$N_2O \rightarrow NO \rightarrow N_2O$	+	6.4
	$NO \rightarrow N_2O$	+	6.4, 6.5
523	NO_2	-	7.1
	$NO_2 \rightarrow N_2O$	-	7.2
	$N_2O \rightarrow NO_2$	-	7.2
593	$N_2O \rightarrow H_2O$	-	8.2

In general, it can be stated that only N_2O neither NO_2 nor NO is capable of generating reactive surface oxygen on the Fe-ZSM-5_{5500}. H_2O, NO or NO_2 treatments after oxygen loading from N_2O resulted in the transformation or removal of $(O)_{Fe}$ so that CO_2 wasn't formed anymore during CO treatment.

4.3. References

1. Dubkov, K. A.; Ovanesyan, N. S.; Shteinman, A. A.; Starokon, E. V.; Panov, G. I., Evolution of iron states and formation of alpha-sites upon activation of FeZSM-5 zeolites. *Journal of Catalysis* **2002,** 207, (2), 341-352.
2. Sobolev, V. I.; Kharitonov, A. S.; Paukshtis, Y. A.; Panov, G. I., Stoichiometric Reaction of Benzene with Alpha-Form of Oxygen on FeZSM-5 Zeolites - Mechanism of Aromatics Hydroxylation by N_2O. *Journal of Molecular Catalysis* **1993,** 84, (1), 117-124.

3. Dubkov, K. A.; Starokon, E. V.; Paukshtis, E. A.; Volodin, A. M.; Panov, G. I., Mechanism of the low-temperature interaction of hydrogen with alpha-oxygen on FeZSM-5 zeolite. *Kinetics and Catalysis* **2004,** 45, (2), 202-208.
4. Panov, G. I.; Uriarte, A. K.; Rodkin, M. A.; Sobolev, V. I., Generation of active oxygen species on solid surfaces. Opportunity for novel oxidation technologies over zeolites. *Catalysis Today* **1998,** 41, (4), 365-385.
5. Parmon, V. N.; Panov, G. I.; Uriarte, A.; Noskov, A. S., Nitrous oxide in oxidation chemistry and catalysis: application and production. *Catalysis Today* **2005,** 100, (1-2), 115-131.
6. Dubkov, K. A.; Paukshtis, E. A.; Panov, G. I., Stoichiometry of oxidation reactions involving alpha-oxygen on FeZSM-5 zeolite. *Kinetics and Catalysis* **2001,** 42, (2), 205-211.
7. Panov, G. I.; Sobolev, V. I.; Kharitonov, A. S., The Role of Iron in N_2O Decomposition on ZSM-5 Zeolite and Reactivity of the Surface Oxygen Formed. *Journal of Molecular Catalysis* **1990,** 61, (1), 85-97.
8. Bulushev, D. A.; Renken, A.; Kiwi-Minsker, L., Role of adsorbed NO in N_2O decomposition over iron-containing ZSM-5 catalysts at low temperatures. *Journal of Physical Chemistry B* **2006,** 110, (22), 10691-10700.
9. Kiwi-Minsker, L.; Bulushev, D. A.; Renken, A., Active sites in HZSM-5 with low Fe content for the formation of surface oxygen by decomposing N_2O: is every deposited oxygen active? *Journal of Catalysis* **2003,** 219, (2), 273-285.
10. Jia, J.; Wen, B.; Sachtler, W. M. H., Identification by Isotopic Exchange of Oxygen Deposited on Fe/MFI by Decomposing N_2O. *Journal of Catalysis* **2002,** 210, (2), 453-459.

Chapter 5

CATALYTIC N_2O DECOMPOSITION

The N_2O decomposition to N_2 and O_2 over Fe-ZSM-5 is known to involve iron containing sites and proceeds via atomic surface oxygen loading and gaseous N_2 formation from N_2O as a first step

$$N_2O + (\ )_{Fe} \rightarrow (O)_{Fe} + N_2 \quad (5.1)$$

and

$$(O)_{Fe} + (O)_{Fe} \rightarrow 2(\ )_{Fe} + O_2 \quad (5.2)$$

the recombination/formation of gaseous oxygen as a second step. Based on these two steps, the dynamics of N_2O decomposition is discussed in this chapter. Different temperatures are used to distinguish these reaction steps in N_2O decomposition.

5.1. Oxygen Loading from N_2O

Fe-ZSM-5, which is an active catalyst for N_2O decomposition at atmospheric pressure, decomposes N_2O under vacuum conditions too. N_2O was repeatedly pulsed with the TAP setup at 593 K over the iron containing zeolite and the responses of reactant, product and inert tracer are illustrated in Figure 5.1. Nitrogen appeared in the reactor outlet almost simultaneously with nitrous oxide, while no molecular oxygen could be observed by the mass spectrometer during these experiments. Thus, the formation of surface atomic oxygen $(O)_{Fe}$ was evidenced by the release of gaseous N_2 through partial decomposition of N_2O. The TAP experiments at low temperatures (593 K and 523 K) are in line with Equation (5.1).

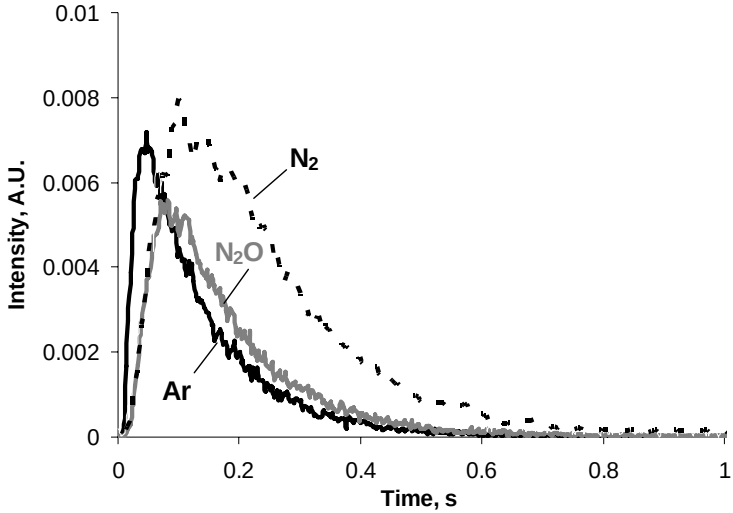

Figure 5.1.: Transient response curves of N_2O, Ar and N_2 obtained after introduction of single N_2O/Ar pulses over the Fe-ZSM-5_{550} catalyst at 593 K.

During a train of N_2O/Ar pulses over the standard pre-treated catalyst, the N_2O conversion as well as the N_2 production were progressively decreasing until no N_2O decomposition was observed anymore meaning that all the active sites were saturated with oxygen. This characteristic is the basis of the following section where the titration of the sites active in N_2O decomposition in the Fe-ZSM-5 sample is described.

5.2. Titration of Active Sites

N_2O reacted at low temperatures (< 600 K) with the catalyst resulting in the formation of gaseous nitrogen and oxygen bound by the catalyst as in Equation (5.1). A complete saturation of the active sites can be reached by N_2O exposure at low temperatures where oxygen was stored and did not desorb. The concentration of active sites of the Fe-ZSM-5, $C_{Fe}^{N_2O}$, was defined as the number of deposited surface atomic oxygen $(O)_{Fe}$ per mass of catalyst. It was indirectly calculated by the amount of decomposed N_2O molecules or released N_2 molecules until saturation. The standard pre-treated catalyst was considered as surface atomic oxygen free.

5.2.1. Pulse Technique under Vacuum

A titration of the active sites of the Fe-ZSM-5_{5500} was achieved with the TAP-system. N_2O/Ar (80/20) pulses were introduced in the TAP reactor at 593 K. The pulse size was about $4.8 \cdot 10^{14}$ molecules/pulse. The N_2O and N_2 responses were measured at the outlet of the reactor and the area below the pulse responses determined. A typical curve resulting from the multi-pulse experiments with N_2O at 593 K is shown in Figure 5.2.

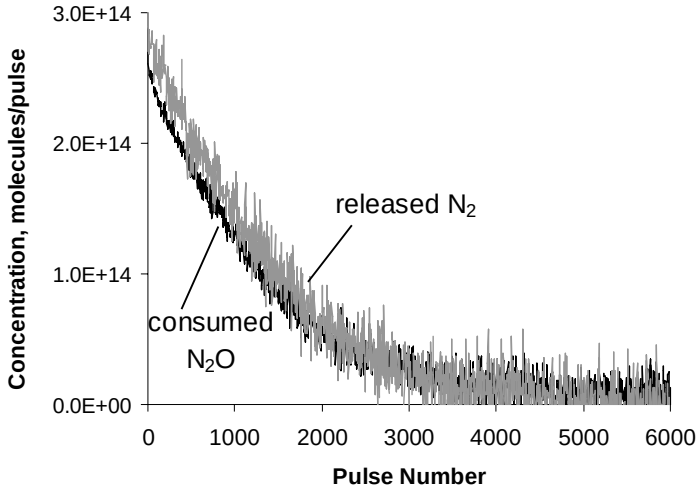

Figure 5.2: Multi-pulse titration experiment. Released amount of N_2 and consumed N_2O during N_2O pulsing at 593 K versus pulse number over 0.0994 g standard pre-treated Fe-ZSM-5_{5500}. Pulse size: $4.8 \cdot 10^{14}$ molecules/pulse.

The amount of produced N_2 and consumed N_2O per pulse is plotted versus pulse number. The N_2O conversion in the first pulse (ca. 60%) decreased with the pulse number as a consequence of the gradual saturation of the active sites in the catalyst. The decrease was sharper during the first 3000 pulses and gradually approached the value of zero conversion after 6000 pulses. The injections continued until the catalyst was saturated which was indicated when all subsequent N_2O peaks remained the same size.

The concentration of active sites ($C_{Fe}^{N_2O}$) was estimated from the amount of N_2 released assuming that a single oxygen atom was chemisorbed on each active site. A summarization of the released amount of N_2 per pulse over 6000 N_2O pulses gave $C_{Fe}^{N_2O}$. An integration of the consumed amount of N_2O over the pulse number represented the amount of decomposed N_2O plus reversibly adsorbed N_2O and can, therefore, deviate from the amount of released N_2. The found concentrations were $(3.0 \pm 0.6)\cdot10^{18}$ molecules/g released N_2 and $(2.8 \pm 0.6)\cdot10^{18}$ molecules/g consumed N_2O for various catalyst loadings between 0.02 and 0.1g. Assuming the validity of Equation (5.1), the amount of released N_2 molecules/g corresponds to the amount of active sites/g.

The equality of the values for the released N_2 and consumed N_2O is in line with the results of Panov [1]. They measured the concentration of active sites in a static vacuum setup from the amount of the N_2 released or the N_2O consumed, since these two amounts were found to be equal. This shows that the reversible adsorption of N_2O isn't very pronounced in vacuum and the amount of released N_2 or consumed N_2O is equal to the amount of active sites. Thus, the concentration of active sites found with the TAP setup was about $3.0\cdot10^{18}$ sites/g.

5.2.2. Transient Flow Method at Atmospheric Pressure

The amount of active sites in the Fe-ZSM-5_{5500} was also measured via transient response method at atmospheric pressure during N_2O decomposition over the catalyst at 523 K. The reaction gas phase was monitored in the reactor outlet after switching in the inlet from He to a mixture of 2 vol% N_2O, 2 vol% Ar in He. The gas-phase composition as a function of time for the Fe-ZSM-5_{5500} catalyst is presented in Figure 5.3.

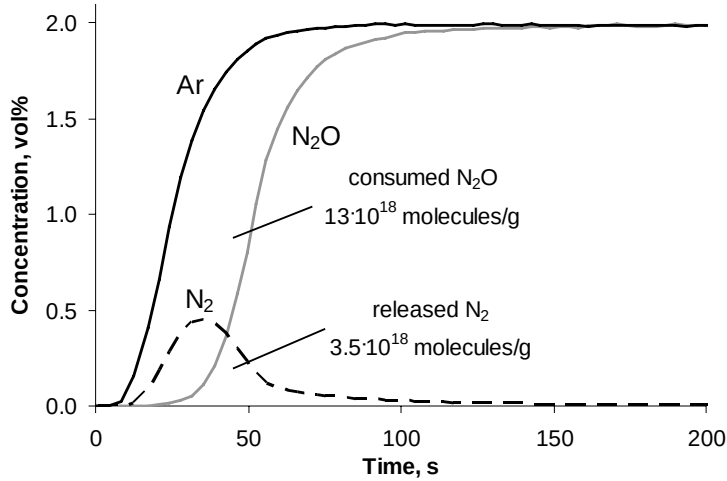

Figure 5.3: Transient responses at 523 K obtained after the switch from He to the 2 vol% N_2O + 2 vol% Ar + 96 vol% He mixture over Fe-ZSM-5_{5500} catalyst.

The reaction was assumed to proceed as in Equation (5.1) through evolution of a stoichiometric amount of N_2 into the gas phase and deposition of one oxygen atom per each Fe(II). The concentration of active sites was determined by integration of the peak of the released nitrogen to $3.5 \cdot 10^{18}$ sites/g. The integration of the area between the Ar and N_2O response allowed the estimation of the amount of consumed N_2O which was found to be $13 \cdot 10^{18}$ molecules/g. The amount of reversibly adsorbed N_2O ($13 \cdot 10^{18}$ molecules/g – $3.5 \cdot 10^{18}$ molecules/g = $9.5 \cdot 10^{18}$ molecules/g) was about three times higher than $C_{Fe}^{N_2O}$. This is different to experiments in vacuum by Panov [1] at 523 K where the amount of consumed N_2O and released N_2 were found to be equal. The difference is attributed to the higher partial pressure of N_2O (2 kPa instead of 0.027-0.053 kPa) in the transient response method.

It could be shown that the pulse experiment in vacuum as well as the transient response method at atmospheric pressure resulted in about the same concentration of active sites (~3-$3.5 \cdot 10^{18}$ sites/g) which was determined from the N_2 release. Taking into consideration that the catalyst sample contained 5500 ppm Fe, only 5% of the total amount of Fe atoms in the zeolite were active in oxygen loading from N_2O. This indicates that a very large fraction of the iron in the zeolite is unable to activate the N_2O molecule under TAP and atmospheric conditions at temperatures below 600 K.

5.3. Molecular Oxygen Formation

Above 600 K the formation of molecular oxygen accompanied by the evolution of N_2 was observed during N_2O decomposition over Fe-ZSM-5. In contrast to lower temperatures (<600 K) surface oxygen recombined and desorbed as in Equation (5.2). The transient responses upon pulsing N_2O at 803 K are presented in Figure 5.4. The inset with a 15 times larger time scale shows O_2 that was desorbed in a broad peak.

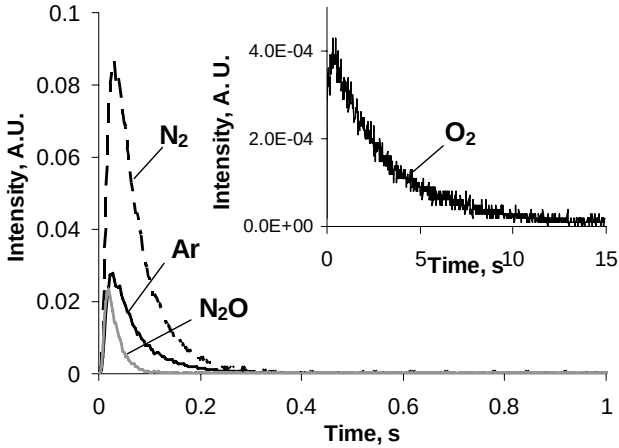

Figure 5.4: Transient response curves of N_2O, Ar and N_2 obtained after introduction of single N_2O/Ar pulses over the Fe-ZSM-5_{5500} catalyst at 803 K. O_2 formation during N_2O decomposition at 803 K (inset).

The N_2O curve didn't intersect the Ar curve which is the diffusion-only case. Gleaves and coworkers [2] have demonstrated that such behavior was indicative of irreversible adsorption and reaction. The conversion of N_2O was about 80%. A large amount of N_2 was produced as well as O_2. These responses provide valuable qualitative information on the reaction mechanism and will be further studied in the next section.

The single-pulse experiment of N_2O was repeated with the Fe-ZSM-5 at even higher temperature 946 K. The height-normalized transient responses of Ar, O_2 and N_2 are illustrated in Figure 5.5. The N_2O conversion at 946 K was about 95%.

Higher temperatures accelerate the diffusion process. The molecules passed the reactor very fast leading to sharp response curves. The normalized Ar and N_2 curves were very similar indicating that the formation of N_2 by N_2O decomposition was very fast and not retarded. The response of O_2 (peak maximum at 0.05 s) was only delayed by

0.03 s with respect to N_2 instead of 0.5 s at 803 K. The sharpening of the O_2 response at 946 K indicated that the oxygen recombination/desorption was faster and significantly accelerated compared to 803 K. However, the delayed O_2 response showed that the recombination/desorption of oxygen was still the slowest step.

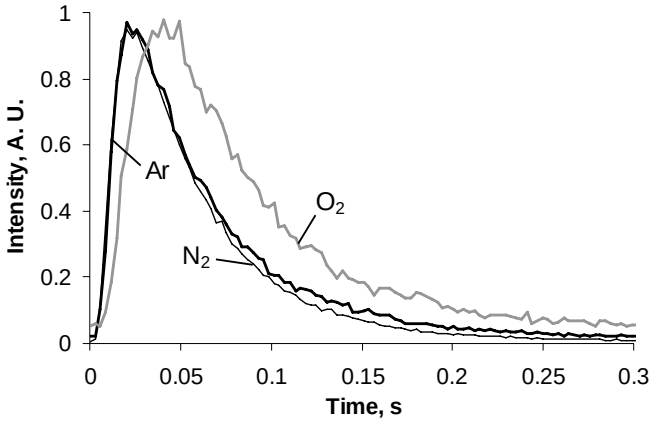

Figure 5.5: Height-normalized transient response curves of Ar, O_2 and N_2 obtained after introduction of single N_2O/Ar pulses over the Fe-ZSM-5_{5500} catalyst at 946 K.

5.4. The Mechanism of Oxygen Formation

5.4.1. Qualitative Assumptions from Pulse Shapes

In order to extract qualitative data from the previous responses the height-normalized responses observed during a N_2O single-pulse experiment at 803 K over Fe-ZSM-5 are shown in Figure 5.6. The pulse shapes were easier to compare in this way. The N_2O, Ar and N_2 were similar in shape compared to the O_2 response signal being much broader and deviating from the other curves. Possible reasons for the shape of O_2 can be mechanistic features of N_2O decomposition or simply the non-reactive adsorption-desorption phenomena of O_2 along the catalyst bed [3]. Therefore, a mixture of O_2 and Ar was pulsed at the same temperature (803 K) over the Fe-ZSM-5_{5500}. The height-normalized response curves are shown in Figure 5.7. The pulse responses of Ar and O_2 were very similar in shape. Ar as inert tracer hardly undergoes adsorption-desorption processes with the zeolite and represents the diffusion-only case [2], so did oxygen. Therefore, the broader and delayed oxygen response from a N_2O pulse

compared to the Ar response in Figure 5.6 is due to mechanistic features of the N_2O decomposition.

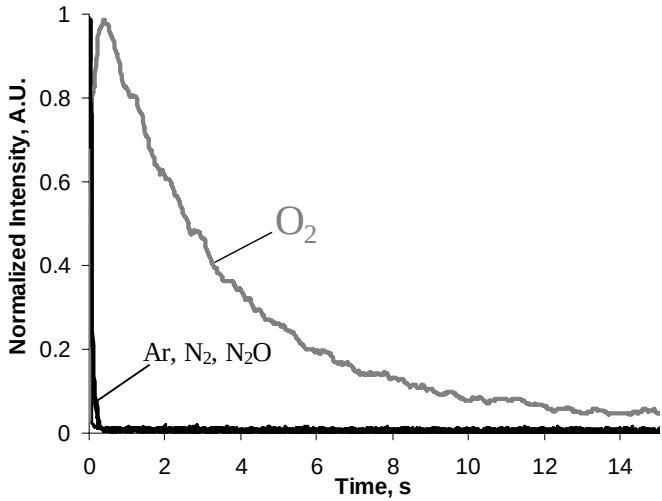

Figure 5.6: Height-normalized transient response curves obtained after introduction of single N_2O/Ar pulses over the Fe-ZSM-5_{5500} catalyst at 803 K.

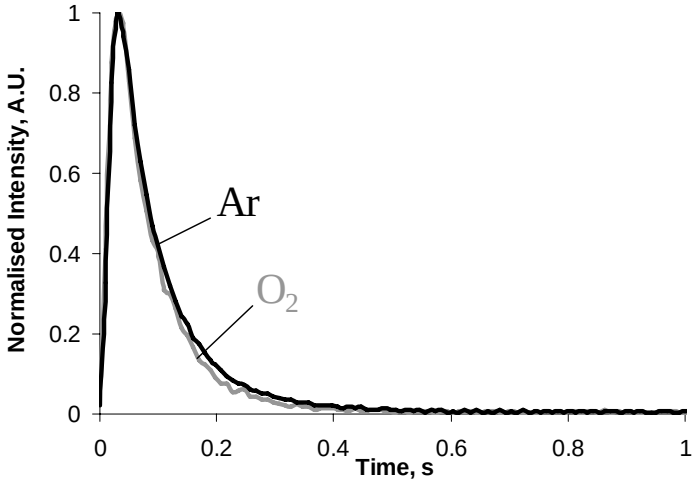

Figure 5.7: Height-normalized transient response curves obtained after introduction of single O_2/Ar pulses over the Fe-ZSM-5_{5500} catalyst at 803 K.

From Figure 5.6 it can be seen that O_2 still desorbed during 15 s from the catalyst even though all N_2O molecules left the reactor within 0.5 s. Additionally, while oxygen still desorbed, no N_2 was produced anymore since N_2 evolved within 0.5 s. Thus, the deposition of active surface oxygen by N_2O was finished within 0.5 s, while the recombination and desorption of oxygen took up to 15 s. Therefore, it can be concluded that the rate-determining step of the N_2O decomposition at 803 K was the recombination/desorption of oxygen.

In the literature two possible rate-determining steps for the N_2O decomposition are discussed. Mechanistic studies have substantiated that O_2 formation is the rate-determining step in N_2O decomposition over iron containing zeolites [3-8]. Basically, two pathways leading to O_2 have been put forward. At one side, the reaction of adsorbed oxygen species, $(O)_{Fe}$, with gas-phase N_2O was proposed to result in O_2 formation over Fe-ZSM-5 [9, 10].

$$(O)_{Fe} + N_2O \rightarrow O_2 + N_2 + (\ )_{Fe} \tag{5.3}$$

On the other side, the recombination of two surface oxygen atoms into molecular oxygen was suggested as a source of O_2 in N_2O decomposition over Fe-ZSM-5 (Equation (5.2)) [3-6, 11].

Heyden et al. have developed a comprehensive mechanistic model for the direct decomposition of N_2O on Fe-ZSM-5 on the basis of DFT calculations [12, 13]. They state that the rate-determining step in the reaction path is N_2O dissociation, releasing a N_2 molecule and leaving an O atom on the site (Equation (5.1)).

In case of Equation (5.3) being the rate-determining step, the TAP experiments should show O_2 production while N_2O is present and N_2 is produced. This could be the case in the first 0.5 s after N_2O introduction while N_2O, N_2 and O_2 evolved simultaneously as seen in Figure 5.6. However, the main part of O_2 was produced when N_2O left the reactor and the formation of N_2 was finished. Therefore, the most reasonable explanation for the observed TAP results is given in Equation (5.2), that oxygen recombination/desorption is the rate-determining step. O_2 was produced in absence of N_2O and without formation of N_2 in parallel.

If the dissociation of N_2O as proposed by Heyden et al. [12, 13] is the rate-determining step while the recombination/desorption of oxygen is fast, then O_2 and N_2 would be produced as long as N_2O is present on the catalyst. When N_2O passed the catalyst bed, oxygen should desorb very fast since this step is not considered to be slow. The desorption of O_2 in TAP experiments took up to 15 s compared to 0.5 s for the N_2O passage and N_2 formation. Thus, TAP experiments are not in line with the third mechanistic proposal. TAP results confirm recombination/desorption of surface oxygen as the rate-determining step.

5.4.2. Kinetic Fit on Oxygen Decay

The kinetics of the oxygen formation was analyzed to derive insights into plausible reaction pathways leading to O_2. At 803 K oxygen was loaded on the catalyst during a N_2O pulse. The N_2O decomposition and N_2 evolution was finished within 0.5 s since N_2O passed the reactor within this time and no gaseous N_2 was produced anymore after this time delay. Only gaseous O_2 was formed up to 15 s. Therefore, it can be assumed that from 0.5 s on after the injection of N_2O only the final step of the catalytic cycle took place: the formation and desorption of oxygen, yielding gas-phase O_2 and free iron sites (Equation (5.2)).

Since re-adsorption of O_2 was negligible in TAP experiments as shown in section 5.4.1, the relative rate of desorption, defined as the change in adsorbate coverage per unit of time, is given by

$$-\frac{d\theta_O}{dt} = k \bullet \theta_O^n \tag{5.4}$$

in which θ_O is the coverage of active sites with oxygen, t the time, n the order of recombination/desorption and k the rate constant. The desorption rate is proportional to the registered O_2 flow at the reactor exit I_{O2} in units of mass per time:

$$-\frac{d\theta_O}{dt} \sim I_{O_2} \tag{5.5}$$

The amount of oxygen on the catalyst at a certain time t' can be calculated by an integration of the area below the oxygen response curve from time t' until all oxygen is desorbed at $t \rightarrow \infty$:

$$\theta_O\left(t = t'\right) \sim \int_{t=t'}^{t\rightarrow\infty} I_{O_2} \cdot dt \tag{5.6}$$

By implementing Equation (5.5) and (5.6) in Equation (5.4), the following expression is reached which contains two kinetic constants and two measurable terms:

$$I_{O_2}\Big|_{t=t'} = k_1 \cdot \left(\int_{t=t'}^{t\rightarrow\infty} I_{O_2} \cdot dt \right)^n \tag{5.7}$$

The desorption of surface oxygen loaded from one N_2O pulse at 803 K is presented in Figure 5.8. As indicated, the oxygen desorption rate was proportional to the gas flow I_{O2} at t' and the amount of adsorbed oxygen species at t' was determined by the

integration of I_{O2} from t' until oxygen desorption was completed in this case at 15 s. The first 0.5 s upon the N_2O injection were not considered since the reaction system is much more complex due to the decomposition of N_2O and the formation of N_2.

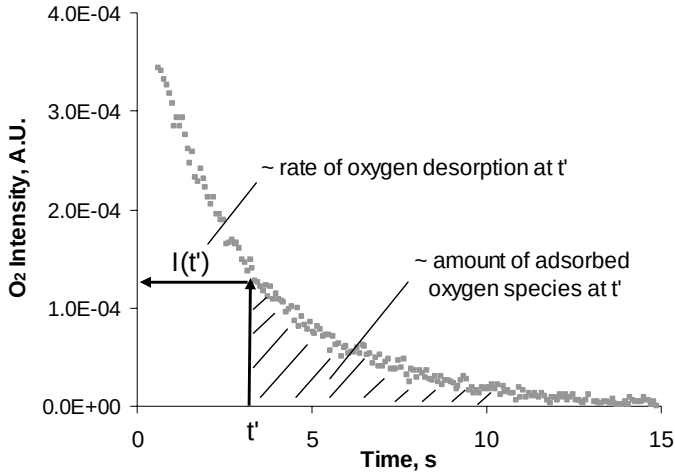

Figure 5.8: Height-normalized transient response O_2 curve obtained after introduction of single N_2O/Ar pulse over the Fe-ZSM-5_{5500} catalyst at 803 K.

Equation (5.8) is the linearised form of Equation (5.7) by taking the logarithm. The slope represents the order of the desorption of oxygen.

$$\underbrace{\ln\left[I_{O_2}\big|_{t=t'}\right]}_{A} = \ln k_1 + n \cdot \underbrace{\ln\left[\int_{t=t'}^{t\to\infty} I_{O_2}\cdot dt\right]}_{B} \qquad (5.8)$$

Figure 5.9 exemplifies ln A versus ln B for the oxygen desorption seen in Figure 5.8. The straight line demonstrates the agreement between experiment and theory while the slope corresponds to the order of oxygen desorption. Several transient responses of O_2 derived from pulse experiments with the TAP reactor were fitted with Equation (5.8) to determine the order of oxygen desorption which was found to be 0.95 ± 0.1.

A desorption order of about one corresponds to a monomolecular desorption. An associative desorption as the recombination of two monoatomic surface oxygen species, $(O)_{Fe}$, proposed in Equation (5.2) would result in an order of two. Therefore, intermediate reactions steps may be added to Equation (5.2) to be in line with the kinetic analysis of the transient TAP experiments. The involvement of adsorbed NO_x species catalyzing the desorption of oxygen can be excluded since the $NO_{x,ads}$ species were

already desorbed at temperatures around 800 K as shown in the TPD experiments in chapter 6.

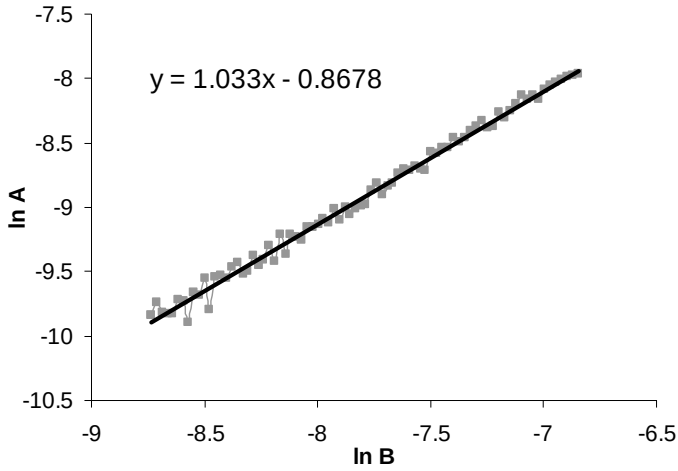

Figure 5.9: Linearization of oxygen desorption curve of Figure 5.8 by Equation (5.8).

The first order dependence of the oxygen desorption can be explained for example by the slow desorption of bimolecular oxygen. Other authors already suggested the formation of oxygen via desorption of a bimolecular oxygen species. Kondratenko et al. [14] concluded from the simultaneous fitting of N_2O, N_2 and O_2 TAP responses upon N_2O decomposition over Fe-ZSM-5 that a biatomic oxygen precursor was formed upon N_2O decomposition over a Fe site with monoatomic adsorbed oxygen species. This biatomic precursor was transformed to another biatomic oxygen species, which decomposed yielding gas-phase O_2 and free iron site. Heyden et al. [13] assumed biatomic oxygen species of different structure and triatomic oxygen species as surface precursors for gaseous O_2 evolution in DFT modeling. Bell and coworkers [8, 15, 16] proposed N_2O decomposition proceeded via dissociative adsorption of N_2O on a vacant iron site, releasing a N_2 molecule and leaving an O atom on the site. A second N_2O molecule decomposed on the same site, so that two O atoms were attached to the same site. These atoms recombined to form an O_2 molecule, which then desorbed from the iron site. The linear dependence of the oxygen desorption rate on the surface coverage of oxygen derived from TAP experiments is in accordance with the suggestions made in literature.

5.5. References

1. Dubkov, K. A.; Ovanesyan, N. S.; Shteinman, A. A.; Starokon, E. V.; Panov, G. I., Evolution of iron states and formation of alpha-sites upon activation of FeZSM-5 zeolites. *Journal of Catalysis* **2002,** 207, (2), 341-352.
2. Gleaves, J. T.; Yablonskii, G. S.; Phanawadee, P.; Schuurman, Y., TAP-2: An interrogative kinetics approach. *Applied Catalysis A-General* **1997,** 160, (1), 55-88.
3. Perez-Ramirez, J.; Kapteijn, F.; Mul, G.; Moulijn, J. A., NO-assisted N_2O decomposition over Fe-based catalysts: Effects of gas-phase composition and catalyst constitution. *Journal of Catalysis* **2002,** 208, (1), 211-223.
4. Bulushev, D. A.; Kiwi-Minsker, L.; Renken, A., Dynamics of N_2O decomposition over HZSM-5 with low Fe content. *Journal of Catalysis* **2004,** 222, (2), 389-396.
5. Kiwi-Minsker, L.; Bulushev, D. A.; Renken, A., Active sites in HZSM-5 with low Fe content for the formation of surface oxygen by decomposing N_2O: is every deposited oxygen active? *Journal of Catalysis* **2003,** 219, (2), 273-285.
6. Mul, G.; Perez-Ramirez, J.; Kapteijn, F.; Moulijn, J. A., NO-assisted N_2O decomposition over ex-framework FeZSM-5: mechanistic aspects. *Catalysis Letters* **2001,** 77, (1-3), 7-13.
7. Pirngruber, G. D., The surface chemistry of N_2O decomposition on iron containing zeolites (I). *Journal of Catalysis* **2003,** 219, (2), 456-463.
8. Wood, B. R.; Reimer, J. A.; Bell, A. T.; Janicke, M. T.; Ott, K. C., Nitrous oxide decomposition and surface oxygen formation on Fe-ZSM-5. *Journal of Catalysis* **2004,** 224, (1), 148-155.
9. Fu, C. M.; Korchak, V. N.; Hall, W. K., Decomposition of nitrous oxide on FeY zeolite. *Journal of Catalysis* **1981,** 68, (1), 166-171.
10. Kapteijn, F.; Marban, G.; Rodriguez Mirasol, J.; Moulijn, J. A., Kinetic analysis of the decomposition of nitrous oxide over ZSM-5 catalysts. *Journal of Catalysis* **1997,** 167, (1), 256-265.
11. Pirngruber, G. D.; Luechinger, M.; Roy, P. K.; Cecchetto, A.; Smirniotis, P., N_2O decomposition over iron-containing zeolites prepared by different methods: a comparison of the reaction mechanism. *Journal of Catalysis* **2004,** 224, (2), 429-440.
12. Heyden, A.; Bell, A. T.; Keil, F. J., Kinetic modeling of nitrous oxide decomposition on Fe-ZSM-5 based on parameters obtained from first-principles calculations. *Journal of Catalysis* **2005,** 233, (1), 26-35.
13. Heyden, A.; Peters, B.; Bell, A. T.; Keil, F. J., Comprehensive DFT study of nitrous oxide decomposition over Fe-ZSM-5. *Journal of Physical Chemistry B* **2005,** 109, (5), 1857-1873.
14. Kondratenko, E. V.; Perez-Ramirez, J., Mechanism and kinetics of direct N_2O decomposition over Fe-MFI zeolites with different iron speciation from temporal analysis of products. *Journal of Physical Chemistry B* **2006,** 110, (45), 22586-22595.
15. Ryder, J. A.; Chakraborty, A. K.; Bell, A. T., Density functional theory study of nitrous oxide decomposition over Fe- and Co-ZSM-5. *Journal of Physical Chemistry B* **2002,** 106, (28), 7059-7064.
16. Ryder, J. A.; Chakraborty, A. K.; Bell, A. T., Density functional theory study of benzene oxidation over Fe-ZSM-5. *Journal of Catalysis* **2003,** 220, (1), 84-91.

Chapter 6

EFFECT OF NO ON N_2O DECOMPOSITION

At 523 K only the formation of surface atomic oxygen $(O)_{Fe}$ on Fe containing sites and gaseous N_2 from N_2O takes place. Oxygen recombines only at higher temperatures indicating that, in general, the accepted rate-determining step in N_2O decomposition is the desorption of oxygen from the catalyst surface [1-3] whereupon is also concluded in chapter 4 based on TAP experiments. The addition of gaseous NO enhances the activity of Fe containing zeolites [1, 3-5]. Slow NO formation on the catalyst surface from N_2O interaction is observed over Fe- and Cu-zeolites [6-10]. NO/NO_2 [3, 5, 11] as well as nitrite/nitrate [12] redox cycles are proposed for active sites regeneration in N_2O decomposition.

Perez-Ramirez et al. [3] studied the N_2O decomposition over homemade isomorphously substituted extra-framework Fe-ZSM-5 with the Multitrack, a TAP like system. It was supposed that adsorbed NO may accommodate oxygen loaded by N_2O on an adjacent site, allowing the deposition of a second oxygen and supporting the recombination of both. Adsorbed NO may even facilitate the migration of atomic oxygen to enhance their recombination. They observed NO-induced NO_2 desorption while they didn't report $NO_{x,ads}$ formation from N_2O in the absence of adsorbed NO.

6.1. $NO_{x,ads}$ Formation from N_2O on Fe-ZSM-5 at Low Temperatures

Adsorbed surface species on the Fe-ZSM-5_{5500} catalyst were investigated by temperature-programmed desorption experiments after different numbers of N_2O pulses at 593 K as well as at 523 K using the TAP setup. At these temperatures N_2O formed gaseous N_2 and atomic surface oxygen, $(O)_{Fe}$, involving Fe containing sites. The formation of gaseous oxygen by N_2O decomposition took place at temperatures higher than 661 K. No gaseous NO/NO_2 was detected while pulsing N_2O in the range of 523 K to 946 K.

After N_2O pulsing over the zeolite at 593 K, only O_2 and NO were detected during the TPD runs which are illustrated in Figure 6.1. Oxygen loaded during the N_2O interaction of 300, 600 and 1800 pulses was released with peaks at 713 K, 701 K and 678 K, respectively (Figure 6.1a). With increasing amount of performed N_2O pulses, the amount of accumulated surface oxygen increased and the maximum temperature of the oxygen desorption shifted to lower temperature (by ~35 K) indicating an easier oxygen desorption. According to Figure 6.1b, which shows the corresponding NO TPD profiles, it increased the amount of NO formed and accumulated on the surface with increasing the number of performed N_2O pulses. It is interesting to note that NO desorbed during these TPD experiments always at the very end of the oxygen desorption with the maxima at 707-757 K. The parallel evolution of O_2 and NO in the TPD experiments suggests a common surface species which decomposes to O_2 and NO. Therefore, the surface NO detected in the TPD runs was assigned to surface $NO_{x,ads}$ species.

At 523 K the loading of oxygen on iron sites from N_2O as well as the formation of $NO_{x,ads}$ was much slower. TPD runs after N_2O multi-pulse experiments showed desorption of gaseous O_2, but the NO concentration was below the detection limit, see Figure 6.3b, curve 1. The absence of detected $NO_{x,ads}$ species at 523 K proved that they did not correspond to an impurity in the dosed N_2O blend at 593 K since adsorption phenomena should be strengthened at lower temperature. Nevertheless, the desorption maxima of oxygen decreased as well (744 K to 730 K) with increasing number of N_2O pulses (600 to 1200, not shown) indicating the existence of surface $NO_{x,ads}$ on the catalyst.

These results evidenced the creation of adsorbed NO_x on the zeolite during N_2O decomposition:

$$(\ )_{Fe} + N_2O \rightarrow (O)_{Fe}, NO_{x,ads} + N_2 \qquad (6.1)$$

As the amount of accumulated NO_x increased, the oxygen desorption temperature shifted to lower temperatures suggesting the ease of oxygen desorption. The

data lead to the conclusion that the formed NO_x surface species ease the desorption of $(O)_{Fe}$. To confirm this, special experiments with NO pre-adsorption are performed and discussed in the following section.

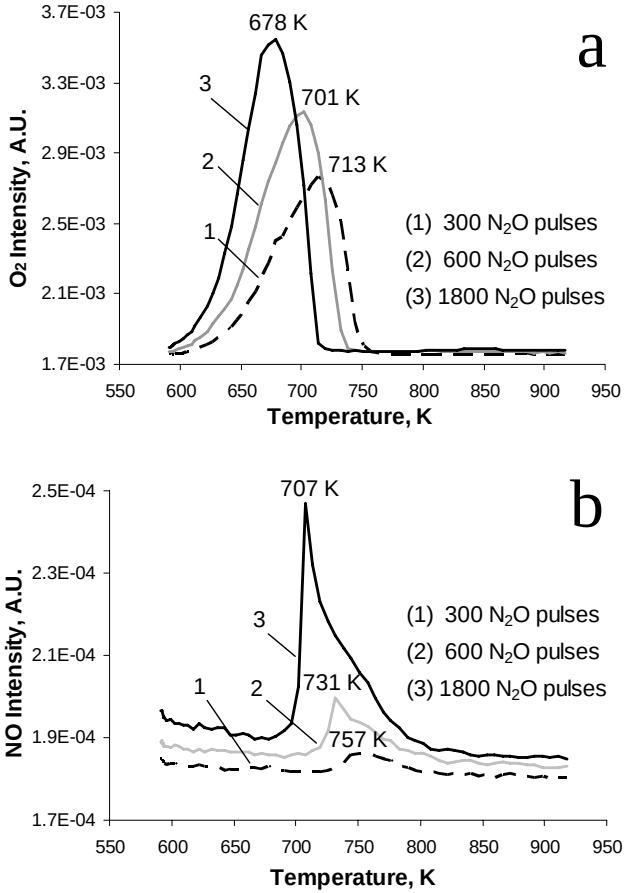

Figure 6.1: O_2 (a) and NO (b) TPD profiles obtained after 300 (1), 600(2) and 1800 (3) pulses of N_2O over the Fe-ZSM-5_{5500} catalyst at 593 K.

6.2. N_2O Interaction with NO Adsorbed on Fe-ZSM-5

The effect of pre-adsorbed NO on the desorption of oxygen loaded from N_2O is studied at 523 K using the TAP setup. NO is adsorbed on the catalyst by NO and

$N_2O \rightarrow NO$ treatments. First only the adsorption of NO on the Fe-ZSM-5_{5500} is discussed in this chapter and then the interaction of N_2O with the NO_{ads} containing zeolite is investigated.

6.2.1. NO Adsorption on Fe-ZSM-5

Only a small amount of irreversible adsorbed NO remained on the catalyst after 600 NO pulses over the Fe-ZSM-5_{5500} at 523 K. In Figure 6.2, curve 1, it can be seen that NO desorbed in a broad peak during the TPD experiment. No oxygen desorbed and, therefore, it was not formed during the interaction of NO with the catalyst.

About 10 times more NO was adsorbed on the catalyst which was pre-treated with 600 N_2O pulses compared to the standard pre-treatment. NO/NO_2 TPD profiles of the catalyst after $N_2O \rightarrow NO$ treatment at 523 K are presented in Figure 6.2, curve 2 and 3. Surface oxygen was loaded from N_2O pulses (600) which was mainly desorbed by the subsequent NO pulses (600) as discussed in detail in section 6.3. Only a small amount of oxygen remained on the catalyst to form $NO_{x,ads}$ species (not shown).

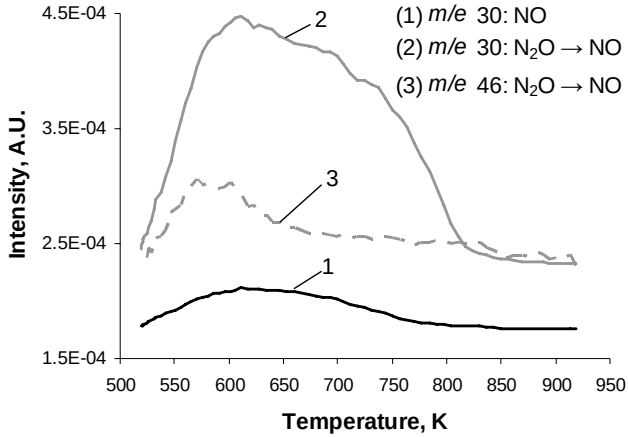

Figure 6.2: NO TPD profiles obtained after pulsing NO (1) and $N_2O \rightarrow NO$ (2), NO_2 TPD profile obtained after pulsing $N_2O \rightarrow NO$ (3) over the Fe-ZSM-5_{5500} catalyst at 523 K.

The concentration of irreversibly adsorbed NO on the Fe-ZSM-5_{5500} was surprisingly around ten times larger on oxygen containing surface as compared to the standard pre-treated catalyst (Figure 6.2). As already mentioned, the initial iron oxidation state is probably +II after the pre-treatment for 30 min at 946 K in vacuum. The interaction of the oxidant N_2O with the Fe-ZSM-5 oxidizes a fraction of the active iron

sites to Fe(III) through the deposition of atomic oxygen. According to infrared studies NO adsorbs strongly on Fe(II) and not to any significant extent on Fe(III) [13, 14]. However, the TAP studies showed much higher affinity of NO with the Fe-ZSM-5 containing $(O)_{Fe}$ species. The same tendency was observed during transient response experiments in [11] where the amount of irreversibly adsorbed NO doubled after N_2O pre-treatment compared to the calcined catalyst. NO adsorption was somehow provided by the $(O)_{Fe}$ sites while forming $NO_{x,ads}$ and initiating the oxygen recombination and desorption even at low temperature as 523 K (discussed in section 6.3).

6.2.2. Interaction of N_2O with Fe-ZSM-5 Containing NO_{ads}

The interaction of N_2O with adsorbed NO on the Fe-ZSM-5_{5500} was studied at 523 K. Therefore, TPD profiles were compared after the interaction of N_2O with the differently pre-treated catalyst: (1) only standard pre-treated ("clean" catalyst), (2) NO, (3) $N_2O \rightarrow NO$. After pre-treatment (1) no surface species were detected. In the other pre-treatments NO was adsorbed. The catalyst contained after pre-treatment (3) about 10 times more NO_{ads} than after pre-treatment (2) which is discussed in the previous section. The amount of performed N_2O pulses (600 pulses) was constant but didn't lead to saturation with atomic oxygen of the catalyst. N_2O pulses over the catalyst with adsorbed NO resulted neither in NO desorption, nor in gaseous NO_2 formation while surface oxygen from N_2O was loaded. The consequent O_2 TPD profiles are presented in Figure 6.3a. The maximum of the oxygen desorption shifted strongly to lower temperatures from 744 K to 646 K and 580 K, respectively. The amount of deposited $(O)_{Fe}$ was 1.3 times larger in the presence of adsorbed NO (Figure 6.3a, curve 2) and was 3.4 times larger after $N_2O \rightarrow NO$ pre-treatment (Figure 6.3a, curve 3) compared to the NO_{ads} free catalyst (Figure 6.3a, curve 1).

Figure 6.3b illustrates the corresponding NO TPD profiles. No NO (curve 1) was detected after the N_2O only pulsing contrary to the NO (curve 2) and $N_2O \rightarrow NO$ (curve 3) pre-treated cases. NO desorbed each time at the very end of the oxygen desorption. Partially NO and O_2 evolved simultaneously which was assigned to a common $NO_{x,ads}$ species. They appeared as sharp peak similar to the NO_x surface species generated during N_2O interaction at 593 K as discussed in section 6.1.

Curve 3 and curve 4 of Figure 6.3b show the responses for the mass to charge ratio (m/e) 30 (NO) and m/e 46 (NO_2) during the TPD after the $N_2O \rightarrow NO \rightarrow N_2O$ multi-pulse sequence. They had the same maxima at 611 K indicating that a common surface species contributed to m/e 30 (NO), 46 (NO_2) and to 32 (O_2). Hence, adsorbed NO_2 or even higher oxidized nitrogen oxide species were formed on the catalyst and their assignment was ambiguous.

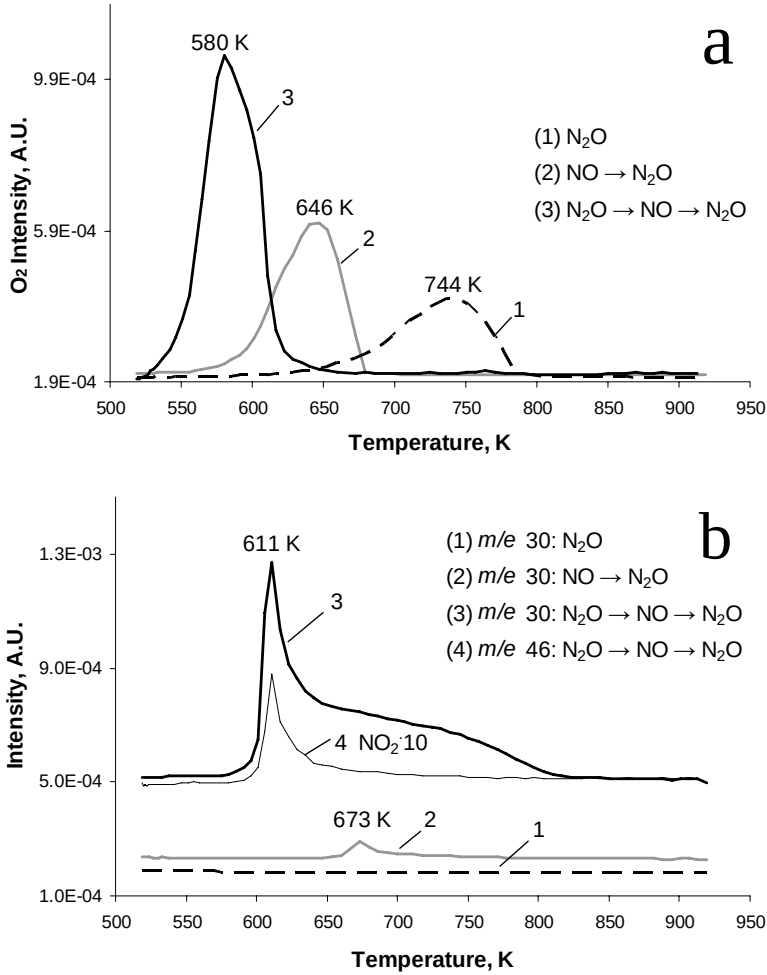

Figure 6.3: O_2 (a) and NO/NO_2 (b) TPD profiles obtained after pulsing N_2O (1), $NO \rightarrow N_2O$ (2), $N_2O \rightarrow NO \rightarrow N_2O$ (3) and NO_2 TPD profile obtained after pulsing $N_2O \rightarrow NO \rightarrow N_2O$ (b, 4) over the Fe-ZSM-5_{5500} catalyst at 523 K.

Pure NO_{ads} (Figure 6.2, curve 1) desorbed in a broad peak during the TPD runs while the $NO_{x,ads}$ species (Figure 6.1b and Figure 6.3b) appeared in a sharp peak. The NO TPD profile (Figure 6.3b, curve 3) after the $N_2O \rightarrow NO \rightarrow N_2O$ multi-pulse sequence showed a sharp peak, to which in parallel NO_2 and O_2 was evolved, and a broad desorption peak of NO only at higher temperatures, which was not accompanied by O_2

or NO_2 desorption. Therefore, it can be concluded that the catalyst after the $N_2O \rightarrow NO \rightarrow N_2O$ multi-pulse sequence contained $NO_{x,ads}$ as well as NO_{ads}.

The amount of loaded $(O)_{Fe}$ was elevated with increasing NO concentration on the catalyst (Figure 6.3) while NO_{ads} is not known to significantly enhanced oxygen loading from N_2O [11]. An explanation on the basis of the reaction mechanism is not evident. However, a transport phenomenon could be the reason for this observation. In TAP studies the transport mechanism into the micro pores was assumed as sorption at the exterior of the zeolite particles and only the adsorbed molecules diffuse into the pores [15-17]. An enhanced surface oxygen migration due to NO_{ads} was proposed in [3]. This would in TAP experiments raise the degree of pore efficiency and explain the increased $(O)_{Fe}$ formation during the N_2O interaction with the catalyst containing more adsorbed NO.

The more NO (Figure 6.2) was preadsorbed on the catalyst prior to the N_2O interaction, the more $NO_{x,ads}$ species were formed during the final N_2O interaction (Figure 6.3b). The increase of the $NO_{x,ads}$ concentration were accompanied by a decrease of the desorption temperatures of oxygen (~160 K, Figure 6.3a) in TPD runs. Thus, $NO_{x,ads}$ species (Figure 6.3b) formed from NO_{ads} and N_2O facilitated the rate-determining step the oxygen recombination/desorption.

In summary, the rate-determining step which is the recombination and desorption of surface atomic oxygen [1-3] is promoted by preadsorbed NO_x species. NO_{ads} did not inhibit oxygen loading from N_2O, however, considerably lowered the desorption temperature of $(O)_{Fe}$. Therefore, different but adjacent sites for NO adsorption and surface atomic oxygen formation from N_2O are proposed. Other studies [3, 4, 11] excluded as well the competitive adsorption of atomic oxygen and NO on the same active sites of Fe-ZSM-5. Adsorbed NO is further oxidized by N_2O to NO_x species acting as a "co-catalyst" in N_2O decomposition.

$$( )_{Fe}, NO_{ads} + N_2O \rightarrow (O)_{Fe}, NO_{x,ads} + N_2 \qquad (6.2)$$

The nature of the $NO_{x,ads}$ species is not definite. Different mechanisms are proposed to explain the promoting effect of them in N_2O decomposition. NO/NO_2 [3, 5, 11] and NO^-_2/NO^-_3 [12] redox cycles are discussed.

6.3. NO Interaction with Fe-ZSM-5 Containing $(O)_{Fe}$

In the previous sections, it is shown that adsorbed NO is formed from N_2O on the Fe-ZSM-5_{550}. $NO_{x,ads}$ species facilitate the desorption of oxygen during TPD

experiments. It is also interesting to investigate the interaction of NO with the catalyst loaded with oxygen from N_2O.

NO pulses over the Fe-ZSM-5_{5500} pre-loaded with $(O)_{Fe}$ from 600 N_2O pulses at 593 K resulted in a strong irreversible adsorption of NO during the first pulses as illustrated in Figure 6.4a. In parallel the desorption of gaseous O_2 was provoked (Figure 6.4b). NO pulses over N_2O pre-treated catalyst at even lower temperature (523 K) caused also oxygen to desorb. The following TPD run is discussed in section 6.2.1 and presented a major NO peak (Figure 6.2, curve 2) and some NO_2 (Figure 6.2, curve 3). NO adsorbed in large quantities while only a small amount of $NO_{x,ads}$ species were formed during NO and $(O)_{Fe}$ interaction. The main part of surface oxygen was desorbed due to NO pulsing:

$$NO + (O)_{Fe} \rightarrow NO, NO_{x,ads} + (\ )_{Fe} + O_2 \qquad (6.3)$$

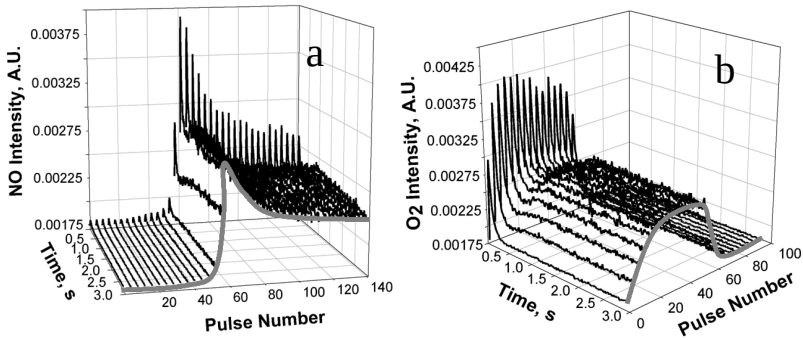

Figure 6.4: NO pulses (a) over the Fe-ZSM-5_{5500} at 593 K after $(O)_{Fe}$ deposition from N_2O provoked the desorption of oxygen (b). Grey line: guide for eyes.

The competition of NO and loaded oxygen for the same sites was excluded since oxygen loading from N_2O (section 6.2) on the catalyst after NO pre-treatments was easy and initiate neither NO, nor NO_2 desorption. The investigation of the interaction of N_2O with preadsorbed NO using the Micromeritics AutoChem 2910 setup at atmospheric pressure showed as well that atomic oxygen was easily loaded [11]. However, the desorption of surface oxygen upon NO interaction was not observed during transient response experiments at atmospheric pressure. The consumption of loaded oxygen by NO was proposed with the formation of adsorbed NO_x species, which could be located not directly on the iron sites [11]:

$$NO + (O)_{Fe} \rightarrow NO_{x,ads} + (\ )_{Fe} \qquad (6.4)$$

The difference is that in TAP experiments the surface oxygen was released by NO interaction and in Micromeritics experiments oxygen was consumed by NO and $NO_{x,ads}$ species were formed. This discrepancy was clarified by flow experiments with the Micromeritics setup. It was assumed that the larger part of the freed oxygen in TAP experiments left the reactor directly since it had hardly any possibility to interact with the next catalyst layer (only thin zeolite layer of 1 mm) where O_2 would oxidise NO_{ads} to $NO_{x,ads}$ species. If this assumption is correct, then it must be possible for molecular oxygen to oxidize NO_{ads}.

The generated surface species from the interaction of NO, NO→O_2 and O_2 with the Fe-ZSM-5_{350} were compared. The TPD profiles after NO treatment for 5 min at 523 K are shown in Figure 6.5a. The evolution of the adsorbed NO as well a small amount of O_2 was observed. The simultaneous desorption of NO and O_2 was always an indication of common $NO_{x,ads}$ species. Thus, $NO_{x,ads}$ species were formed on the catalyst from NO only at atmospheric pressure. The TPD profiles after the interaction of O_2 for 5 min at 523 K with the NO pre-treated (5 min at 523 K) Fe-ZSM-5_{350} are illustrated in Figure 6.5b.

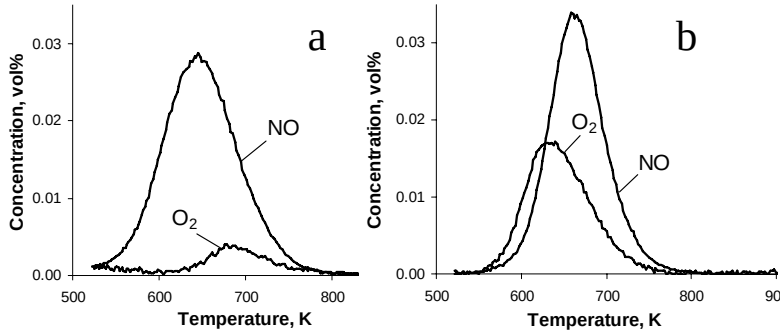

Figure 6.5: TPD profiles obtained after interaction of NO (0.5 vol%, 5 min) (a) and consecutive interaction of NO (0.5 vol%, 5 min) and O_2 (1.5 vol%, 5 min) (b) with the Fe-ZSM-5_{350} at 523 K.

The subsequent interaction of NO_{ads} and O_2 led to the formation of more $NO_{x,ads}$ species than after NO interaction only as seen by the increased amount of desorbed oxygen. It is important to note that O_2 was not found in TPD experiments (not shown) after the interaction of O_2 for 5 min with the standard pre-treated catalyst. In summary, O_2 didn't adsorb on the "clean" catalyst but it interacted with the NO pre-treated catalyst forming $NO_{x,ads}$ species.

TAP experiments showed that NO pulses led to the desorption of surface atomic oxygen, $(O)_{Fe}$, at low temperatures (523 K and 593 K) where the desorption of O_2 was not observed during N_2O interaction with the Fe-ZSM-5. NO adsorbed in large amounts on the catalyst and formed a minor part of $NO_{x,ads}$ species. In contrast to TAP results,

the desorption of oxygen upon NO interaction with $(O)_{Fe}$ at 523 K was not observed in transient experiments at atmospheric pressure [11]. The thin catalyst bed in the TAP reactor was left quickly by O_2 whereas during experiments at atmospheric pressure the freed O_2 had the possibility to react further with NO_{ads} or with gas phase NO forming finally $NO_{x,ads}$ species. That is a possible explanation for the difference to flow experiments where the desorption of oxygen during the interaction of NO with $(O)_{Fe}$ was not observed.

6.4. $NO_{x,ads}$ Species Reactivity in CO Oxidation

In the previous sections it was shown that $NO_{x,ads}$ species are formed by the interaction of N_2O with the standard pre-treated Fe-ZSM-5_{5500} and even more with the NO pre-treated catalyst. These $NO_{x,ads}$ species facilitate the oxygen desorption in TPD experiments and are proposed as "co-catalyst" in the N_2O decomposition. Their reactivity concerning CO oxidation is discussed in this section as well as their influence on the reactivity of atomic surface oxygen loaded from N_2O.

Only a small amount of irreversibly adsorbed NO remained on the catalyst after 600 NO pulses over the Fe-ZSM-5_{5500} at 523 K. In Figure 6.6b, curve 1 it can be seen that NO desorbed in a broad peak during the TPD experiment. No oxygen (Figure 6.6a, curve 1) desorbed and was, therefore, not formed during NO treatment. 600 N_2O pulses subsequent to the NO pre-treatment loaded surface oxygen which desorbed in a TPD run with a maximum at 640 K (Figure 6.6a, curve 2). NO evolved (Figure 6.6b, curve 2) in a sharp peak at the end of the oxygen desorption indicating $NO_{x,ads}$ species. The interaction of CO with the surface species formed after NO→N_2O treatment led to the formation of CO_2. CO oxidation took place. In the following TPD run it could be observed that all surface oxygen was removed by CO (Figure 6.6a, curve 3) and NO desorbed in a broad peak as irreversibly adsorbed NO (Figure 6.6b, curve 3). Thus, CO was oxidized by surface oxygen and the $NO_{x,ads}$ species were reduced to adsorbed NO.

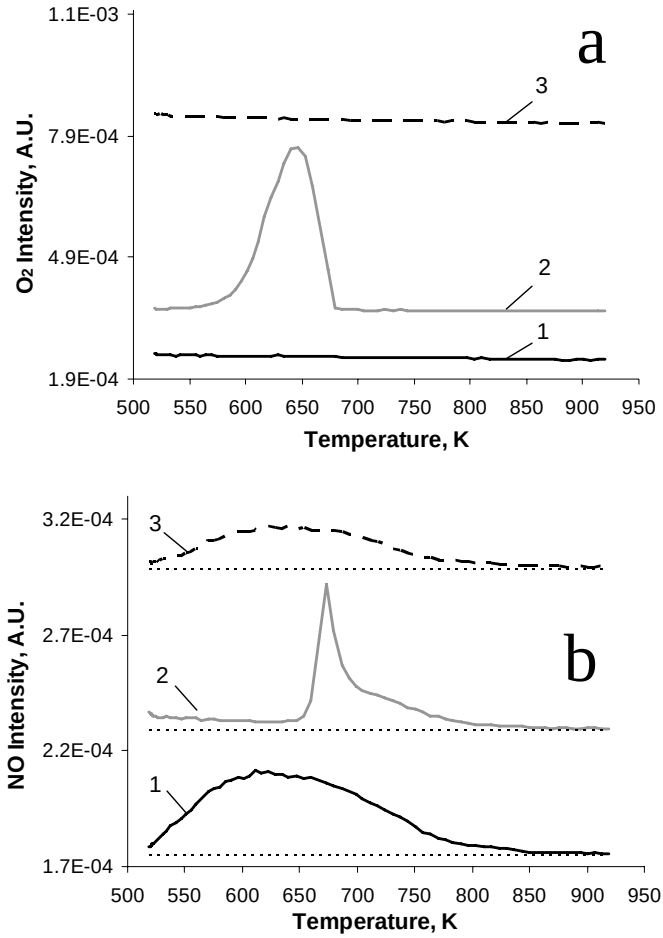

Figure 6.6: O_2 (a) and NO (b) TPD profiles obtained after pulsing NO (1), NO→N_2O (2) and NO→N_2O→CO (3) over the Fe-ZSM-5_{5500} catalyst at 523 K.

About 10 times more NO was adsorbed at 523 K on the catalyst which was pre-treated with 600 N_2O pulses loading surface oxygen as compared to the standard pre-treatment. In section 6.3 it is shown that NO provoked the desorption of the main part of the surface oxygen, only a small amount remained on the catalyst to form $NO_{x,ads}$ species. Several CO pulses reduced these $NO_{x,ads}$ species to NO_{ads} only. Hence, after a N_2O→NO→CO treatment of the Fe-ZSM-5_{5500} at 523 K the TPD experiment indicated only NO (Figure 6.7a and b, curve 1) which desorbed in a broad peak as already observed in Figure 6.6b, curve 1. 600 N_2O pulses over the N_2O→NO pre-treated catalyst resulted in the generation of surface oxygen and $NO_{x,ads}$ species which is

discussed in section 6.2 but for easier comparison once more presented in Figure 6.7a and b, curve 2.

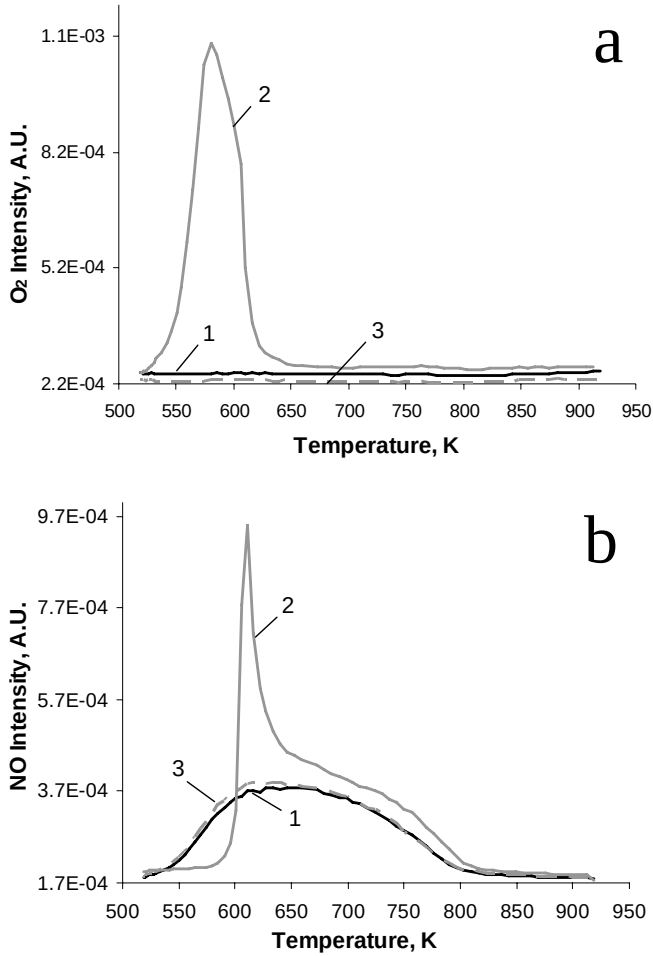

Figure 6.7: O_2 (a) and NO (b) TPD profiles obtained after pulsing $N_2O \rightarrow NO \rightarrow CO$ (1), $N_2O \rightarrow NO \rightarrow N_2O$ (2) and $N_2O \rightarrow NO \rightarrow N_2O \rightarrow CO$ (3) over the Fe-ZSM-5_{5500} catalyst at 523 K.

The interaction of CO with the surface species formed during the $N_2O \rightarrow NO \rightarrow N_2O$ treatment generated CO_2 at 523 K. The residual surface species are illustrated in Figure 6.7a and b, curve 3. Oxygen was completely removed and the $NO_{x,ads}$ species were reduced to NO_{ads}. NO desorbed again as broad peak such as after the $N_2O \rightarrow NO \rightarrow CO$ treatment (Figure 6.7a and b, curve 1) very similar to the desorption of

only NO in Figure 6.6b, curve 1 and 3. The only difference was that the $N_2O \rightarrow NO$ pre-treatment (Figure 6.7) led to a 10 times larger amount of adsorbed NO as compared to the NO pre-treatment (Figure 6.6). Thus, even in the presence of much higher NO concentrations, the whole surface oxygen was removed by CO and the $NO_{x,ads}$ species were reduced to NO_{ads}.

The same NO and O_2 TPD profiles were generated upon the treatment of the $(O)_{Fe}$ and $NO_{x,ads}$ containing catalyst with CO as after the adsorption of gaseous NO as seen in Figure 6.6 and Figure 6.7. Only NO_{ads} was detected and no oxygen could be found upon increasing the temperature to 916 K in vacuum. The interaction of CO with the catalyst produced CO_2 in the presence of adsorbed NO_x species, reduced them to NO_{ads} and efficiently scavenged off all atomic oxygen. Thus, the reactivity of $(O)_{Fe}$ in CO oxidation was not diminished by the presence of $NO_{x,ads}$ species on the catalyst in TAP experiments. These observations are summarized in the following equation:

$$(O)_{Fe}, NO_{x,ads} + CO \rightarrow ( )_{Fe}, NO_{ads} + CO_2 \qquad (6.5)$$

In line with these conclusions are results from El-Malki et al. [7]. Nitro and nitrate groups were detected in FTIR spectra obtained by N_2O exposure to Fe/MFI at 473 K. Additionally, the same bands were observed over Fe/MFI samples upon simple exposure to a flow of NO and O_2 in He at the same temperature. It is interesting that a treatment with CO at 473 K of samples containing nitro and nitrate bands led to the disappearance of them, indicating their high reactivity towards CO. The bands of the NO_x groups disappeared also upon contacting the sample with benzene vapor at 473 K but remained intact at room temperature.

Studies at atmospheric pressure reported an inhibiting effect of adsorbed NO/NO_x species on the oxygen reactivity in CO oxidation [11]. By using the transient response method it was observed that the presence of $NO_{x,ads}$ did not inhibit the surface oxygen loading from N_2O at 523 K. However, the reactivity of $(O)_{Fe}$ towards CO oxidation at low temperatures (< 523 K) was drastically diminished for a catalyst with pre-adsorbed NO/NO_x species. Surface NO_x species probably blocked the sites necessary for CO activation, which were in vicinity of the loaded atomic oxygen as was concluded. The concentration of NO_{ads} on the catalyst in the vacuum system was certainly lower than at atmospheric pressure and, therefore, a diminished reactivity of the surface oxygen in CO oxidation was not observed in TAP experiments.

In summary, NO has a catalytic effect in direct N_2O decomposition by accelerating the O_2 desorption whereas CO as reducing agent regenerates active iron sites. Apparently the catalytic surface species, $NO_{x,ads}$, were formed during N_2O interaction with the assistance of NO_{ads} and were easily reduced by CO to irreversibly

adsorbed NO_{ads}. Adsorbed NO underwent a redox cycle where N_2O oxidizes NO_{ads} to $NO_{x,ads}$ which was reduced by CO to NO_{ads} as schematically pictured below:

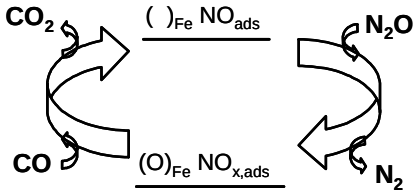

6.5. Deposited Oxygen Reactivity in Presence of Reversibly Adsorbed NO

NO pulses at 523 K over the Fe-ZSM-5_{5500} using the TAP setup resulted in a very broad NO response, indicating the strong adsorption of NO on the catalyst. It took about 5 min to desorb the reversibly adsorbed NO from the catalyst after the NO introduction was stopped. Irreversibly adsorbed NO stayed on the catalyst and desorbed only by increasing the reactor temperature. The role of irreversibly adsorbed NO is elucidated in section 6.1 to 6.4. It was either formed during N_2O interaction or adsorbed during NO treatments. The influence of reversibly adsorbed NO on the activity of oxygen loaded from N_2O was studied in N_2O/CO pump-probe experiments at 523 K. Oxygen was loaded from N_2O which formed with CO the product CO_2 in case that the loaded oxygen was active in CO oxidation. N_2O was pulsed at 0 s and CO at 5 s. The cycle time was 10 s.

At first, the catalyst was pre-treated with 600 NO pulses. Thereafter, the reversibly adsorbed NO desorbed during a period of 10 min without pulses. In a subsequent N_2O/CO pump-probe experiment was observed that reversibly adsorbed NO was completely desorbed (Figure 6.8a). CO_2 was formed from the oxygen loaded from N_2O and CO as from the very first cycle (Figure 6.8b).

In a second experiment, the catalyst was again pre-treated with 600 NO pulses and the N_2O/CO pump-probe experiment was performed right after the NO treatment so that reversibly adsorbed NO was still on the catalyst. The desorption of reversibly adsorbed NO is shown in Figure 6.9a. During the first 15 cycles NO was detected and desorbed. At the same time CO_2 was not formed as presented in Figure 6.9b. Only after the 15^{th} cycle, CO_2 was created from the surface oxygen loaded from N_2O and CO.

The reversibly adsorbed NO inhibited the formation of CO_2 by blocking sites necessary for the activation of the reactants CO or surface oxygen. Another possibility is that oxygen was not loaded from N_2O in the presence of reversibly adsorbed NO which could not be found out in TAP experiments. A TPR experiment (section 7.3) with a mixture of NO and N_2O at atmospheric pressure with the Micromeritics AutoChem 2910 setup showed that oxygen loading from N_2O at 523 K or the N_2O decomposition at higher temperatures was never suppressed by the presence of gaseous NO. Thus, oxygen loaded from N_2O on the catalyst was not active in CO oxidation in the presence of reversibly adsorbed NO in vacuum conditions.

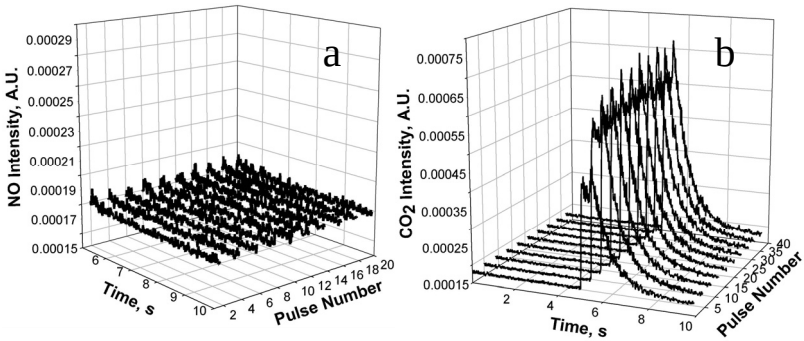

Figure 6.8: NO (a) and CO_2 (b) responses obtained during the oxidation of CO, pulsed at 5 s, with $(O)_{Fe}$ loaded from a N_2O pulse at 0 s over the Fe-ZSM-5_{5500} at 523 K in the absence of reversibly adsorbed NO.

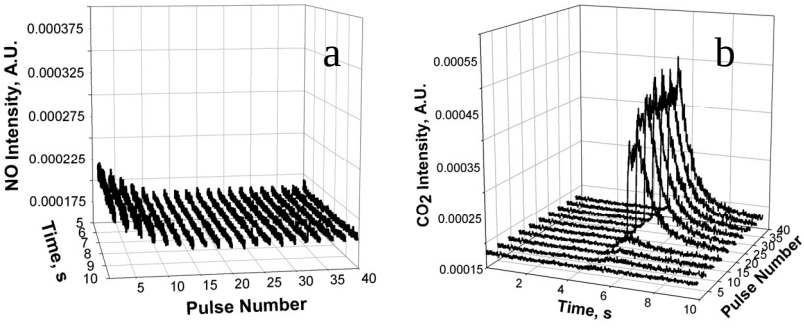

Figure 6.9: NO (a) and CO_2 (b) responses obtained during the oxidation of CO, pulsed at 5 s, with $(O)_{Fe}$ loaded from a N_2O pulse at 0 s over the Fe-ZSM-5_{5500} at 523 K in the presence of reversibly adsorbed NO during the first 15 pulses.

Irreversibly adsorbed NO promoted the N_2O decomposition by accelerating the desorption of surface oxygen and reversibly adsorbed NO inhibited the oxidation of CO

with surface oxygen. The dual role of NO, acting as a promoter in N_2O decomposition and as an inhibitor in N_2O reduction with CO was also discussed for experiments at atmospheric pressure and the findings were attributed to the presence of different iron species [18]. NO was found to selectively inhibit the reduction of N_2O of isolated iron sites at low temperature, disabling CO and N_2O activation.

Pirngruber et. al. [19] proposed that de-hydroxylation at 873 K created vacancies in the coordination sphere of iron that allowed the adsorption of two or even three molecules of NO on one site. Bulushev et al. [6] assigned in DRIFTS studies thermally stable NO species during NO interaction to mononitrosyl $Fe^{2+}(NO)$ species involved in surface bi- and oligonuclear iron species, probably with aluminum in vicinity. Dinitrosyl $Fe^{2+}(NO)_2$ or trinitrosyl $Fe^{2+}(NO)_3$ species also existed while the iron Fe-ZSM-5 was exposed to gaseous NO. However, they were found to be unstable in inert gas flow. Therefore, the promoting effect of irreversibly adsorbed NO was assigned to mononitrosyl species while dinitrosyl and trinitrosyl sites were related to reversibly adsorbed NO.

In general, iron species accepting two or three NO molecules should possess high coordinative unsaturation and are probably isolated. The amount of produced CO_2 in the presence of reversibly adsorbed NO was almost negligible. This would mean that the majority of active sites were highly coordinative unsaturated.

In summary, NO possesses a dual role acting as promoter in N_2O decomposition and as an inhibitor in N_2O reduction with CO. The inhibiting effect was shown by reversibly adsorbed NO with TAP experiments in vacuum. Oxygen loaded from N_2O on the catalyst was not active in CO oxidation in the presence of reversibly adsorbed NO.

6.6. Effect of NO on N_2O Decomposition Studied in Pump-Probe Experiments

NO promotes the N_2O decomposition over Fe-ZSM-5. Mechanistic studies at different temperatures (593-946 K) were performed using so-called pump-probe experiments. The Fe-ZSM-5_{5500} and the Fe-ZSM-5_{200} catalyst were tested and compared to check for the importance of the inactive part of Fe. The Fe-ZSM-5_{200} contained only 7% inactive Fe and the Fe-ZSM-5_{5500} around 95%. Generally, the results were quite similar to the results obtained with the Multitrack system [3].

6.6.1. N_2O/NO Pump-Probe Experiments

The effect of NO on the N_2O interaction was studied using pump-probe experiments, in which pulses of N_2O and NO were consecutively fed to the reactor. A pulse of N_2O was followed by a pulse of NO. Before each alternating pulse experiment the catalyst was heated at 946 K for 30 min followed by approximately 1000 pulses of N_2O ($3.8 \cdot 10^{14}$ molecules/pulse) at the studied temperature.

N_2O and NO were sequentially introduced over the Fe-ZSM-5_{5500} at 661 K. The time interval between the two pulses was varied from 1 to 9.5 s and the alternate pulsing was repeated in cycles of 10 s. Some oxygen responses are exemplified in Figure 6.10 for N_2O at 0 s (curve 1) and for a delay time of 1 s (curve 2), 4 s (curve 3) and 9.5 s (curve 4) between the N_2O pulse at 0 s and the NO pulse. Only nitrous oxide interaction with the Fe-ZSM-5_{5500} at 661 K (curve 1) resulted in very slow oxygen desorption which can be observed through a very broad response. In the case of 1 s (curve 2) and 4 s (curve 3) delay time, NO was introduced, when the oxygen from the previous N_2O pulse was still in adsorbed state. The amount of evolved oxygen per cycle was independent of the time interval between the N_2O and the NO pulse. The NO pulse provided the appearance of an additional very sharp O_2 response. This sharp peak was not observed when Ar was pulsed instead of NO. It was not accompanied by nitrogen or NO_2 evolution. The NO response itself was very broad (not shown). Initial sharpening of the oxygen response at the time of the N_2O pulse was observed especially when the NO pulse was short-time before the N_2O pulse as in Figure 6.10, curve 4 with 0.5 s between the NO and N_2O pulses (9.5s between the N_2O and NO pulses). This indicates that NO or NO_x species were in adsorbed state before the N_2O pulse. Switching off NO pulsing resulted in NO desorption and transition of the catalyst behavior to the original one, with a very broad O_2 response (not shown) like that shown in Figure 6.10, curve 1 in accordance with the data reported in [3].

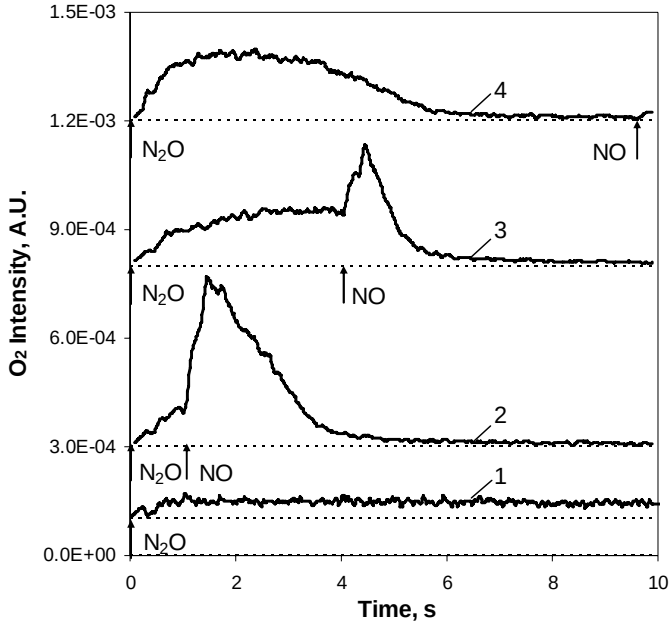

Figure 6.10: Oxygen response profiles obtained during catalytic decomposition of N_2O over Fe-ZSM-5_{5500} at 661 K pulsing only N_2O at 0 s (1) and pulsing N_2O at 0 s and NO at 1 s (2), 4 s (3), 9.5 s (4), respectively.

During the NO addition the O_2 profile (curve 2 to 4) sharpened at the time of the N_2O pulse, indicating a significantly faster O_2 desorption in N_2O/NO alternating cycles, than in the experiment with N_2O only. Additionally, the NO pulse led to a sharp O_2 response. It is shown in chapter 5 that surface oxygen from N_2O was loaded very quickly and there was no O_2 re-adsorption on the Fe-ZSM-5 catalyst. Hence, the shape of the O_2 response was provided by its desorption as a rate-determining step for N_2O decomposition. Consequently the NO pulse accelerated the desorption of the loaded oxygen.

NO/N_2O pump-probe experiments were also performed with the Fe-ZSM-5_{5500} at 661 K and shown in Figure 6.11. NO was pulsed 0.1 s, 0.5 s and 3 s before the N_2O pulse and repeated in a 10 s cycle. It is seen that the oxygen peak sharpened with decreasing time between the NO and N_2O pulse from 3 to 0.1 s. The decrease of the time interval resulted in higher concentration of adsorbed NO/NO_x species during the N_2O pulse. The oxygen desorbed during the N_2O pulse much faster in case when NO was adsorbed before the N_2O pulse, which is in line with the data [3]. The amount of desorbed oxygen per cycle was constant and independent of the time interval. Thus, adsorbed NO species facilitated oxygen desorption in accordance with TPD data (section

6.1 and 6.2) without the conversion of NO_{ads} to gaseous products as no NO_2 in the gas phase was observed.

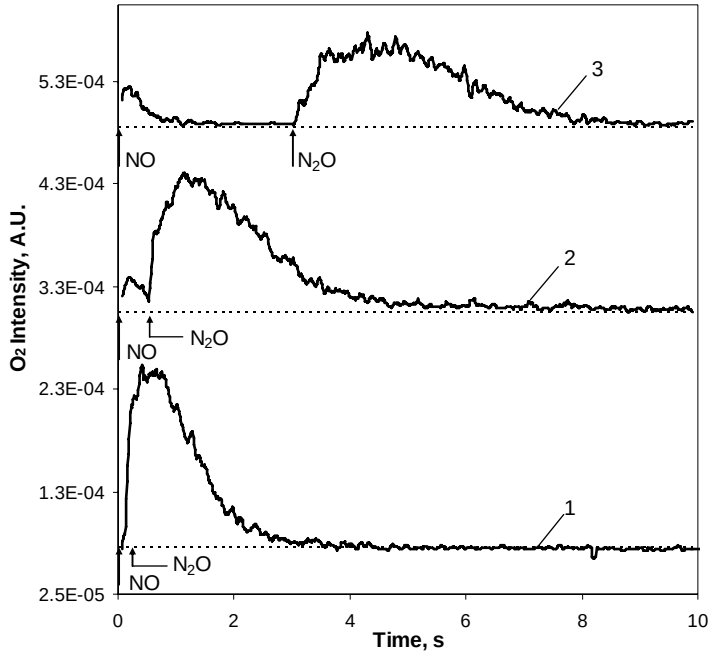

Figure 6.11: Oxygen response profiles obtained during pulsing NO at 0 and N_2O at 0.1 s (1), 0.5 s (2) and 3 s (3), respectively over Fe-ZSM-5_{5500} at 661 K.

Similar initial sharpening of the oxygen response was observed at 661 K during N_2O/NO experiments (Figure 6.10), which showed that NO or NO_x species were in adsorbed state before the N_2O pulse. The difference of N_2O/NO to NO/N_2O pump-probe experiments was that NO was introduced, when the oxygen from the previous N_2O pulse was still in adsorbed state (Figure 6.10) contrary to the pulse consequence, when the NO pulse was introduced 0.1-3 s before the N_2O pulse (Figure 6.11). In the latter case oxygen already desorbed before the NO pulse. No gaseous NO_2 was detected during the reaction under any reported conditions contrary to the results of Perez-Ramirez et al. [3] at 773 K. Decomposition of NO to N_2 and O_2 was never observed during those mechanistic studies of the NO-assisted N_2O decomposition.

At 803 K N_2O decomposed into N_2 and O_2 while O_2 desorbed from the catalyst within 10 s. In N_2O/NO pump-probe experiments the time interval between the N_2O, always pulsed at 0 s, and NO pulses was varied from 1 to 9 s and repeated in cycles of 10 s. Some oxygen responses are exemplified in Figure 6.12. The oxygen response didn't get significantly sharpened at the N_2O pulse but oxygen desorbed very fast while NO

was introduced. The integration of the oxygen response showed that the amount of released O_2 per cycle was constant and absolutely independent of the time interval at 803 K as well as at 661 K.

In contrast with the studies at 661 K where a few alternating pulse experiments cycles had to be performed in order to obtain a constant oxygen desorption profile, the promoting effect on the reaction at 803 K was already with the first NO pulse completely developed. This suggests a slow accumulation of NO on the catalyst at 661 K while at higher temperatures NO is only very weakly bonded to the catalyst and, therefore, almost instantaneously desorbed.

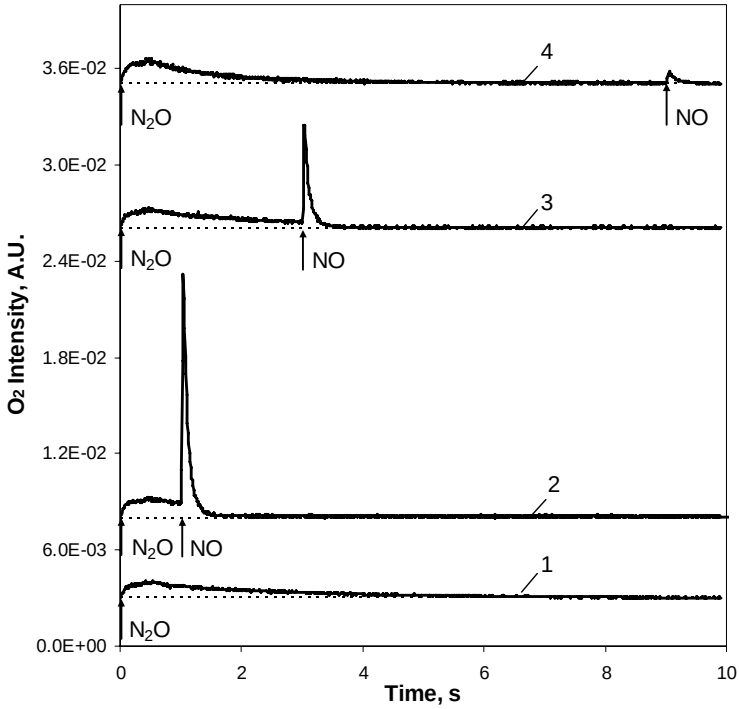

Figure 6.12: Oxygen response at 803 K during catalytic decomposition of N_2O over Fe-ZSM-5_{5500}: pulsing only N_2O at 0 s (1) and NO-assisted by pulsing N_2O at 0 s and NO after different time intervals: 1 s (2), 3 s (3) and 9 s (4).

A N_2O/NO pump-probe experiment at high temperature (946 K) with a time interval of 3 s between the N_2O and NO pulse is illustrated in Figure 6.13. The cycle time was 10 s. The O_2 profiles received by introducing N_2O only or sequentially pulsing N_2O and NO strongly resembled each other, indicating that the promotion of NO was negligible. Obviously, oxygen was completely desorbed before the NO pulse was introduced and NO was desorbed before N_2O was pulsed. Additionally, the oxygen

recombination/desorption at 946 K was already much faster compared to lower temperatures as discussed in chapter 5 and more difficult to accelerate further.

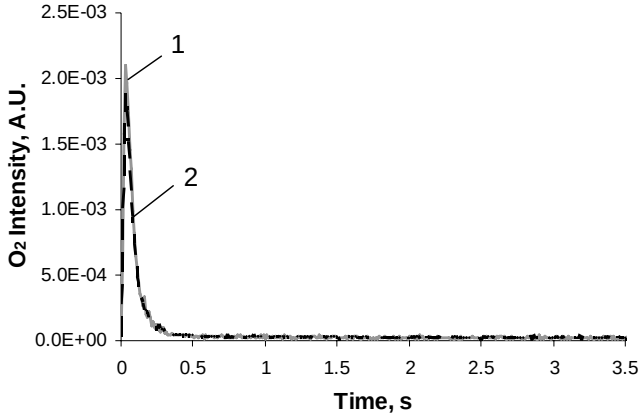

Figure 6.13: Oxygen profiles obtained during catalytic decomposition of N_2O over Fe-ZSM-5_{5500} at 946 K: pulsing N_2O at 0 s (1) and pulsing N_2O and NO at 0 s and 3 s (2), respectively.

All the experiments presented in this section were repeated with another Fe-ZSM-5 sample. The zeolite contains only 200 ppm Fe and different to the catalyst applied so far as no binder was used during fabrication. Therefore, the Fe-ZSM-5_{5500} contains iron compounds and provides more than 95% inactive Fe atoms. The home-made Fe-ZSM-5_{200} catalyst contains almost exclusively active iron sites (93%).

In general, the same results were obtained for the 200 ppm and the 5500 ppm Fe sample in N_2O/NO pump-probe experiments in the range of 593 to 946 K which proved that the observed effects were related to iron sites active in N_2O decomposition and not to inactive Fe atoms from the binder. The oxygen response after the interaction from N_2O and NO with the Fe-ZSM-5_{200} at 661 K is exemplified in Figure 6.14. Curve 1 shows the nitrous oxide interaction with the zeolite which resulted in very slow oxygen desorption observed through a very broad response. Curves 2, 3, and 4 illustrate the oxygen profile during catalytic decomposition of nitrous oxide pulsing N_2O at 0 s and NO at 1 s during the 1st, 2nd and 20th cycle, respectively in pump-probe experiments. The O_2 profile sharpened during the NO addition at the time of the N_2O pulse and the NO pulse with increasing cycle number. NO slowly accumulated on the catalyst and augmented its promoting effect on the oxygen desorption with increasing cycle number resulting in a constant response after 20 cycles.

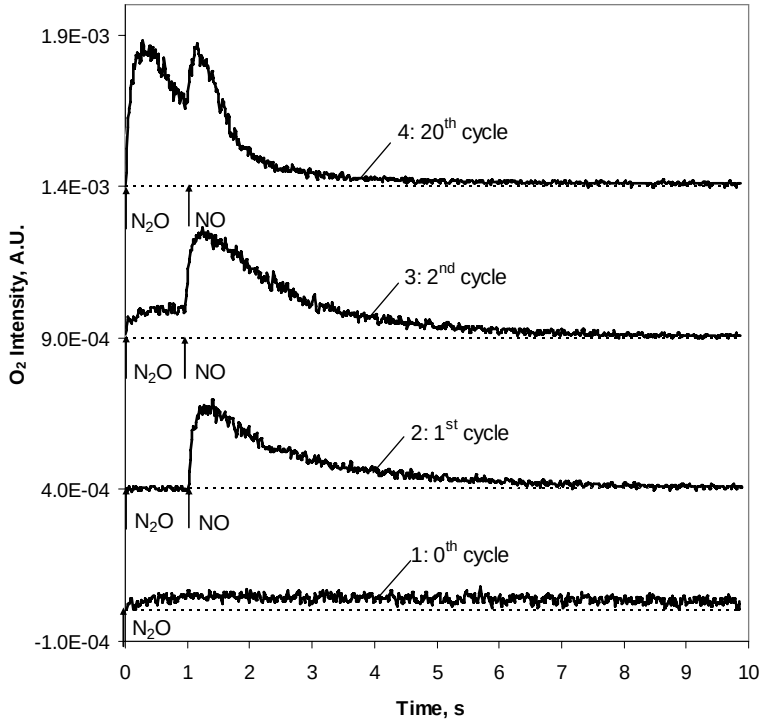

Figure 6.14: Oxygen profiles obtained during catalytic decomposition of N_2O over Fe-ZSM-5_{200} at 661 K pulsing only N_2O at 0 s (1) and pulsing N_2O and NO at 0 and 1 s (curve 2-4), respectively. The 1st, 2nd and 20th cycle of the N_2O/NO pump-probe experiment are shown in curve 2 to 4.

6.6.2. Discussion

The effect of NO on surface atomic oxygen deposited on Fe-ZSM-5 from N_2O was investigated in N_2O/NO pump-probe experiments at different temperatures. In TAP experiments the promoting effect of NO on the oxygen recombination/desorption was observed at 661 K where oxygen desorption usually took place but only very slowly (Figure 6.10, curve1). The presence of adsorbed NO facilitated the oxygen recombination/desorption significantly during the N_2O pulse (Figure 6.10, curve 2 to 4). Additionally, the NO pulse led to a spontaneous oxygen release of the residual surface oxygen (Figure 6.10, curve 2 and 3). The sharp oxygen evolution during the NO pulse as observed in Figure 6.10 was not reported earlier. The explanation of this peak is connected to the interaction of gaseous NO with loaded oxygen species forming gaseous

oxygen. In similar studies Perez-Ramirez et al. [3] did not observe O_2 desorption at the time of the NO pulse which was probably connected to a delayed NO pulse respectively to the time period of O_2 desorption. If all oxygen species were already desorbed, the addition of NO had no instant effect.

Both adsorbed NO from previous cycles and introduced NO accelerated the desorption of surface oxygen. A constant amount of oxygen desorbed per cycle independently of the time interval between the two pulses. Probably $NO_{2,ads}$ was formed during the interaction of added NO with adsorbed oxygen on the catalyst:

$$NO_{ads} + (O)_{Fe} \rightarrow NO_{2,ads} + (\ )_{Fe} \tag{6.6}$$

This $NO_{2,ads}$ transferred oxygen to adsorbed oxygen quickly and decomposed back to NO_{ads} and molecular oxygen in the next step:

$$NO_{2,ads} + (O)_{Fe} \rightarrow O_2 + NO_{ads} + (\ )_{Fe} \tag{6.7}$$

NO_2 was not detected in the gas phase. Perez-Ramirez et al. [3] observed a decoupled formation of O_2 and NO_2. NO_2 was considered to be mainly released due to displacement by NO and probably by thermal desorption, while O_2 was formed during the N_2O pulses. Adsorbed NO is suggested to facilitate the oxygen transfer through NO_2 intermediates, enhancing the change of recombination to O_2.

TAP studies showed that NO had an enduring effect at least until the next N_2O pulse where it accelerated the O_2 recombination/desorption as compared to the N_2O only case seen by the initial sharpening in Figure 6.10. In line with this observation are the data of Figure 6.11 where smaller time delays between the NO and N_2O pulse led to faster oxygen desorption by the time of the N_2O pulse. The sharpening of the oxygen response during the N_2O pulse could be expressed by the following equation in which adsorbed NO facilitates the desorption of oxygen without the conversion of NO_{ads} to gaseous products:

$$(O)_{Fe} + NO_{ads} + (O)_{Fe} \rightarrow O_2 + NO_{ads} + 2(\ )_{Fe} \tag{6.8}$$

Temperature-programmed desorption in vacuum (section 6.1 and 6.2) and transient response experiments at atmospheric pressure [1, 11] confirmed as well that $NO_{x,ads}$ species facilitate the rate-determining step - the oxygen desorption.

At 803 K oxygen desorbs relatively fast within 10 s upon a N_2O pulse. N_2O/NO pump-probe studies presented also a spontaneous oxygen release of the residual surface oxygen during the NO pulse (Figure 6.12). Oxygen is permanently released whereas the NO pulse increased the desorption rate of the residual surface oxygen rapidly,

exemplified in Figure 6.12. The initial sharpening during the N_2O pulse was much less pronounced at 803 K than at 661 K since NO is quickly desorbed from the catalyst surface at this elevated temperature. A constant amount of oxygen was desorbed during a cycle independently of the time delay between the N_2O and NO pulse.

At higher temperatures as 946 K no obvious effect of NO on the oxygen desorption could be detected (Figure 6.13). The addition of NO had no measurable influence on the oxygen release and consequently on the N_2O decomposition since the oxygen desorption was already very fast at this temperature which is discussed in chapter 5.

All the results found in section 6.6.1 could be reproduced with a home-made catalyst Fe-ZSM-5_{200} (exemplified in Figure 6.14) containing almost only active Fe sites compared to the discussed commercial Fe-ZSM-5_{5500} with the majority of inactive iron from a binder. This evidences that the presented results originate from iron sites active in N_2O decomposition and they were not influenced by inactive iron which was also present in the Fe-ZSM-5_{5500}.

6.7. Summary

The interaction of N_2O and NO with the Fe-ZSM-5_{5500} at 523 K and 593 K were investigated by the TAP reactor for further mechanistic insight into the N_2O decomposition. Surface species were studied in temperature-programmed desorption experiments and the reactivity of surface oxygen was characterized by its capacity to oxidize CO. Table 6.1 summarizes these experiments. In addition, N_2O/CO pump-probe experiments served for the elucidation of the effect of reversibly adsorbed NO. The NO–assisted N_2O decomposition was studied with N_2O/NO pump-probe experiments at higher temperatures (661 K to 946 K).

During the interaction of N_2O with the zeolite at 593 K atomic surface oxygen was loaded and $NO_{x,ads}$ species were formed accompanied by N_2 evolution (section 6.1). The concentration of surface oxygen and $NO_{x,ads}$ species increased with increasing number of performed N_2O pulses. At the same time the temperature of maximum oxygen desorption decreased by ~35 K. Adsorbed NO_x acts as "co-catalyst" and facilitate the desorption of oxygen which is, in general, accepted as the rate-determining step of the N_2O decomposition. At 523 K all reactions of N_2O with the Fe-ZSM-5_{5500} were slower. Therefore, less surface oxygen was loaded and the $NO_{x,ads}$ species were below the detection limit.

Table 6.1: Summary of formed surface species and their capacity to oxidize CO upon different treatments of the Fe-ZSM-5_{5500} with N_2O and NO at 523 and 593 K using the TAP setup.

Temperature, K	*Treatment*	TPD responses			CO_2 evolution during CO interaction
		O_2	NO	NO_x	
523	N_2O	+	-	-	+
	NO	-	+	-	-
	$N_2O \rightarrow NO$	-	+	+	very little
	$N_2O \rightarrow NO \rightarrow N_2O$	+	+	+	+
	$NO \rightarrow N_2O$	+	+	+	+
593	N_2O	+	+	+	+
	$N_2O \rightarrow NO$	-	+	+	very little

The interaction of N_2O with the Fe-ZSM-5_{5500} containing adsorbed NO showed the formation of $NO_{x,ads}$ species (section 6.2). An increasing $NO_{x,ads}$ species concentration was accompanied by a shift of the oxygen desorption to significantly lower temperatures (by ~160 K) in TPD runs. Hence, $NO_{x,ads}$ species formed from pre-adsorbed NO and N_2O facilitated the desorption of oxygen.

NO pulses over the $(O)_{Fe}$ containing catalyst led to the recombination and desorption of surface atomic oxygen at low temperatures (523 K and 593 K) where the desorption of O_2 was not observed during N_2O interaction with the Fe-ZSM-5_{5500} (section 6.3). NO adsorbed in large amounts at the same time on the catalyst and formed a minor part of $NO_{x,ads}$ species. NO/NO_x adsorbed finally on adjacent sites to the N_2O decomposing sites since the reloading of oxygen from N_2O took place without any difficulty (section 6.2).

The $NO_{x,ads}$ species which were formed during N_2O interaction with the assistance of NO_{ads} were easily reduced to irreversibly adsorbed NO_{ads} (section 6.4). Hence, adsorbed NO underwent a redox cycle where N_2O oxidizes NO_{ads} to $NO_{x,ads}$ which was reduced by CO to NO_{ads}. In addition, the atomic surface oxygen loaded from N_2O was fully reactive in CO oxidation. The reactivity of $(O)_{Fe}$ was not diminished by the presence of $NO_{ads}/NO_{x,ads}$ species on the catalyst in TAP experiments.

N_2O/CO pump-probe experiments showed that oxygen loaded from N_2O on the catalyst was not active in CO oxidation in the presence of reversibly adsorbed NO in vacuum conditions (section 6.5). The reversibly adsorbed NO probably blocked sites necessary for the activation of the reactants CO or surface oxygen. Irreversibly adsorbed NO promoted the N_2O decomposition and reversibly adsorbed NO inhibited the oxidation of CO with surface oxygen.

N_2O/NO pump-probe experiments at 661 K demonstrated an accelerated oxygen desorption at the time of the N_2O pulse due to adsorbed NO/NO_x species. The subsequent NO pulse accelerated the desorption of the residual surface oxygen at 661 K and 803 K. At both temperatures a constant amount of oxygen was desorbed during a cycle independent of the time delay between the N_2O and NO pulse. NO promoted the desorption of oxygen. Adsorbed NO accommodated oxygen from N_2O forming higher oxidized nitrogen oxide species which decomposed back to NO_{ads} and molecular oxygen. Thus, the recombination of surface oxygen loaded from N_2O was accelerated by a NO/NO_x redox cycle.

At higher temperature such as 946 K the desorption of oxygen was already fast that no effect of NO was observed on the recombination and desorption of surface oxygen.

The findings from the N_2O/NO pump-probe experiments were reproduced with a home-made catalyst Fe-ZSM-5_{200} containing almost only active Fe sites compared to the discussed commercial Fe-ZSM-5_{5500} with 95% inactive iron. This evidences that the presented results originated from iron sites active in N_2O decomposition.

6.8. References

1. Bulushev, D. A.; Kiwi-Minsker, L.; Renken, A., Dynamics of N_2O decomposition over HZSM-5 with low Fe content. *Journal of Catalysis* **2004,** 222, (2), 389-396.
2. Kiwi-Minsker, L.; Bulushev, D. A.; Renken, A., Low temperature decomposition of nitrous oxide over Fe/ZSM-5: Modelling of the dynamic behaviour. *Catalysis Today* **2005,** 110, (3-4), 191-198.
3. Perez-Ramirez, J.; Kapteijn, F.; Mul, G.; Moulijn, J. A., NO-assisted N_2O decomposition over Fe-based catalysts: Effects of gas-phase composition and catalyst constitution. *Journal of Catalysis* **2002,** 208, (1), 211-223.
4. Mul, G.; Perez-Ramirez, J.; Kapteijn, F.; Moulijn, J. A., NO-assisted N_2O decomposition over ex-framework FeZSM-5: mechanistic aspects. *Catalysis Letters* **2001,** 77, (1-3), 7-13.
5. Sang, C. M.; Kim, B. H.; Lund, C. R. F., Effect of NO upon N_2O decomposition over Fe/ZSM-5 with low iron loading. *Journal of Physical Chemistry B* **2005,** 109, (6), 2295-2301.
6. Bulushev, D. A.; Renken, A.; Kiwi-Minsker, L., Formation of the surface NO during N_2O interaction at low temperature with iron-containing ZSM-5. *Journal of Physical Chemistry B* **2006,** 110, (1), 305-312.
7. El-Malki, E. M.; van Santen, R. A.; Sachtler, W. M. H., Active sites in Fe/MFI catalysts for NO_x reduction and oscillating N_2O decomposition. *Journal of Catalysis* **2000,** 196, (2), 212-223.
8. Grubert, G.; Hudson, M. J.; Joyner, R. W.; Stockenhuber, M., The room temperature, stoichiometric conversion of N_2O to adsorbed NO by Fe-MCM-41 and Fe-ZSM-5. *Journal of Catalysis* **2000,** 196, (1), 126-133.
9. Shimokawabe, M.; Tadokoro, K.; Sasaki, S.; Takezawa, N., Temperature programmed desorption and infrared spectroscopic studies of nitrogen monoxide

adsorbed on ion-exchanged copper mordenite catalysts. *Applied Catalysis A-General* **1998,** 166, (1), 215-223.
10. Turek, T., Kinetics of nitrous oxide decomposition over Cu-ZSM-5. *Applied Catalysis B-Environmental* **1996,** 9, (1-4), 201-210.
11. Bulushev, D. A.; Renken, A.; Kiwi-Minsker, L., Role of adsorbed NO in N_2O decomposition over iron-containing ZSM-5 catalysts at low temperatures. *Journal of Physical Chemistry B* **2006,** 110, (22), 10691-10700.
12. Sang, C. M.; Lund, C. R. F., Possible role of nitrite/nitrate redox cycles in N_2O decomposition and light-off over Fe-ZSM-5. *Catalysis Letters* **2001,** 73, (1), 73-77.
13. Joyner, R.; Stockenhuber, M., Preparation, characterization, and performance of Fe-ZSM-5 catalysts. *Journal of Physical Chemistry B* **1999,** 103, (29), 5963-5976.
14. Lobree, L. J.; Hwang, I. C.; Reimer, J. A.; Bell, A. T., An in situ infrared study of NO reduction by C_3H_8 over Fe-ZSM-5. *Catalysis Letters* **1999,** 63, (3-4), 233-240.
15. Delgado, J. A.; Nijhuis, T. A.; Kapteijn, F.; Moulijn, J. A., Determination of adsorption and diffusion parameters in zeolites through a structured approach. *Chemical Engineering Science* **2004,** 59, (12), 2477-2487.
16. Fierro, V.; Schuurman, Y.; Mirodatos, C.; Duplan, J. L.; Verstraete, J., Study of the cracking reaction of linear and branched hexanes under protolytic conditions by non-stationary kinetics. *Chemical Engineering Journal* **2002,** 90, (1-2), 139-147.
17. Keipert, O. P.; Baerns, M., Determination of the intracrystalline diffusion coefficients of alkanes in H-ZSM-5 zeolite by a transient technique using the temporal-analysis-of-products (TAP) reactor. *Chemical Engineering Science* **1998,** 53, (20), 3623-3634.
18. Boutarbouch, M. N. D.; Cortes, J. M. G.; El Begrani, M. S.; de Lecea, C. S. M.; Perez-Ramirez, J., Catalytic conversion of N_2O over FeZSM-5 zeolite in the presence of CO and NO. *Applied Catalysis B-Environmental* **2004,** 54, (2), 115-123.
19. Pirngruber, G. D.; Roy, P. K., A look into the surface chemistry of N_2O decomposition on iron zeolites by transient response experiments. *Catalysis Today* **2005,** 110, (3-4), 199-210.

Chapter 7

NO_2 INTERACTION WITH Fe-ZSM-5

Nitrogen dioxide (NO_2) is a reddish brown, highly reactive and more toxic than NO and N_2O. NO_2 is in equilibrium with NO and O_2:

$$NO_2 \rightleftarrows NO + \tfrac{1}{2}O_2 \qquad (7.1)$$

The decomposition of NO_2 is endothermic with a standard reaction enthalpy of 57.09 kJ/mol which is about constant from 298 to 1200 K [1]. Therefore, the equilibrium is shifted to the right with increasing temperature. With a standard reaction Gibbs energy of 35.27 kJ/mol, the equilibrium constant is unity at 780 K. The equilibrium between $NO+O_2$ and NO_2 is swiftly established over Fe-ZSM-5 [2].

A simple two-step mechanism involving cation redox cycles on extra-framework Fe sites is often considered for the N_2O decomposition such as described in chapter 5. Additional pathways involving NO/NO_2 [3-5] and NO_2/NO_3 [6] species are discussed when NO_x species are produced as surface or gas phase species. Adsorbed NO_2 is an intermediate of the catalytic N_2O decomposition cycle and is formed when adsorbed NO accommodates oxygen from N_2O leading to the facilitation of oxygen recombination/desorption [3, 4, 7-9]

It was hypothesized that NO_2 is also able to produce adsorbed (atomic) oxygen which could be used as selective oxidant [4]. The interaction of gaseous NO_2 with Fe-ZSM-5 is rarely studied especially at low temperatures where the NO/NO_2 equilibrium is shifted to NO_2. It is interesting to know whether NO_2 can similarly to N_2O provide atomic surface oxygen which can also oxidize CO already at 523 K. Furthermore, to what extent does NO_2 resemble the autocatalytic effect of $NO_{x,ads}$ species or the assisting role of NO in the N_2O decomposition? TAP experiments in vacuum and transient response experiments at atmospheric pressure were performed to elucidate the function of NO_2 in the N_2O decomposition network over Fe-ZSM-5 at 523 K.

The transient experiments which were performed at 523 K with NO_2 using the TAP setup in vacuum with the Fe-ZSM-5_{5500} and the Micromeritics Analyzer at atmospheric pressure with the Fe-ZSM-5_{350} are summarized in Table 7.1. Temperature-programmed reaction (TPR) flow experiments at atmospheric pressure with N_2O, NO_2, N_2O+NO and N_2O+NO_2 mixtures are discussed in section 7.3. The surface species formed from NO_2 on the catalyst were investigated with in situ DRIFTS and the findings are presented in section 7.4.

Table 7.1: Summary of NO_2 interactions with Fe-ZSM-5 at 523 K performed with the TAP setup and the Micromeritics Analyzer.

Catalyst Treatment	*TAP setup*	*Micromeritics Analyzer*	*Section*
NO_2	+	+	7.1
$NO_2 \rightarrow CO$	+	+	7.1
$NO_2 \rightarrow N_2O$	+	+	7.2
$NO_2 \rightarrow N_2O \rightarrow CO$	+	-	7.2
$N_2O \rightarrow NO_2$	+	+	7.2
$N_2O \rightarrow NO_2 \rightarrow CO$	+	+	7.2

7.1. Formation of Surface Species from NO_2

7.1.1. Pulse Experiments with TAP Setup under Vacuum

NO_2 is described as reactive intermediate in the N_2O decomposition over Fe-ZSM-5. Furthermore, it was proposed that NO_2 could provide reactive oxygen as N_2O does. In order to elucidate this hypothesis NO_2 was dosed over Fe-ZSM-5_{5500} and the formed surface species were studied in TPD and CO oxidation experiments. 300 pulses

of NO_2 were introduced at 523 K over the Fe-ZSM-5_{5500}. The NO_2 and NO pulse responses are seen in Figure 7.1. The NO_2 pulse response was very broad, probably due to strong reversible adsorption:

$$NO_2 \quad \rightleftarrows \quad NO_{2,ads} \tag{7.2}$$

NO desorbed very slowly. The similar shape of NO_2 and NO was certainly due to NO_2 fragmentation to NO and oxygen inside the ionization chamber of the mass spectrometer [10].

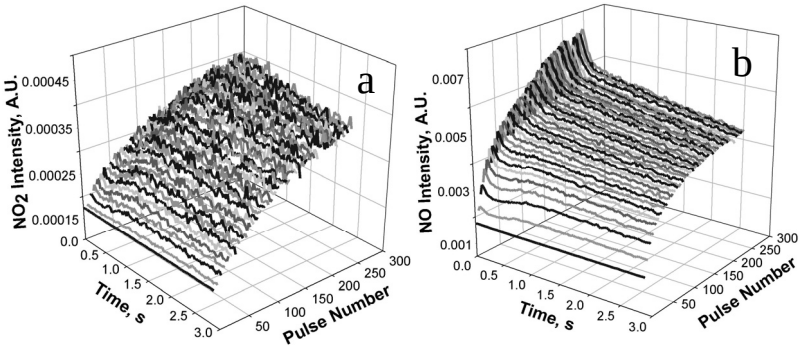

Figure 7.1: NO_2 (a) and NO (b) responses during the introduction of NO_2 pulses over the Fe-ZSM-5_{5500} at 523 K.

However, the peak at the beginning of the NO response was clearly not present in the NO_2 response and indicated the production of NO from NO_2. The oxygen response didn't contain this initial peak. It can be assumed that the oxygen formed during NO_2 decomposition was adsorbed on the catalyst surface:

$$NO_{2,ads} \quad \rightarrow \quad NO \quad + \quad O_{ads} \tag{7.3}$$

The surface species formed during NO_2 interaction with the catalyst were studied in a subsequent TPD experiment. Figure 7.2 shows the TPD profiles of AMU 46, 32 and 30. A desorption maxima was observed around 573 K in the profiles of AMU 46, 32 and 30 indicating the decomposition of a $NO_{x,ads}$ species. A shoulder around 793 K was only observed in the AMU 32 and 30 profiles indicating the desorption of an additional, different surface species. The desorption profiles with a maxima around 573 K and a shoulder around 773 K indicated two different species on the catalyst or two different sites which interacted with NO_2.

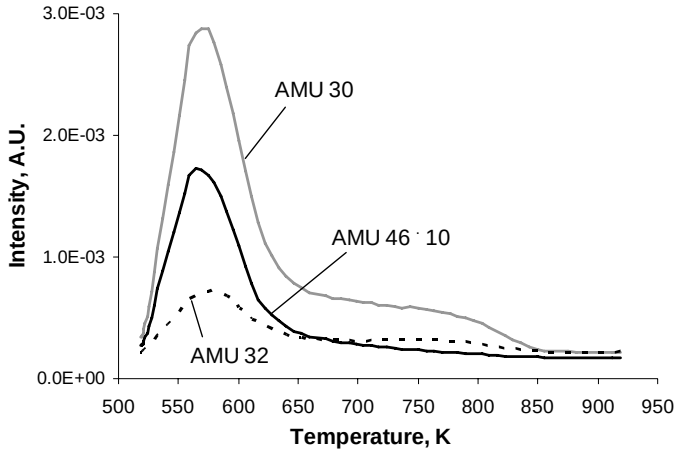

Figure 7.2: TPD profiles of AMU 46, 32, 30 after 300 pulses of NO_2 in Ar over Fe-ZSM-5_{5500} at 523 K.

The existence of active atomic surface oxygen can be clarified by a comparison of the AMU 32 profile with typical $(O)_{Fe}$-TPD profiles. Figure 7.3 summarizes the AMU 32 TPD profiles recorded after different treatments of the Fe-ZSM-5_{5500} at 523 K: (1) 300 pulses NO_2 and (2) 600 pulses N_2O. Profile (2) presents reactive atomic oxygen loaded from N_2O. Neither the desorption maxima, nor the shape of the $(O)_{Fe}$-TPD profiles were similar to the AMU 32 profile after NO_2 interaction with the catalyst. The formation of reactive atomic surface oxygen from NO_2 seemed to be unlikely.

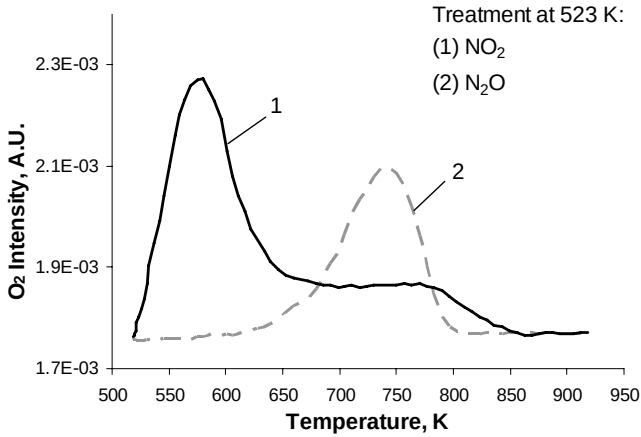

Figure 7.3: Comparison of AMU 32 TPD profiles after: 300 pulses NO_2 (1) and 600 pulses N_2O (2) over Fe-ZSM-5_{5500} at 523 K.

In order to verify the reactivity of the surface species, formed from NO_2, CO pulses were introduced after exposing the catalyst to NO_2 at 523 K. No formation of CO_2 was observed which would be the case in the presence of reactive atomic oxygen on the catalyst. This is summarized in the following equations:

$$\begin{aligned} O_{ads}\ from\ NO_2 \ + \ CO \ &\not\rightarrow \ CO_2 \\ O_{ads}\ from\ NO_2 \ &\neq \ (O)_{Fe}\ from\ N_2O \end{aligned} \tag{7.4}$$

Thus, it can be concluded that NO_2 adsorbed on the catalyst, accompanied by NO release, forming two different $NO_{x,ads}$ species which were inactive in CO oxidation. The TPD profiles (not shown) obtained upon NO_2→CO treatment were identical to that shown in Figure 7.2 after NO_2 only treatment. This is in line with the inactivity of the surface species from NO_2 with respect to CO oxidation to CO_2.

In order to get quantitative information, the interaction of NO_2 with Fe-ZSM-5_{350} was investigated in transient response experiments at atmospheric pressure.

7.1.2. Quantitative Flow Experiments at Atmospheric Pressure

The interaction of gaseous NO_2 and the Fe-ZSM-5_{350} was investigated during transient response experiments at atmospheric pressure and 523 K. The possibility of NO_2 to provide active surface oxygen was of special interest. The gas composition at the outlet as a function of time after a step change in the reactor inlet from He to a mixture of 0.5 vol% NO_2, 0.5 vol% Ar in He for the Fe-ZSM-5_{350} sample is presented in Figure 7.4.

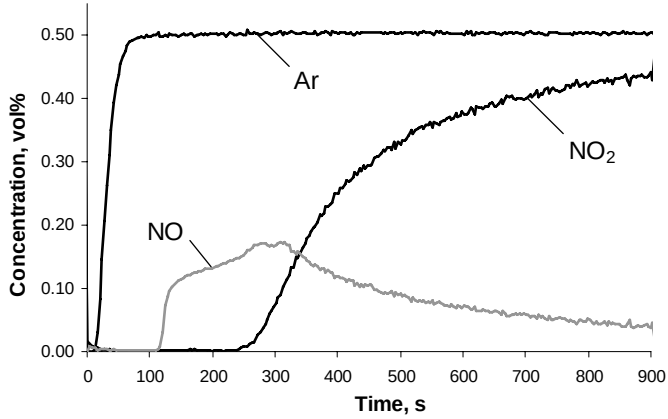

Figure 7.4: Response curves of Ar, NO_2 and NO obtained at 523 K during introduction of the 0.5 vol% NO_2, 0.5 vol% Ar mixture in He on the Fe-ZSM-5_{350} catalyst.

The non-ideal reactor behavior, as compared to the plug flow, was represented by the concentration-time profile of the inert tracer Ar. NO_2 evolution was delayed with respect to Ar due to decomposition and adsorption on the catalyst surface:

$$NO_2 \rightarrow NO_{2,ads} \tag{7.5}$$

The formation of NO was observed during the NO_2 interaction for 15 min with the catalyst but no N_2 and O_2 evolution took place. $50 \cdot 10^{18}$ molecules/g NO_2 were adsorbed/decomposed and $16 \cdot 10^{18}$ molecules/g NO were produced. The transient production of NO was assigned to the decomposition of NO_2 on the catalyst to gaseous NO and adsorbed oxygen (Equation (7.3)). The evolution of gaseous NO was delayed by 100 s to the introduction of NO_2. Probably, initially formed NO was adsorbed on the zeolite. A blank experiment with quartz pellets in the reactor did not show NO formation during a NO_2 step response experiment at 523 K (not shown). Therefore, the Fe-ZSM-5_{350} was necessary for the decomposition of NO_2 at low temperature.

The surface species formed on the Fe-ZSM-5_{350} during the NO_2 interaction were investigated by a TPD experiment. The catalyst was purged for 10 min with He before the TPD in order to remove all weakly adsorbed species. Figure 7.5 shows the evolution of AMU 30, 32 and 46 during the TPD. Their overlapping profiles indicated $NO_{x,ads}$ species. The concentration ratio from AMU 30 and AMU 32 is illustrated in the inset of Figure 7.5. It approached with increasing temperature a plateau with the value 2. At 723 K all molecules which contributed to the AMU 46 profile were desorbed. The interpretation of this finding is that in the temperature range from 673 to 873 K, where AMU 30 divided by AMU 32 equals 2, only one surface species desorbed contributing to AMU 30 and AMU 32, while at lower temperatures with a non-constant ratio different surface species desorbed contributing to AMU 30, 32 and 46. On that basis, the deconvolution of the TPD profiles resulted in two main surface compounds.

An AMU 32' profile was derived from the experimental AMU 30 profile assuming a constant AMU 30/AMU 32 ratio of 2 and is shown together with the experimental AMU 30 profile in Figure 7.6a. This TPD pattern was assigned to $NO_{2,ads}$ as the ratio of NO:O_2 equals 2:1. By subtracting the AMU 32' profile from the experimental AMU 32 profile, the AMU 32" profile was derived. In order to close the mass balance of the TPD, the AMU 32" profile was correlated with the experimental AMU 46 profile in Figure 7.6b. The areas below the AMU 46 and AMU 32" profiles had a ratio of 2:1. In addition, the shapes of the AMU 46 and AMU 32" profile were similar. Therefore, a common surface species, $NO_{3,ads}$, was proposed for this TPD pattern. Thus, the TPD profiles after the NO_2 interaction could be fully interpreted.

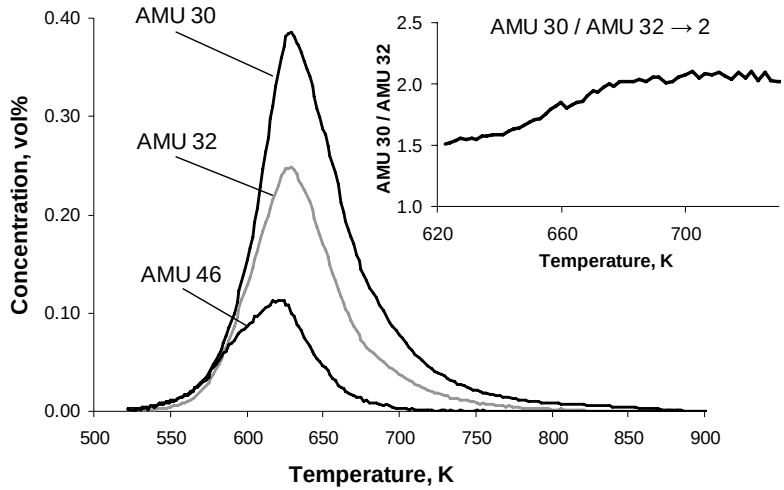

Figure 7.5: TPD profiles of AMU 46, 32, 30 after 15 min NO_2 interaction (0.5 vol%) with Fe-ZSM-5_{350} at 523 K. Inset: Concentration ratio from AMU 30 and AMU 32 versus temperature.

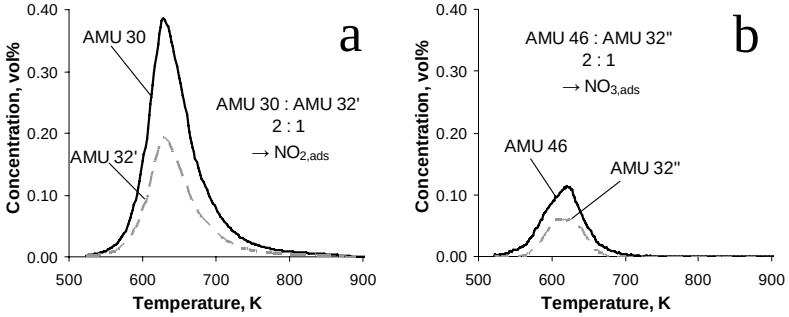

Figure 7.6: Assignment of the TPD profiles after 15 min NO_2 interaction (0.5 vol%) with Fe-ZSM-5_{350} at 523 K to $NO_{2,ads}$ (a) and $NO_{3,ads}$ (b) surface species.

First, $3.0 \cdot 10^{18}$ molecules/g $NO_{3,ads}$ species desorbed with a maximum at 623 K contributing to AMU 32 and 46 with the ratio 2:1. Shortly after with a maximum at 623 K $12 \cdot 10^{18}$ molecules/g $NO_{2,ads}$ evolved contributing to AMU 30 and 32 with a ratio 2:1. Consequently, NO_2 adsorption on the zeolite was accompanied by its decomposition via the formation of adsorbed $NO_{3,ads}$ and gaseous NO which is qualitatively summarized in the following equation:

$$NO_2 \rightarrow NO_{2,ads}, NO_{3,ads} + NO \quad (7.6)$$

$(O)_{Fe}$, formed during N_2O interaction with Fe-ZSM-5_{350}, desorbed during the TPD at lower temperature than the NO_x species and mainly without the parallel desorption of NO or NO_2 species [3]. Thus, the TPD after NO_2 interaction did not indicate atomic surface oxygen, $(O)_{Fe}$, since the simultaneous desorption of oxygen with NO or NO_2 during TPD runs resulted from decomposing NO_x surface species. Furthermore, $(O)_{Fe}$ loaded from N_2O possessed high reactivity in the oxidation of CO to CO_2. The activity of the surface species formed during NO_2 interaction was also characterized by their capacity to oxidize CO. The CO_2 and NO responses during the CO interaction with the NO_2 pre-treated catalyst are presented in Figure 7.7.

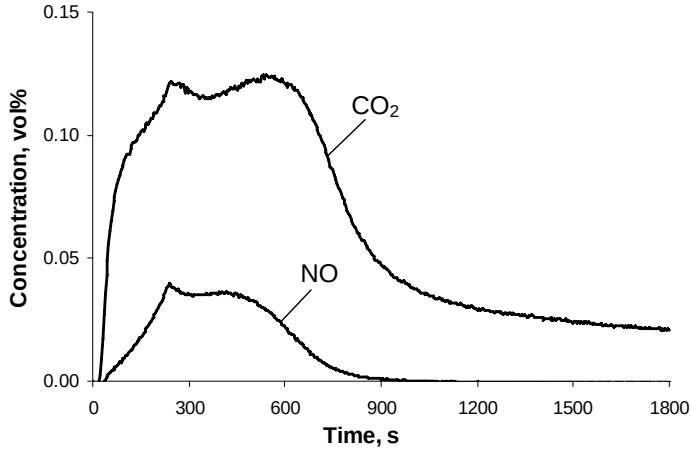

Figure 7.7: CO_2 and NO response curves obtained during interaction of 3 vol% CO in He at 523 K with the Fe-ZSM-5_{350} after exposure to NO_2 (0.5 vol% NO_2, 0.5 vol% Ar in He) for 15 min at 523 K.

The formation of CO_2 was slow and still ongoing after 30 min of CO interaction. At the beginning it was accompanied by NO desorption. The integration of the peak area gave the total amount of $25 \cdot 10^{18}$ molecules/g produced CO_2 and $3.9 \cdot 10^{18}$ molecules/g desorbed NO. The reason was probably a partial reduction of $NO_{2,ads}$,$NO_{3,ads}$ which released NO at the same time:

$$NO_{2,ads}, NO_{3,ads} + CO \rightarrow NO_{x,ads} + NO + CO_2 \quad (7.7)$$

Figure 7.8 published in [11] shows the CO_2 response curve obtained during interaction of CO with oxygen deposited from N_2O at 523 K on the Fe-ZSM-5_{200} which is very similar to the Fe-ZSM-5_{350} apart from the amount of active sites. Intensive

formation of CO_2 was observed and finished within 120 s due to the consumption of reactive oxygen loaded from N_2O on the NO_x free surface. However, oxygen loaded from N_2O on the surface saturated with $NO_{x,ads}$ species was not reactive with respect to CO oxidation to CO_2 [3]. Surface $NO_{x,ads}$ species probably blocked the sites necessary for CO activation, which may be in the vicinity of the loaded oxygen. Therefore, the formation of α-oxygen from NO_2 cannot be evidenced with CO oxidation since a large amount of $NO_{2,ads}$,$NO_{3,ads}$ were present which would make surface oxygen inactive with respect to CO oxidation to CO_2.

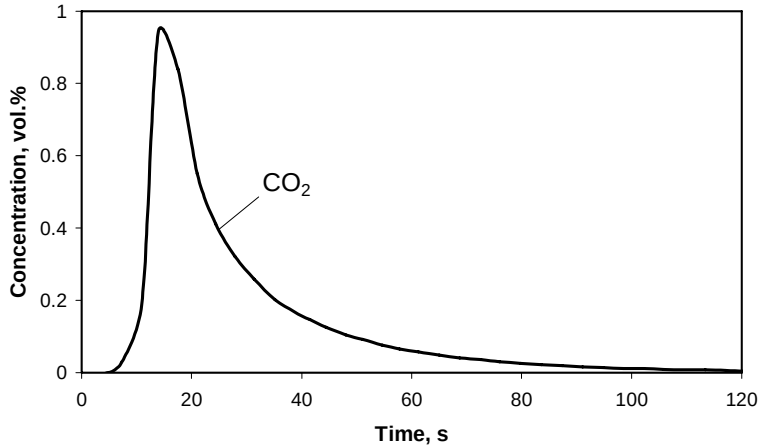

Figure 7.8: CO_2 response curve obtained during interaction of CO (3 vol% CO in He, 523 K) with oxygen deposited from N_2O on the Fe-ZSM-5_{200} catalyst at 523 K. Taken from [11].

7.1.3. Summary

The interaction of gaseous NO_2 with Fe-ZSM-5 at 523 K in vacuum and at atmospheric pressure showed the formation of two different NO_x surface species accompanied by the evolution of gaseous NO (Equation (7.6)). $NO_{2,ads}$ and $NO_{3,ads}$ species were identified in TPD experiments at atmospheric pressure. The amount of surface species after NO_2 interaction was an order of magnitude higher than the amount of active sites which can be loaded with atomic oxygen from N_2O. The surface species formed by NO_2 at atmospheric pressure oxidized CO only slowly compared to reactive surface oxygen from N_2O. TAP experiments clearly showed that the interaction of NO_2 with the Fe-ZSM-5 didn't lead to surface oxygen at 523 K which was active in CO oxidation. This is in line with Sobalik et al. reporting that NO_2 didn't form active oxygen on Fe-ferrierites at 473-523 K [12].

Bulushev et al. showed that oxygen loaded from N_2O on the surface saturated with $NO_{x,ads}$ species was not reactive with respect to CO oxidation to CO_2 [3]. Thus, the

formation of α-oxygen from NO_2 cannot be evidenced with CO oxidation since a large amount of $NO_{x,ads}$ species was present on the catalyst surface after NO_2 interaction.

7.2. Role of NO_2 in N_2O Decomposition

7.2.1. Pulse Experiments with TAP Setup under Vacuum

NO_2 was used as pre-treatment in order to study its effect on the N_2O decomposition. 300 pulses of NO_2 were introduced at the Fe-ZSM-5_{5500} at 523 K followed by 600 N_2O pulses. The subsequent TPD profiles are presented in Figure 7.9. The intensities, maxima and shape of the response were very similar to the ones after 300 pulses of NO_2 (Figure 7.2).

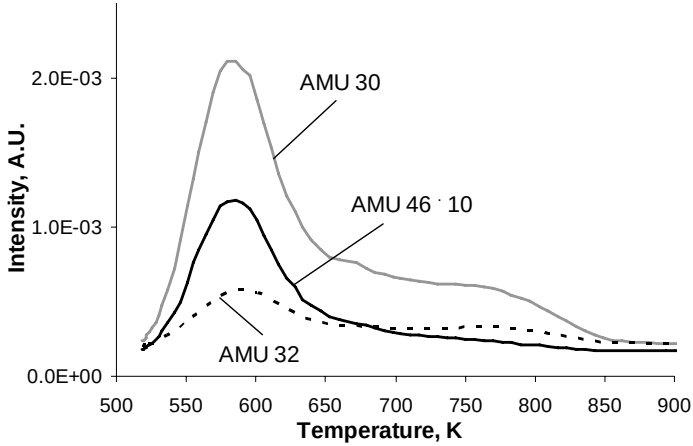

Figure 7.9: TPD profiles of AMU 46, 30, 32 after 300 pulses of NO_2 in Ar followed by 600 pulses N_2O over the Fe-ZSM-5_{5500} catalyst at 523 K.

Thus, NO_2 formed surface species on the catalyst at 523 K which were not affected by N_2O pulses. Active surface oxygen, $(O)_{Fe}$, was not loaded from N_2O after the NO_2 pre-treatment. Furthermore, the species created on the catalyst after the $NO_2 \rightarrow N_2O$ treatment were inactive in CO oxidation (not shown). It seems like the active sites for oxygen loading from N_2O got already occupied during the NO_2 treatment. It should be mentioned that NO did not block the active sites for oxygen loading from N_2O but facilitated the oxygen desorption during TPD runs.

The role of NO_2 in N_2O decomposition was investigated by pulse experiments with the TAP setup. The interaction of NO_2 pulses with the catalyst containing $(O)_{Fe}$ loaded from 600 N_2O pulses at 523 K was studied. The response curves of NO_2 (a) and O_2 (b) are illustrated in Figure 7.10. The first ten NO_2 pulses were completely adsorbed on the catalyst and led to desorption of oxygen which was as well observed while pulsing NO over the N_2O pre-treated Fe-ZSM-5_{5500}. The formed surface species were inactive with respect to CO oxidation.

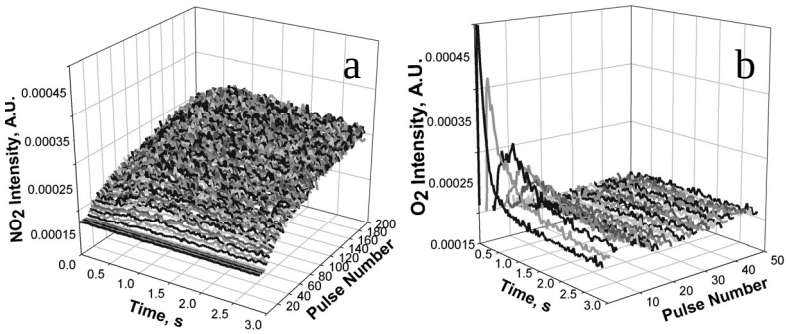

Figure 7.10: NO_2 (a) and O_2 (b) response curves during the introduction of 300 NO_2 pulses at 523 K over Fe-ZSM-5_{5500} containing $(O)_{Fe}$.

The TPD experiment performed after to the $N_2O \rightarrow NO_2$ pulse sequence gave qualitatively and quantitatively the same result as after pulsing only NO_2 seen in Figure 7.2. Thus, NO_2 provoked the desorption of reactive atomic oxygen loaded from N_2O and formed the same surface species as on the standard pre-treated catalyst.

Similar but quantitative experiments were performed with the Micromeritics setup at atmospheric pressure in order to further clarify the effect of NO_2 on N_2O decomposition at 523 K.

7.2.2. Quantitative Flow Experiments at Atmospheric Pressure

Whether NO_2 can provide the same effects as NO on the N_2O decomposition was studied at 523 K in step response and subsequent TPD experiment. As already presented in section 6.1, the slow formation of NO_{ads} on the catalyst was observed from N_2O catalyzing the N_2O decomposition. Surface NO_{ads} can be further oxidized to adsorbed NO_2 species ($NO_{2,ads}$) which led to the facilitation of $(O)_{Fe}$ recombination/desorption. The presence of $NO_{x,ads}$ formed from NO did not inhibit the surface oxygen loading from N_2O at 523 K as observed by a transient response method. However, the reactivity of $(O)_{Fe}$ toward CO oxidation at low temperatures (< 523 K) was drastically diminished [3].

The temperature of 523 K was low enough to ensure the study of the effect of NO_2 and not of a NO/NO_2 mixture since NO_2 decomposes to O_2 and NO at higher temperatures as seen in Equation (7.1). The Fe-ZSM-5_{350} interacted for 15 min with NO_2 at 523 K, was purged for 10 min in He and then exposed to N_2O. The response curves obtained during the introduction of 2 vol% N_2O are shown in Figure 6.10.

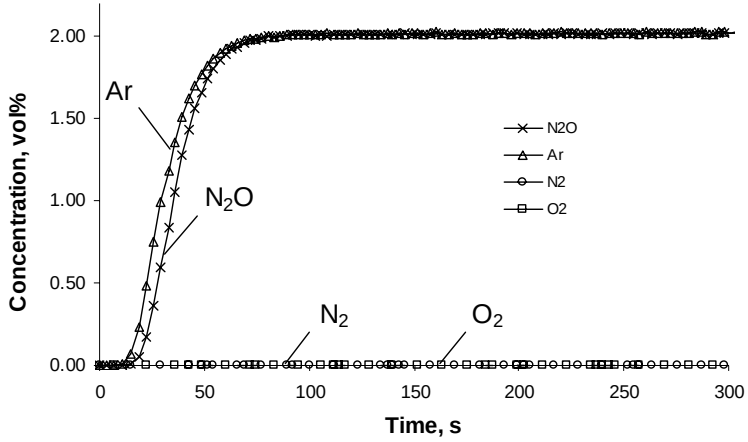

Figure 7.11: Response curves of N_2O, Ar, N_2 and O_2 obtained at 523 K during introduction of the 2 vol% N_2O, 2 vol% Ar mixture in He on the Fe-ZSM-5_{350} catalyst after NO_2 interaction (0.5 vol% NO_2, 0.5 vol% Ar in He for 15 min at 523 K).

Only N_2O and Ar appeared at the reactor outlet. The absence of N_2 formation indicated the absence of oxygen loading on the catalyst from N_2O which was usually observed during the N_2O interaction with a standard pre-treated catalyst. A delay of the N_2O to the Ar response showed that N_2O was reversibly adsorbed. Integration of the area between the two responses (Ar and N_2O) gave $2.1 \cdot 10^{18}$ molecules/g of reversible adsorbed N_2O. The amount of reversible adsorbed N_2O after NO_2 pre-treatment was close to its value upon N_2O interaction with the standard pre-treated catalyst ($2.4 \cdot 10^{18}$ molecules/g). Thus, NO_2 blocked the sites for $(O)_{Fe}$ loading from N_2O but hardly influenced the sites for reversible N_2O adsorption. The TPD run after the NO_2 followed by N_2O interaction with the catalyst at 523 K gave qualitatively and quantitatively the same result as already present in Figure 7.5 after NO_2 only interaction. This indicates that N_2O did not undergo any reaction with the NO_2 pre-treated catalyst. N_2O was only reversibly adsorbed. NO_2 blocked the active sites for N_2O decomposition at low temperatures as 523 K.

For a better understanding of a possible role of NO_2 in the N_2O decomposition mechanism, the interaction of NO_2 with $(O)_{Fe}$ loaded from N_2O was investigated. The

transient responses during NO_2 introduction over the Fe-ZSM-5 which was saturated with $(O)_{Fe}$ loaded from N_2O are shown in Figure 7.12.

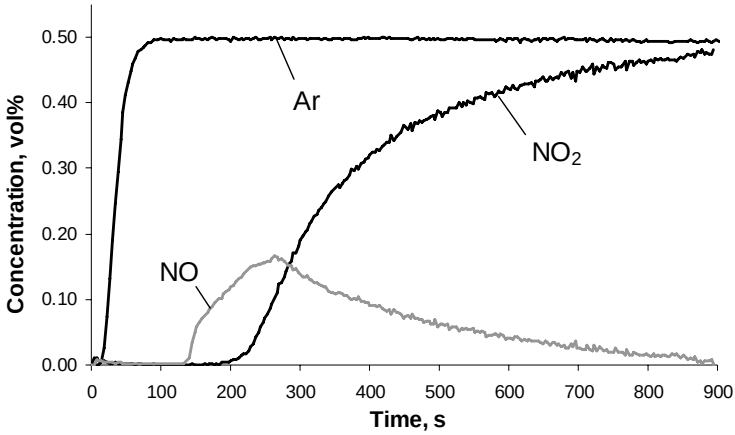

Figure 7.12: Response curves of N_2O, Ar and NO obtained at 523 K during introduction of the 0.5 vol% NO_2, 0.5 vol% Ar mixture in He on the Fe-ZSM-5_{350} catalyst after N_2O interaction (2 vol% N_2O, 2 vol% Ar in He for 5 min at 523 K).

Ar, the inert tracer, accounted for the hydrodynamic reactor behavior. NO_2 evolution was delayed with respect to Ar. NO was produced and its formation was nearly finished after 15 min. The area between the concentration-time profile of Ar and NO_2 was proportional to the amount of adsorbed/reacted NO_2: $40 \cdot 10^{18}$ molecules/g. The integration of the NO response gave the amount of produced NO: $11 \cdot 10^{18}$ molecules/g. The concentrations of produced N_2, reversibly adsorbed N_2O, adsorbed NO_2 and produced NO during transient response experiments with 2 vol% N_2O or 0.5 vol% NO_2 are summarized in Table 7.2.

During the NO_2 interaction with the oxygen saturated catalyst, $10 \cdot 10^{18}$ molecules/g of NO_2 less were consumed and $5 \cdot 10^{18}$ molecules/g of NO less were produced as with the standard pre-treated catalyst. However, the TPD run (not shown) after the $N_2O \rightarrow NO_2$ interaction gave qualitatively and quantitatively the same results as the TPD after NO_2 interaction with the Fe-ZSM-5_{350} which is shown in Figure 7.5. Hence, it can be concluded that the loaded oxygen from N_2O ($2.7 \cdot 10^{18}$ molecules/g) interacted with NO_2 forming $NO_{2,ads}$,$NO_{3,ads}$ species. Therefore, less NO_2 decomposed to provide oxygen for the surface species formation and a smaller amount of NO was produced.

Table 7.2: Concentrations of produced or adsorbed molecules during transient response experiments at 523 K with the Fe-ZSM-5_{350} catalyst determined with the Micromeritics Analyzer.

Treatment for 15 min	*N_2 produced, 10^{18} molec./g*	*N_2O rev. ads., 10^{18} molec./g*	*NO_2 ads., 10^{18} molec./g*	*NO produced, 10^{18} molec./g*
2 vol% N_2O	2.7	2.4	-	-
0.5 vol% NO_2	-	-	50	16
2 vol% N_2O after 15 min 0.5 vol% NO_2	-	2.1	-	-
0.5 vol% NO_2 after 15 min 2 vol% N_2O	-	-	40	11

The possibility of having reactive $(O)_{Fe}$ left on the catalyst after the $N_2O \rightarrow NO_2$ interaction was tested by CO introduction at 523 K. The response was similar to Figure 7.7 during CO oxidation after NO_2 treatment. Only slow oxidation of CO was observed which was not characteristic for the interaction of CO with reactive $(O)_{Fe}$. This could indicate that the oxygen loaded from N_2O was completely consumed with NO_2 for the formation of $NO_{2,ads}$,$NO_{3,ads}$ species. Furthermore, oxygen loaded from N_2O on the surface saturated with $NO_{x,ads}$ species was shown to be not reactive with respect to CO oxidation to CO_2 [3].

7.2.3. Summary

NO_2 pre-treatments inhibited the loading of oxygen from N_2O in transient response and TAP experiments. The formation of gaseous nitrogen was not observed during the exposure of the NO_2 pre-treated catalyst to N_2O. NO_2 blocked the sites for oxygen loading from N_2O but the amount of reversibly adsorbed N_2O stayed constant compared to the standard pre-treated catalyst. The blockage of the sites which were active in N_2O decomposition through NO_2 pre-treatment had not been reported so far. Only kinetic analysis of the NO oxidation over MFI zeolites at temperatures from 473 to 623 K revealed the occurrence of a strong reaction inhibition by adsorbed NO_2 [13]. In chapter 6, it is shown that adsorbed NO did not inhibit the surface oxygen loading from N_2O at 523 K.

NO_2 interaction with $(O)_{Fe}$ containing catalyst led to the formation of $NO_{2,ads}$,$NO_{3,ads}$ species as upon NO_2 interaction with the standard pre-treated catalyst. The oxygen deposited by N_2O pre-treatment was consumed for the formation of $NO_{x,ads}$ species in experiments at atmospheric pressure. Since oxygen was already present on the catalyst, less oxygen was needed from NO_2 and, therefore, less gaseous NO was

produced during NO_2 interaction with the N_2O pre-treated Fe-ZSM-5 as compared to a standard pre-treated sample. In TAP experiments oxygen was released during the interaction of NO_2 with $(O)_{Fe}$ loaded Fe-ZSM-5_{5500}. The same phenomenon was observed during the interaction of NO with $(O)_{Fe}$. In contrast to TAP results, the desorption of oxygen was not observed in transient experiments at atmospheric pressure. A possible explanation is that the thin catalyst bed in the TAP reactor was left quickly by formed O_2 whereas during experiments at atmospheric pressure the freed O_2 had the possibility to react further with $NO_{x,ads}$ species. More details and the corresponding experiments are given in section 6.3.

7.3. Temperature-Programmed Reaction at Atmospheric Pressure

Temperature-programmed reaction is often used to study the reaction dynamics and activation energy. Here, the interaction of N_2O, NO_2, N_2O+NO and N_2O+NO_2 mixtures were studied by temperature-programmed reaction and compared with each other in terms of reactivity and apparent activation energy. The influence of NO and NO_2 on the reaction system was of special interest.

7.3.1. Treatments before Temperature-Programmed Reaction

Before the TPR experiments, pre-treatments of the Fe-ZSM-5_{350} with the N_2O (1 vol%), NO_2 (0.25 vol%), N_2O (1 vol%)+NO (0.25 vol%) and N_2O (1 vol%)+ NO_2 (0.25 vol%) in Ar/He mixture at 523 K were performed to load surface species on the catalyst. During the 15 min treatment, different processes took place as listed below: The loading of oxygen, $(O)_{Fe}$, from N_2O accompanied by N_2 production, the adsorption of N_2O, NO, and NO_2 on the catalyst, formation of NO and O_2 from NO_2 and vice versa, and the creation of $NO_{x,ads}$ species from N_2O as well as from NO_2.

$$N_2O + (\ )_{Fe} \rightarrow N_2 + (O)_{Fe} \tag{7.8}$$

$$N_2O,\ NO,\ NO_2 \rightarrow N_2O_{ads},\ NO_{ads},\ NO_{2,ads} \tag{7.9}$$

$$NO_2 \rightleftarrows NO + \tfrac{1}{2} O_2 \tag{7.10}$$

$$N_2O \rightarrow N_2 + NO_{x,ads} \tag{7.11}$$

$$NO_2 \rightarrow NO_{x,ads} + NO \tag{7.12}$$

The concentrations of produced or adsorbed species are summarized in Table 7.3. They were determined as described in section 7.1 and 7.2. The treatment with N_2O showed oxygen loading via N_2 evolution as discussed in section 5.2. The exposure of the catalyst to NO_2 resulted in NO production and $NO_{x,ads}$ formation such as in Figure 7.4. More interesting were the observations during the N_2O+NO_2 and N_2O+NO treatments and will be discussed in detail in the following.

Table 7.3: Characteristic concentrations of produced or adsorbed molecules during transient response experiments at 523 K with the Fe-ZSM-5_{350} catalyst determined with the Micromeritics Analyzer.

Treatment for 15 min	*N_2 produced, 10^{18} molec./g*	*N_2O rev. ads., 10^{18} molec./g*	*NO ads., 10^{18} molec./g*	*NO_2 ads., 10^{18} molec./g*	*NO prod., 10^{18} molec./g*
1 vol% N_2O	2.4	1.3	-	-	-
0.25 vol% NO_2	-	-	-	33	9.5
1 vol% N_2O + 0.25 vol% NO	1.5	1.3	5.2	-	-
1 vol% N_2O + 0.25 vol% NO_2	2.5	1.5	-	24	12

The most significant reaction, which was the loading of the catalyst with oxygen, $(O)_{Fe}$, from N_2O (Equation (7.8)) will be compared for different transient experiments. It was indirectly observed by the characteristic initial N_2 production from N_2O which was not accompanied by gaseous oxygen formation. Therefore, the N_2 response profiles obtained during N_2O interaction with the Fe-ZSM-5_{350} at 523 K are summarized in Figure 7.13 for the different cases. Curve (1): N_2O interacted with the standard pre-treated catalyst. Curve (2): The catalyst was exposed to a mixture of N_2O+NO_2. Curve (3): N_2O interacted with the NO_2 pre-treated catalyst. Curve (4): The catalyst was exposed to a mixture of N_2O+NO.

The amount of produced N_2 was about the same during 1 vol% N_2O interaction (Figure 7.13, curve 1, $2.4 \cdot 10^{18}$ molecules/g N_2) and during 1 vol% N_2O+0.25 vol% NO_2 interaction (Figure 7.13, curve 2, $2.5 \cdot 10^{18}$ molecules/g N_2) with the standard pre-treated catalyst. The amount of reversibly adsorbed N_2O on the Fe-ZSM-5_{350} was also the same for the N_2O and the N_2O+NO_2 mixture. Thus, the loading of active sites with oxygen was fully achieved even in the presence of 0.25 vol% NO_2. However, pre-adsorbed NO_2, which was discussed in section 7.2, completely inhibited the oxygen loading from N_2O (Figure 7.13, curve 3, no N_2 evolution). Only reversible adsorption of N_2O takes place. The loading of surface oxygen from the N_2O+NO_2 mixture showed that the interaction

of N_2O with the catalyst was faster than the blockage of the active sites by surface species formed from NO_2.

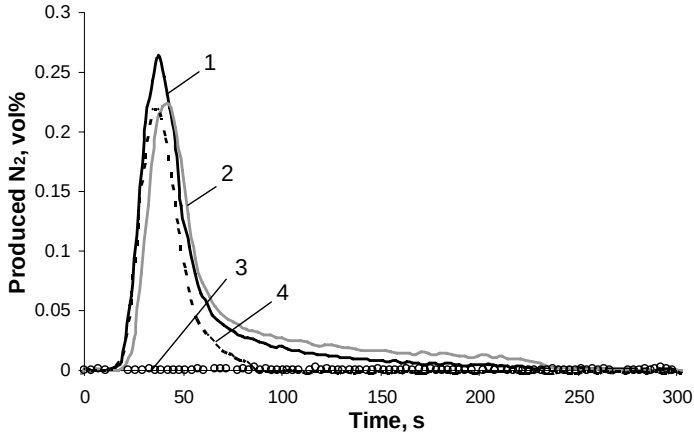

Figure 7.13: Response curves of N_2 obtained at 523 K during introduction of 1 vol% N_2O, 1 vol% Ar in He (1), 1 vol% N_2O, 0.25 vol% NO_2, 1.25 vol% Ar in He (2), 2 vol% N_2O, 2 vol% Ar in He after NO_2 interaction (0.5 vol% NO_2, 0.5 vol% Ar in He for 15 min at 523 K) (3) and 1 vol% N_2O, 0.25 vol% NO, 1.25 vol% Ar in He (4) over the Fe-ZSM-5_{350} catalyst.

The loading of oxygen from N_2O took also place during the treatment with N_2O+NO. The amount of formed N_2 was $1.5 \cdot 10^{18}$ molecules/g (Figure 7.13, curve 4) in contrast to $2.4 \cdot 10^{18}$ molecules/g (Figure 7.13, curve 1) when only N_2O was interacting with the catalyst. In the presence of NO the N_2 evolution from N_2O was finished within 100 s (curve 4) while a tailing up to 250 s was observed during the interaction of N_2O only (curve 1). Thus, in the presence of NO, pathways leading to a slow formation of N_2 from N_2O were absent. The slow creation of $NO_{x,ads}$ species from N_2O was evidenced in section 6.1. The loading of $(O)_{Fe}$ and the formation of $NO_{x,ads}$ species from N_2O was accompanied by N_2 formation as seen in the following equations:

$$\begin{aligned} fast: \quad & N_2O \rightarrow (O)_{Fe} + N_2 \\ slow: \quad & N_2O \rightarrow NO_{x,ads} + N_2 \end{aligned} \tag{7.13}$$

These $NO_{x,ads}$ species which were usually formed by N_2O in a slow process were probably created faster by simple adsorption of NO from the N_2O+NO mixture accompanied by a diminished N_2 release.

7.3.2. Temperature-Programmed Reaction Profiles

In this section the responses of the temperature-programmed reactions of N_2O, NO_2, N_2O+NO and N_2O+ NO_2 are presented and discussed. The catalyst was exposed to the reaction mixture of the TPR for 15 min at 523 K prior to the temperature ramp of 10 K/min from 523 to 873 K. The pre-treatment with the different reaction mixtures is discussed in the previous section.

Figure 7.14 shows the conversion of 1 vol% N_2O versus temperature. The decomposition to N_2 and O_2 started above 577 K and reached 100% at 650 K.

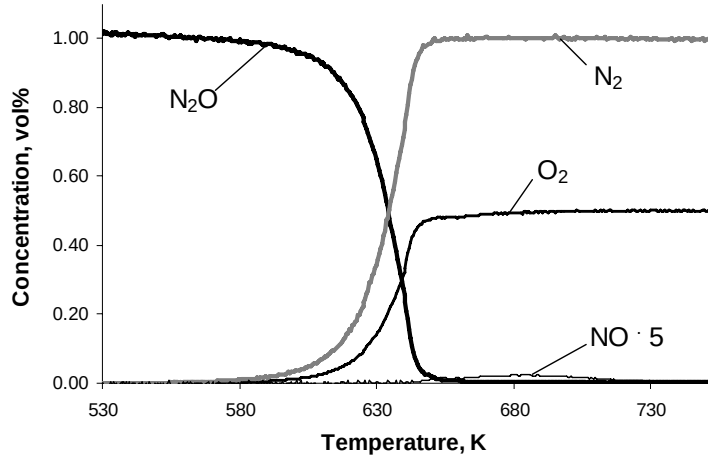

Figure 7.14: Temperature-programmed reaction profiles observed during the passage of 1 vol% N_2O, 1 vol% Ar mixture in He over the Fe-ZSM-5_{350} catalyst.

The ratio of N_2/O_2 remained equal to two during the entire studied temperature range and the amount of detected NO or NO_2 around 683 K was negligible:

$$N_2O \rightarrow N_2 + \tfrac{1}{2} O_2 \qquad (7.14)$$

Surface oxygen was already loaded during the 15 min of N_2O pre-treatment accompanied by the formation of $2.4 \cdot 10^{18}$ molecules/g of N_2.

The TPR profiles of 0.25 vol% NO_2 is shown in Figure 7.15. Upon heating the catalyst, an excess of NO_2 was observed due to desorption of reversibly adsorbed NO_2 accumulated on the catalyst during the pre-treatment. At higher temperature NO_2 decomposed to NO and O_2:

$$NO_2 \rightarrow NO + \frac{1}{2} O_2 \quad (7.15)$$

Based on this equation the theoretical profiles for the produced NO and O_2 were calculated from the amount of decomposed NO_2 and are illustrated in Figure 7.15b. It is seen by the difference of the experimental and calculated responses that the evolved amount of NO and O_2 was over-stoichiometric with respect to the decomposed amount of NO_2. The excess of NO and O_2 was assigned to the desorption of $NO_{x,ads}$ species which were accumulated on the catalyst during the pre-treatment.

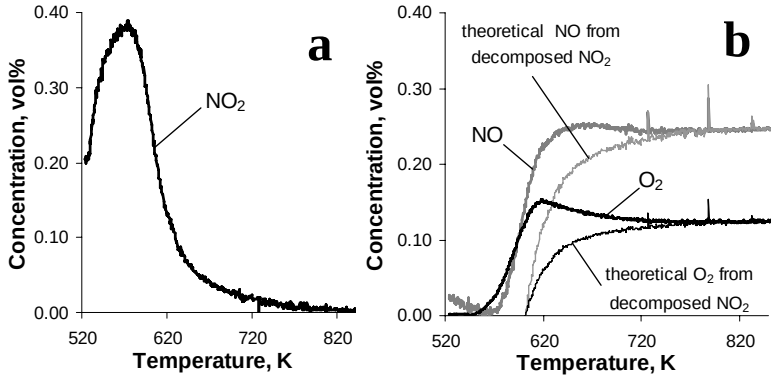

Figure 7.15: Temperature-programmed reaction profiles observed during the passage of 0.25 vol% NO_2, 0.25 vol% Ar mixture in He over the Fe-ZSM-5_{350} catalyst. Reactant (a), products (b).

The effect of NO_2 on the N_2O decomposition was investigated in a TPR using a mixture of 0.25 vol% NO_2 and 1 vol% N_2O. The responses in Figure 7.16 show the stoichiometric decomposition of N_2O to N_2 starting at 570 up to 688 K for 100% conversion. NO_2 decomposed with progressing temperature to NO and O_2. Thus, NO was formed during the TPR. The concentrations of NO_2 as well as NO were always changing. A stoichiometric decomposition of NO_2 as in Equation (7.15) was assumed and the corresponding profiles for the produced NO and O_2 were calculated from the amount of decomposed NO_2. The stoichiometric decomposition of N_2O (Equation (7.14)) was also accounted for the determination of the theoretically produced amount of O_2. Figure 7.16b includes the calculated O_2 and NO responses in which the N_2O and NO_2 decomposition was considered. As already observed at the NO_2 TPR, an excess of NO desorbed between 523 K and 723 K whereas an excess of O_2 was hardly observed in the N_2O+NO_2 TPR. NO originated from NO_{ads} species accumulated on the catalyst during the pre-treatment.

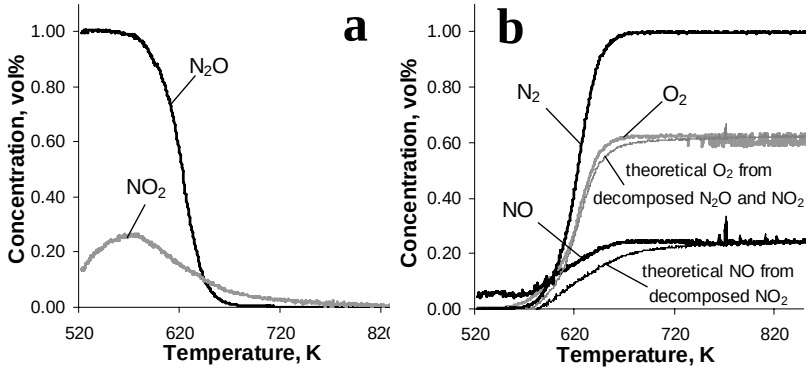

Figure 7.16: Temperature-programmed reaction profiles observed during the passage of 0.25 vol% NO_2, 1 vol% N_2O, 1.25 vol% Ar mixture in He over the Fe-ZSM-5_{350} catalyst. Reactants (a), products (b).

Since NO was constantly formed during N_2O-NO_2-TPR, a N_2O-NO-TPR was performed for comparison. Figure 7.17 illustrates the TPR profiles of 1 vol% N_2O and 0.25 vol% NO. N_2O decomposed stoichiometrically to N_2 from 543 to 693 K. Based on a stoichiometric decomposition of N_2O (Equation (7.14)), the theoretical O_2 response was calculated and illustrated in Figure 7.17b.

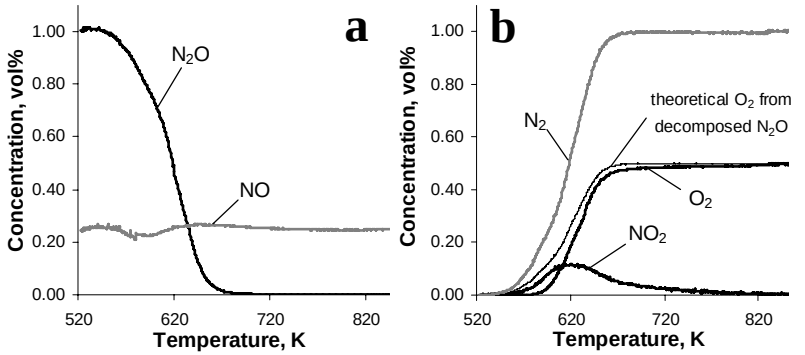

Figure 7.17: Temperature-programmed reaction profiles observed during the passage of 0.25 vol% NO, 1 vol% N_2O, 1.25 vol% Ar mixture in He over the Fe-ZSM-5_{350} catalyst. Reactants (a), products (b).

A deficit of the produced oxygen was observed by comparing the theoretical with the experimental O_2 response. Obviously, oxygen reacted partially with NO forming NO_2. For the amount of evolved NO_2 during the experiment an equivalent amount of

NO had to be consumed. The consumption of a small amount of NO was observed by the sink in the NO response around 598 K in Figure 7.17a. The outstanding amount of NO for the NO_2 formation was probably already adsorbed on the catalyst during the pre-treatment. The accumulation of NO during the pre-treatment as well as the O_2 consumption was shifted to fewer time/temperature compared to the appearance of NO_2 (desorption maximum at 623 K). It can be concluded that NO_2 was formed on the catalyst surface and not in a gas phase reaction.

$$NO_{ads} + O_{ads} \rightarrow NO_2 \tag{7.16}$$

7.3.3. Apparent Activation Energy

In this section the N_2O conversion as function of the temperature is compared for different reaction mixtures: 1 vol% N_2O + 1 vol% Ar, 1 vol% N_2O + 0.25 vol% NO + 1.25 vol% Ar, 1 vol% N_2O + 0.25 vol% NO_2 + 1.25 vol% Ar in He. The apparent activation energy is presented.

Figure 7.18 shows the relation between conversion and temperature of the N_2O decomposition over Fe-ZSM-5_{350} for different mixtures (N_2O, N_2O+NO and N_2O+NO_2). It can be seen that the conversion increased with the increase of the temperature and reaches 100% at 673 K for all three mixtures. The addition of NO_2 and NO to N_2O decreased the temperature whereas the decomposition started by 8 and 34 K lower, respectively.

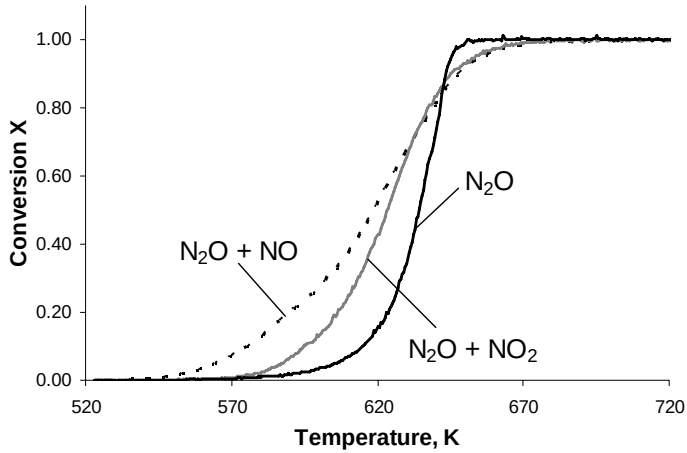

Figure 7.18: Temperature dependence of N_2O conversion of the Fe-ZSM-5_{350} for different reaction mixtures: 1 vol% N_2O + 1 vol% Ar, 1 vol% N_2O + 0.25 vol% NO + 1.25 vol% Ar, 1 vol% N_2O + 0.25 vol% NO_2 + 1.25 vol% Ar in He.

The N_2O+NO and N_2O+NO_2 curve overlapped at temperatures higher than 623 K. The reason is that the concentration profiles of NO and NO_2 during the TPR were about the same above 623 K for the N_2O+NO and N_2O+NO_2 mixture. At lower temperatures the NO and NO_2 concentration profiles for the two mixtures were significantly different as can be seen in Figure 7.16 and Figure 7.17. The promoting effect of NO is clearly seen in Figure 7.18 by higher conversions at the same temperature for the N_2O+NO mixture compared to N_2O only. NO_2 was also enhancing the N_2O decomposition but to a lower extent. Since the interconversion of NO_2 and NO took place, they coexisted on the catalyst or in the reaction mixture and it was difficult to determine in which way NO or NO_2 contributed to the N_2O decomposition.

The N_2O conversion obtained during temperature-programmed reaction of only N_2O and mixtures of N_2O+NO and N_2O+NO_2 from 539 K to 623 K are shown in the form of an Arrhenius plot in Figure 7.19.

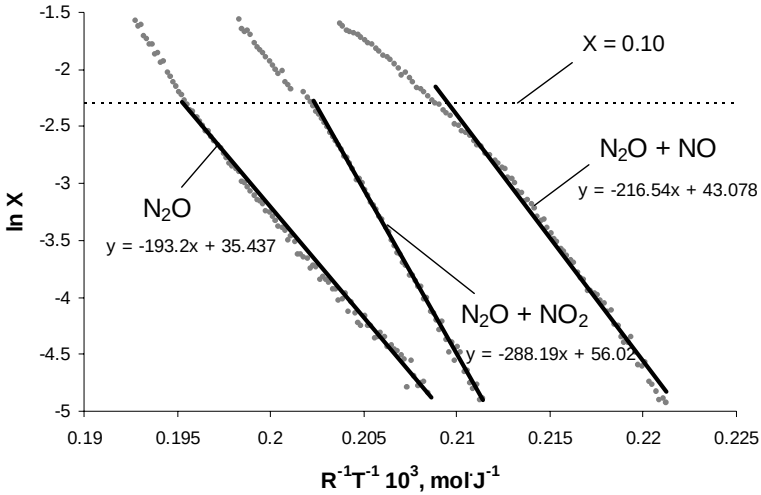

Figure 7.19: Arrhenius plot generated from the results of Figure 7.18 for the N_2O decomposition over Fe-ZSM-5_{350} for different reaction mixtures: 1 vol% N_2O + 1 vol% Ar, 1 vol% N_2O + 0.25 vol% NO + 1.25 vol% Ar, 1 vol% N_2O + 0.25 vol% NO_2 + 1.25 vol% Ar in He.

A differential flow reactor was considered with a constant rate at all points within the reactor. Since rates were concentration-dependent it was only reasonable for small conversions ($X \leq 0.10$). Our results in the transient period [14] and other investigators' results [15, 16] indicated that the N_2O decomposition is a first-order reaction (n=1). On the basis of Equation (7.17) the apparent activation energy was calculated from the slope

of the straight line and the preexponential factor from the axis intercept, respectively. The results are summarized for the different reaction mixtures in Table 7.4.

$$c_{N_2O_{,0}} \cdot \frac{\Delta X}{\tau_{res}} = A e^{(-E_a/RT)} \cdot c_{N_2O}^{n} \qquad (7.17)$$

For N_2O decomposition the apparent activation energy was found to be E_a = 193 kJ/mol. This value agreed with those published by Kiwi-Minsker et al.: 169 kJ/mol [14], Bell and coworkers: 179 kJ/mol [17] and 185 kJ/mol [18], Perez-Ramirez et al.: 161 kJ/mol [4], Zhu et al.: 136-213 kJ/mol [19] and Sang et al.: 194 kJ/mol [5].

The addition of NO or NO_2 caused an increase in the rate of N_2O decomposition. However, the apparent activation energy was higher for the mixtures than for pure N_2O, 217 kJ/mol for N_2O+NO and 288 kJ/mol for the N_2O+NO_2 mixture. The increase of the activity in the presence of NO was not reflected in a decrease in E_a as was observed by Perez-Ramirez et al.: 106 kJ/mol [4] and Sang et al.: 165 kJ/mol [5]. Simultaneously with E_a increased the preexponential factor. The higher activity was, thus, explained by the compensation effect, resulting in an increase of the preexponential factor in the order of ~10^5-10^9.

Table 7.4: Apparent Arrhenius Parameters for First-Order Kinetic Fits for N_2O decomposition obtained from the results of Figure 7.18.

Reaction Mixture	*(X = 0 - 0.10)*	
	E_a, kJ·mol^{-1}	ln A (A: s^{-1})
N_2O	193	35
N_2O+ NO	217	43
N_2O + NO_2	288	56

7.3.4. Summary

Temperature-programmed reaction at atmospheric pressure of N_2O showed the expected stoichiometric decomposition into N_2 and O_2. The reaction started above 577 K and reaches 100% conversion at 650 K. The formation of gaseous NO or NO_2 was negligible. The TPR of NO_2 showed its decomposition with increasing temperature to NO and O_2. The TPR with a mixture of N_2O+NO_2 and N_2O+NO was accompanied by the interconversion of NO_2↔NO which made an assignment of effects to NO and NO_2, respectively, very difficult. In addition, NO_x surface species were formed during the pre-treatment of 15 min in the reaction mixture. The desorption of the accumulated surface species interfered with the processes of the TPR.

NO_2 was formed in the TPR with the N_2O+NO mixture. It is interesting to note that the release of NO_2 was time/temperature delayed with respect to the consumption of NO from the N_2O+NO mixture indicating a surface instead of a gas-phase reaction.

During the pre-treatment with the N_2O+NO_2 mixture at 523 K, $(O)_{Fe}$ loading tooks place to the full extent. As discussed above, the catalyst pre-treated with NO_2 did not uptake oxygen from N_2O since the active sites were blocked by $NO_{2,ads}$,$NO_{3,ads}$ species. It can be concluded that the loading of $(O)_{Fe}$ from N_2O was faster than the adsorption and formation of $NO_{2,ads}$,$NO_{3,ads}$ species from NO_2.

During the simultaneous introduction of N_2O and NO at 523 K, $(O)_{Fe}$ was loaded which was measured by the N_2 release. The amount of produced N_2 was only about 60% compared to surface oxygen loaded from N_2O in the absence of NO. In the presence of NO, pathways leading to a slow formation of N_2 from N_2O were absent. The slow formation of NO_{ads} species accompanied by N_2 evolution from N_2O was reported in [14]. These $NO_{x,ads}$ species which were usually formed by N_2O in a slow process were probably created faster by simple adsorption of NO from the N_2O+NO mixture accompanied by a diminished N_2 release.

The apparent activation energy for N_2O decomposition calculated from a TPR experiment was 193 kJ/mol. The temperature-programmed reaction might not be in steady state during the whole experiment since N_2O formed $NO_{x,ads}$ species only slowly [20] which co-catalysed the N_2O decomposition. Nevertheless, the apparent activation energy was close to the value (169.4 ± 5.5 kJ/mol) obtained by steady-state measurements with the same Fe-ZSM-5_{350} catalyst [14].

It was observed that the addition of sub-stoichiometric amount of NO and NO_2, respectively, caused an increase in the rate of N_2O decomposition. The increase in activity was not reflected in a decrease in the apparent activation energy as it was the case in [4, 5] by ca. 40-60 kJ/mol. On the contrary, the activation energy increased by 22 kJ/mol and 73 kJ/mol due to the addition of NO and NO_2, respectively. Simultaneously, the apparent preexponential factor increased in the order of ~10^5-10^9. Thus, the higher activity can be explained by the compensation effect.

7.4. NO_2 DRIFTS in Situ

Adsorbed NO_x species were formed from NO_2 during contact with Fe-ZSM-5 catalysts at 523 K. The formation of these species was further investigated by infrared spectroscopy. The zeolite was exposed to a flow of 20 ml (STP)/min of 0.5 vol% NO_2, 0.5 vol% Ar in He. The DRIFT spectra presented in Figure 7.20, spectrum 1 were obtained after 15 min of NO_2 interaction with the zeolite at room temperature in the presence of gaseous NO_2. It shows absorption frequencies at 2198, 2133, 1742, and

between 1635 and 1577 cm^{-1}. The bands at 2198 and 2134 cm^{-1} were assigned to $[NO^+][N_2O_4]$ and NO^+, respectively [21-24]. The 1744 cm^{-1} band was unambiguously assigned to N_2O_4 [21, 22, 24]. The band at 1635 and 1627 cm^{-1} was attributed to some form of adsorbed NO_2 [21, 24]. The frequencies around 1602 cm^{-1} were assigned to nitro and nitrate groups [21, 24] while the low intensity band at 1577 cm^{-1} with low intensity was attributed to adsorbed NO_3 groups [21, 22, 24]. The assignments for the FT-IR bands are summarized in Table 7.5. The band assignment for frequencies below 1650 cm^{-1} was not evident since many NO_x species (NO_2, NO^-_2, NO^-_3) absorbed at about 1650-1600 cm^{-1} [25]. Bands in the range of 1920–1750 cm^{-1} attributed to mononitrosyl and dinitrosyl complexes with Fe(II) on zeolite did not appear upon NO_2 interaction. In summary, strong bands for NO^+ and N_2O_4 were observed while the bands of the nitro and nitrate groups were not well resolved and their assignment was ambiguous.

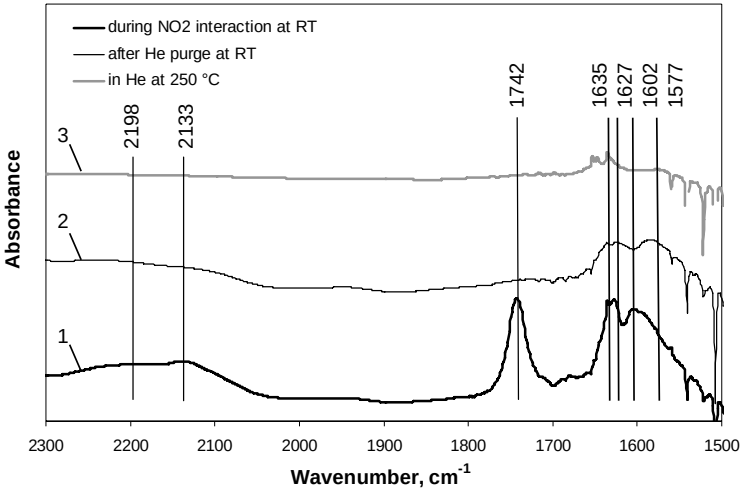

Figure 7.20: DRIFT spectra obtained during NO_2 interaction (0.5 vol%, 15 min) at room temperature (1), subsequent He purge (5 min) at room temperature (2) and the spectra at 523 K in He (3).

The spectra of the adsorbed species after a He purge of 5 min is also presented in Figure 7.20, spectrum 2 in order to see the difference between strongly and weakly adsorbed species. The bands of N_2O_4 and NO^+ disappeared upon the He purge and the bands of the nitro and nitrate groups decreased in intensity. The spectra upon heating to 523 K (Figure 7.20, spectrum 3) in He showed only very weak bands at 1635 and 1577 cm^{-1} assigned to adsorbed NO_2 and NO_3 species, respectively.

In this case DRIFTS was not a suitable way to study the formation of $NO_{x,ads}$ species on the Fe-ZSM-5_{350} during NO_2 interaction at 523 K and their desorption at higher temperatures since the bands of the nitrite and nitrate groups had a very low

intensity already at low temperatures as 523 K. The sample size was only 50 mg and the concentration of active sites with $2.7 \cdot 10^{18}$ sites/g was very low. This showed again the general problem of characterizing Fe-ZSM-5 active in N_2O decomposition due to the small concentration of active sites.

Table 7.5: Summary of the assignment of the different FT-IR bands.

Band position (Wavenumber, cm^{-1})	*Assignment to adsorbed*	*Reference*
2198	$[NO^+][N_2O_4]$	[21, 22]
2133	NO^+	[21-24]
1742	N_2O_4	[21, 22, 24]
1711	N_2O_4	[22]
1635	NO_2	[21, 24]
1627	NO_2	[21, 24]
1602	NO_2	[21, 24]
	NO_3	
1577	NO_3	[21, 22, 24]

DRIFT spectroscopy was applied to further elucidate the interaction of NO_2 with the Fe-ZSM-5_{350}. The idea was to study the formation of surface species by NO_2 and to observe their stability upon heating the catalyst. However, already at 523 K the intensities of nitro/nitrate groups were very weak. Additional bands of interest in the range of 2300 to 1500 cm^{-1} were not observed, which made the method not suitable to study the interaction of NO_2 with the particular catalyst. At room temperature strong bands for NO^+ and N_2O_4 were observed while the bands of the nitro and nitrate groups were not well resolved and their assignment was ambiguous.

7.5. References

1. Lide, D. R., *CRC Handbook of Chemistry and Physics*. 82nd ed.; CRC Press: Boca Raton, 2001-2002.
2. Chen, H. Y.; Voskoboinikov, T.; Sachtler, W. M. H., Reduction of NO_x over Fe/ZSM-5 catalysts: Adsorption complexes and their reactivity toward hydrocarbons. *Journal of Catalysis* **1998,** 180, (2), 171-183.
3. Bulushev, D. A.; Renken, A.; Kiwi-Minsker, L., Role of adsorbed NO in N_2O decomposition over iron-containing ZSM-5 catalysts at low temperatures. *Journal of Physical Chemistry B* **2006,** 110, (22), 10691-10700.
4. Perez-Ramirez, J.; Kapteijn, F.; Mul, G.; Moulijn, J. A., NO-assisted N_2O decomposition over Fe-based catalysts: Effects of gas-phase composition and catalyst constitution. *Journal of Catalysis* **2002,** 208, (1), 211-223.

5. Sang, C. M.; Kim, B. H.; Lund, C. R. F., Effect of NO upon N_2O decomposition over Fe/ZSM-5 with low iron loading. *Journal of Physical Chemistry B* **2005,** 109, (6), 2295-2301.
6. Sang, C. M.; Lund, C. R. F., Possible role of nitrite/nitrate redox cycles in N_2O decomposition and light-off over Fe-ZSM-5. *Catalysis Letters* **2001,** 73, (1), 73-77.
7. Mul, G.; Perez-Ramirez, J.; Kapteijn, F.; Moulijn, J. A., NO-assisted N_2O decomposition over ex-framework FeZSM-5: mechanistic aspects. *Catalysis Letters* **2001,** 77, (1-3), 7-13.
8. Pirngruber, G. D.; Pieterse, J. A. Z., The positive effect of NO on the N_2O decomposition activity of Fe-ZSM-5: A combined kinetic and in situ IR spectroscopic study. *Journal of Catalysis* **2006,** 237, (2), 237-247.
9. Kogel, M.; Abu-Zied, B. M.; Schwefer, M.; Turek, T., The effect of NO_x on the catalytic decomposition of nitrous oxide over Fe-MFI zeolites. *Catalysis Communications* **2001,** 2, (9), 273-276.
10. Corna, A.; Massot, R., *Compilation of Mass Spectroscopy Data.* Heyden: London, 1966.
11. Kiwi-Minsker, L.; Bulushev, D. A.; Renken, A., Transient response method for characterization of active sites in HZSM-5 with low content of iron during N_2O decomposition. *Catalysis Today* **2004,** 91-92, 165-170.
12. Novakova, J.; Sobalik, Z., Comparison of O-18 isotopic exchange after and during the interaction of N_2O, NO, and NO_2 with Fe ions in ferrierites. *Catalysis Letters* **2003,** 89, (3-4), 243-247.
13. Brosius, R.; Habermacher, D.; Martens, J. A.; Vradman, L.; Herskowitz, M.; Capek, L.; Sobalik, Z.; Dedecek, J.; Wichterlova, B.; Tokarova, V.; Gonsiorova, O., NO oxidation kinetics on iron zeolites: influence of framework type and iron speciation. *Topics in Catalysis* **2004,** 30-31, (1-4), 333-339.
14. Kiwi-Minsker, L.; Bulushev, D. A.; Renken, A., Low temperature decomposition of nitrous oxide over Fe/ZSM-5: Modelling of the dynamic behaviour. *Catalysis Today* **2005,** 110, (3-4), 191-198.
15. El-Malki, E. M.; van Santen, R. A.; Sachtler, W. M. H., Active sites in Fe/MFI catalysts for NO_x reduction and oscillating N_2O decomposition. *Journal of Catalysis* **2000,** 196, (2), 212-223.
16. Kapteijn, F.; Marban, G.; RodriguezMirasol, J.; Moulijn, J. A., Kinetic analysis of the decomposition of nitrous oxide over ZSM-5 catalysts. *Journal of Catalysis* **1997,** 167, (1), 256-265.
17. Wood, B. R.; Reimer, J. A.; Bell, A. G., Studies of N_2O adsorption and decomposition on Fe-ZSM-5. *Journal of Catalysis* **2002,** 209, (1), 151-158.
18. Wood, B. R.; Reimer, J. A.; Bell, A. T.; Janicke, M. T.; Ott, K. C., Nitrous oxide decomposition and surface oxygen formation on Fe-ZSM-5. *Journal of Catalysis* **2004,** 224, (1), 148-155.
19. Zhu, Q.; Mojet, B. L.; Janssen, R. A. J.; Hensen, E. J. M.; van Grondelle, J.; Magusin, P.; van Santen, R. A., N_2O decomposition over Fe/ZSM-5: effect of high-temperature calcination and steaming. *Catalysis Letters* **2002,** 81, (3-4), 205-212.
20. Bulushev, D. A.; Renken, A.; Kiwi-Minsker, L., Formation of the surface NO during N_2O interaction at low temperature with iron-containing ZSM-5. *Journal of Physical Chemistry B* **2006,** 110, (1), 305-312.
21. Chen, H. Y.; El-Malki, E. M.; Wang, X.; van Santen, R. A.; Sachtler, W. M. H., Identification of active sites and adsorption complexes in Fe/MFI catalysts for NO_x reduction. *Journal of Molecular Catalysis A-Chemical* **2000,** 162, (1-2), 159-174.

22. Hadjiivanov, K.; Knozinger, H.; Tsyntsarski, B.; Dimitrov, L., Effect of water on the reduction of NO_x with propane on Fe-ZSM-5. An FTIR mechanistic study. *Catalysis Letters* **1999,** 62, (1), 35-40.
23. Hadjiivanov, K.; Saussey, J.; Freysz, J. L.; Lavalley, J. C., FT-IR study of NO+O_2 co-adsorption on H-ZSM-5: re-assignment of the 2133 cm^{-1} band to NO^+ species. *Catalysis Letters* **1998,** 52, (1-2), 103-108.
24. Lobree, L. J.; Hwang, I. C.; Reimer, J. A.; Bell, A. T., An in situ infrared study of NO reduction by C_3H_8 over Fe-ZSM-5. *Catalysis Letters* **1999,** 63, (3-4), 233-240.
25. Hadjiivanov, K. I., Identification of neutral and charged N_xO_y surface species by IR spectroscopy. *Catalysis Reviews-Science and Engineering* **2000,** 42, (1-2), 71-144.

Chapter 8

H_2O INTERACTION WITH Fe-ZSM-5

A significant deactivation during N_2O decomposition was several times observed upon water introduction into the reaction mixture [1-5]. The water inhibition was studied theoretically and compared with experimental results by Heyden et al. [6, 7]. The authors concluded that water impurity (< 100 ppm) may strongly affect the kinetics of N_2O decomposition. Water is often already present in reaction mixtures as an impurity. This chapter addresses the water effect on N_2O decomposition over isomorphously substituted Fe-ZSM-5 at different temperatures. It is aimed on further understanding under which conditions water inhibits the N_2O decomposition and the reaction steps involved. Vacuum conditions and small amounts of reactants in the TAP setup facilitate the de-hydroxylation of the catalyst compared to atmospheric pressure experiments.

8.1. H_2O Influence on Catalytic Activity

8.1.1. Transient Experiments under Vacuum

The effect of water on the activity of the Fe-ZSM-5_{5500} catalyst was studied in vacuum under transient conditions at different temperatures using the TAP system. At temperatures below 600 K N_2O decomposed via N_2 evolution and atomic surface oxygen loading. The decomposition proceeded until the catalyst was saturated with oxygen and stopped completely thereafter. Consequently, a catalytic activity measurement was not possible at low temperatures. H_2O pulses subsequently to N_2O pulses provoked the partial desorption of oxygen and transformed the residual surface oxygen. This experiment gives valuable information about the interaction of $(O)_{Fe}$ with water and is described in detail in section 8.2.

At 703 K N_2O decomposed over Fe-ZSM-5_{5500} by forming gaseous N_2 and gaseous O_2. The O_2 response from a N_2O pulse over the dry catalyst is shown in Figure 8.1, curve 1. Subsequently to the introduction of about 100 N_2O pulses for reaching a representative conversion, the Fe-ZSM-5_{5500} was saturated with water at 703 K followed by N_2O pulsing during two hours. The catalyst was completely deactivated upon the introduction of water. No oxygen release was observed during N_2O interaction with the catalyst (Figure 8.1, curve 2). However, during continuous N_2O pulsing thereafter, H_2O desorbed and 95% of the initial conversion was recovered after 2 h (Figure 8.1, curve 3). Thus, the effect of water on the catalyst at 703 K can be considered reversible in vacuum.

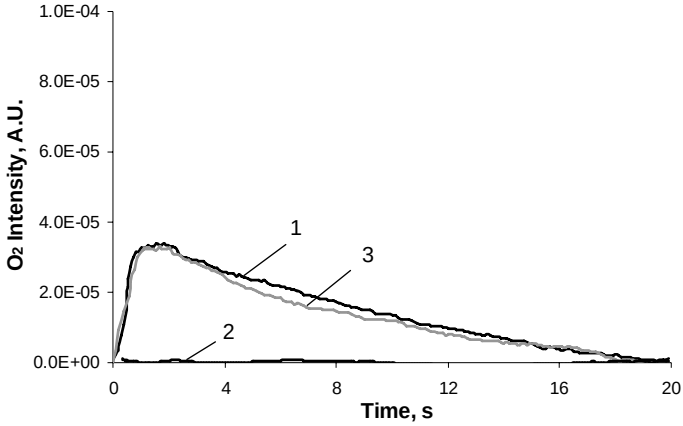

Figure 8.1: O_2 responses during the introduction of N_2O pulses at 703 K over dry Fe-ZSM-5_{5500} (1), over the catalyst saturated with water (2) and after 2h of N_2O pulsing over the wet catalyst (3).

The effect of water on the N_2O decomposition at 803 K was studied with the same catalyst using a pump-probe experiment. After the standard pre-treatment of the Fe-ZSM-5_{5500}, about 100 pulses of N_2O were introduced to the reactor every 20 s to acquire a representative conversion. Afterwards, pulses of N_2O (80 vol% N_2O in Ar) and H_2O were consequently fed to the reactor. N_2O was introduced at t = 0 s time and H_2O was pulsed after a delay at t = 10 s. The total cycle time was 20 s. The N_2O decomposition to N_2 (not shown) and O_2 (Figure 8.2a) was observed in agreement with the steady-state results. Under these conditions water adsorbed reversibly and gave a very broad peak. A part of this H_2O peak starting from the moment of N_2O introduction, is seen in Figure 8.2b. The area under the peak was proportional to the water amount present on the surface before the N_2O pulse.

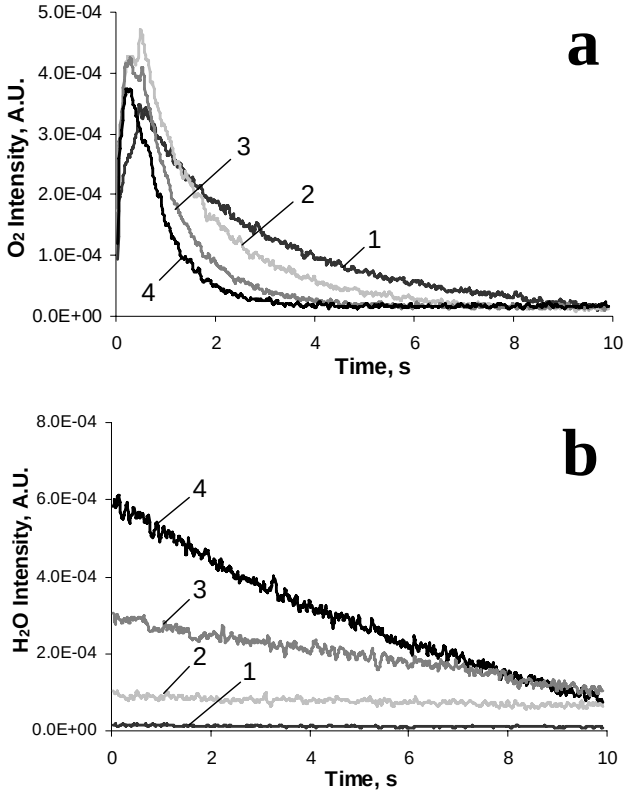

Figure 8.2: Oxygen (a) and water (b) responses obtained at 803 K during N_2O interaction (0 s) with the Fe-ZSM-5_{5500} catalyst containing different amounts of water: without H_2O (1), with increasing amount of water (2), (3), (4).

The oxygen response area decreased with increasing surface water amount. A difference of approximately two times was observed between the oxygen response area without water (curve 1) and with maximal water coverage (curve 4). This indicates that water blocked considerably active iron sites for the reaction even though it was only reversibly adsorbed at 803 K. At the conditions of the experiment Ar, N_2O and N_2 peaks (not shown) were quite narrow (< 0.5 s) as compared with the oxygen peak, which was quite broad and sharpened with increasing amount of H_2O (from 10 to 4 s, Figure 8.2a). The shape of the oxygen responses provide valuable qualitative information on the reaction mechanism and is discussed in section 8.3.

8.1.2. Steady-state Experiments at Atmospheric Pressure

To study the effect of water on N_2O decomposition under steady-state conditions, experiments were performed with the Micromeritics AutoChem 2910 setup at atmospheric pressure. A water pulse of 2 μl was introduced into the reaction mixture passing through the Fe-ZSM-5_{5500} catalyst at different temperatures after the steady-state was attained within 65 min. The conversions before and after water introduction are presented in Table 8.1. It is seen that with the dry catalyst the increase of the temperature from 523 to 673 K increased the conversion up to about 100%. Water introduction led to the complete deactivation of the catalyst towards N_2O decomposition.

Table 8.1: Water effect on the steady-state conversion during the N_2O decomposition (2 vol% N_2O in Ar, total flow rate 20 ml/min) over Fe-ZSM-5_{5500} (0.4 g).

Temperature, K	*Conversion after 65 min in the reaction mixture*	
	Before H_2O introduction	*After H_2O introduction*
523	0	0
603	0.15	0
673	1.0	0

8.1.3. Summary

In summary, the presence of H_2O decreased the catalyst activity in N_2O decomposition at any studied temperature (523–803 K) in experiments with the TAP and the Micromeritics setup. The de-hydroxylation of the catalyst was facilitated in vacuum. The effect of water on the N_2O decomposition at 703 K led to complete deactivation but it was reversible. At 803 K the N_2O conversion was diminished to about the half in N_2O/H_2O pump probe experiments. Water injection on the catalyst at atmospheric pressure (523-673 K) inhibited completely the N_2O decomposition.

8.2. Interaction of H_2O with Surface Oxygen loaded from N_2O

The interaction of H_2O with surface oxygen loaded from N_2O was studied with the Fe-ZSM-5_{5500} at 593 K using the TAP reactor. At these conditions the formation of surface atomic oxygen $(O)_{Fe}$ and gaseous N_2 from N_2O took place, but the formation of gaseous oxygen was not observed. The active sites were loaded with oxygen by multiple N_2O pulsing. Afterwards, pulses of water were introduced. It is seen in Figure 8.3 that the first water pulses provoked an O_2 release. This suggests the competitive adsorption of water on the iron sites containing oxygen. Oxygen evolved as a very broad peak. After 30 pulses of water oxygen did not desorb anymore, while water continued to accumulate on the catalyst until the saturation after ca. 300 pulses.

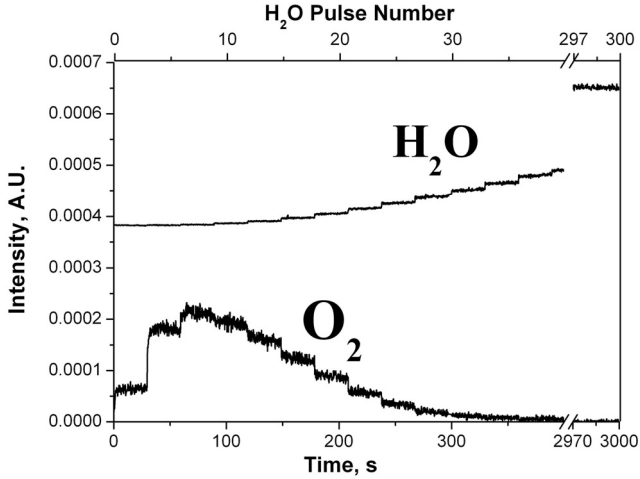

Figure 8.3: Oxygen desorption provoked by water pulses after oxygen loading from N_2O on the Fe-ZSM-5_{5500} catalyst in the TAP reactor at 593 K.

A TPD experiment was performed in order to investigate residual surface species after the water treatment of the $(O)_{Fe}$ containing catalyst. Figure 8.4 summarizes TPD profiles of O_2 evolution for different pre-treatments at 593 K. Curve 1 shows the TPD profile of oxygen after $(O)_{Fe}$ loading from N_2O. Curve 2 illustrates the O_2 evolution in the TPD after the interaction of H_2O with the $(O)_{Fe}$ containing catalyst. As indicated by a shift of the temperature of maximal desorption rate from 715 to 849 K the presence of water clearly transformed the residual adsorbed oxygen. Kiwi-Minsker et al. reported as well that the oxygen recombination/desorption was more difficult from the water saturated surface as from the dry catalyst [8].

It was shown earlier that $(O)_{Fe}$ loaded from N_2O possessed high reactivity in CO oxidation already at low temperatures (423-473 K) [9]. The surface oxygen transformed by H_2O was inactive in CO oxidation as seen by the absence of CO_2 formation during CO interaction (not shown). Curve 3 in Figure 8.4 shows the TPD profile of the O_2 evolution after the $N_2O \rightarrow H_2O \rightarrow CO$ treatment of the Fe-ZSM-5_{5500} at 593 K. It is almost identical to curve 2 confirming the inactivity of the surface oxygen with respect to CO oxidation.

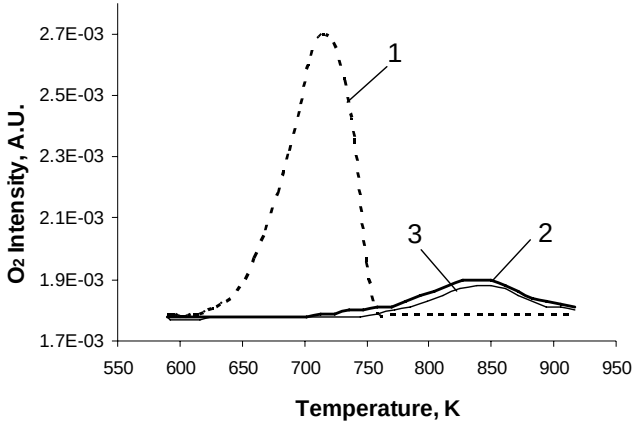

Figure 8.4: TPD profiles of oxygen after its loading from N_2O (1), after N_2O interaction followed by water saturation (2) and after N_2O interaction followed by water saturation and CO treatment (3) at 593 K of the Fe-ZSM-5_{5500}.

Thus, water interaction with $(O)_{Fe}$ at 593 K provoked the evolution of O_2 and transformed residual oxygen into an inactive form which can not oxidize CO to CO_2. The observations upon the interaction of H_2O with $(O)_{Fe}$ containing zeolite are summarized in the following equation:

$$(O)_{Fe} + H_2O \rightarrow H_2O_{ads} + O_2 + \{O\}_{Fe} \qquad (8.1)$$

Similar experiments were performed in the Micromeritics AutoChem 2910 setup with the Fe-ZSM-5_{5500} catalyst at 523 K. 2 µl water were injected in the reaction mixture consisting of 2 vol% N_2O, 2 vol% Ar in He after surface oxygen loading for 2.5 min It is seen in Figure 8.5 that O_2 and N_2O were desorbed upon the water pulse. H_2O was detected at the reactor outlet 140 s after the injection (not shown). Thus, water adsorption was accompanied by the evolution of $0.57 \cdot 10^{18}$ molecules/g oxygen and the desorption of N_2O which was only weakly adsorbed and amounts $7.0 \cdot 10^{18}$ molecules/g. Important is that the amount of oxygen induced by water adsorption ($1.1 \cdot 10^{18}$ atoms/g)

was less than the amount of loaded oxygen ($3.5 \cdot 10^{18}$ atoms/g). Hence, water substituted only a part of the loaded $(O)_{Fe}$ leading to its desorption as O_2.

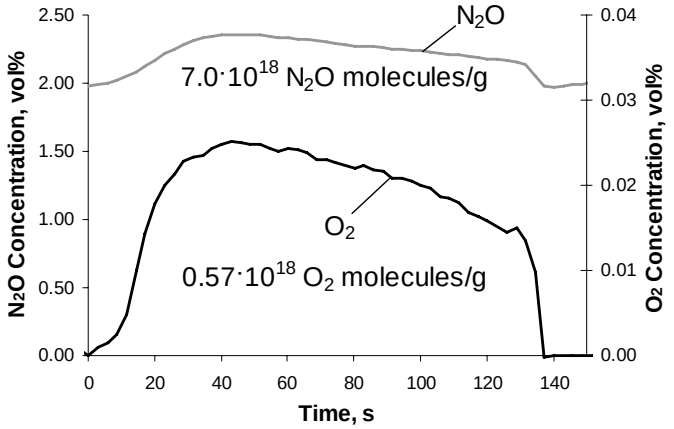

Figure 8.5: O_2 and N_2O desorption provoked by the injection of 2 µl water into the reaction mixture of 2 vol% N_2O, 2 vol% Ar in He after oxygen loading from N_2O on the Fe-ZSM-5_{5500} catalyst at 523 K.

A TPD run was performed after the water assisted oxygen desorption in order to study the residual surface species. Figure 8.6 shows the AMU 32 and AMU 30 TPD. $NO_{x,ads}$ species desorbed around 729 K contributing to AMU 30 and AMU 32. $NO_{x,ads}$ species were known to be slowly formed from N_2O as reported in [1, 10] and acted as co-catalyst [11, 12] in N_2O decomposition. They were stronger attached to the catalyst than water. Supplementary, oxygen was desorbed showing a broad peak with a maximum at 959 K similar to the profile when oxygen loading was performed on the water saturated surface which was inactive in CO oxidation [8, 13]. Water participated in the transformation of the active iron sites into inactive ones.

It can be concluded that water affected $(O)_{Fe}$ by provoking its partial desorption as O_2 and transforming the residual oxygen into an inactive form as already summarized in Equation (8.1). Very good agreement was found between the TAP reactor data obtained at vacuum conditions and catalytic data at atmospheric pressure. $NO_{x,ads}$ species formed from N_2O resisted the water treatment while weakly adsorbed N_2O desorbed during the water pulse at atmospheric pressure.

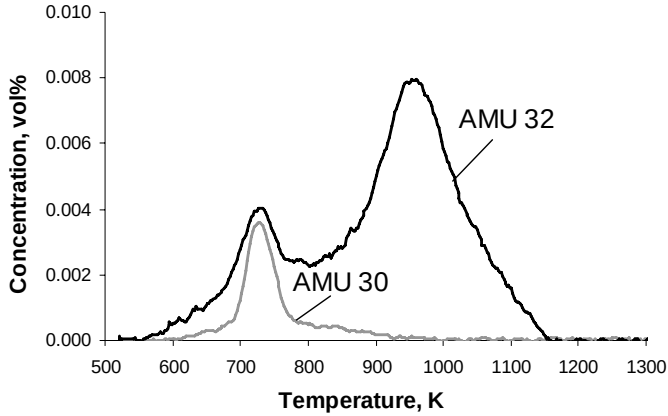

Figure 8.6: TPD profiles of AMU 32 and 30 after oxygen loading from 2 vol% N_2O, 2 vol% Ar in He for 2.5 min on the Fe-ZSM-5_{5500} catalyst at 523 K followed by the injection of 2 µl water into the reaction mixture.

8.3. Effect of H_2O on Oxygen Desorption during N_2O Decomposition

N_2O/H_2O pump probe experiments with the Fe-ZSM-5_{5500} at 803 K which are presented in section 8.1 showed a diminished N_2O conversion over the wet zeolite. In Figure 8.2 it can be seen that the area of the O_2 response becomes smaller with increasing amount of H_2O on the catalyst. However, the oxygen responses shifted also to lower times with increasing surface water amount. To understand the reasons of the broad shape of the O_2 response on the dry surface and narrow on the wet one, O_2/Ar pulses were introduced on the dry and wet catalyst at the same temperature. It is seen in Figure 8.7 that the Ar and O_2 responses were similar and extremely narrow (< 0.4 s) independently on the water pre-treatment. Hence, oxygen re-adsorption did not take place on the zeolite and mass transport of oxygen did not play an important role in the conditions of N_2O decomposition on the dry as well as on the wet surfaces. The results indicate that the oxygen recombination/desorption is the rate-determining step of N_2O decomposition which is discussed in detail in chapter 5.

However, the O_2 response shift to lower times on the wet surface points out a larger rate constant of the oxygen recombination/desorption in the presence of water. The latter is in line with the observed water assisted oxygen desorption taking place at temperatures as low as 523 K and 593 K (section 8.2) contrary to normal oxygen desorption, which was not observed below 600 K in TAP experiments.

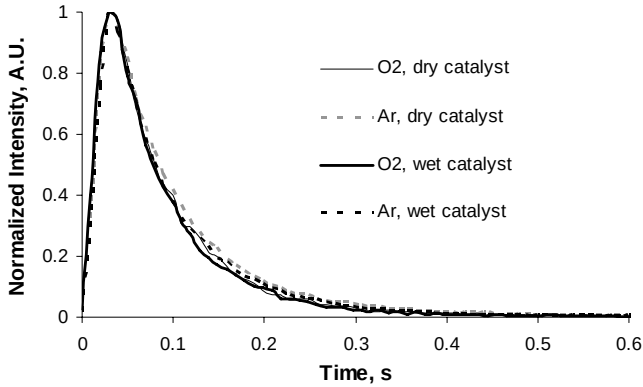

Figure 8.7: Height-Normalized oxygen and argon responses obtained during introduction of the O_2/Ar mixture on the dry and wet Fe-ZSM-5_{5500} catalyst at 803 K.

8.4. H_2O Assisted NO Desorption

The effect of water on adsorbed NO was investigated with the TAP setup at 593 K. NO adsorbs strongly on Fe(II) and is, therefore, frequently used as a probe molecule. Depending on the coordinative unsaturation of the Fe(II) sites NO can adsorb as mono-, di- and trinitrosyl [14, 15]. The Fe-ZSM-5_{5500} was loaded with NO by 600 NO pulses. Consequent water pulses provoked the desorption of NO as seen in Figure 8.8.

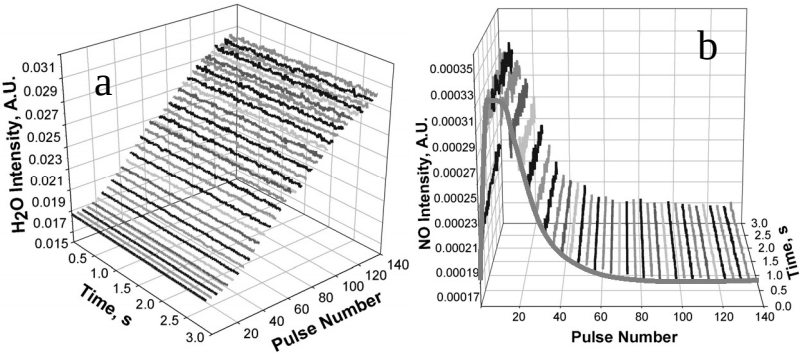

Figure 8.8: Water pulses (a) provoke NO desorption (b) from the NO containing Fe-ZSM-5_{5500} catalyst at 593 K. Grey line: guide for eyes.

H_2O desorbed in a very broad peak and accumulated on the catalyst over 140 pulses. NO desorbed as well in a very broad peak during the first 40 water pulses. This observation points out the preference of the H_2O molecules for certain sites which were occupied by NO_{ads}. NO TPD profiles before and after water interaction with the NO containing Fe-ZSM-5_{5500} are compared in Figure 8.9. Evidently, the main part of NO_{ads} was desorbed during water pulsing.

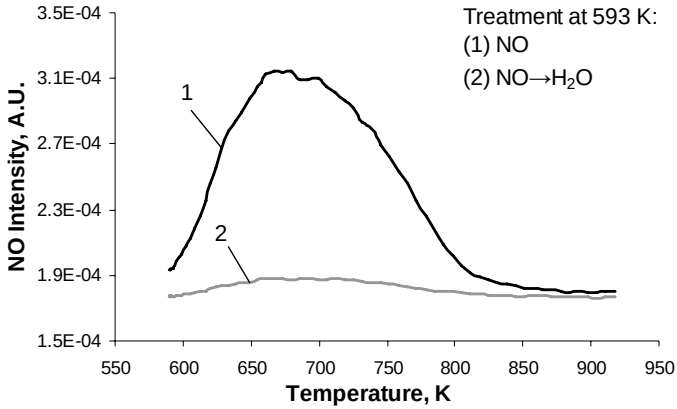

Figure 8.9: NO TPD profiles after introducing 600 NO pulses (1) and 600 NO pulses followed by 140 H_2O pulses (2) over the Fe-ZSM-5_{5500} catalyst at 593 K.

The affinity of H_2O and NO to the Fe-ZSM-5 was further investigated by pulsing NO over the wet Fe-ZSM-5_{5500} at 593 K. Figure 8.10 illustrates the NO pulses responses. Clearly, NO passed the TAP-reactor within 3 s when the catalyst was saturated with water. NO pulses over the dry zeolite (not shown) were much broader and need more than 10 s to traverse the reactor. The large mean residence time of NO was the result of reversible ad- and desorption processes with the catalyst. The reduced mean residence time of NO with the wet Fe-ZSM-5 indicated less interaction of NO with the catalyst. A possible explanation is that water blocked sites which participate in dry conditions in NO adsorption. In accordance with the reduced NO affinity to the wet catalyst are IR spectroscopy data from Pirngruber et al. [16]. They concluded that de-hydroxylation of Fe-ZSM-5 prepared by CVD created vacancies in the coordination sphere of iron that allowed the adsorption of two or even three molecules of NO on one site.

It can be concluded that there was competitive adsorption of H_2O and NO on the same sites while water had a stronger affinity to the Fe-ZSM-5 than NO. H_2O provoked the desorption of NO_{ads} and occupied different sites. NO interacted only weakly with the wet catalyst since sites for NO adsorption were already saturated by water.

$NO_{x,ads}$ species formed by N_2O interaction with the catalyst at atmospheric pressure were not desorbed by water as described in section 8.2, Figure 8.6. Thus, water desorbed NO_{ads} but not $NO_{x,ads}$ species showing the strong bonding of the $NO_{x,ads}$ species to the catalyst.

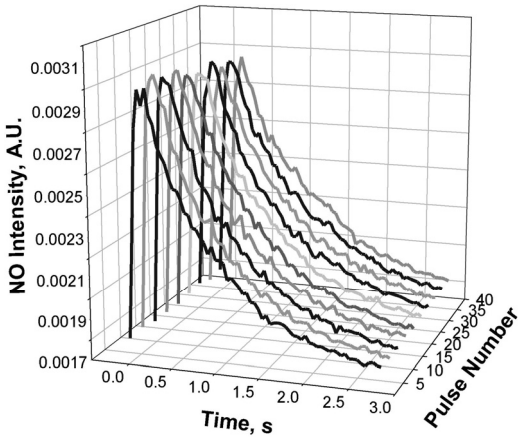

Figure 8.10: NO pulses over the water containing Fe-ZSM-5_{5500} catalyst at 593 K.

8.5. Summary

Adsorbed water strongly influenced the N_2O decomposition inhibiting it completely at least at temperatures ≤ 673 K. The latter occurred because the oxygen recombination/desorption, considered as the rate-determining step of N_2O decomposition, did not take place from the water saturated surface rendering the zeolite catalyst inactive toward N_2O decomposition [1]. During TAP experiments only small amounts of water were dosed and the water desorption was facilitated due to vacuum conditions. Therefore, the recovery of the initial catalyst activity at 703 K was observed 2 h after water treatment. The effect of water at this temperature can be considered reversible.

The observed partial desorption of the loaded $(O)_{Fe}$ as O_2 at 523-593 K induced by water adsorption, indicated its competition with water for the same adsorption sites. During N_2O/H_2O pump probe experiments at 803 K oxygen desorbed significantly faster with increasing water amount on the catalyst suggesting as well the water assisted O_2 desorption. At the same time, the catalyst activity decreased to about the half of the initial N_2O conversion over the dry zeolite.

At 523 and 593 K only a part of oxygen loaded from N_2O was desorbed from the catalyst by water. The residual adsorbed oxygen desorbed during TPD experiments with

the TAP setup at 849 K instead of 715 K for oxygen loaded from N_2O on the dry catalyst. However, the most important is that the oxygen on the wet catalyst can not oxidize CO to CO_2. It means that the active sites were transformed into an inactive form in the presence of water. The oxygen which stayed on the catalyst seemed to participate in the Fe(II) oxidation to the hydroxylated Fe(III) species, as proposed in a simplified scheme reported in [13]. These Fe(III) species were inactive in N_2O decomposition and could be activated again by high-temperature treatment in He or in vacuum.

Other reaction steps were also influenced by water adsorption. Reversibly adsorbed N_2O at atmospheric pressure desorbed upon H_2O interaction. $NO_{x,ads}$ species formed during N_2O interaction at 523 K remained on the catalyst while NO_{ads} desorbed during water treatment. Water adsorbed strongly on several sites of the zeolite and was able to provoke the desorption of reversibly adsorbed N_2O, NO_{ads} and a part of $(O)_{Fe}$.

NO showed much weaker interaction with the wet catalyst than with the dry one at 593 K. This is understood as NO can adsorb among others on Fe(II) sites, which become highly coordinative saturated by adsorbed water.

Good agreement was found between the TAP reactor data obtained at vacuum conditions and steady-state data at atmospheric pressure. The results on water assisted O_2 desorption and catalyst deactivation by water were published by us [17].

8.6. References

1. Bulushev, D. A.; Kiwi-Minsker, L.; Renken, A., Dynamics of N_2O decomposition over HZSM-5 with low Fe content. *Journal of Catalysis* **2004,** 222, (2), 389-396.
2. El-Malki, E. M.; van Santen, R. A.; Sachtler, W. M. H., Active sites in Fe/MFI catalysts for NO_x reduction and oscillating N_2O decomposition. *Journal of Catalysis* **2000,** 196, (2), 212-223.
3. Roy, P. K.; Pirngruber, G. D., The surface chemistry of N_2O decomposition on iron-containing zeolites(II) - The effect of high-temperature pretreatments. *Journal of Catalysis* **2004,** 227, (1), 164-174.
4. Yuranov, I.; Renken, A.; Kiwi-Minsker, L., Zeolite/sintered metal fibers composites as effective structured catalysts. *Applied Catalysis A-General* **2005,** 281, (1-2), 55-60.
5. Zhu, Q.; Mojet, B. L.; Janssen, R. A. J.; Hensen, E. J. M.; van Grondelle, J.; Magusin, P.; van Santen, R. A., N_2O decomposition over Fe/ZSM-5: effect of high-temperature calcination and steaming. *Catalysis Letters* **2002,** 81, (3-4), 205-212.
6. Heyden, A.; Peters, B.; Bell, A. T.; Keil, F. J., Comprehensive DFT study of nitrous oxide decomposition over Fe-ZSM-5. *Journal of Physical Chemistry B* **2005,** 109, (5), 1857-1873.

7. Heyden, A.; Bell, A. T.; Keil, F. J., Kinetic modeling of nitrous oxide decomposition on Fe-ZSM-5 based on parameters obtained from first-principles calculations. *Journal of Catalysis* **2005,** 233, (1), 26-35.
8. Kiwi-Minsker, L.; Bulushev, D. A.; Renken, A., Active sites in HZSM-5 with low Fe content for the formation of surface oxygen by decomposing N_2O: is every deposited oxygen active? *Journal of Catalysis* **2003,** 219, (2), 273-285.
9. Dubkov, K. A.; Paukshtis, E. A.; Panov, G. I., Stoichiometry of oxidation reactions involving alpha-oxygen on FeZSM-5 zeolite. *Kinetics and Catalysis* **2001,** 42, (2), 205-211.
10. Bulushev, D. A.; Renken, A.; Kiwi-Minsker, L., Formation of the surface NO during N_2O interaction at low temperature with iron-containing ZSM-5. *Journal of Physical Chemistry B* **2006,** 110, (1), 305-312.
11. Bulushev, D. A.; Renken, A.; Kiwi-Minsker, L., Role of adsorbed NO in N_2O decomposition over iron-containing ZSM-5 catalysts at low temperatures. *Journal of Physical Chemistry B* **2006,** 110, (22), 10691-10700.
12. Kiwi-Minsker, L.; Bulushev, D. A.; Renken, A., Low temperature decomposition of nitrous oxide over Fe/ZSM-5: Modelling of the dynamic behaviour. *Catalysis Today* **2005,** 110, (3-4), 191-198.
13. Kiwi-Minsker, L.; Bulushev, D. A.; Renken, A., Transient response method for characterization of active sites in HZSM-5 with low content of iron during N_2O decomposition. *Catalysis Today* **2004,** 91-92, 165-170.
14. Berlier, G.; Spoto, G.; Ricchiardi, G.; Bordiga, S.; Lamberti, C.; Zecchina, A., IR spectroscopy of adsorbed NO as a useful tool for the characterisation of low concentrated Fe-silicalite catalysts. *Journal of Molecular Catalysis A-Chemical* **2002,** 182, (1), 359-366.
15. Berlier, G.; Zecchina, A.; Spoto, G.; Ricchiardi, G.; Bordiga, S.; Lamberti, C., The role of Al in the structure and reactivity of iron centers in Fe-ZSM-5-based catalysts: a statistically based infrared study. *Journal of Catalysis* **2003,** 215, (2), 264-270.
16. Pirngruber, G. D.; Roy, P. K., A look into the surface chemistry of N_2O decomposition on iron zeolites by transient response experiments. *Catalysis Today* **2005,** 110, (3-4), 199-210.
17. Bulushev, D. A.; Prechtl, M. P.; Renken, A.; Kiwi-Minsker, L., Water Vapor Effects in N_2O Decomposition over Fe-ZSM-5 Catalysts with Low Iron Content. *Industrial & Engineering Chemistry Research* **2007,** 46, (12), 4178 - 4185.

Chapter 9

CONCLUSIONS AND PERSPECTIVES

9.1. Conclusions

Mechanistic aspects of the N_2O decomposition to N_2 and O_2 over Fe-ZSM-5 containing small amounts of active iron were studied with transient pulse experiments in vacuum and transient flow experiments at atmospheric pressure. Both approaches showed that the mechanism strongly depends on the reaction temperature, but in all cases the reaction proceeds via atomic surface oxygen loading and gaseous N_2 formation from N_2O as a first step. A complete saturation of the active sites can be attained by N_2O exposure at low temperatures ($T < 600$ K in vacuum, $T < 523$ K at atmospheric pressure) where oxygen is stored and does not desorb. On that basis, the concentration of sites active in surface atomic oxygen loading from N_2O were determined in pulse experiments using the TAP setup. The concentration of active sites was found to be the same as in a flow experiment with the Micromeritics analyzer.

The mechanism of surface atomic oxygen recombination and desorption as O_2 depends on the temperature. At high temperature ($T > 773$ K) the atomic surface oxygen recombines probably directly and desorbs as O_2. The oxygen recombination/desorption was found to be delayed to N_2O decomposition and N_2 evolution at 803 K which

indicates that oxygen formation is the rate-determining step. A curve fit of the oxygen desorption response resulted in a first order dependence of the oxygen desorption rate on the oxygen surface coverage.

In the range of 523 to 773 K, the O_2 formation is facilitated by NO. The formation of $NO_{x,ads}$ species was observed during the interaction of N_2O with the zeolite at 593 K. The temperature of maximum desorption rate of oxygen in TPD experiments decreases with increasing amount of $NO_{x,ads}$ species. The effect is enhanced by pre-adsorbed NO on the catalyst. Adsorbed NO_x acts as co-catalyst and facilitates the desorption of oxygen which is in general accepted as the rate-determining step of the N_2O decomposition.

NO pulses over the catalyst containing atomic surface oxygen provoke the recombination and desorption of atomic surface oxygen at low temperatures (523 K and 593 K) where the desorption of O_2 is not observed during N_2O interaction with the Fe-ZSM-5_{5500}. NO adsorbs in large amounts at the same time on the catalyst on adjacent sites to the N_2O decomposing sites since the reloading of oxygen from N_2O takes place without any difficulty.

N_2O/NO pump-probe experiments at 661 K demonstrated an accelerated oxygen desorption at the time of the N_2O pulse due to adsorbed NO/NO_x species. The subsequent NO pulse accelerate the desorption of the residual surface oxygen at 661 K and 803 K. Adsorbed NO accommodates oxygen from N_2O forming higher oxidized nitrogen oxide species which decompose back to NO_{ads} and molecular oxygen. Thus, the recombination of surface oxygen loaded from N_2O is accelerated by a NO/NO_x redox cycle.

In general, NO_2 is considered as intermediate of the catalytic cycle of N_2O decomposition and functions as intermediate oxygen storage. At temperatures above 600 K the interconversion of $NO_2 \leftrightarrow NO$ takes place whereas at lower temperature NO_2 compared to NO shows a different effect on the oxygen loading from N_2O.

The interaction of gaseous NO_2 with Fe-ZSM-5 at 523 K in vacuum and at atmospheric pressure showed the formation of two different NO_x surface species accompanied by the evolution of gaseous NO. In general, oxygen loaded from N_2O on the surface saturated with $NO_{x,ads}$ species is not reactive with respect to CO oxidation to CO_2. Therefore, the formation of α-oxygen from NO_2 could not be evidenced with CO oxidation since a large amount of $NO_{x,ads}$ species is present on the catalyst surface after NO_2 treatment.

NO_2 pre-treatments inhibit the loading of oxygen from N_2O in transient response experiments. NO_2 blocks the sites for oxygen loading from N_2O but the amount of reversible adsorbed N_2O stays constant compared to the standard pre-treated catalyst. Unlike the surface species formed upon NO_2 treatment, adsorbed NO doesn't prevent the surface oxygen loading from N_2O at 523 K.

NO_2 interaction with $(O)_{Fe}$ containing catalyst leads to the formation of $NO_{2,ads}$,$NO_{3,ads}$ species as upon NO_2 interaction only. The oxygen deposited by N_2O pre-

treatment is consumed for the formation of $NO_{x,ads}$ species in experiments at atmospheric pressure.

Adsorbed water strongly influences the N_2O decomposition inhibiting it completely at least at temperatures ≤ 673 K. During TAP experiments only small amounts of water were dosed and the water desorption is facilitated due to vacuum conditions. Therefore, the recovery of the initial catalyst activity at 703 K was observed 2 h after water treatment. The effect of water at this temperature is considered reversible.

The observed partial desorption of the loaded atomic surface oxygen as O_2 at 523 and 593 K induced by water adsorption, indicates the competition of water for the same adsorption sites. During N_2O/H_2O pump-probe experiments at 803 K oxygen desorbs significantly faster with increasing water amount on the catalyst suggesting as well the water assisted O_2 desorption. At the same time, the catalyst activity decreases to about the half of the initial activity of the dry zeolite.

At 523 and 593 K only a part of oxygen loaded from N_2O is desorbed from the catalyst by water. The residual adsorbed oxygen desorbs during TPD experiments with the TAP setup at 849 K instead of 715 K for oxygen loaded from N_2O on the dry catalyst. However, the most important is that the oxygen on the wet catalyst can not oxidize CO to CO_2. It means that the active sites are transformed into an inactive form in the presence of water. The oxygen which stays on the catalyst seems to participate in the Fe(II) oxidation to the hydroxylated Fe(III) species. These Fe(III) species are inactive in N_2O decomposition and could be activated again by high temperature treatment in He or in vacuum.

Very good agreement was found between the TAP reactor data obtained under vacuum and results obtained by transient flow experiments at atmospheric pressure. It follows that the mechanism of the N_2O decomposition over Fe-containing ZSM-5 depends strongly on the reaction temperature as well as on the presence of other gases such as NO, H_2O and NO_2.

9.2. Perspectives

It would be interesting to further investigate the interaction of NO_2 with the Fe-ZSM-5 using the TAP setup in particular whether atomic surface oxygen can be generated from NO_2 such as from N_2O. NO_2 interacts with the catalyst via NO evolution and oxygen loading. Since a large amount of $NO_{2,ads}$,$NO_{3,ads}$ species is also formed on the catalyst, the loaded oxygen could not be tested for its reactivity in CO oxidation to CO_2. Active surface oxygen from N_2O was shown to be inactive with respect to CO oxidation in the presence of $NO_{x,ads}$ species. The dosing of small amounts of NO_2 with the TAP setup could separate the formation of active surface oxygen and of

$NO_{x,ads}$ species. This could give useful information on the fate of the deposited oxygen from NO_2.

The study of another iron containing zeolite, for example BEA framework, would be beneficial to get more information on the influence of the host matrix on the catalyst properties. A comparison with the MFI-type zeolite could reveal further mechanistic aspects, in particular concerning the desorption of oxygen and the effect of NO, NO_2 and H_2O on the N_2O decomposition.

CURRICULUM VITAE

Petra Prechtl
Petra.Prechtl@a3.epfl.ch

German
Born - 10.11.1977

EDUCATION

2002-2007 **PhD in Chemical Engineering**

- Swiss Federal Institute of Technology Lausanne (EPFL), Switzerland, Laboratory of Chemical Reaction Engineering
- "Study of N_2O Decomposition over Fe-ZSM-5 with Transient Methods"

2000-2002 **Master of Science in Chemical Engineering, with distinction**

- University of Erlangen-Nuremberg, Germany
- Diploma thesis: "Entwicklung einer Druck- und Kleinstvolumen-strom-Regelung für in situ DRIFTS im pressure gap"

1996-2000 **Engineering Diploma in Technical Chemistry, with distinction**

- University of Applied Sciences Nuremberg, Germany
- Diploma thesis: "Neuartiges Nanoliter-Injektionssystem auf Piezo-Mikromanipulator-Basis für die Kapillarelektrophorese"
- Awards from Bavarian Ministry of Science and Max Buchner Foundation for excellent diploma thesis

PROFESSIONAL EXPERIENCE

2002-2007 **Assistant/Researcher at the EPFL, Lausanne, Switzerland**

- Supervised one master and two semester theses
- Assisted the course: Advanced Chemical Reaction Engineering
- Coached practical laboratory work in Chemical Engineering

1999 **6-month internship at Degussa-Hüls AG, Theodore, AL, USA**

- Acquired and evaluated production process data
- Performed laboratory experiments for plant start-up
- Developed analytical procedures

LANGUAGES

German	Native speaker
English	Fluent (spoken & written)
French	Fluent (spoken & written)

ARTICLES

P.M. Prechtl, D.A. Bulushev, B.K. Bromley, A. Renken, L. Kiwi-Minsker, *Transient kinetics of the influence of NO on N_2O decomposition over Fe-ZSM-5.* in preparation.

D.A. Bulushev, P.M. Prechtl, A. Renken, L. Kiwi-Minsker, *Water Vapor Effects in N_2O Decomposition over Fe-ZSM-5 Catalysts with Low Iron Content*. Industrial & Engineering Chemistry Research, 46 (12) 2007, 4178-4185.

F. Kiesslich, P.M. Prechtl, H. Gerhard, M.A. Liauw, N. Popovska, G. Emig, *Development of a Dosing Concept for Minute Flow Rates*. Chemical Engineering Technology, 27 (5) 2004, 553-558.

POSTERS

P.M. Prechtl, D.A. Bulushev, A. Renken, L. Kiwi-Minsker, *Oxygen desorption in N_2O decomposition over Fe-ZSM-5 studied by TAP*. Europacat VIII, 26-31.08.2007, Turku, Finland.

P.M. Prechtl, B.K. Bromley, D.A. Bulushev, A. Renken, L. Kiwi-Minsker, *N_2O Zersetzung im TAP-System über Fe-ZSM-5*. GVC/DECHEMA-Jahrestagung, 26-28.09.2006, Wiesbaden, Germany.

P.M. Prechtl, B.K. Bromley, D.A. Bulushev, A. Renken, L. Kiwi-Minsker, *TAP reactor to study N_2O decomposition over Fe-ZSM-5*. International Symposium on Chemical Reaction Engineering, 03-06.09.2006, Potsdam, Germany.

P.M. Prechtl, L. Kiwi-Minsker, A. Renken, *Temporal Analysis of Products (TAP): NO effects on N_2O decomposition.* University Conference of Occidental Switzerland, Seminar on chemistry, "Modern Concepts for Environmentally Benign Synthesis", 11-15.09.2005, Villars, Switzerland.

P.M. Prechtl, L. Kiwi-Minsker, A. Renken, *Temporal Analysis of Products: reactor system, basic principles, and application.* University Conference of Occidental Switzerland, Seminar on inorganic chemistry and chemical engineering, "Frontiers in Catalysis", 28.09.-02.10.2003, Champery, Switzerland.